Investigation of binary polar solvent mixtures, solubilized ferroelectric salts and Paraffin-based derivatives using dielectric spectroscopy

INAUGURALDISSERTATION
zur
Erlangung der Würde eines Doktors der Philosophie
vorgelegt der
Philosophisch-Naturwissenschaftlichen Fakultät
der Universität Basel

von

Dana Daneshvari
aus Tehran / Iran

Basel, 2007

Genehmigt von der Philosophisch-Naturwissenschaftlichen Fakultät auf Antrag von

Herrn Prof. Dr. Hans Leuenberger (Fakultätsverantwortlicher und Dissertationsleiter)

Herrn Prof. Dr. Isodoro Caraballo (Korreferent)

Basel, den 27.06.2007

Prof. Dr. Hans-Peter Hauri
Dekan

Acknowledgments

This work was carried out at the Department of Pharmaceutical Technology, University of Basel / Switzerland.

I would like to express my profound gratitude to my supervisor Prof. Dr. H. Leuenberger for his invaluable support, encouragement, supervision and useful suggestions throughout this research work. Many thanks for giving me this opportunity to work with you. It has been a great pleasure and an honour for me working with you.

I wish to express my gratitude to the co-referee of the present dissertation Prof. Dr. Isodoro Caraballo.

For the financial support of my PhD I want to acknowledge the University of Basel.

I warmly thank Mr. Stephan Winzap for his kindness and never lasting help during my work. My thanks also go to Ms. Christina Erb for her warm and kind help.

My special acknowledgement is expressed to Dr. Maxim Puchkov for his big support when I needed him.

My sincere thanks go to my friends and co-workers especially Thomas Meyer, David Blaser, Marcel Schneider, Franziska Müller, Miriam Reiser, Michael Lanz, Johannes von Orelli, Matthias Plitzko, Heiko Nalenz, sonija Reutlinger and all other colleagues at Pharmacenter. Thank you for the wonderful working atmosphere and great laughs during Coffee and lunch breaks. I'm grateful for getting to know such good friends during my PhD studies.

Many thanks also to my other colleagues at Industrial Pharmacy Lab.

Last but not least, I would also like to thank all my family specially my father and my mother for their never lasting support during all these years. There are no words to express my gratitude to you and I love you for believing in me and never giving up on me. To my sister Didar and her fabulous family (Ramin, Niki and Nami), thank you for your support and for making me feel at home since my arrival in Switzerland, and many thanks to my brother Danesh for his kind support from long distance.

List of Content

Symbols and abbreviations I
Summary IV

Part A : Binary polar solvent mixtures

Chapter 1: Introduction **1**

Chapter 2: Theory **4**
2.1 Water 4
2.1.1 Molecule 5
2.1.2 Hydrogen bonding network in water clusters 6
2.1.3 Physical properties of water 7
2.1.4 Structural differences between a solid, liquid and gas 9
2.1.5 Water clusters, structured water and biowater 11
2.1.5.1 So-called “structured water” 11
2.1.5.2 Biowater 12
2.2 Dielectric spectroscopy 13
2.3 Properties of isolating material in electric fields 15
2.3.1 Permanent and induced electric dipolemoments 15
2.3.2 Dielectric constant 16
2.3.3 The Clausius-Mossotti and Debye equations and their modification according to Leuenberger 18
2.3.4 Kirkwood-Fröhlich equation and g-valuse obtained from it (Stengele et al., 2001) 24
2.3.5 Broadband dielectric spectroscopy 25
2.3.5.1 The Debye equation applied for complex dielectric permittivity (ε*). 26
2.3.6 Relaxation behavior 28
2.3.6.1 Relaxation behavior according to Cole-Davidson and its superposition with the Debye equation 28
2.3.6.2 The Havriliak-Negami equation and its description of relaxation times 29
2.3.6.3 The dependence on temperature 30
2.4 Electromagnetic alternate fields in the microwave range and their applications in pharmaceutical research and development 32
2.4.1 Analytics 33
2.4.2 Heating procedures 33
2.5 Application of percolation theory to liquid binary mixtures 35

Chapter 3 : Materials and methods **43**
3.1 Materials 43
3.1.1 Solvents 43
3.1.2 Apparatus 48
3.1.3 Computer Software 50
3.2 Methods 51
3.2.1 Sample preparation 51
3.2.2 Measurement of static permittivity and Conductivity 51
3.2.2.1. Measuring principle 51
3.2.2.2. Apparatus and Measuring Procedure 54
3.2.2.3. Accuracy and reproducibility of the measurement 55

3.2.3 Measurement of complex permittivity 57
3.2.3.1. Measuring principle 57
3.2.3.2. Apparatus and Measuring Procedure 59
3.2.3.3. Accuracy and reproducibility of measurement 60
3.2.4 Measurement of density 62
3.2.4.1. Measuring principle 62
3.2.4.2. Apparatus and measuring procedure 63
3.2.4.3. Accuracy and reproducibility of the measurement 64
3.2.5 Measurement of refractive index 66
3.2.5.1. Measuring principle 66
3.2.5.2. Apparatus and measuring procedure 67
3.2.5.3. Accuracy and reproducibility of measurement 68
3.2.6 Data analysis 68
3.2.6.1. Determination of additional physical properties 68
3.2.6.2. Nonlinear regression of dielectric raw data 69
3.2.6.3. Subdivision of curves into segments by means of nonlinear regression 71
3.2.6.4. Software 72

Chapter 4: Results and discussions **74**
4.1. Application of percolation theory in comparison of DMSO and its analogues (DMF, DMAC, NMP) in water as well as 1,4-Dioxane binary mixtures using dielectric spectroscopy 74
4.1.1. Percolation phenomena observed in the binary mixtures based on the results of the modified Clausius-Mossotti-Debye equation 76
4.1.2. Percolation phenomena observed in the binary mixtures based on the results of gvalues according to the Kirkwood-Fröhlich equation 83
4.1.3. Relaxation time according to the Debye equation for the complex dielectric permitivity ε* 87
4.1.4. Conclusions 90
4.2. Investigation of Formamide and its mono & dimethylated form in water using dielectric spectroscopy 92
4.2.1. Percolation phenomena observed in the binary mixtures of Formamide and methylated forms (Mono and Dimethylated) based on the results of the modified Clausius-Mossotti-Debye equation 94
4.2.2. Percolation phenomena observed in the binary mixtures of Formamide and methylated forms based on the results of gvalues according to the Kirkwood-Fröhlich equation 97
4.2.3. Relaxation time of Formamide and methylated forms according to the Debye equation for the complex dielectric permitivity ε* 100
4.2.4. Conclusions 101
4.3. Calculation of percolation threshold from experimental data using first and second derivatives 103

References **106**

Part B : Solubilized ferroelectric salts

Chapter 1: Introduction **112**

Chapter 2: Theory **116**
2.1 Ferroelectric Terms 116
2.1.1 Polar Axis 116
2.1.2 Pyroelectric Effect 117

2.2 Ferroelectric Materials 117
2.2.1 Polarization 118
2.2.2 Spontaneous Polarization 118
2.2.3 Permanent Dipole Moment of polar molecules 118
2.2.4 Behavior of Dielectrics in Electric Fields: Classification of Polar Materials (Crystalse and liqiud crystals) 120
2.2.5 Ferroelectric Domains 127
2.2.6 Phase Transition 127
2.2.7 Ferroelectric Curie Point T_C 128
2.2.8 Curie-Weiss Temperature 128
2.2.9 Paraelectric Phase 129
2.3 Dielectric Constant 129
2.3.1 Complex Permitivity 132
2.3.2 Static or Differential Permittivity 133
2.4 Dielectric Spectroscopy 133
2.5 Polymorphism 134
2.5.1 Polymorphism in pharmaceuticals 135
2.6 Water 136
2.7 Rochelle Salt (Sodium Potassium tartrate NaK(C4H4O6)4H2O) 137
2.7.1 The Rochelle Salt Period 137
2.7.2 Crystal Structure of Rochelle Salt (NaK(C4H4O6)4H2O) 139
2.7.3 Polymorphism of Rochelle Salt 140
2.8 Potassium dihydrogen phosphate (KDP) 142
2.9 Amonium dihydrogen phosphate (ADP) 148

Chapter 3 : Materials and methods 150
3.1 Materials 150
3.2 Apparatus 154
3.3. Computer Software 157
3.4. Methods 158
3.4.1. Sample Preparation 158
3.4.2. Measurement of Dielectric Constant ε 158
3.4.2.1. Measuring principle 158
3.4.3. Measuring procedure 159
3.4.4. Data analyses 160

Chapter 4: Results and discussions 161
4.1 Investigation of ferroelectric activity in pure Seignette Salt and its binary and ternary mixtures of H2O and H2O/Dioxane in different temperatures 161
4.1.1 Influence of temperature on Pure Seignette Salt, Pure Water and Pure Dioxan 162
4.1.1.1 Pure Seignette Salt, Melted measurement 162
4.1.1.2 Pure Seignette Salt Relative measurement 163
4.1.2 Pure Water 165
4.1.3 Pure 1,4-Dioxane 168
4.1.4 Influence of the volume fraction on the ferroelectric properties of the Seignette Salt-Water solutions 169
4.1.5 Influence of the temperature on the ferroelectric properties of the Seignette salt-Water solutions 173
4.1.6 Ternary Seignette Salt-Water-1,4-Dioxane solutions 176
4.1.6.1 Water-1,4-Dioxane solutions 177
4.1.6.2 1,4-Dioxane-Seignette salt solutions 179
4.1.6.3 Ternary Seignette salt-Water-1,4-Dioxane solutions 180
4.1.7 Relaxation behavior of pure Seignette salt and the binary mixtures of Seignette salt / H2O 184

4.2 Discussion 190
4.2.1 Investigation of ferroelectric activity in KDP/water binary mixtures using dielectric spectriscopy at temperature range between 10 and 70 192
4.2.2 Influence of the volume fraction on the dielectric properties of the KDP/water solutions 192
4.2.3 Influence of the temperature on the dielectric properties of the KDP/water solutions 200
4.2.4 Relaxation behavior of KDP/water solutions 205
4.2.5 Discussion 210
4.3 Investigation of ferroelectric activity in ADP/water binary mixtures using dielectric spectriscopy at temperature range between 10 and 70 212
4.3.1 Influence of the volume fraction on the dielectric properties of the ADP/water solutions 212
4.3.2 Influence of the temperature on the dielectric properties of the ADP/water solutions 221
4.3.3 Relaxation behavior of ADP/water solutions 227
4.3.4 Discussion 232
4.4 Conclusions 233

References **235**

Part C : Paraffin-based derivatives

"Effect of peg number on dielectric properties of paraffin base-peg polymers at microwave frequencies" **237**
Abstract 237
Introduction 237
Experimental method 238
Results 239
Discussion 240
Conclusions 244
References 244

"Cole-Cole plot analysis of dielectric behavior of paraffin labeled with different PEG-chains" **246**
Abstract 246
1. Introductions 247
2. Definitions and theoretical background of Cole-Cole plot 247
3. Experimental Method 249
3.1 Materials 249
3.2 Equipments for Dielectric Measurement 249
3.3 Method 251
3.4 Melting point measurement 251
4. Results 251
5. Discussion 254
5.1 Linear region of Cole-Cole plot 254
5.2 Circular region of Cole-Cole plot 256
5.3 Transition from circular to linear curve 257
6. Conclusion 258
Acknowledgement 259
References 259

Appendix **260**

Symbols and Abbreviations

Latin symbols

A	area [m^2]
A*	apparatus specific constant of density meter
B*	apparatus specific constant of density meter
B	susceptance, imaginary part of admittance [S]
C	capacitance [F]
c	cohesive energy density [$Jmol^{-1}$]
C_0, C_{vacuum}	capacitance of the condenser in vacuum [F]
C_{mut}	capacitance of material under test [F]
D_{OH}	density of OH-groups per volume [cm^{-3}]
$D_{\mu\mu}$	density of the square of the dipole moment per molar volume [D^2molcm^{-3}]
E	electric field [Vm^{-1}]
E_e	external electric field [Vm^{-1}]
E_i	internal electric field [Vm^{-1}]
E_L	Lorenz-field
E_{local}	local electric field [Vm^{-1}]
E_{sph}	electric field caused by induced dipoles outside the sphere, causing charges on the surface
E_T, $E_T(30)$	Dirmroth-Reichardt parameter [$Kcalmol^{-1}$]
E_T^N	normalized values of the Dirmroth-Reichardt parameter
G	conductance [$S=\Omega^{-1}$]
g	Kirkwood-Fröhlich correlation factor
ΔH	molar vaporization enthalpy [$Jmol^{-1}$]
i	imaginary unit $(-1)^{1/2}$
I	weight factor of the relaxation time
k	Boltzmann constant = $1.38 \cdot 10^{-23}$ [JK^{-1}]
K	Cell constant [m^{-1}]
L	Inductance [H]
$\lvert m \rvert$	slope of the linear regression $(E_i/E) = f(1/T)$
b	interception of the linear regression $(E_i/E) = f(1/T)$

M_r	molecular weight [$gmol^{-1}$]
$M_{r,m}$	molecular weight of the mixture [$gmol^{-1}$]
N	number of the molecules per volume [m^{-3}]
n	refractive index
N_A	Avogadro constant = $6.02 \cdot 10^{23}$ [mol^{-1}]
P_{atm}	atmospheric pressure [Torr]
p	occupation probability
p_c	percolation threshold
P	polarization [Cm^{-2}]
P_M	molar polarization [$Cmol^{-1}$]
Q	total electric charge
q	critical exponent
q	charge
R	resistance [Ω]
R	gas constant [8.314 $Jmol^{-1}K^{-1}$]
R*	resistance of the standard [Ω]
r	distance
S	scale/proportionality factor
STDEV	standard deviation
T	temperature [K]
T*	oscillation period of the sample-filled U-tube [s]
T	transmittance
V_1	volume fraction of liquid 1
V_2	volume fraction of liquid 2
V_A/V	volume fraction of A in A+B
V_m	molar volume [m^3mol^{-1}]
V	potential difference between the plates
X	reactance, imaginary part of impedance [Ω]
Y	admittance, Y = G+iB [s]
Z	impedance, Z = R+iX [s]

Greek symbols

α	angle of incidence
α	polarizability [C m^2V^{-1}]

β	Cole-Davidson parameter for asymmetric distribution of relaxation times
β	angle of refraction
Γ	reflection coefficient
δ	phase of admittance, dielectric loss angle; tan $\delta = \frac{\varepsilon''}{\varepsilon'}$
$\delta+$, $\delta-$	charge of the dipole
ε_{exp}	experimentally obtained permittivity values
ε_{lit}	permittivity values in literature
ε_m	measured quasi-static dielectric constant for the mixtures
ε, ε_{stat}, ε_{rel}	static permittivity; relative permittivity or dielectric constant
ε_0	electric field constant in vacuum = $8.85410 \cdot 10^{-12}$ [$C^2\ J^{-1}m^{-1}$]
ε_∞	dielectric constant characteristic for induced polarization, measured at a frequency low enough that both atomic and electronic polarization are the same as in static electric field and high enough so that the permanent dipoles can no longer follow the field
ε^*	complex permittivity
ε'	real part of complex permittivity
ε''	imaginary part of complex permittivity
μ	permanent dipole moment [Cm]
μ_g	permanent dipole moment in the gas phase [Cm]
	1 Debye = $3.33564 \cdot 10^{-30}$ Cm
μ_i	induced dipole moment [Cm]
μ^*	complex permeability
ν	frequency [s^{-1}]
ρ	density [kgm^{-3}]
ρ_m	density of the mixture [kgm^{-3}]
σ	specific conductivity [Sm^{-1}]
τ	dielectric relaxation time [s]
τ_0	main dielectric relaxation time [s]
θ	phase of impedance
ω	angular frequency [s^{-1}]
ω_{res}	resonance frequency [s^{-1}]

Summary

Water properties are the subject of investigations in physics, chemistry, biology and different applied fields of natural science.

Liquid dosage forms, generally based on aqueous solutions, take an important role in drug administration e.g. as parenteral preparations, ophthalmic formulations or as oral solutions for children and elderly patients. Sufficient drug solubility in water is a prerequisite for orally administrated solid dosage forms such as tablets, capsules, etc. to show a sufficient bioavailability. The solubility of a drug is determined by intermolecular forces. While these can be reasonably well characterized in gaseous and solid material, no satisfying description has yet been found for liquid systems, especially for nonideal solutions. The presence of several types of intermolecular interactions let water show rather a complex associated structure due to which it has a number of its abnormal properties.

In part A of this work, the intermolecular forces in pure solvents and binary mixtures at 298.2 K (25°C) are investigated, using quasistatic low-frequency and AC high-frequency broadband (0.2-20 GHz) dielectric spectroscopy.

The data were interpreted using for the low frequency measurements the modified Clausius-Mossotti-Debye equation according to Leuenberger and Kirkwood-Fröhlich equation. For the description of the dielectric relaxation in the high frequency range there are different models available which describe the relaxation behaviour of a polar liquid. The most simple equation is the Debye equation, which will be described and will be compared with the other models in the theory chapter. It has to be kept in mind that the resulting relaxation times (τ) depend on the mathematical model applied. If the mean corrected R^2 coefficient does not differ significantly for the mathematical models used, it is not possible to make an unambiguous choice of model.

In part A of this work, we collect a wide study of percolation phenomena in DMSO and its analogues (DMAC, DMF & NMP) in binary mixtures with water, to investigate any similarity in their behaviour. In addition, we investigated these solvents in 1,4-

dioxane binary mixtures to study their behaviour in a nonpolar environment. Furthermore, we studied Formamide and its mono and dimethylated form in binary mixtures with water to investigate the effect of adding a methyl group to a molecular structure using percolation phenomena.

In pharmaceutical science the polymorphism of the Active Pharmaceutical Ingredients (APIs) is of an important interest. More than 50% of all APIs show polymorphism. However, it is very difficult to predict in which condition, which type of polymorph is formed. In part B of this work we try to detect pre-formation of crystalline order in the liquid and to investigate the different polymorphism during this process at different temperature and different concentrations.

As a model compound, Seignette salt was chosen due to its ferroelectric activity and high solubility in water. The binary mixtures of Salt-water and ternary mixtures of Salt-water-1,4-dioxane were the subject of the investigation. The relaxation behaviour of these mixtures was studied using Debye model and percolation phenomena. Furthermore, any sudden increase or decrease in their complex permittivity (real and imaginary part) was studied at temperatures between 10-70°C and at different concentration from low salt content to saturated and supersaturated solutions.

To have a broader investigation, aqueous binary mixtures of KDP and ADP which both posses a ferroelectric activity with high water solubility were studied.

Part C of this work is collaboration with “Swiss Federal Institute for Materials Science & Technology Research and Testing, EMPA”. Paraffin based PEG derivatives were the subject of the investigation. These labeled polymers with different PEG number were studied to find which one is more appropriate to use as a binder in ceramic production. Dipolar losses in the microwave range are used in modern technology for accelerating thermal processing of polymers (tempering, curing etc...). In the other hand, the importance of removing binders in pharmaceutical and material science is well known.

The results of this part will be presented in “International symposium HES-07, Padua, Italy” on June 2007 with the title of “Effect of PEG Derivative Number on Dielectric

Properties of Paraffin Based-PEG Polymers at Microwave Frequencies". In addition, "The Cole-Cole plot analysis of dielectric behavior of paraffin labeled with different PEG-chains" has been submitted to the Polymer International, Journal (www3.interscience.wiley.com) on 16.05.2007.

Part A:

Binary polar solvent mixtures

Chapter 1

Introduction

Life as we know could not exist without water. Nearly 70% of the human body is composed of this unique liquid, which beyond all doubt does not merely serve as filling material between other molecules. Aqueous solutions constitute the reaction medium for chemical processes occurring in biological systems and water is clearly involved in determination of structural and functional properties of macromolecules.

In drug administration, liquid dosage forms play an important role, e.g. as oral solutions for children and elderly patients, ophthalmic formulations, injectible drug preparations, etc. So far, the predictability of drug solubility is only of qualitative nature. A simple and fast method for determining the solubility and miscibility behavior of solvents and solvent mixtures would be an important contribution to a more rational development of robust liquid drug formulations, which could also shorten the time-to-market.

The solubility and miscibility are determined by intermolecular forces. While these can be reasonably well characterized in gaseous and solid material, no satisfying description has yet been found for liquid systems, especially for nonideal solutions.

At present, neither the theory nor the applications of dielectric analysis are widely known within the pharmaceutical sciences. Dielectric spectroscopy involves the study of the response of a material to an applied field. By appropriate interpretation of the data, it is possible to obtain information on the structural properties of the sample through its electrical properties.

In this work, the intermolecular forces in pure solvents and binary mixtures are investigated. For this, the material is examined using quasistatic low-frequency and AC high-frequency dielectric spectroscopy, in addition, the density and refractive indices are determined.
The Debye -equation, which describes well the behavior in quasistatic electric fields of nonpolar gaseous and liquid material, and polar molecules in the gas phase, was modified in the work of Rey (1998; see also Stengele et al., 2001). The reintroduction of the internal electric field *Ei* allowed a description of close interaction forces and thus the application of the Debye -equation to polar, hydrogen-bonding liquids.

In this work, aqueous binary mixtures and pure liquids of pharmaceutical and/or theoretical interest are investigated at room temperature (298.2K). The values for E_i/E, the relation between the internal and the external electric field, are compared to other parameters describing the system, such as the Kirkwood-Fröhlich correlation factor *g,* the dielectric relaxation behavior, or the partial molar volume for liquid mixtures.

The Kirkwood-Fröhlich correlation factor *g* ([Fröhlich, 1958], [Kirkwood, 1939]) is well-established parameter describing the alignment of molecules. The drawbacks are that it can only be applied to polar molecules and that the results are of ambiguous nature.

The behavior of molecules in a high frequency AC field gives us information about the dynamics in a liquid, about the mobility of molecules and molecular units in the liquid.

These various parameters lead to an overall picture of the properties of the investigated materials, which may help us to derive information about the macrostructures of the investigated liquids, and about the influence of structural changes, such as the modification of a side chain.

The applicability of percolation theory, a method of statistical physics to describe for example cluster formation, critical phenomena, and diffusion, to liquid mixtures is a key element for the interpretation of the results obtained.

Percolation theory predicts that the behavior of a system changes not linearly as a function of e.g. the volume fraction of water but that at certain critical volume fractions, major changes occur influencing the properties of the system. The results obtained by Rey (1998) showed that not for all investigated systems and parameters critical volume fractions could be detected. This could mean that the sensibility of the parameters in regard to the structural changes may vary; this aspect is also part of the investigation.

The data in this work were interpreted using for the low frequency measurements the modified Clausius-Mossotti-Debye equation according to Leuenberger and the Kirkwood-Frohlich equation. For the description of the dielectric relaxation in the high frequency range there are different mathematical models available which describe the relaxation behavior of a polar liquid. The most simple equation is the Debye equation, which will be described in the chapter of theory. To fit the ε', ε"- data in a best way it is also possible to use the Cole-Davidson distribution function or superposition of the Debye function with the Cole-Davidson function. It has to be kept in mind that the resulting relaxation times (τ) depend on the mathematical model applied. If the mean corrected R^2 coefficient does not differ significantly for the mathematical models used, it is not possible to make an unambiguous choice of model. The goal is to use the model with an adequate corrected R^2 and with the lower number of parameters to be adjusted.

In the two papers (Stengele et al., 2001; Stengele et al., 2002) it was shown, that the Clausius-Mossotti-Debye equation for the quasi-static dielectric constant (ε) could be extended to liquids if the parameter E_i/E is introduced. E_i corresponds to the local mean field due to close molecule-molecule interactions after the application of an external electric field E.

Chapter 2

Theory

2.1 Water

Life as known on earth would not be possible if the physical properties of water were different.

Water is a tasteless, odorless substance that is essential to all known forms of life and is known as the *universal solvent*. It appears mostly in the oceans (saltwater) and polar ice caps, but also as clouds, rain water, rivers, freshwater aquifers, lakes, and sea ice. Water in these bodies continuously moves through a cycle of evaporation, precipitation, and runoff to the sea. Clean water is essential to human health.

Thales of Miletus, an early Greek philosopher, known for his analysis of the scope and nature of the term "landscaping", believed that "all is water."

Liquid dosage forms, generally based on aqueous solutions, take an important role in drug administration e.g. as parenteral preparations, ophthalmic formulations or as oral solutions for children and elderly patients. A sufficient drug solubility in water is a prerequisite for orally administrated solid dosage forms such as tablets, capsules, etc. to show a sufficient bioavailability. The solubility of a drug is determined by intermolecular forces. While these can be reasonably well characterized in gaseous and solid material, no satisfying description has yet been found for liquids systems, especially for non ideal solutions. The presence of several types of intermolecular interactions let the water show rather a complex associated structure due to which it has a number of its abnormal properties *(Hernandez, 2004)*.

2.1.1 Molecule

The water molecule, H_2O, shows, C_{2v} symmetry, both protons being equivalent. The dipole moment vector bisects H-O-H angle. It points form the negative oxygen atom to the positive region between the hydrogen atoms. The OH bond lengths are 0.9584Å, and H-O-H bond angle 104.45°; these free-molecule values are not obtained in the liquid. The dipole moments is 1.8546± 0.0004 D *(Buckingam, 1986)*.

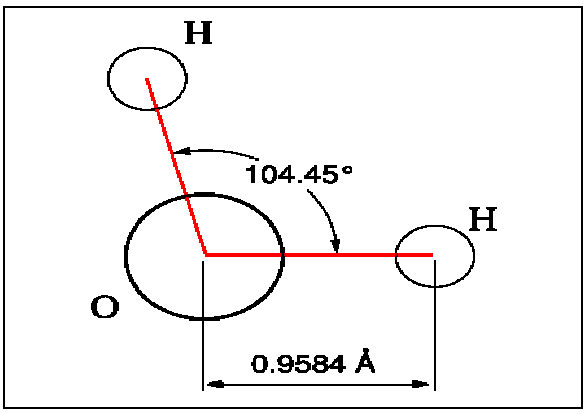

Fig. 2.1. Water molecule dimensions

Two atoms, connected by a covalent bond, may exert different attractions for the electrons of the bond. In such cases the bond is polar, with one end slightly negatively charged (-) and the other slightly positively charged (+).

The water molecule has an neutral charge, but the electrons are asymmetrically distributed. The oxygen nucleus draws electrons away from the hydrogen nuclei, leaving these nuclei with a small net positive charge. The excess of electron density on the oxygen atom creates weakly negative regions at the other two corners of an imaginary tetrahedron. Fig. 2.2.

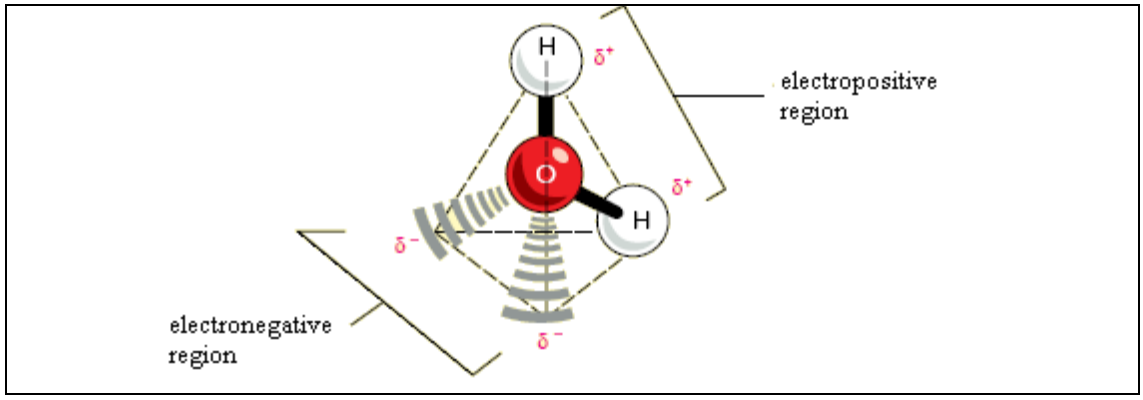

Fig. 2.2. Electric dipole of the molecule of water.

2.1.2 Hydrogen bonding network in water clusters

Clusters of water molecules are held together by hydrogen bonding networks. These networks are differentiated by the participation of the individual water molecules in the hydrogen bonds either as proton donors (d), proton acceptors (a), or their combinations. These hydrogen bonds represent an intermediate case between the weakly bonded Van der Waals systems (~0.3kcal/mol) and those held together by strong covalent forces (~100kcal/mol) *(Vegiri et al., 1993)*.

The cohesive nature of water is responsible for many of its unusual properties, such as high surface tension, specific heat, and heat of vaporization.

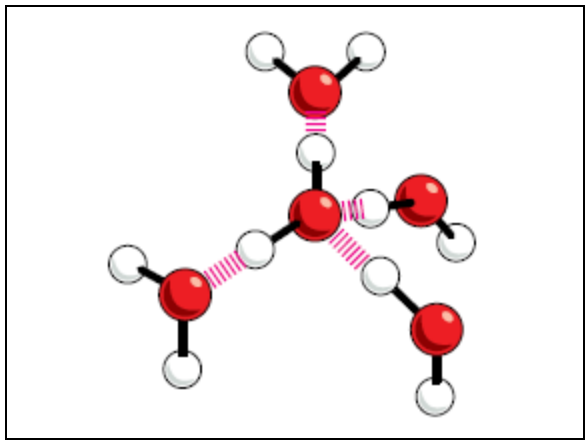

Fig. 2.1. Water structure

Small clusters of water molecules can be considered as prototypes for understanding the fundamental interactions that govern hydrogen bonding. The vibration-rotation-tunneling (VRT) microwave experiments of Saykally and co-workers have confirmed earlier theoretical predictions suggesting that the global minima of the trimer through pentamer clusters have “ring” structures. For the water hexamer in isolated or the presence of benzol in the gas phase, the experimentally obtained global minimum were best fit by a cage rather than a ring structure resembling the basic structure of an ice-modification with a higher density. However, in a nitrogen containing organic compound, monocyclic chair-conformation water hexamer has been identified *(Xantheas, 2000), (Ugalde et al., 2000)*.

2.1.3 Physical properties of water

Water is not a simple liquid, being better known for its anomalous behavior than for its ordinary liquid state properties. The presence of hydrogen bonds together with the tetrahedric coordination of the molecule of water constitutes the key to explain its unusual properties.

Property	
Molecular weight [g/mol]	18.0151
Melting point [°C]	0.00
Boiling point [°C]	100.00
Temperature of maximum density [°C]	3.984
Maximum density [g/cm^3]	1.0000
Density at 25°C [g/cm^3]	0.99701
Density at 100°C [g/cm^3]	0.958
Density of ice at 0°C [g/cm^3]	0.9168
Vapor pressure [mmHg]	23.75
Dielectric constant ε	78.39
Electric conductivity [ohm^{-1} cm^{-1}]	5.7x10^{-8}
Heat capacity [J(molK)$^{-1}$]	75.2
Surface tension [mJm^{-2}]	72
Viscosity [Poise=10^{-1}kgm^{-1}s^{-1}]	0.01

Table 2.1.Some physical properties of water at 25°C unless otherwise stated.

For example, water is almost unique among the more than 15 million known chemical substances in that its solid form is less dense that the liquid. Fig. 2.4 shows how the volume of water varies with the temperature; the large increase (about 9%) on freezing shows why ice floats on water and why pipes burst when they freeze. The expansion between 4°C and 0°C is due to the formation of larger clusters. Above 4°C, thermal expansion sets is as thermal vibrations of the O-H bonds becomes vigorous, tending to shove the molecules apart more *(Lower, 2001)*.

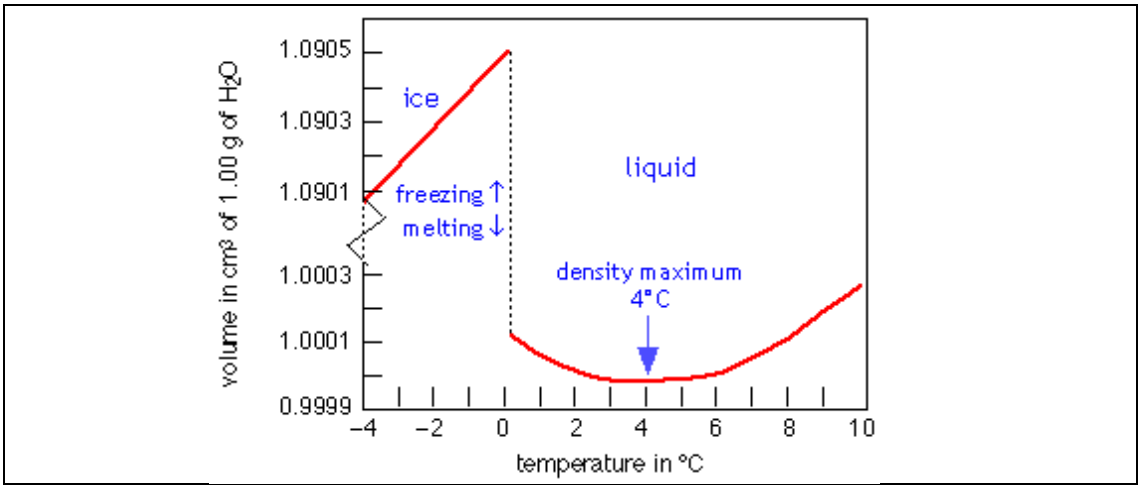

Fig. 2.3. Volume of water as a function of the temperature *(Lower, 2001)*.

The boiling point of water is other anomalous property of water. Fig. 2.5 shows that over 150 K higher than expected by extrapolation of the boiling points of other Group A hydrides, here shown compared with Group B hydrides. It is also much higher than O_2 (90 K) or H_2 (20 K). See also below for further comparisons.

There is considerable hydrogen bonding in liquid water resulting in high cohesion (water's cohesive energy density is 2.6 times that of methanol), which prevents water molecules from being easily released from the water's surface. Consequentially, the vapor pressure is reduced. As boiling cannot occur until this vapor pressure equals the external pressure, a higher temperature is required. The pressure/temperature range of liquidity for water is much larger

than for most other materials (*e.g.* under ambient pressure the liquid range of water is 100°C whereas for both H_2S and H_2Se it is about 25°C) *(Lower, 2001)*.

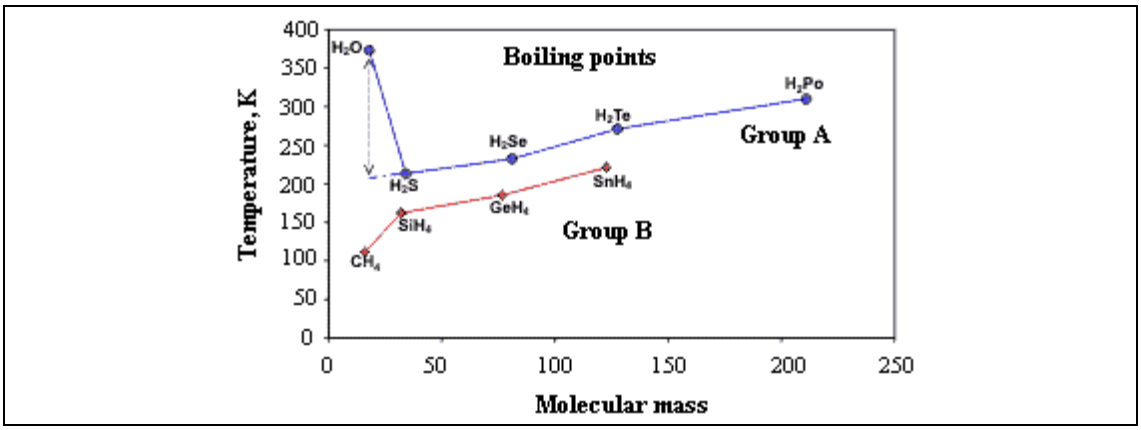

Fig. 2.4. Influence of H-bonding on the boiling point.

2.1.4 Structural differences between a solid, liquid and gas

The single combination of pressure and temperature at which water, ice, and water vapour can coexist in a stable equilibrium occurs at exactly 273.16 kelvins (0.01 °C) and a pressure of 611.73 pascals (ca. 6 millibars, .006037 Atm). At that point, it is possible to change all of the substance to ice, water, or vapour by making infinitesimally small changes in pressure and temperature. (Note that the pressure referred to here is the vapor pressure of the substance, not the total pressure of the entire system.

Water has an unusual and complex phase diagram, although this does not affect general comments about the triple point. At high temperatures, increasing pressure results in first liquid, and then solid water (above around 10^9 Pa a crystalline form of ice which is denser than water forms). At lower temperatures the liquid state ceases to appear with compression causing the state to pass directly from gas to solid.

At a constant pressure higher than the triple point, heating ice necessarily passes from ice to liquid then to steam. In pressures below the triple point, such

as in outer space where the pressure is low, liquid water cannot exist: Ice skips the liquid stage and becomes steam on heating, in a process known as sublimation.

Triple point cells are useful in the calibration of thermometers. For exacting work, triple point cells are typically filled with a highly pure chemical substance such as hydrogen, argon, mercury, or water (depending on the desired temperature). The purity of these substances can be such that only one part in a million is a contaminant; what is called “six-nines" because it is 99.9999% pure. When it is a water-based cell, a special isotopic composition called VSMOW water is used because it is considered to be representative of “average ocean water” and produces temperatures that are more comparable from lab to lab. Triple point cells are so effective at achieving highly precise, reproducible temperatures, an international calibration standard for thermometers called ITS–90 upon triple point cells for delineating six of its defined temperature points.

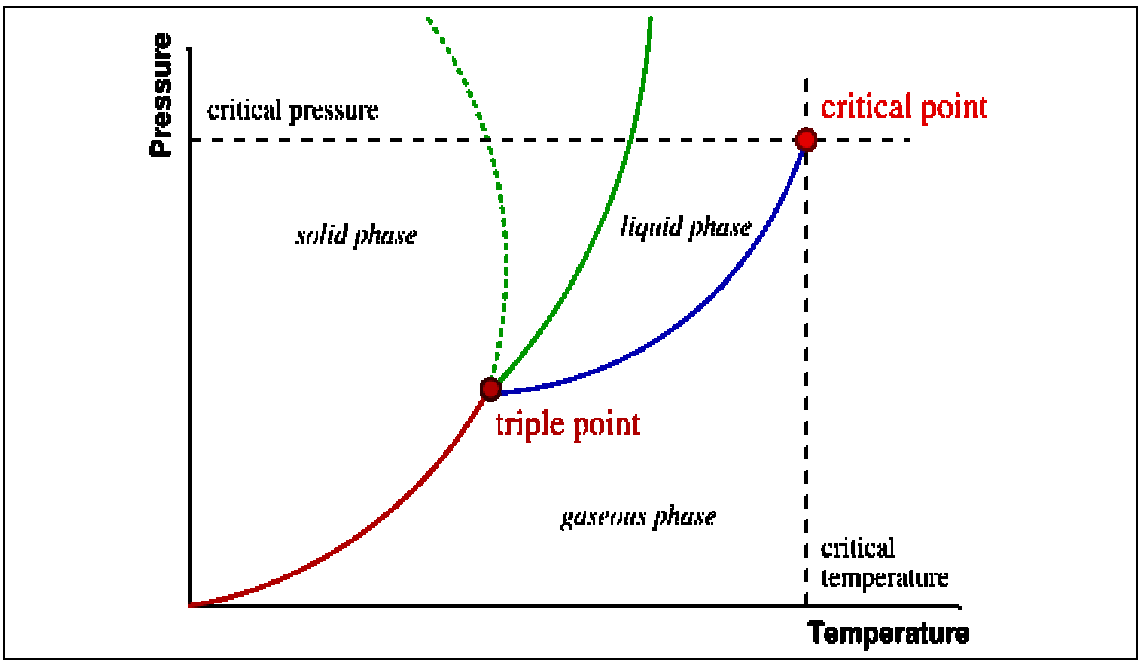

Fig. 2.5. Triple point of the water.

2.1.5 Water clusters, structured water and biowater

Since the 1930s, chemists have described water as an "associated" liquid, meaning that hydrogen-bonding attractions between H2O create loosely-linked aggregates. Because the strength of a hydrogen bond is comparable to the average thermal energy at ordinary temperatures, these bonds are disrupted by thermal motions almost as quickly as they form. Theoretical studies have shown that certain specific cyclic arrangements ("clusters") of 3, 4, and 5 H2O molecules are especially stable, as is a three-dimensional hexamer (6 molecules) that has a cage-like form. But even the most stable of these clusters will flicker out of existence after only about 10 picoseconds. It must be emphasized that no clustered unit or arrangement has ever been isolated or identified in pure liquid water (see Fig. 2.7).

2.1.5.1 So-called “structured water”

Water molecules interact strongly with non-hydrogen bonding species as well .A particularly strong interaction occurs when an ionic substance such as sodium chloride (ordinary salt) dissolves in water. Owing to its high polarity, the H2O molecules closest to the dissolved ion are strongly attached to it, forming what is known as the primary hydration shell. Positively charged ions such as Na + attract the negative (oxygen) ends of the H2O molecules, as shown in Fig. 2.8. The ordered structure within the primary shell creates, through hydrogen bonding, a region in which the surrounding waters are also somewhat ordered; this is the outer hydration shell, or cybotactic region.

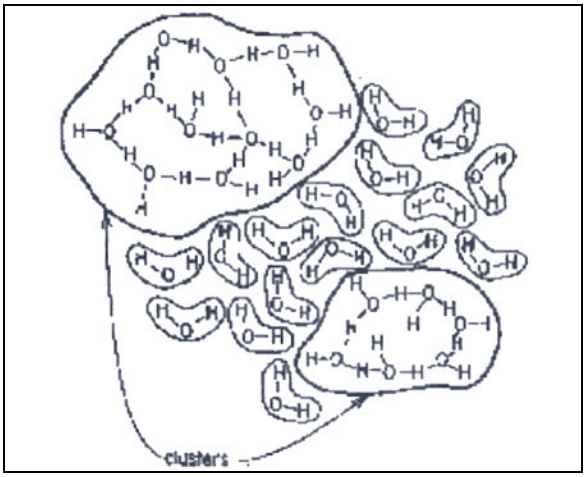

Figure 2. 7 Liquid water can be thought of as a seething mass of water molecules in which hydrogen-bonded clusters are continually forming, breaking apart, and re-forming. Theoretical models suggest that the average cluster may encompass as many as 90 HzO molecules at 0°C, so that very cold water can be thought of as a collection of ever-changing ice-like structures. At 70C, the average cluster size is probably no greater than about 25 *(Lower, 2001)*.

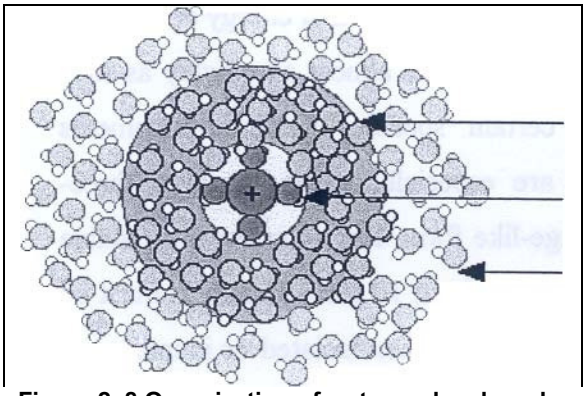

Outer hydration shell (cybotactic region, semi-ordered)
Inner hydration shell (chemisorbed and ordered water)
Bulk water (random arrangement)

Figure 2. 8 Organization of water molecules when an ionic substance such as sodium chloride (ordinary salt) is dissolved *(Lower, 2001).*

2.1.5.1 Biowater

Water can hydrogen-bond not only to itself, but also to any other molecules that have - OH or -NH2 units hanging off of them. This includes simple molecules such as alcohols, surfaces such as glass, and macromolecules such as proteins. The biological activity of proteins (of which enzymes are an important subset) is critically dependent not only on their composition but also on the way these huge molecules are folded; this folding involves hydrogen-bonded interactions with water, and also between different parts of the molecule itself Anything that disrupts these intramolecular hydrogen bonds will denature the protein and destroy its biological activity. This is essentially what happens when you boil an egg; the bonds that hold the egg white protein in its compact folded arrangement break apart so that the molecules unfold into a tangled, insoluble

mass which, be cannot be restored to their original forms. Note that hydrogen-bonding need not always involve water; thus the two parts of the DNA double helix are held together by H-N-H hydrogen bonds.

It is now known that the intracellular water very close to any membrane or organelle (sometimes called *vicinal water)* is organized very differently from bulk water, and that this structured water plays a significant role in governing the shape (and thus biological activity) of large folded biopolymers. It is important to bear in mind, however, that the structure of the water in these regions is imposed solely by the geometry of the surrounding hydrogen bonding sites.

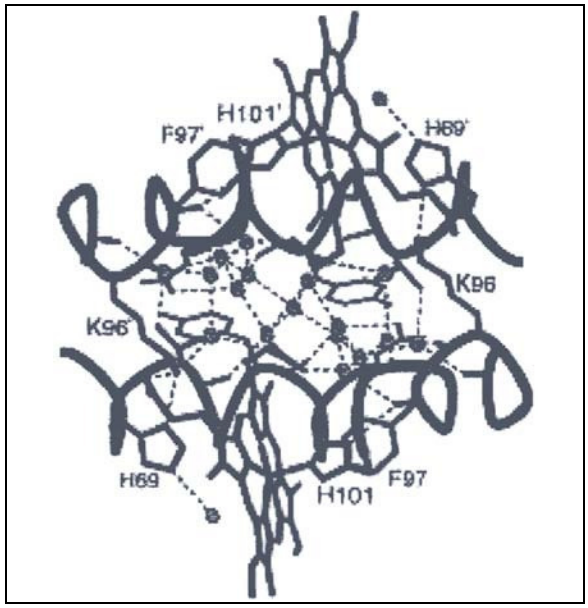

Figure 2. 9 This picture, taken from the work of William Royer Jr. of the U. Mass. Medical School, shows the water structure (small green circles) that exists in the space between the two halves of a kind of dimeric hemoglobin. The thin dotted lines represent hydrogen bonds. Owing to the geometry of the hydrogen-bonding sites on the heme protein backbones, the H2O molecules within this region are highly ordered; the local water structure is stabilized by these hydrogen bonds, and the resulting water cluster in turn stabilizes this particular geometric form of the hemoglobin dimer. *(Lower,2001)*

2.2 Dielectric spectroscopy

Dielectric spectroscopy involves the study or response of material to an applied electric field. By appropriate interpretarion of the data, it is possible to obtain structural information on a range of samples using this technique. While the use of dielectric spectroscopy technique has previously been largely confined to the field of physics, the generality of dielectric behavior has led to the technique being used in more diverse fields such as colloid science, polymer sience and, more recently, the pharmaceutical sciences *(Craig,1995)*.

Most pharmaceutical systems may be described as dielectrics, which contain dipoles. In principle, therefore the majority of such materials may be studied using this technique.

The use of the information obtained may be broadly divided into two categories:

1. Dielectric data may be used as fingerprint with which to compare samples prepared under different conditions; this therefore has implications for the use of dielectric spectroscopy as a quality control.
2. Each spectrum may be interpreted in terms of the structure and behavior of the sample, therefore leading to more specific information in the sample under study.

Both approaches are useful and obviously require different levels of understanding regarding the theory the technique.

As with any technique, there are associated advantages and disadvantages.

The advantages are:

- The sample preparation is generally very simple.
- Samples with a range of sizes and shapes may therefore studied; solid compacts, powders, gels or liquids may be esily measured.
- The method and conditions of measurement may be varied. For example, the sample may be examined under a range of tempeeratures, humidities, pressures, etc. *(Craig,1995)*.

The principal disadvantages of the technique with respect to pharmaceutical uses are

1. Not all samples may be usefully analyzed, a fault which is common to all analytincal methods.

2. The second disadvantage lies with the general inaccessibility of the dielectrics literature to pharmaceutical sciences. This has arisen largely for historical reasons, as most of the dielectric literature has been written on the (hitherto) reasonable assumption that any reader interested in the subject will already have a prior knowledge of dielectrics (or at least physics) *(Craig, 1995)*.

2.3 Properties of isolating material in electric fields

2.3.1 Permanent and induced electric dipole moments

A polar molecule is a molecule with a permanent electric dipole moment that arises from the partial change on atoms linked by polar bonds. Non-polar molecules may acquier a dipole moment in an electric field o acccount of the distortion the field causes in their electronic distributions and nuclear positions. Similarly, polar molecules may have their existing dipole moments modified by the applied field.

Permanent and induced dipole moments are important in chemistry through their role in intermolecular forces and their contribution to he ability of a substance to act as a solvent for ionic solids. The latter ability stems from the fact that one end of a dipole may be coulombically attracted to an ion of opposite charge and hence contribute an exothermic to the enthalpy of solution.

The average electric dipole moment per unit volume of a sample is called its polarization (P).

The polarization of a fluid sample is zero in the absence of an applied field because the molecules adopt random orientations and the average dipole moment is zero. In the presence of a field the dipoles are partially aligned and there is an additional contribution from the dipole moment induced by the field.

Hence, the polarization of a medium in the presence of an applied field is non-zero (see Fig. 2.10).

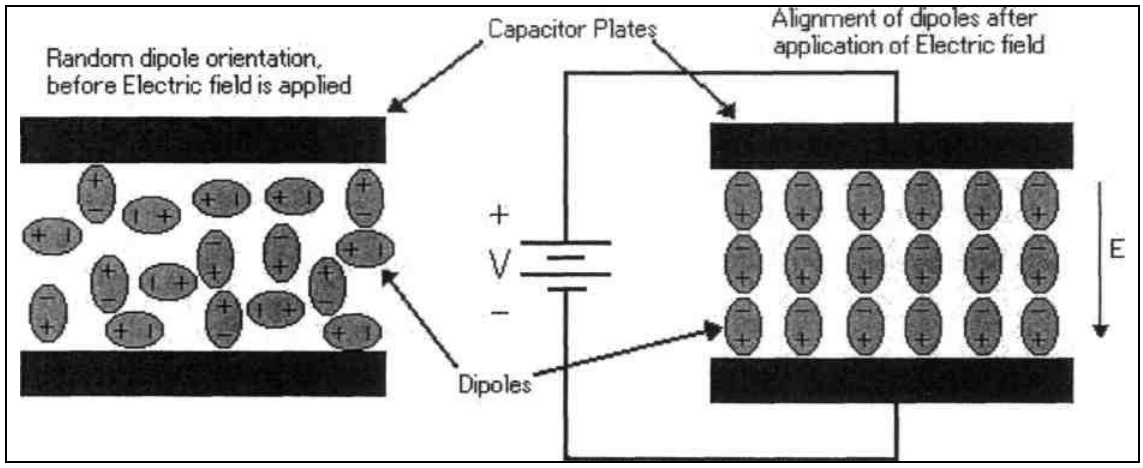

Fig. 2.10. Orientation of dipole moments.

2.3.2 Dielectric constant

The dielectric constant or permittivity of a material is a measure of the extent to which the electric charge distribution in the material can be distorted or "polarized" by the application of an electric field. The individual charges do not travel continuously for relatively large distances, as in the case in electrical conduction by transport. But there is nevertheless a flow of charge in the polarization process, for example, by the rotation of polar molecules, which tend to line up in the direction of the field.

The total electric charge (Q) of two parallel plates of a condenser at equilibrium is proportional to the potential difference (V) between the plates. The capacitance (C) is the proportionality factor between these values.

$$Q = C \times V \tag{2.1}$$

The capacitance of a condenser depends on its geometry and the medium between the plates.

As a standard, the capacitance of a condenser in vacuum is used.

$$C_0 = \frac{\varepsilon_0 \cdot A}{r} \qquad (2.2)$$

C_0 = capacitance of the condenser in vacuum
ε_0 = electric field constant in vacuum = $8.854 \cdot 10^{-12}$ [C^2 /Jm]
A = surface area of each plate
r = distance between parallel plates

The relationship between capacitance (C) in the dielectric to capacitance in vacuum (C_0) is described as dielectric constant *(ε_{rel})*.

$$\varepsilon_{rel} = \frac{C}{C_0} \qquad (2.3)$$

The dielectric constant ($\varepsilon_{re/}$) is dimensionless, substance-specific and equals to one for vacuum according to its definition.

The electric charge of a dielectric in a condenser is polarized by the electric field. The electric field causes the charges to shift in the direction of the field. When the applied field changes direction periodically, the permanent dipole moments reorientate and follow the field. The electric field can also induce dipole in a system, which is actually dipole-free.

The dielectric constant is dependent on the polarizability of the dielectric. As the polarizability increases, the dielectric constant increases with it.

The dielectric constant is also frequency dependent. Dielectric constant measured at low frequencies is called static permittivity, at high frequencies complex permittivity. Depending on the frequency, different polarization types of the dielectric can be observed.

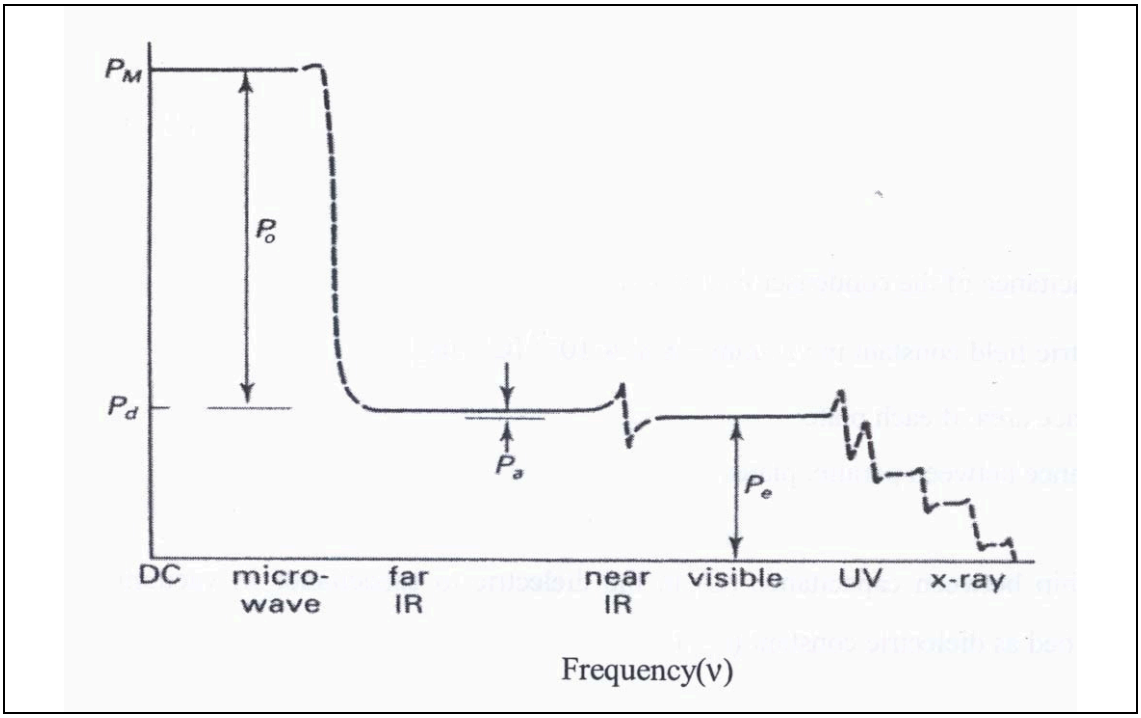

Fig. 2.11. Frequency dependence of the molar polarisation of permanent dipoles. (Shoemaker et al., 1989) where PM = molar polarization; P0 = orientational polarization; Pa = atomic polarization; Pe = electronic polarization; Pd = distortion polarization.

The total polarization is measured on static conditions (alternating current at low frequencies). The static electric constant is also called static permittivity (ε_{stat}) or relative permittivity (ε_{rel}).

$$\varepsilon = \varepsilon_{real} = \varepsilon_{stat} = \frac{C}{C_0} \qquad (2.4)$$

In this work, static dielectric constant (ε_{stat}) will be abbreviated as (ε).

(Alonso et al., 1992), (Shoemaker et al., 1989)

2.3.3 The Clausius-Mossotti and Debye equations and their modification according to Leuenberger

Pure pharmaceutical solvents, for example water and ethanol, are dielectrics, i.e. insulating materials. Every kind of insulation material consists at an atomic level of negative and positive charges balancing each other in microscopic as well as in more macroscopic scales. Macroscopically, some localized space charge may be present, but even then an overall charge neutrality exists.

As soon as the material is exposed to an electric field (as generated by a voltage across electrodes between which the dielectric is embedded), very different kinds of dipoles become excited even within atomic scales. A local charge imbalance is thus "induced" within the neutral species (atoms or molecules) as the "centers of gravity" for the equal amount of positive and negative charges, ± *q,* become separated by a small distance *(d),* thus creating a dipole with a dipole moment, $\mu = q * d$, which is related to the "local" or "microscopic" electric field *(E_{Local})* acting in close vicinity of the species. Thus, the dipole moment can also be written as:

$$\mu = \alpha \cdot E_{Local} \tag{2.5}$$

where α= polarizability [$Cm^2\ V^{-1}$] of the species or material under consideration.

It is necessary to point out that E_{Local} refers to the local field rather than the applied field. This distinction is drawn because the local field will be the vectorial sum of the applied field and the fields generated by the presence of the surrounding charges (i.e. the other dipoles). The question then arises as to how the local field may be related to the applied electric field. One of the earliest approaches involves the general relationship between polarization and the applied electric field strength:

$$P = (\varepsilon - 1) \cdot \varepsilon_0 \cdot E_e \tag{2.6}$$

where P = polarization, dipole density [Cm $^{-2}$], 8 = relative permittivity or dielectric constant and ε_0 = electric field constant in vacuum = 8.85410-12 [C^2 J^{-1} m^{-1}]; E_e = external electric field, produced by the applied voltage *(Craig, 1995)*

The local field was first calculated by Lorenz (1909) by considering all the electric fields influencing the molecule in the cavity:

$$E_{Local} = E_i + E_e - E_{sph} \tag{2.7}$$

E_{Local} = local electric field
E_i = internal electric field, caused by interactions with other induced dipole in the sphere.
E_e = external electric field, produced by the applied voltage.
E_{sph} = electric field caused by the induced dipoles outside the sphere, causing charges on the surface.

In an ideal gas, E_{sph} and E_i are zero. In liquids, neighboring molecules show a polarising effect leading to charges on the sphere's boundary, resulting in

$$E_{sph} = -\frac{P}{3 \cdot \varepsilon_0} \tag{2.8}$$

By combining Eqs. (2.6), (2.7), and (2.8) we obtain for local field:

$$E_{Local} = E_i + E_e \cdot \left(\frac{\varepsilon + 2}{3} \right) \tag{2.9}$$

If $E_i = 0$, E_{Local} is reduced to the Lorenz field (E_L):

$$E_{Local} = E_L = \frac{\varepsilon + 2}{3} \cdot E_e \tag{2.10}$$

According to Clausius and Mossotti we obtain for nonpolar molecules of constant polarization the following relation:

$$P = N \cdot \mu_i \tag{2.11}$$

Where P = polarization, dipole density [Cm^{-2}]; N = number of molecules per volume and μ_i = induced dipole moment.

By combining Eq. (2.5) with (2.11) we get:

$$P = N \cdot \mu_i = N \cdot \alpha \cdot E_{Local} \tag{2.12}$$

Combination of Eq. (2.6), (2.10) and (2.12) lead to the **Clausius-Mossotti equation for nonpolar molecules** (Eq. (2.13) and (2.14))

$$\frac{(\varepsilon - 1)}{(\varepsilon + 2)} = \frac{N \cdot \alpha}{3 \cdot \varepsilon_0} \tag{2.13}$$

Where $N = \frac{N_A}{V_M} = \frac{N_A \cdot \rho}{M_r}$ is the number of polarisable molecules per unit volume.

Therefore, the Eq. (2.13) can be defined as molar polarization P_M (Eq. (2.14))

$$P_M = \frac{\varepsilon - 1}{\varepsilon + 2} \cdot \frac{M_r}{\rho} = \frac{N_A}{3 \cdot \varepsilon_0} \cdot \alpha \tag{2.14}$$

Where P_M = molar polarization [m^3mol^{-1}] and N_A = Avogadro's constant = 6.023×10^{23} [mol^{-1}]

(Clausius, 1879) (Lorenz, 1909) (Mossotti, 1847)

The Clausius-Mossotti equation was extended by Debye to polar molecules:

$$\frac{\varepsilon-1}{\varepsilon+2}\cdot\frac{M_r}{\rho}=\frac{N_A}{3\cdot\varepsilon_0}\cdot\left(\alpha+\frac{\mu_g^2}{3\cdot k\cdot T}\right) \qquad (2.15)$$

With ε = quasi-static relative dielectric constant; M_r = molecular weight; ρ = density; N_A = Avogadro number, $6.023x10^{23}$ (mol^{-1}); ε_0 =electric field constant in the vacuum, $8.854xl0^{-12}$ ($C^2\ J^{-1}\ m^{-1}$); α = polarizability of the molecule ($Cm^2\ V^{-1}$); μ_g = dipole moment in the state of an ideal gas (C m); k = Boltzmann's constant, $1.38xl0^{-23}$ ($J\ K^{-1}$); T = temperature (K).

The Debye equation (Eq. (2.15)) is only valid for gas under low pressure and highly diluted solutions of polar molecules in nonpolar solvents, as dipole-dipole interactions are neglected. Therefore, it is not valid for polar liquids but can be used to estimate quite accurately the dipole moment μ_g of water in a highly diluted solution of water in 1,4-dioxane simulating an ideal gas state condition *(Hedestrand, 1929)*.

(Debye, 1912)(Böttcher, 1973)

The essential point of the original derivation of the Clausius-Mossotti-Debye equation consisted in the fact that the local mean field E_i being the result of short range Van der Waals interactions and of hydrogen bonding of neighboring molecules was neglected. The introduction of the term E_i/E with E = applied external electric field leads to the following modification:

$$\frac{\varepsilon-1}{3\frac{E_i}{E}+(\varepsilon+2)}\cdot\frac{M_r}{\rho}=\frac{N_A}{3\cdot\varepsilon_0}\cdot\left(\alpha+\frac{\mu_g^2}{3\cdot k\cdot T}\right) \qquad (2.16)$$

E_i/E for binary mixtures was calculated according to the following Eq. (2.17)

$$\frac{E_i}{E} = \frac{M_{r,m}}{3 \cdot \rho_m} \cdot \frac{\varepsilon_m - 1}{\frac{N_A}{3 \cdot \varepsilon_0}\left[V_1\left(\alpha_1 + \frac{\mu_{g,1}^2}{3 \cdot K \cdot T}\right) + V_2\left(\alpha_2 + \frac{\mu_{g,2}^2}{3 \cdot k \cdot T}\right)\right]} - \frac{\varepsilon_m + 2}{3} \qquad (2.17)$$

Where ρ_m = density of mixture; $M_{r;m}$ = molecular weight of the mixture; ε_m = measured quasi-static relative dielectric constant for the mixture; V_1 = volume fraction of liquid 1; V_2 = volume fraction of liquid 2.

For calculating the respective contributions of the liquids, their volume contributions are considered. For the description of binary mixtures by means of percolation theory, the volume fractions are used, as they are more meaningful for the characterization of three-dimensional networks than molar fractions.

The **Clausius-Mossotti-Debye equation modified according to Leuenberger** (Stengele et al., 2001) (Eq. (2.16)) can be used to characterize polar liquids. In case of a highly polar liquid such as water the value of E_i/E is -21.0 at room temperature. The parameter E_i/E is temperature dependent and can be modeled as follows:

$$\frac{E_i}{E} = -|m| \cdot \left(\frac{1}{T}\right) + b \qquad (2.18)$$

Interestingly an empirical relationship between | m | and the Hildebrand solubility parameter (δ) could be established (Stengele et al., 2001). This relationship has to be judged with caution as it is often neglected that δ is temperature dependent. The values of δ which are listed in tables such as in the book of Barton (Barton, 1991) are estimated values valid at room temperature. The slope |m| on the other hand is a temperature independent parameter. If the temperature T is kept constant, the parameter (|m| /T) is a constant, too, and the correlation between the Hildebrand solubility parameter (δ) and (|m| /T) is still valid. One can expect that as a consequence the value E_i/E at room temperature may directly yield a good correlation with the total Hildebrand

solubility parameter (δ_t). Thus it should be possible to find an empirical relationship between the values of E_i/E and the total Hildebrand solubility parameter (δ_t) at room temperature. This evaluation as well as the study of the correlation of E_i/E value with the partial Hanson solubility parameters and structural properties of the polar liquid is part of a publication by Hernandez-Perni – Stengele et al. (2005).

(Stengele et al., 2001)

2.3.4 Kirkwood-Fröhlich equation and g-valuse obtained from it (Stengele et al., 2001)

Short-range interactions between dipoles are considered by the Kirkwood-Frohlich Equation (Eq. (2.19)), which was introduced by Kirkwood (Kirkwood, 1939) and further developed by Frölich (Frölich, 1958).

$$\frac{(\varepsilon - \varepsilon_\infty)\cdot(2\cdot\varepsilon + \varepsilon_\infty)}{\varepsilon\cdot(\varepsilon_\infty + 2)^2} = \frac{N_A}{9\cdot\varepsilon_0\cdot k\cdot T}\cdot\frac{\rho}{M}\cdot\mu_g^2\cdot g \qquad (2.19)$$

Where ε, respectively ε_∞ correspond to the is dielectric constant characteristic for induced polarization, measured at a frequency low enough that both atomic and electronic polarization are the same as in the static field respectively high enough so that the permanent dipoles can no longer follow the field; *g* is the correlation factor.

The correlation factor *g* was calculated following the Kirkwood-Frohlich equation for binary mixtures (Hasted, 1973), using the volume fractions for calculations instead of molar fractions, so that the results are comparable to the values for E_i/E (Section 2.3.3):

$$\frac{(\varepsilon_m - \varepsilon_{\infty,m})\cdot(2\cdot\varepsilon_m + \varepsilon_{\infty,m})}{\varepsilon_m(\varepsilon_{\infty,m} + 2)^2} = \frac{N_A}{9\cdot\varepsilon_0\cdot k\cdot T}\cdot\frac{\rho_m}{M_{r,m}}\cdot(V_1\mu_{g,1}^2 + V_2\mu_{g,2}^2)\cdot g \qquad (2.20)$$

The correlation factor *g* is a measure of intermolecular correlations, considering one dipole surrounded by its z next neighbors:

$$g = 1 + z\left\langle \cos\phi_{ij} \right\rangle \tag{2.21}$$

$\left\langle \cos\phi_{ij} \right\rangle$ is the average of the cosine of the angle between two neighboring molecules i and j.

So we find for parallel alignment of molecules, i.e. $\left\langle \cos\phi_{ij} \right\rangle$=1, $g > 1$, and for an antiparallel alignment, i.e. $\left\langle \cos\phi_{ij} \right\rangle$ = -1, $g < 1$.

Values for the induced polarization ε_∞ are not easily gained through experiment. It may be replaced by the square of the refractive index n, usually measured at λ=598.3 nm $\left(n_D^2\right)$, making use of the Maxwell relation: $\varepsilon_\infty = n^2$.

(Fröhlich, 1958) (Kirkwood, 1939)

The Kirkwood-Fröhlich Equation (Eq. (2.19)) is only valid for polar molecules. The value of *g* is ambiguous, as *g* = 1 stands either for an ideal disorder or equal amounts of parallel and antiparallel aligned molecules outweighing each other.

2.3.5 Broadband dielectric spectroscopy

The broad-band dielectric spectroscopy measures as direct data the complex dielectric permittivity (ε*) consisting of the real part (ε') and the imaginary part (ε"). There are different mathematical models available which describe the relaxation behavior of a polar liquid. The most simple equation is the Debye equation, which will be described in the next section. To fit the ε', ε"-data in a

best way it is also possible to use the Cole-Davidson distribution function or superposition of the Debye function with the Cole-Davidson function.

It is evident to check first whether the application of the Debye equation may be sufficient in order to avoid a distribution with the additional parameter β. Thus, before using a more complex distribution, which is just "descriptive" it is favorable to analyze 1) the superposition of two Debye-equations 2) to model the relaxation behavior with the Cole-Davidson distribution function and 3) whether a superposition of the Debye-equation with the Cole-Davidson distribution function describes satisfactory the relaxation behavior for the binary mixtures.

It has to be kept in mind that the resulting relaxation times (τ) depend on the mathematical model applied. If the mean corrected R^2 coefficient does not differ significantly for the mathematical models used, it is not possible to make an unambiguous choice of model.

2.3.5.1 The Debye equation applied for complex dielectric permittivity (ε*)

The Debye equation describes the behavior of the frequency (ω) dependence of the complex dielectric permittivity $\varepsilon^* = \varepsilon', \varepsilon''$:

$$\varepsilon^*(\omega) = \varepsilon_\infty + \frac{\varepsilon - \varepsilon_\infty}{1 + i\omega\tau} \tag{2.22}$$

With ε* = complex permittivity, ε = quasi-static dielectric permittivity (dielectric constant at ca. zero frequency) and ε_∞ = dielectric permittivity for induced polarization, measured at a frequency low enough that both atomic and electronic polarization are the same as in the static field and high enough so that the permanent dipoles can no longer follow the field ($\omega \rightarrow \infty$), τ = characteristic relaxation time [s^{-1}]. ω = angular frequency [s^{-1}] and í = imaginary unit = $(-1)^{1/2}$.

Eq. (2.22) can be split for the real (ε') and imaginary part (ε") of the complex permittivity:

$$\varepsilon'(\omega) = \varepsilon_\infty + (\varepsilon - \varepsilon_\infty)\frac{1}{1+\omega^2\tau^2} \tag{2.23}$$

and

$$\varepsilon''(\omega) = (\varepsilon - \varepsilon_\infty)\frac{1}{1+\omega^2\tau^2} \tag{2.24}$$

Eqs. (2.23) and (2.24) can be interpreted as follows: At low frequencies the dipole moment of the polar molecules, i.e. the molecule, orients in the applied electric field. Thus the real part (ε') is approximately constant and the imaginary part (ε") is close to zero. At a specific ω_{res} the imaginary part (ε") assumes a maximum value, which corresponds to a maximal energy absorption. At higher frequencies the dipole can no longer follow the directions of the external applied field. Thus ε' and ε" assume rather low values (see Fig. 2.12).

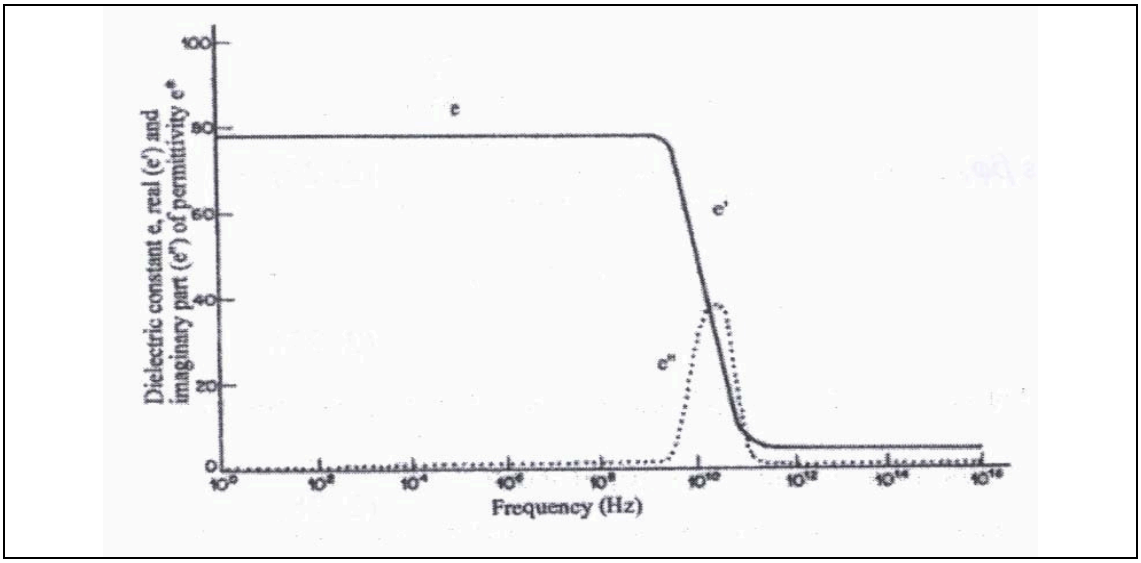

Fig. 2.12. Dielectric permittivity of a polar substance as a function of frequency (after Decareau et al., 1985)

A single relaxation time (τ) is an exception. One has to imagine that all dipoles relax “in phase”, i.e. in a cooperative way i.e. highly synchronized. In fact one has to assume that long- range forces must exist to achieve a high order of its dynamical behavior. In a less organized system more than one relaxation time exists. It may be assumed that the addition of a certain volume percentage of 1,4-dioxane to water may only slightly modify the water structure, giving rise to more than one single relaxation time. Thus, the case for two relaxation times can be modeled as follows:

$$\varepsilon^*(\omega) = \varepsilon_\infty + (\varepsilon - \varepsilon_\infty)\left\{\frac{l_1}{1+i\omega\tau_1} + \frac{l_2}{1+i\omega\tau_2}\right\} \quad (2.25)$$

With relaxation times τ_1, τ_2 and corresponding weights l_1, l_2 being $l_1 + l_2 = 1$. The following equations and the Cole-Davidson equation represent distribution functions describing a more chaotic behavior of the relaxation process.

2.3.6 Relaxation behavior

2.3.6.1 Relaxation behavior according to Cole-Davidson and its superposition with the Debye equation

The Cole-Davidson relaxation behavior can be described as follows, taking into account the real and the imaginary part:

$$\varepsilon'(\omega) = \varepsilon_\infty + (\varepsilon - \varepsilon_\infty)(\cos\phi)^\beta \cos\beta\phi \quad (2.26)$$

$$\varepsilon''(\omega) = (\varepsilon - \varepsilon_\infty)(\cos\phi)^\beta \sin\beta\phi \quad (2.27)$$

with

$$\phi = \arctan\left(\omega\tau_0\right) \tag{2.28}$$

In case of β = 1 the Cole-Davidson equation is identical with the Debye-equation (Eq. (2.22)).

It is evident to check first whether the application of the Debye equation may be sufficient in order to avoid a distribution with the additional parameter β. Thus before using a more complex distribution, which is just "descriptive" it is favorable to analyze 1) the superposition of two Debye-equations 2) to model the relaxation behavior with the Cole-Davidson distribution function and 3) whether a superposition of the Debye-equation with the Cole-Davidson distribution function (Eqs. (2.29), (2.30)) describes satisfactory the relaxation behavior for the binary mixtures:

$$\varepsilon'(\omega) = \varepsilon_\infty + \left(\varepsilon - \varepsilon_\infty\right)\left[l_1\left(\frac{1}{1+\omega^2\tau_1^2}\right) + l_2\left((\cos\phi)^\beta \sin\beta\phi\right)\right] \tag{2.29}$$

$$\varepsilon''(\omega) = \left(\varepsilon - \varepsilon_\infty\right)\left[l_1\left(\frac{\omega\tau_1}{1+\omega^2\tau_1^2}\right) + l_2\left((\cos\phi)^\beta \sin\beta\phi\right)\right] \tag{2.30}$$

with $\phi = \arctan\left(\omega\tau_0\right)$, and $l_1 + l_2 = 1$.

2.3.6.2 The Havriliak-Negami equation and its description of relaxation times

The Havriliak-Nagami equation (2.31) is a more generalize description, taking into account several relaxation times, i.e. a distribution of τ around the main relaxation time τ_0.

$$\varepsilon^*(\omega) = \varepsilon_\infty + \frac{\varepsilon - \varepsilon_\infty}{\left\{1 + \left(i\omega\tau_0\right)^{1-\alpha}\right\}^\beta} \tag{2.31}$$

τ_0 = main relaxation time

α = Cole-Cole symmetric distribution parameter (0≤ α ≤ 1)

β = Cole-Davidson asymmetric distribution parameter (0≤ β ≤ 1)

The separation of the real and the imaginary parts gives the following expression:

$$\varepsilon'(\omega) = \varepsilon_\infty + (\varepsilon - \varepsilon_\infty)\frac{\cos\beta\phi}{\left\{1 + 2(\omega\tau_0)^{1-\alpha}\sin\frac{1}{2}\pi\alpha + (\omega\tau_0)^{2(1-\alpha)}\right\}^{\frac{\beta}{2}}} \quad (2.32)$$

$$\varepsilon''(\omega) = (\varepsilon - \varepsilon_\infty)\frac{\sin\beta\phi}{\left\{1 + 2(\omega\tau_0)^{1-\alpha}\sin\frac{1}{2}\pi\alpha + (\omega\tau_0)^{2(1-\alpha)}\right\}^{\frac{\beta}{2}}} \quad (2.33)$$

where

$$\phi = \arctan\left[\frac{(\omega\tau_0)^{1-\alpha}\cos\frac{1}{2}\pi\alpha}{\left\{1 + (\omega\tau_0)^{1-\alpha}\sin\frac{1}{2}\pi\alpha\right\}}\right] \quad (2.34)$$

It must be note that the relaxation time is the reciprocal of the frequency in **radians per second** whereas the electromagnetic frequency is commonly reported in **cycles per second (Hz)**.

(Böttcher et al., 1978; a, b), (Carig, D.Q.M., 1995; a), (Decareau et al., 1985; c)

2.3.6.3 The dependence on temperature

While a depolarization process will occur through the switching off of the applied electric field, it can also happen through an increased temperature. For a large number of systems, the temperature dependence can be described as:

$$\tau_0 = A\exp(E/RT), \tag{2.35}$$

or as

$$k = \frac{1}{A}\exp(-E/RT). \tag{2.36}$$

τ_0 = main relaxation time (s)
k = reorientation rate (s^{-1})
A = constant (s)
E = constant ($Jmol^{-1}$)
R = gas constant = 8.314 ($Jmol^{-1}K^{-1}$)

The depolarization process in a liquid may take place as a rotational diffusion process or as reorientation by discrete, instantaneous jumps. While the first concept is based on the assumption of a liquid being similar to a dense gas, the second theory emphasizes the similarities between the liquid and solid state.

The concept of reorientation by jumps assumes that for each molecule in a crystal exists an orientation-dependent potential energy with one or more minima. The molecules will be situated for finite intervals in the different potential wells and the probability of switching from one well to another will depend on the height of the potential energy barrier between them. If these potential wells are steep enough, the molecule will usually be oriented in the direction corresponding with the minimal potential energy. Small changes and oscillations occurring in this well may be neglected. If the presence in the well is long compared to the time necessary to switch from one well to another, the

latter may be neglected, which allows us to assume a reorientation by instantaneous jumps.

In liquids, small, quasi-crystalline regions are assumed. Thus, the reorientation process can take place as outlined above for molecular crystals. Alternatively, it can be suggested that the orientation of a molecule is fixed as long as the quasi-crystalline region exists, and that the change in orientation is due to the transition from one quasi-crystalline arrangement to another. *(Böttcher et al., 1978; d)*

While *E* was originally introduced as a purely empirical quantity, it's physical interpretation as the activation energy for the reorientation was introduced by Glasstone et al. in 1941 and is called Eyring's theory of activated rate processes:

$$k = \frac{kT}{h}\exp\left(-\Delta H_a / RT\right)\exp\left(\Delta S_a / RT\right) \qquad (2.37)$$

k = Boltzmann's constant = 1.38 x 10^{-23} (JK^{-1})
h = Planck's constant = 6.626E-34 (Js)
R = gas constant = 8.314 ($Jmol^{-1}K^{-1}$)
ΔH_a = activation enthalpy for the relaxation process ($Jmol^{-1}$)
ΔS_a = activaton entropy for relaxation time process ($Jmol^{-1}K^{-1}$)

Thus, plotting $\ln\left(\frac{1}{\tau_0 T}\right)$ versus $\frac{1}{T}$ allows the calculation of ΔH_a and ΔS_a:

$$\ln\left(\frac{1}{\tau_0 T}\right) = -\frac{\Delta H_a}{R}\cdot\frac{1}{T} + \left[\frac{\Delta S_a}{R} + \ln\left(\frac{k}{h}\right)\right] \qquad (2.38)$$

2.4 Electromagnetic alternate fields in the microwave range and their applications in pharmaceutical research and development

Electromagnetic waves wuth frequencies in the macrowave range ($\omega \approx 10^9 - 10^{11} s^{-1}$) are used in a wide spectrum of fields, which can be roughly divided in analytics and heating procedures.

2.4.1 Analytics

Dielectric spectroscopy in the microwave range has found its place in analysis since the technical advances gained through radar research during World War 2. It has been used for some time in physical and chemical research for the investigation of inter- and intramolecular interactions, but the interest in the applicability of these results in the pharmaceutical field has grown only recently.

(Böttcher et al., 1978), (Carig, D.Q.M., et al., 1995), (Hasted, J.B., 1973)

Microwaves have been used to determine the water content of e.g. gelatin films and polyethylene glycols.

Low-frequency dielectric analysis has been used as a non-destructive method for the quality control of powders, creams, gels, and tablets, such as monitoring of ageing processes.

(Bremecker, K-D., 1983), (Carig, D.Q.M. et al., 1991), (Carig, D.Q.M., 1995), (Goggin, P.L., 1998)

2.4.2 Heating procedures

The main application field of microwaves in pharmaceutics so far lies in material heating.

The volumetric power absorption is proportional not only to the strength of the electric field, but also to the imaginary part ε'' of the permittivity, ε'' is also known as the loss factor, relevant for the energy absorbed in the material when an AC electric field is applied.

$$\frac{P}{V} = \omega \varepsilon_0 E^2 \varepsilon'' \qquad (2.39)$$

P = power (W)

V = volume (m^3)

The penetration depth of an electromagnetic wave, i.e. the depth at which *1/e* of the power at the surface is not attenuated or absorbed, can be described as follows:

$$z = \frac{c}{\omega} \sqrt{\frac{2}{\varepsilon' \left[\sqrt{\left(1 + \tan^2 \delta\right)} - 1 \right]}} \qquad (2.40)$$

z = penetration depth [m]

tanδ = $\frac{\varepsilon''}{\varepsilon'}$

In order to achieve fast and even heating, a compromise has therefore to be found for the applied frequency, a compromise between a high frequency providing rapid heating, and a low frequency allowing an adequate penetration depth. Usually, 2.45 ± 0.05 GHz is used, a frequency assigned by international agreements for industrial, scientific, and medical use. *(Decareau et al., 1985; a, b)*

To shorten drying time, microwaves are used in wet granulation (e.g. GP General Processor from Aeromatic - Fielder Ltd.; Ultima from Collette) and have been applied in tablet coating processes. *(Agoston et al., 2000), (Kiekens et al., 1999), (Joshi et al., 1989).*

The quick heating of liquids has found its way into chemistry, e.g. shortening synthesis time of molecules for high throughput testing, and reducing time for urinary drug screening. *(Larhed et al., 2001), (Criado et al., 2000).*

It is used in processes of reducing microbiological load, e.g. on contact lenses and on plant material, and in the sterilization of injection ampoules, a process recognized in the Japanese Pharmacopoeia. It was shown for pyridoxamine phosphate that drug stability is positively influenced by the short heating time compared to autoclavation. The question if there may be additional effects of microwaves on microorganisms besides the heating, e.g. interaction with the bacterial membrane molecules, has not yet been answered conclusively. (Hiti et al, 2001), (Portner, 1992), (Sasaki et al., 1996), (Janske, 1987).

2.5 Application of percolation theory to liquid binary mixtures

Percolation process were first developed by Flory (1941) and Stockmayer (1943) to describe how small branching molecules react and form very large macromolecules in the gelation process, however, the terminology of percolation was presented later by Broadbent and Hammersley (1957). It was not until late eighties that percolation theory found its way to the field of pharmaceutics *(Leuenberger, 1987).*

In the framework of this thesis, it is certainly impossible to provide a through introduction to the theory of percolation. For deeper understanding of percolation theory it is therefore recommendable to read basic textbooks on this subject as for example "Introduction of percolation theory" by Stauffer and Aharony (1985) and the PhD Thesis of Kuentz (1999).

It often happens that in order to define a concept, one first presents an example that illuminates the most important features of the problem at hand and then uses the insights gained in this way, to obtain a more formal definition.

This is the path we are going to follow in order to introduce percolation theory. The example we are going to present is inspired from (Stauffer, 1985). The first step is to consider a square lattice, like the one presented in Fig. 2.14. Intuitively it is clear what is the meaning of the word lattice. More formally one would say that we consider is a point lattice. Its definition is presented below.

A **point lattice** is an infinite array of discrete points with an arrangement and orientation that appears exactly the same, from whichever of the points the array is viewed.

One can see that the lattice we considered in Fig. 2.13 fulfils this condition. If we imagine the lattice to be infinitely extended in all directions, then all points are equivalent. In this case there is a certain freedom connected to what one could call the points or sites in the lattice. They could be either the squares determined by the gridlines or the points where these lines intersect. For this example we are going to assume the squares to be the relevant entities.

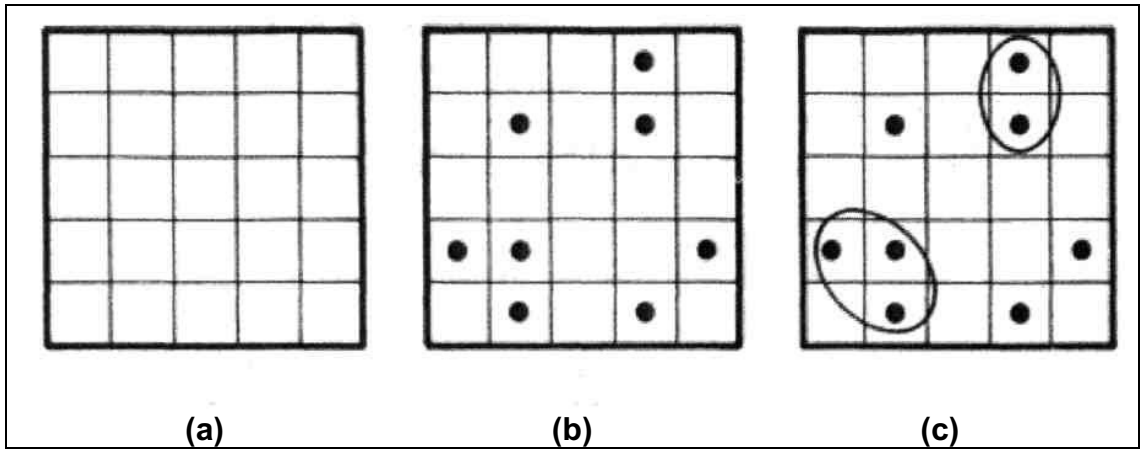

Fig. 2.13 Definition of percolation and its clusters: a) shows parts if a square lattice; in b) some squares are occupied with big dots; in c) the 'clusters', groups of neighbouring occupied squares, are encircled except when the 'cluster' consists of a single square (Stauffer, 1985).

Let us assume that one places a mark in each of the squares determined by the grid lines with probability p. One possible outcome of such an experiment is

presented in Fig. 2.13 (C). One can observe the formation of clusters, which in the present situation are defined as groups of neighboring squares occupied by a dot. Therefore, a **cluster** can be defined as a group of nearest neighboring occupied sites. In the lattice above (Fig. 2.13 c), we have one cluster of size 3 and a cluster of size 2.

One can also observe that the result of the percolation depends on the probability with which each site is occupied. For a low probability a small number of the squares will be occupied. The result might look like the lattice in Fig. 2.14 (A). On the other hand if the probability to occupy one square is high then a big number of squares will be occupied. The result might look like the lattice in Fig. 2.14 (B). An important feature of the second case is the existence of a cluster that connects the top and bottom, left and right sides of the lattice. Such a cluster is called a percolating cluster and its presence represents a qualitative chance in the structure of the lattice from a disconnected state to a connected one. As we will see later, such a transition usually suggests an important transformation in the system that is modeled. Moreover, one could ask what is the smallest probability for which a percolating cluster appears and what is its structure?

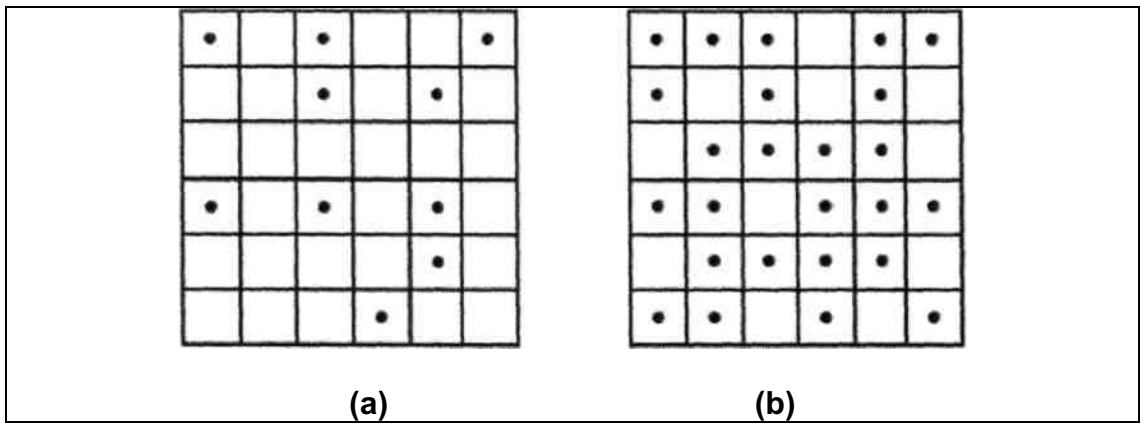

Fig. 2.14 Percolation on a square lattice for two percolation probabilities: a) low probability; b) high probability.

These are typical questions that one can investigate and answer in the framework of percolation theory. It is now an appropriate moment to give the definition that this example prepared.

Percolation theory studies the formation and structure of clusters in a large lattice whose sites or bonds are present with a certain probability.

The example we considered above has an important number of the characteristics of problems approached by percolation theory, but of course it is not the most general situation. The ultimate goal is to restate real life problems in the language of percolation theory, but in order to do such an analysis one needs to expand the model described above. One can easily imagine that percolation on a square lattice will prove fast enough its limitations. Thus the next step we will take is going to expand our model, by considering more general cases of percolation.

In the first place we are going to expand on a feature that we already noticed above. Given a lattice, the relevant entities for the percolation problem can be either the sites or the bonds between the sites. Thus the first distinction we can make is between **site and bond percolation.** As the name suggests the former considers the sites to be the relevant entities, which can be present with probability p, while for the latter the same role is played by the bonds between the sites. Fig. 2.15 presents an example for both site and bond percolation on a square lattice.

In the **bond percolation problem,** the bonds of the network are either *occupied* (i.e., they are open to flow, diffusion and reaction, they are microscopic conducting elements of a composite, etc.), randomly and independently of each other with probability *p,* or are *vacant* (i.e., they are closed to flow or current, or have been plugged, they are insulating elements of composite, etc.) with probability *1-p.* For a large network, this assignment is equivalent to removing a fraction *1-p* of all bonds at random. Two sites are called *connected* if there exists at least one path between them consisting solely of occupied bonds. As we defined, A set of connected sites bounded by vacant bonds is called *cluster.* If the network is of very large extent and if *p* is sufficiently small, the size of any

connected cluster is small. But if *p* is close to 1, the network should be entirely connected, apart from occasional small holes. At some well-defined value of *p*, there is a transition in the topological structure of the random network from a macroscopically disconnected structure to a connected one; this value is called the *bond percolation threshold,* p_{cb}. This is the *largest* fraction of occupied bonds below, which there is no sample-spanning cluster of occupied bonds.

Similarly, in the **site percolation problem** sites of network are occupied with *probability 1–p* and vacant with probability *1-p*. Two nearest-neighbor sites are called connected if they are both occupied, and connected clusters on the network are again defined in the obvious way. There is a *site percolation threshold* p_{cs} above which an infinite (sample-spanning) cluster of occupied sites spans the network.

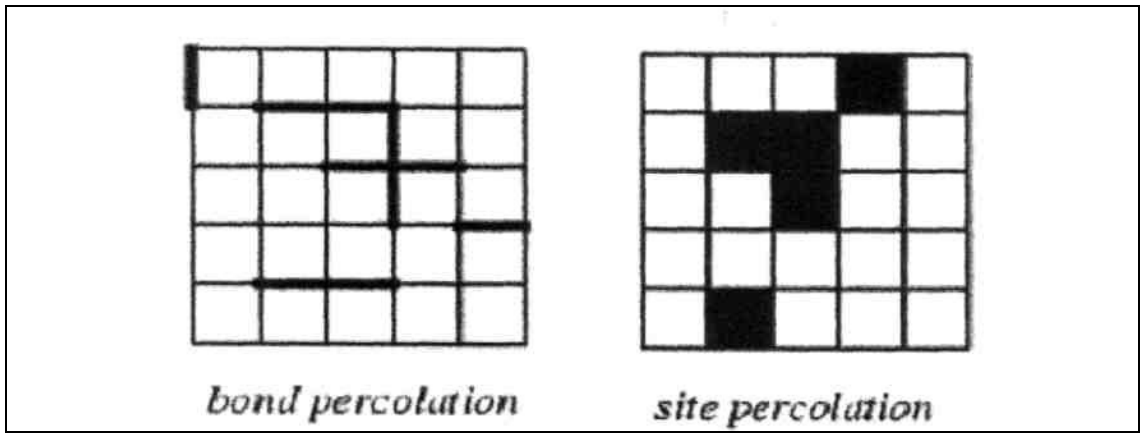

Fig. 2.15 Site and bond percolation on a square lattice Credit for the picture: http://mathworld.wolfram.com/PercolationTheory.litml, May22, 2003

One can also consider the combined situation in which the sites are occupied with probability p and the bonds between neighboring sites are open with probability x. This corresponds to site-bond percolation, for which an example is presented in Fig. 2.16. In this case we are interested in cluster of occupied sites connected by open bonds. *(Stauffer, 1985)*.

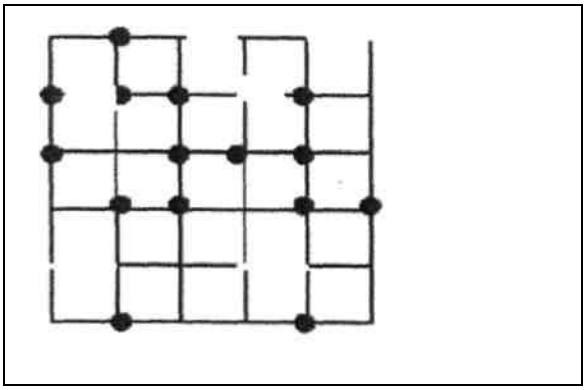

Fig. 2.16. Site-bond on a square lattice.

Lattice	Site	Bond	Coordination number z
Honeycomb	0.6962	0.65271	3
Square	0.592746	0.50000	4
Triangular	0.500000	0.34729	6
Diamond	0.43	0.388	4
Simple cubic	0.3116	0.2488	6
BCC	0.246	0.1803	8
FCC	0.198	0.119	12
Bethe	$1/(z-1)$	$1/(z-1)$	z

Table. 2.1 Site and bond percolation thresholds for different lattices (Sahimi, 1994)

It is also conceivable that percolation thresholds of an ideal system occupied by isometric particles depends on the lattice type, the type of percolation (bond or site) and on the dimension of the lattice (see Table 2.1). In an ideal system the lattice size is extremely large, i.e. infinite compared to the size of a unit lattice cell. Unfortunately, for most of the lattices the percolation thresholds (p_c) cannot be calculated in a straightforward way, but have to be estimated experimentally by computer simulation of such a lattice and its random occupation.

Close to the percolation threshold a property X of the system follows the scaling law of the percolation theory. The following relationship expresses the scaling law:

$$X = S * \left| p - p_c \right|^q \text{ where } 0 \le p \le 1 \qquad (2.41)$$

X = property studied

p = occupation probability

p_c = the percolation threshold

q = the critical exponent

S = scaling factor

The percolation threshold at $p = p_c$ gives the position of a phase transition where the system changes its behavior qualitatively for one peculiar value of a continuously varying parameter. In the percolation case, if p increases smoothly from zero to unity, then we have no percolating cluster for $p < p_c$ and (at least) one percolating cluster for $p > p_c$. Thus at $p = p_c$, and only there, for the first time an infinite cluster is formed. *(Stauffer, 1985), (Siegmund et al., 1999), (Sahimi, 1994), (Kirkpatrick, 1973).*

Finally, one can leave the two dimensional world of plane lattices and consider lattices in three or even, in general, in d dimensions.

Percolation theory is used in many fields. It can be applied to model forest fires or in the case of the oil industry it can be used as a key issue to predict the amount of oil that a well will produce. Percolation theory can be used in this case as a simple idealized model for the distribution of the oil or gas inside porous rocks or oil reservoirs.

Percolation theory has produced an important number of significant results and continues to be an active area of research. Even though it may not present the final solution to some of the problems it addresses, in conjunction with other techniques, it can offer at least a valid point from which further ideas can be advanced. *(Stauffer, 1985).*

In case of a binary mixture between a polar and a nonpolar liquid it is of interest to apply the concepts of percolation theory (Stengele et al., 2002; Stauffer and Aharony, 1998).

Peyrelasse et al., 1988 studied the conductivity and permittivity of various water/AOT/oil systems (AOT = surfactant active agent = sodium bis(2-ethylhexyl) sulfosuccinate) being able to interpret the results according to the phenomenon of percolation. In a second step they studied the viscosity of those systems and they concluded that the shape of viscosity curves could also be interpreted, at least qualitatively, in the framework of percolation theory. They also suggested that the phenomenon of percolation must be involved in other physical properties.

The aim of part A of this thesis is to study the phenomenon of percolation in binary solvent mixtures trying to find a connection between different physical properties.

Chapter 3

Materials and Methods

3.1 Materials

3.1.1 Solvents

For investigation the following solvents and solvent mixtures were chosen:

Water/1,4-dioxane: the measurement of these two very different substances allows us to investigate a nonpolar/polar mixture. 1,4-dioxane, a cyclic flexible diether, possesses through its symmetry no overall dipole moment, but it is miscible with water due to hydrogen bonding to the exposed oxygen atoms.

In order to know more about the influence of aprotic substances on water structure we investigated **DMSO/water** and we compared this mixture with, **DMF/water**, **DMAC/water** and **NMP/**water as DMSO analogues, to also know more about these important pharmaceutical and chemical solvents, and also have a broader investigation to a publication by *Hernandez-Perni G., Leuenberger H. 2004, The characterization of polar liquids and percolation phenomena in DMSO-water mixtures*.

We also measure **Sulpholane/water** mixture as a candidate to compare it with DMSO mixtures as they both have nearly the same dielectric constant and for assurance of correct method we also measured **THF/water** and compared our results with that of *Hernandez-Perni G., 2004*. We also investigated the **Formamide/water**, **Methylformamide/water** and compared them with **dimethylformamide/water** mixture to investigate changes in dielectric constant with addition of methyl groups. ($\varepsilon_{Formamide}$ = 109.5, $\varepsilon_{Methylformamide}$ = 182.4, $\varepsilon_{Dimethylformamide}$ = 37).

In order to know more about the structure and behaviour of these aprotic liquids, we also investigated them in a nonpolar/polar system, and 1,4-dioxane was chosen as the nonpolar part of liquid binary mixtures due to cyclic flexible diether, which possesses through its symmetry no overall dipole moment, but it is miscible with other liquids (polar part of the binary mixture) due to hydrogen bonding to the exposed oxygen atoms. (**DMSO/1,4-dioxane**, **NMP/1,4-dioxane, THF/1,4-dioxane**, **DMAC/1,4-dioxane**, **DMF/1,4-dioxane**, **Formamide/1,4-dioxane**, **methylformamide/1,4-dioxane**).

All mixtures and pure liquids were investigated at room temperature.

The physical properties of these compounds are described below.

Substance	1,4-dioxane	Dimehylacrylamine	Dimethylformamide	DMSO	Methylpyrrolidone
	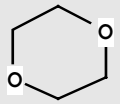	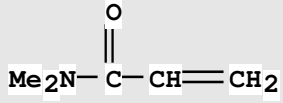	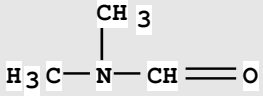	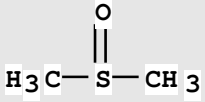	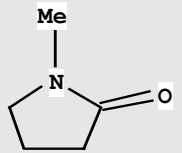
CA registry number	123-91-1	2680-03-7	68-12-2	67-68-5	872-50-4
Molecular formula	$C_4H_8O_2$	C_5H_9NO	C_3H_7NO	C_2H_6OS	C_5H_9NO
Molecular weight mw [g/mol]	88.11	99.13	73.20	78.13	99.13
Density ρ [kg/m^3]	1.02797	0.945	0.94800	1.10000	1.027
Static permittivity ε	2.21	37.8	38.25	47.24	32.2
Dipole moment μ_{Gas} [D]	0.00	3.72	3.73	3.96	4.09
Molecular polarizability α' [$\cdot 10^{-30}$m^3]	8.60	10.14	7.90	7.99	10.66
Hildebrand parameter δ/Mpa$^{0.5}$	20.50	22.50	24.80	26.70	23.10

Table 3. Literature values of some physical properties of the measured solvents at 298.2 K [Barton, 1991], [CRC Handbook of Chemistry and Physics, 1997], [Fluka, 2006], [ChmDAT, 2001], [Merck Index, 1983], [Purohit et al., 1991]

Substance	Formamide	Sulfolane	N,Methylformamide	Tetrahydrofuran	Water
		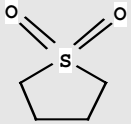	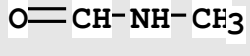	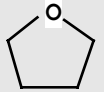	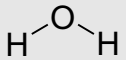
CA registry number	75-12-7	126-33-0	123-39-7	109-99-9	7732-18-5
Molecular formula	CH_3NO	$C_4H_8O_2S$	C_2H_5NO	C_4H_8O	H_2O
Molecular weight mw [g/mol]	45.04	120.17	59.07	72.11	18.02
Density ρ [kg/m^3]	1.1292	1.2600	0.9988	0.88700	0.99705
Static permittivity ε	109.5	43.3	182.4	7.52	78.54
Dipole moment μ_{Gas} [D]	3.4	4.8	3.8	1.75	1.85
Molecular polarizability α' [$\cdot 10^{-30}$m^3]	4.22	10.73	6.01	7.93	1.47
Hildebrand parameter δ/Mpa$^{0.5}$	39.30	27.40	32.90	19.40	47.80

Table 3. (continued) Literature values of some physical properties of the measured solvents at 298.2 K [Barton, 1991], [CRC Handbook of Chemistry and Physics, 1997], [Fluka, 2006], [ChmDAT, 2001], [Merck Index, 1983], [Purohit et al., 1991]

The described substances were used of the following qualities:

Dioxane puriss.
Fluka Chemie GmbH CH-9471 Buchs
Article number 42512

Dimethyl sulfoxide puriss.
Fluka Chemie GmbH CH-9471 Buchs
Article number 41644

Tetrahydrofuran
Fluka Chemie GmbH CH-9471 Buchs
Article number 87362

N, N-Dimethylformamide puriss.
Fluka Chemie GmbH CH-9471 Buchs
Article number 40228

N-Methylformamide purum
Fluka Chemie GmbH CH-9471 Buchs
Article number 66900

N, N-Dimethylacrylamide purum
Fluka Chemie GmbH CH-9471 Buchs
Article number 38873

Sulfolane purum
Fluka Chemie GmbH CH-9471 Buchs
Article number 86150

Formamide puriss.
Fluka Chemie GmbH CH-9471 Buchs

Article number 47670

1-Methyl-2-pyrrolidone. puriss

Fluka Chemie GmbH CH-9471 Buchs

Article number 69118

Water, bidistilled

Freshly prepared by means of Büchi Fontavapor 285

3.1.2 Apparatus

The following apparatus were used for sample preparation and analysis:

Abbé Refractometer

A. Krüss Optronic GmbH D-22297 Hamburg

AR8; 30098

Analytical balance

Mettler-Toledo AG CH-8606 Greifensee

AT 460 Delta Range; 1115330561

Bidistilling Apparatus

Büchi AG CH-9230 Flawil

Fontavapor 285; 499982

Cylinder Condensator

By courtsey of Ramsden PhD (Mechanische Werkstatt Biozentrum, Universität Basel)

Density Meter

Anton Paar AG A-8054 Graz

DMA 58;8

Digital Thermometer

Haake GmbH D- 76227 Karlsruhe

DT 10; -

Pt. 100 platinum resistance thermometer

High- Temperature Dielectric Probe Kit

Agilent Technologies Inc. USA-Palo Alto CA 94304-1185

HP 85070B OPT 002; -

Network Analyser

Agilent Technologies Inc. USA-Palo Alto CA 94304-1185

HP 8720D; US38111202

Precision LCR Meter

Agilent Technologies Inc. USA-Palo Alto CA 94304-1185

HP 4284A; 2940J01533

Thermostat

B. Braun Biotech International GmbH D-34209 Melsungen

Thermomix UB; 852042/9; 9012498

Frigomix U-1; 852 042/ 0; 8836 004

Test Fixture

Agilent Technologies Inc. USA-Palo Alto CA 94304-1185

HP 16047C; -

Ultrasound Bath

Retsch GmbH & Co. D-42781 Haan

UR 1; 306072082

Vortex Mixer

Scientific Industries Inc. USA-8ohemia NY 11716

G 560- E; 2-48666

Water Bath

Salvis AG CH-6015 Reussbiihl

W8R-4; 333127

3.1.3 Computer Software

The following software were used for sample analysis:

HP VEE

Agilent Technologies Inc. USA-Palo Alto CA 94304-1185

Version 5.01

HP 85070B Software Program

Agilent Technologies Inc. USA-Palo Alto CA 94304-1185

Version B.01.05

The following software were used for data analysis:

Excel

Microsoft Corp. USA-Redmond W A 98052-6399

Version 2000

SYSTAT for Windows

SPSS Inc. USA-Chicago IL 60606-6307

Version 7.0

3.2 Methods

3.2.1 Sample preparation

Apparatus Analytic Balance

Mettler- Toledo AG CH-8606 Greifensee

AT 460 Delta Range; 1115330561

Vortex Mixer

Scientific Industries Inc. USA-Bohemia NY 11716

G 560- E; 2-48666

Preparation:

Samples were prepared by weighing the necessary amounts of solvents/solutes into glass flasks.

The samples were then shaken vigorously for 15 seconds and then stirred for 1 minute using a Vortex mixer.

3.2.2 Measurement of static permittivity and conductivity

3.2.2.1. Measuring principle

The static permittivity and conductivity in this work are measured via the impedance and conductance, respectively, by means of a LCR Meter at a low ac frequency (υ), so the measured permittivity corresponds to the dielectric constant measured in direct current (dc).

LCR meters (inductance (L), capacitance (C), and resistance (R)) measure the impedance of a material at specific frequencies. The impedance (Z) is defined as the total opposition a device or circuit offers to the flow of an alternating current at a given frequency (υ). It is a complex expression

$$Z = R + iX = |Z|e^{i\theta} \tag{3.1}$$

$$X = 2\pi\nu L \tag{3.2}$$

Z = impedence [Ω]

R = resistance [Ω]

X = reactance [Ω]

θ = phase of impedance

L = inductance [H]

ν = frequency

The reciprocal of impedance is the admittance (Y)

$$Y = G + iB = |G|e^{i\delta} = \frac{1}{Z} = \frac{1}{R + iX} \tag{3.3}$$

$$B = 2\pi\nu C_{MUT} \tag{3.4}$$

Y = admittance [S]

G = conductance [S]

B = susceptance [S]

δ = phase of admittance, dielectric loss angle

C = capacitance [F]

The static permittivity ε – for $\nu << \nu_{rel}$ – equals the real part of the permittivity

$$\varepsilon' = \frac{C_{MUT}}{C_{vacuum}} \tag{3.5}$$

ε' = real part of permittivity ε^*

C_{MUT} = capacitance of material under test [F]

C_{vacuum} = capacitance of vacuum [F]

In the present work, the measured C_{air} is substituted for C_{vacuum}, the calculated values for ε are corrected via a calibration curve (equation 3.10).

The tangent of δ is called the dielectric dissipation factor,

$$\tan\delta = \frac{G}{|B|} = \frac{G}{2\pi\nu C_{MUT}} \quad (3.6)$$

In a parallel circute, the conductance (G) is reciprocal of the parallel resistance (R_p)

$$G = \frac{1}{R_p} \quad (3.7)$$

and the specific conductivity (σ)

$$\sigma = K \times G \quad (3.8)$$

K = cell constant [cm^{-1}]

For materials relaxing in the frequency range of the LCR meter (20 Hz – 1 MHz), the imaginary part ε'' of the permittivity ε^* can be calculated as following:

$$\varepsilon'' = \varepsilon' \cdot \tan\delta = \frac{1}{R_p \omega C_{vacuum}} \quad (3.9)$$

$$\omega = 2\pi\nu \quad (3.10)$$

(Agilent Technologies Inc., 1988), (Agilent Technologies Inc., 1994)

3.2.2.2. Apparatus and Measuring Procedure

Apparatus Precision LCR Meter (Agilent Technologies Inc. HP 4284A; 2940J01533), Test Fixture (Agilent Technologies Inc. USA-Palo Alto CA 94304-1185 HP 16047C.

To the test fixture connected:
Cylinder Condensator (by courtesy of Ramsden PhD (Mechanische Werkstatt Biozentrum, Universitat Basel)
inner electrode: diameter 12.92mm, height 9.85 mm
outer electrode: diameter 18.74 mm

To the cylinder condensator connected:
Thermostat (B. Braun Biotech International GmbH D-34209 Melsungen: Thermomix UB; 852 042/ 9; 9012 498/ Frigomix U-l; 852 042/ 0; 8836 004), allowing temperature control of ±0.1 K

The temperature of the cylinder condensator was checked by means of:
Digital Thermometer (Haake GmbH D-76227 Karlsruhe DT 10; -), Pt. 100 platinum resistance thermometer (±0.1 K)

For the measurement set-up used in this work the capacitance C and the conductance G are measured in a parallel circuit mode [Lehnert, 1992]. As test frequency 100 kHz was chosen, giving stable results and being 10^3 - 10^5 lower than the relaxation frequencies of the liquids measured in this work.

The measurements were made by means of a personal computer connected to the LCR Meter, using the software HP VEE 5.01 (Agilent Technologies Inc. USA-Palo Alto CA 94304-1185).

Measuring procedure The cylinder condensator is brought to the measuring temperature and filled with sample. 5 minutes after the required temperature is reached, the sample is measured 5 times, waiting for 1 minute after each

measurement. Using the before determined capacitance of the empty condensator and the calibration curve (equation 3.10), the static permittivity is calculated.

3.2.2.3. Accuracy and reproducibility of the measurement

Accuracy Due to the effects of boundary fields, the cylinder condensator is to be calibrated. The calibration is performed by measuring pure solvents of known static permittivities at 298.2 K.

Taking the geometry of the condensator into consideration, the calibration curve is

$$\varepsilon_{lit} = 2.7394 \cdot \varepsilon_{\exp} - 1.8031 \qquad r^2 = 1.000 \qquad (3.11)$$

Solvent	ε_{exp}	ε_{lit}[1]
n-pentane	1.324	1.836
cyclohexane	1.379	2.015
tetrachlormethane	1.471	2.228
1,2-dichlorethane	4.438	10.360
1-propanol	8.093	20.100
methanol	12.482	32.630
water bidest.	29.340	78.540

Table. 3.1. Literature and experimental static permittivities of pure solvents at 298.2 K.

The correction of measured values by means of equation (3.11) leads to values for the dielectric constant of good accuracy (see Table 3.2) compared to literature values. In this work, e will stand for experimental values corrected with equation (3.11).

Reproducibility The values for the static permittivity used in this work are based on three measurements per sample. The standard deviations are of the same order of magnitude as those for the nonpolar 1,4 dioxane and for the highly polar, hydrogen-bonding water listed in Table 3.3. therefore no further listing of standard deviations for the measured static permittivities is made.

Solvent	$\varepsilon_{exp,corr}$	ε_{lit}[1]	Accuracy[2]
benzene	2.30	2.27	1.21
n-butanol	17.82	17.51	1.74
glycerol	42.80	42.50	0.60

Table 3. 2 Accuracy of the corrected values for the static permittivities of pure solvents at 298.2K.

	1,4 Dioxane		Water, bidistilled	
Temperature[K]	**ε**	**rel. STDEV [%]**	**ε**	**rel. STDEV [%]**
290.7	2.260	1.21	82.203	0.35
298.2	2.255	0.62	78.994	0.23
305.7	2.243	0.43	75.904	0.13
313.2	2.226	0.38	72.431	0.50
320.7	2.209	0.34	69.583	0.21
328.2	2.169	1.11	66.327	0.45
335.7	2.145	0.97	63.403	0.34
343.2	2.116	1.33	60.829	0.95

Table 3. 3 Reproducibility of measurements of static permittivity (n=3).

[1] *(Riddick et al., 1972), (CRC Handbook of Chemistry and Physics, 1997)*

[2] $\frac{\left|\varepsilon_{lit}-\varepsilon_{\exp,corr}\right|\cdot 100}{\varepsilon_{\exp}}[\%]$

3.2.3 Measurement of complex permittivity

3.2.3.1. Measuring principle

The measuring system consists of a dielectric probe connected to a network analyzer by means of a semi-rigid coaxial cable. An electromagnetic signal is generated by the network analyzer and transmitted into the material under test (MUT) via cable and probe. The signal is reflected by the MUT and its phase and amplitude are compared by the network analyzer to those of the incident e.m. wave.

Both phase and amplitude of the reflected e.m. wave are determined by the intrinsic impedence Z:

$$Z = \sqrt{\frac{\mu^*}{\varepsilon^*}} \tag{3.12}$$

Z = intrinsic impedance [Ω]

μ^* = complex permittivity interaction of a material with a magnetic field
ε^* = complex permittivity interaction of a material with an electric field

The reflection coefficient Γ of MUT and line is defined as:

$$\Gamma = \frac{Z_{MUT} - Z_{line}}{Z_{MUT} + Z_{line}} \tag{3.13}$$

Γ = reflection coefficient
Z_{MUT} = impedance of sample [Ω]
Z_{line} = impedance of line [Ω]

For calculating ε' and ε'' the S_{11}-parameter is used, the scattering parameter, comparing incidented and reflected signal at port 1.

$$S_{11} = \frac{(1-T^2)\cdot\Gamma}{1-T^2\cdot\Gamma} \tag{3.14}$$

T = transmission coefficient

Assuming the sample to be infinite size, we receive for Γ:

$$\Gamma = \frac{Z_{MUT} - Z_{line}}{Z_{MUT} + Z_{line}} = \frac{\sqrt{\frac{\mu^*}{\varepsilon^*}} - 1}{\sqrt{\frac{\mu^*}{\varepsilon^*}} + 1} \tag{3.15}$$

Assuming the MUT to be non-magnetic ($\mu^* = 1$) we receive:

$$\Gamma = \frac{\sqrt{\frac{1}{\varepsilon^*}} - 1}{\sqrt{\frac{1}{\varepsilon^*}} + 1} \tag{3.16}$$

In dielectrics the energy absorption is very high, so T≈0:

$$S_{11} = \frac{(1-T^2)\cdot\Gamma}{1-T^2\cdot\Gamma} = \frac{\Gamma}{1} = \frac{\sqrt{\frac{1}{\varepsilon^*}} - 1}{\sqrt{\frac{1}{\varepsilon^*}} + 1} \tag{3.17}$$

For calculation of ε' and ε'' the following relationships are used:

$$\left|\varepsilon^*\right| = \sqrt{\varepsilon'^2 + \varepsilon''^2} \tag{3.18}$$

$$\tan\delta = \frac{\varepsilon''}{\varepsilon'} \tag{3.19}$$

δ = loss angle, phase difference between dielectric displacment and dielectric field

(Agilent Technologies Inc., 1985), (Agilent Technologies Inc., 1993), (Rauxel-Dornik, 1991)

3.2.3.2. Apparatus and Measuring Procedure

Apparatus Network Analyzer
Agilent Technologies Inc. USA-Palo Alto CA 94304-1185
HP 8720D;US38111202

To the Network Analyzer connected:

High-Temperature Dielectric Probe Kit
Agilent Technologies Inc. USA-Palo Alto CA 94304-1185 HP 85070B OPT 002; -

The sample was kept at the required temperature through immersion in:
Thermostat (B. Braun Biotech International GmbH D-34209 Melsungen: Thermomix UB; 852 042/ 9; 9012 498 / Frigomix U-1; 852 042/ 0; 8836 004), allowing temperature control of ±0.1 K.

The temperature was checked by means of:
Digital Thermometer (Haake GmbH D-76227 Karlsruhe DT 10; -), Pt. 100 platinum resistance thermometer (±0.1 K)

The measurements were made by means of a personal computer connected to the Network Analyzer, using software HP 85070B Probe Software Program (Agilent Technologies Inc. USA-Palo Alto CA 94304-1185).

Measuring procedure Measurements were made between 0.2 and 20 GHz at 401 frequencies.

The dielectric probe was calibrated at the measurement temperature T_{meas} by air, a metal block, and bidistilled water. The computer software requires a fast performance of these calibration steps which does not allow for an exact temperature adjustment. Therefore, this operation was followed by a calibration refresh procedure, using bidistilled water at T_{meas} ± 0.1 K. Calibration and refresh calibration were made before starting measurements at T_{meas} and after every fifth sample.

For measurement, the probe was immersed in the sample, which was brought to T_{meas} by means of a water bath/refrigerator. Special attention has to be paid to avoid air bubbles in the probe and the stability of the coaxial cable. Using the thermostat as a water bath, the sample was stabilized at T_{meas}± 0.1 K before starting the measurement.

3.2.3.3. Accuracy and reproducibility of measurement

In order to check accuracy and reproducibility of measurements, air and water at three temperatures were measured three times after the calibration procedure, and compared to literature values. As only few data of high frequency measurements are available in literature, it was decided to use water at 278.2, 298.2, and 283.2 K, as these have only recently been closely reinvestigated by Kaatze (1989).

Frequency [GHz]	Literature		Experimental		Accuracy[3]	
	ε'	ε''	ε'	ε''	ε'	ε''
1.150	85.1	8.56	85.0	9.3	0.12	7.78
1.800	83.7	13.2	83.5	14.1	0.23	6.26
2.786	80.8	19.5	80.2	20.7	0.75	5.68
3.723	76.0	24.6	76.3	26.0	0.35	5.51
5.345	69.8	31.8	68.4	33.0	2.03	3.77
7.762	58.6	37.8	56.4	38.7	3.88	2.20
12.82	38.9	39.2	36.9	39.3	5.38	0.24
15.06	33.6	37.1	31.0	37.6	8.31	1.35
17.35	28.1	35.8	26.4	35.5	6.49	0.80

Table 3. 4 Experimental values of water at 278.2 K compared to those given by Kaatze (1989).

For air, ε' should be 1 and ε'' 0, invariant of frequency. The measured values were ε' = 1.02 ± 0.02 and ε'' = 0.03 ± 0.02. This shows that while the measurements are well comparable to the theoretical values for air, ε'' is more hampered by noise than ε'.

The average relative standard deviation for water at 278.2 K is 0.10 % for ε' (2.78 % for ε'), at 298.2 K is 0.08 % and 2.71 %, and at 283.2 K 0.13 % and 2.74 %. This means that the measurements lead to an excellent reproducibility for ε' and to an acceptable reproducibility for ε'', in accordance with the data for typical reproducibility of 1-2.5 % given by Agilent Technologies Inc. (1993).
The accuracy of measurements (see Table 3.4, 3.5, 3.6) lies in general very well in the range given by Agilent Technologies Inc. (1993) of ε' ± 5 % and tanδ ± 0.05 %. Nevertheless, it must be noticed that best accuracy is obtained at room temperature and that in many cases measurements of ε' are more accurate than those of ε''.

[3] $\frac{|lit - \exp| \cdot 100}{\exp}[\%]$

Frequency [GHz]	Literature		Experimental		Accuracy[4]	
	ε'	ε''	ε'	ε''	ε'	ε''
2.000	77.9	7.57	77.6	7.79	0.40	7.78
2.628	77.1	9.86	77.0	10.11	0.16	6.26
3.773	75.3	14.5	75.6	14.0	0.37	5.68
5.433	73.1	19.3	72.6	19.4	0.62	5.51
6.300	71.2	21.6	70.9	21.9	0.40	3.77
6.958	69.7	23.3	69.5	23.7	0.28	2.20
7.850	67.9	25.6	67.5	25.8	0.62	0.24
8.579	66.8	27.2	65.8	27.4	1.57	1.35
11.73	58.5	32.3	58.1	32.5	0.75	0.80
13.38	54.0	34.0	54.1	34.2	0.19	0.70
16.60	47.0	35.9	46.8	36.0	0.38	0.39
19.02	41.7	36.2	42.0	36.5	0.68	0.70

Table 3. 5 Selection of experimental values of water at 298.2 K compared to those given by Kaatze (1989).

Frequency [GHz]	Literature		Experimental		Accuracy[4]	
	ε'	ε''	ε'	ε''	ε'	ε''
7.707	67.2	14.5	66.2	14.7	1.47	1.26
12.47	61.5	21.4	61.3	21.7	0.33	1.37
17.46	56.3	27.2	55.1	26.9	2.13	1.04

Table 3. 6: Experimental values of water at 323.2 K compared to those given by Kaatze (1989).

3.2.3 Measurement of density

3.2.4.1. Measuring principle

The densities are measured by means of a vibrating-tube densimeter (VTB).

[4] $\frac{|lit - \exp| \cdot 100}{\exp}[\%]$

A U-shaped tube, both stationary ends anchored, is filled with the sample and brought to out-of-plane oscillations. The resonant frequency of the tube depends on its total mass m_{total}. As the volume V of the vibrating part is fixed through clamping, m_{total} depends on the known mass of the tube m_{tube} and of the density ρ of the sample:

$$m_{total} = m_{tube} + V \cdot \rho \tag{3.20}$$

The resonance frequency of this measuring system, which can be viewed to consist of an undamped spring with the mass m attached, is described as following:

$$f = \frac{1}{2\pi}\sqrt{\frac{k}{m_{tube} + V \cdot \rho}} = \frac{1}{T^*} \tag{3.21}$$

k = spring constant

T^* = period of oscillation

The density can be calculated from (3.20):

$$\rho = T^{*2} \cdot \frac{k}{4\pi^2 V} - \frac{m_{tube}}{V} = A^* \cdot T^{*2} - B \tag{3.22}$$

Calibration using air and bidistilled water determines the instrument constant A^* and B^*.

(Davis et al., 1992)

3.2.4.2. Apparatus and measuring procedure

Apparatus Density Meter (Anton Paar AG A-8054 Graz: DMA 58; 8)

Measuring procedure We calibrated the apparatus for each measuring temperature every 100 days, as standards are air and bidistilled water used.

The sample is de-gassed in an ultrasound-bath and brought to measurement temperature (water bath/refrigerator).

2ml sample is filled into the tube using a disposable syringe. After stabilization, the indicated period of oscillation is recorded.

3.2.4.3. Accuracy and reproducibility of the measurement

In order to examine the accuracy and reproducibility of density measurements pure solvents were measured three times and the results were compared to literature data.

Accuracy The measurements showed an excellent agreement with literature data *(Riddick et al., 1972)* (see Table 3.7).

Reproducibility The densities of solvents were measured three times at different temperatures. The reproducibility proved to be independent of the measuring temperature [Rey, 1998]. The values for the density used in this work are based on three measurements per sample and temperature. The standard deviations are of the same order of magnitude as those listed in Table 3.7. Therefore, no further listing of standard deviations for the measured densities are made.

Solvent	$Density_{lit}$ [kg/cm^3]	$Density_{exp}$ [kg/cm^3]	Reproducibility Rel. STDEV [%]	Accuracy[5]
benzylalcohol	1.04127	1.04135	0.004	0.008
1,4-dioxane	1.02797	1.02829	0.011	0.031
ethanol	0.78504	0.78535	0.007	0.039
toluene	0.86231	0.86193	0.100	0.044
water, bidistilled	0.99705	0.99705	0.002	0.000

Table 3. 7 Experimental values of some pure solvents 323.2 K compared to those given by Riddick (1972).

5 $\frac{\left|\rho_{lit} - \rho_{\exp}\right| \cdot 100}{\rho_{\exp}} [\%]$

3.2.5 Measurement of refractive index

3.2.5.1. Measuring principle

When light passes the interface of two substances of different optical densities both its velocity and direction are changed.

The refractive index n of a transparent medium is defined as the relation of the velocity of the light in vacuum c to that in the medium CM:

$$n = \frac{c}{c_M} \tag{3.23}$$

For practical reasons, the refractive index is determined, using the velocity of light in air instead of in vacuum as reference system. Thus, the absolute refractive index 1.0000.

On condition of medium 1 being the optical less dense material, viz air, the following relationship can be applied:

$$n_2 = \frac{n_2}{n_1} = \frac{\sin\alpha}{\sin\beta} \tag{3.24}$$

α = angle of incidence
β = angle of refraction,

the reference system being the normal to the two media's interface.

The refractive index depends on the wavelength of the light source, usually it is referred to the D-line of sodium *(λ* = 589.3 nm) measured at 20.0 ± 0.5°C $\left(n_D^{20}\right)$.

The Abbé Refractometer determines the critical angle of total reflection α_{crit}, i.e. the incident light is full reflected. The optical denser medium is a glass prism of a known refractive index n_{glass} and α is set at 90°, so (3.23) can be written as:

$$\frac{n_{glass}}{n_{medium}} = \frac{\sin 90^{\circ}}{\sin \beta} = \frac{1}{\sin \beta} \quad (3.25)$$

$$n_{medium} = n_{glass} \cdot \sin \beta \quad (3.26)$$

(Rücker et al., 1992)

3.2.5.2. Apparatus and measuring procedure

Apparatus Abbe Refractometer (A.Kriiss Optronic GmbH D-22297 Hamburg; AR8, 30098)
Thermostat (B.Braun Biotech International GmbH D-34209 Melsungen: Thermomix UB; 852 042/9; 9012 498 / Frigomix U-l; 852 212/0; 8836 004)

Measuring procedure The refractometer was brought to the measurement temperature of 298.2 K ± 0.1 K by means of the thermostat. 15 minutes after reaching stable temperature, we calibrated the refractometer using freshly bidistilled water. In order to achieve correct values over a broad range of refractive indices, water, tetrachloromethane and toluene were measured before the start of a measurement series; this allowed a correction of the determined values. For measuring, a drop of liquid was brought onto the prism of the refractometer. After 5 seconds, the refractive index was taken three times through bringing a dark bar to the crosshair in the reading field.

3.2.5.3. Accuracy and reproducibility of measurement

The measured refractive indices show excellent reproducibility and accuracy compared to literature values (Table 3.8).

Solvent	nD_{lit}	nD_{exp}	Reproducibility Rel. STDEV [%]	Accuracy[6]
Methanol	1.3265	1.3267	0.012	0.019
Water, bidistilled	1.3325	1.3325	0.003	0.004
Ethanol	1.3594	1.3594	0.008	0.001
Tetrachloromethane	1.4574	1.4576	0.012	0.015
Toluene	1.4941	1.4939	0.009	0.011

Table 3. 8 Accuracy and reproducibility of refractive index measurements (pure liquids at 298.2K; n=3

3.2.6 Data analysis

3.2.6.1. Determination of additional physical properties

Physical properties, which were necessary for calculations, such as the dipole moment in the gas phase μ_g and the polarizability α of the investigated compounds, were taken from the literature. If they were not reported, they were determined experimentally.

For the dipole moment, highly diluted solutions of the compound in 1,4-dioxane were measured, μ of the pure liquid was approximated through extrapolation of the calculated values of μ for the mixtures to an infinitely diluted solution of the compound, corresponding to $V_{1,\,4\text{-dioxane}} = 1$. *(Rey, 1998)*

6 $\frac{\left|n_{lit} - n_{\exp,corr}\right| \cdot 100}{n_{\exp}} [\%]$

The polarizability was determined via the Lorenz-Lorenz-equation (2.32).
(Rey, 1998)

3.2.6.2. Nonlinear regression of dielectric raw data

Principle In order to find the values for such parameter as the relaxation time τ or distribution parameter α, the raw data $\varepsilon'(\omega)$, $\varepsilon''(\omega)$ of the dielectric relaxation measurements must be fitted to an equation describing the process.
Close attention must be paid to choosing an adequate equation and fitting procedure, and the number of fitting parameters.

Usually a compromise has to be found between a large number of free parameters, offering a most adequate fit of the data, and a small number, providing robust and meaningful results, especially when data of e.g. various water concentrations are to be compared.

Equation	Free parameters
Debye	3 (ε; ε_∞; τ)
Cole-Cole	4 (ε; ε_∞; τ_0; α)
Cole-Davidson	4 (ε; ε_∞; τ_0; β)
Havrilak-Negami	5 (ε; ε_∞; τ_0; α; α)
2 Debye	5 (ε ; ε_∞ ; τ_1; τ_2; I_1 ($I_1 + I_2 = 1$))

Table 3. 9 Number of free parameters for equations describing relaxation phenomena *(Böttcher et al., 1978; a, b).*

The number of free parameter can be reduced through additional measurements (ε at $v << v_{rel}$) or assumptions made re the values for α, β, ε_∞. Many pure liquids and binary mixtures can be adequately described using either the Cole-Cole- or Cole-Davidson-equation *(Böttcher et al., 1978)*.

The choice of equation was based on literature and on the comparison of fit results re correlation coefficient R^2 and overall look.

Two fitting softwares were compared for evaluation: SYSTAT 7.0 (SPSS Inc., Chicago) and Easy-Fit 2.0 (Prof. Klaus Schittkowski, University of Bayreuth, Germany). The latter allowed a simultaneously fitting of the real and imaginary part of the equation (see equations 2.32, 2.33), but only 100 points (every fourth) could be included. For SYSTAT 7.0, the inclusion of both real and imaginary parts for fitting can be made as the term ($\varepsilon - \varepsilon_\infty$) occurs in both parts. This allows reformulation of equation (2.31) as:

$$\varepsilon'(\omega) = \varepsilon_\infty + \varepsilon''(\omega) \cdot \cot \beta\phi \qquad (3.27)$$

$$\varepsilon'(\omega) = \varepsilon_\infty + \varepsilon''(\omega) \cdot \cot \beta\phi \qquad (3.28)$$

The fitting softwares were compared to each other using a broad selection of data [water (298.2 and 343.2 K), ethanol (298.2 and 343.2 K), glycerol (298.2 K), ethanol/water V_{H2O} /V_{total} = 0.07 (298.2 and 343.2 K), glycerol/water V_{H2O} /V_{total} = 0.17 (320.7 K), and dioxane/water V_{H2O}/V_{total} = 0.30 (298.2 and 328.2 K)].

Data	R^2 SYSTAT 7.0	R^2 Easy-Fit 2.0
water, 298.2 K	0.99996	0.99989
water, 343.2 K	0.99997	0.99964
ethanol, 298.2 K	0.99811	0.98801
ethanol, 343.2 K	0.99547	0.99280
glycerol, 298.2 K	0.99860	0.99865
ethanol/water V_{H2O} /V_{total} = 0.07, 298.2 K	0.99811	0.99039
ethanol/water V_{H2O} /V_{total} = 0.07, 343.2 K	0.98697	0.99283
glycerol/water V_{H2O} /V_{total} = 0.17, 320.7 K	0.99860	0.99731
dioxane/water V_{H2O} /V_{total} = 0.30, 298.2 K	0.98805	0.98986
dioxane/water V_{H2O} /V_{total} = 0.30, 328.2 K	0.99104	0.72709

Table 3.10 Evaluation of fitting software *(Stengele, 2002)*

Often data sets, SYSTAT 7.0 led in 7 cases to better results, both for the values of r^2 and the overall look.

Software Systat for Windows

SPSS Inc. USA-Chicago IL 60606-6307 Version 7.0

Procedure The data, i.e. the mean based on three separate measurements, are fitted to the chosen equation using nonlinear regression (Gauss-Newton with Least Squares estimation).

3.2.6.3. Subdivision of curves into segments by means of nonlinear regression

Principle From theory, we assume that the properties of a binary mixture should behave like the volume-wise addition of the properties if the pure liquids. If deviations from this theoretical assumption occur, the splitting up of the curve onto small number of segments leads to the distinction of percolation

thresholds, critical volume fractions, and to a better description of properties of the system. The subdivision of data into a number of segments may be appropriate if the number of segments is small, the mathematical model describing the segments simple, via straight lines, and if there are sharp transitions between the segments.
(Belman et al., 1969), (Seber et al., 1989)

3.2.6.4. Software

Systat for Windows
SPSS Inc. USA-Chicago IL 60606-6307 Version 7.0

Procedure The data were inspected in order to decide about a suitable number of sub-segments and potential critical concentrations. For the following example (see Table 3.11), three sub-segments seem appropriate with critical values for x_{crit} ≈ 4-6 and 8-10.

The data were arbitrary split into three straight subsegments around these possible x_{crit}, e.g. the first four points to subsegment A, the next four to subsegment B, the last four to subsegment C. Using nonlinear regression, the data were fitted to the following equation:

$$y = A(m_1 x + b_1) + B(m_2 x + b_2) + C(m_3 + b_3) \quad (3.29)$$

The final decision to which segment the data are to be assigned is made considering the correlation coefficient r^2 for the overall fit. For this example, the best fit (r^2 = 0.9985) was received for a distribution 5 / 3 / 4 (A: y= -0.62x + 13.78; B: -2.10x + 21.8; C: 0.35x + 0.25).

x	y	Data belong to segment		
		A	B	C
1.0	13.0	1	0	0
2.0	12.6	1	0	0
3.0	12.1	1	0	0
4.0	11.4	1	0	0
5.0	10.5	0	1	0
6.0	9.2	0	1	0
7.0	7.1	0	1	0
8.0	5.0	0	1	0
9.0	3.6	0	0	1
10.0	3.5	0	0	1
11.0	4.0	0	0	1
12.0	4.6	0	0	1

Table 3.11 Subdivision of curves into segments: example

Chapter 4

Results and discussion

4.1. Application of percolation theory in comparison of DMSO and its analogues (DMF, DMAC, NMP) in water as well as 1,4-Dioxane binary mixtures using dielectric spectroscopy

Peyrelasse et al., 1988 studied the conductivity and permittivity of various water/AOT/oil systems (AOT= surfactant active agent = sodium bis(2-ethylhexyl) sulfosuccinate) being able to interpret the results according to the phenomenon of percolation. In a second step they studied the viscosity of those systems and they concluded that the shape of viscosity curves could also be interpreted, at least qualitatively, in the framework of percolation theory. They also suggested that the phenomenon of percolation must be involved in other physical properties.

The aim of this work is to study the phenomenon of percolation in binary solvent mixtures parameters by analyzing parameters derived from dielectric spectroscopy trying to find a connection between different physical properties.

We chose the DMSO-water system and compare it to its analogues for our studies because the mixtures exhibit higher viscosities than either of the two pure components, with a large viscosity maximum near 35% mole fraction in DMSO (32% (V_{wa}/V)) *(Marshall et al., 1987).* Moreover, there have been many attempts to revel the structure of the DMSO-water mixture in order to understand the maximum deviations detected at 30-40 mol % DMSO (63-72% (V_{DMSO}/V) corresponding to 60-70 mol % water (28-37% (V_{wa}/V)) observed for a wide range of properties, such as freezing point *(Hamvemeyer, 1966)*, density and viscosity *(Soper and Luzar, 1992)*. Kaatze at al., 1990 found a typically

minimum at mole fraction around 30% of DMSO (37% (V_{wa}/V)) for the adiabatic compressibility suggesting the existence of homogeneous hydrogen-bonded networks rather than the presence of stoichiometrically well-defined DMSO: $2H_2O$ complexes.

Soper and Luzar, 1992, could moreover demonstrate through a neutron diffraction study of DMSO-water mixture that although there is clearly some disordering of the water structure, the broadly tetrahedral coordination of water molecules remains intact: part of the hydrogen bonding has simply been transferred from the water-water complex to water-DMSO complex, and the proportion of this transfer increases with increasing concentration of DMSO (Fig.4.1)

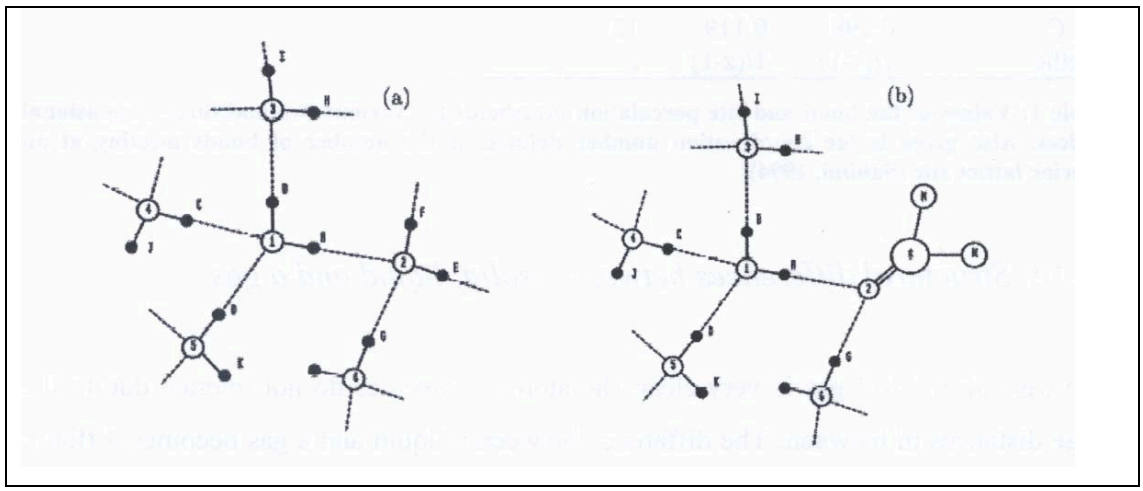

Figure 4.1: Schematic view of hydrogen bonding in pure water (a) and DMSO/water (b). Solid lines represent intermolecular bonds, dashed lines represent hydrogen bonds. In (a) water molecule 1 is coordinated by 5 other molecules, 2, 3, 4, 5 and 6, with the first four at roughly tetra-hedral positions the hydrogen A at the origin it sees 1 hydrogen (B) at 1.55 Å, 4 hydrogens (C, D, E, F) at ≈2.3 Å, 1 hydrogen (G) at ≈3.0 Å, and 4 hydrogens (H, I, J, K) at ≈3.8 Å, with a broad range of additional positions available due to the disorder. In (b) molecule 2 has been re-placed by DMSO molecule, which is roughly 50% larger than the water molecule it replaces and adds two or three lone pair electrons, but no hydrogens, to form hydrogen bonds. Now hydrogens E and F have disappeared, so substantially reducing the height of peaks at 2.3 Å and 3.8 Å, and, if DMSO contributes three lone pairs, emphasizing the peak at ≈ 3 Å. If DMSO were to form much stronger hydrogen bonds with water than water does to itself, this reduction in peak height should become marked at high concentration (Soper and Luzar, 1992).

Percolation thresholds of an ideal system occupied by isometric particles depends on the lattice type, the type of percolation (bond or site) and on the euclidean dimension of the lattice (see Table 4.1). In the following work only the case of site percolation is discussed. In an ideal system the lattice size is extremely large, i.e. infinite compared to the size of a unit lattice cell. Unfortunately, for most of the lattices the percolation thresholds (p_c) cannot be calculated in a straightforward way, but have to be estimated experimentally by computer simulation of such a lattice and its random occupation.

Lattice	Site	Bond	Coordination Number z
Honeycomb	0.696	0.653	3
Square	0.593	0.500	4
Triangular	0.500	0.347	6
Diamond	0.430	0.388	4
Simple cubic	0.312	0.249	6
BCC	0.246	0.180	8
FCC	0.198	0.119	12
Bethe	1/(z-1)	1/(z-1)	z

Table 4.1: Values of the bind and site percolation thresholds for various two and three dimentional lattices. Also given is the coordination number defined as the number of bonds meeting at an interior lattice site *(Sahimi, 1994)*

4.1.1. Percolation phenomena observed in the binary mixtures based on the results of the modified Clausius-Mossotti-Debye equation

The E_i/E-values for the investigated DMSO-water, DMAC-water, DMF-water and NMP-water binary mixtures at room temoerature (25°C) are represented in figures 4.2 – 4.5. The E_i/E-values can be subdivided in three linear segments. The intersections show the lower and upper percolation threshold. The lower intersection for all 4 solvents can be interpreted as the percolation threshold of water. The second one can be assumed as upper percolation threshold, where

DMSO, DMAC, NMP and DMF starts to form isolated clusters and is no longer percolating the system.

DMSO-water, DMAC-water, NMP-water and DMF-water mixtures represents one of the more complicated binary systems, namely an associating component (water) plus a second component (DMSO, DMAC, NMP and DMF) acting only as a hydrogen bond acceptor *(Luzar, 1990).*

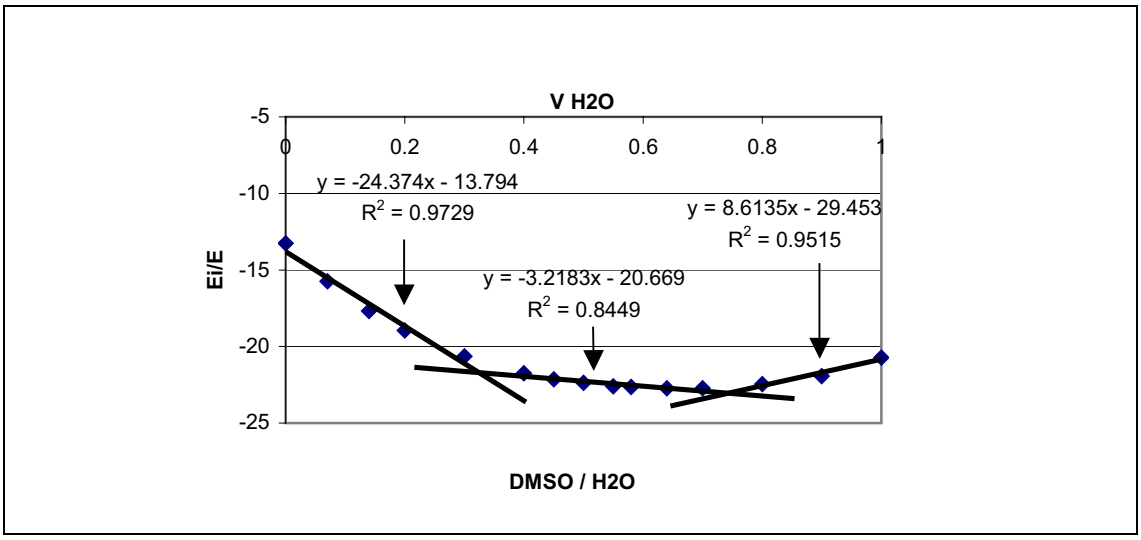

Figure 4.2: Ei/E values of the DMSO-water binary mixtures at 25°C. The intersections are located at ca. 0.32 and 0.74 (Vwa/V).

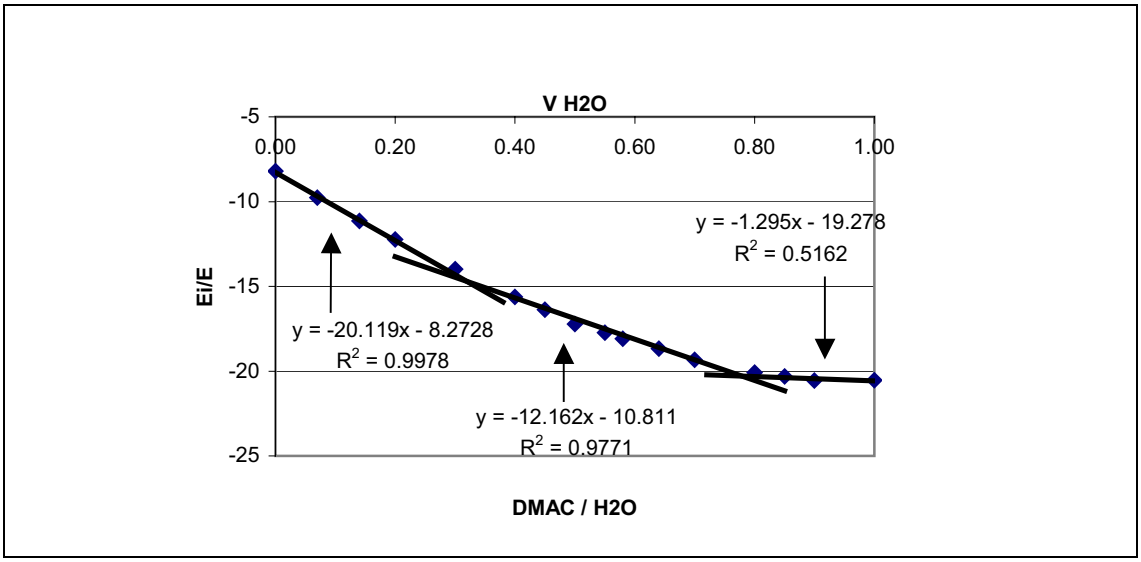

Figure 4.3: Ei/E values of the DMAC-water binary mixtures at 25°C. The intersections are located at ca. 0.32 and 0.78 (Vwa/V).

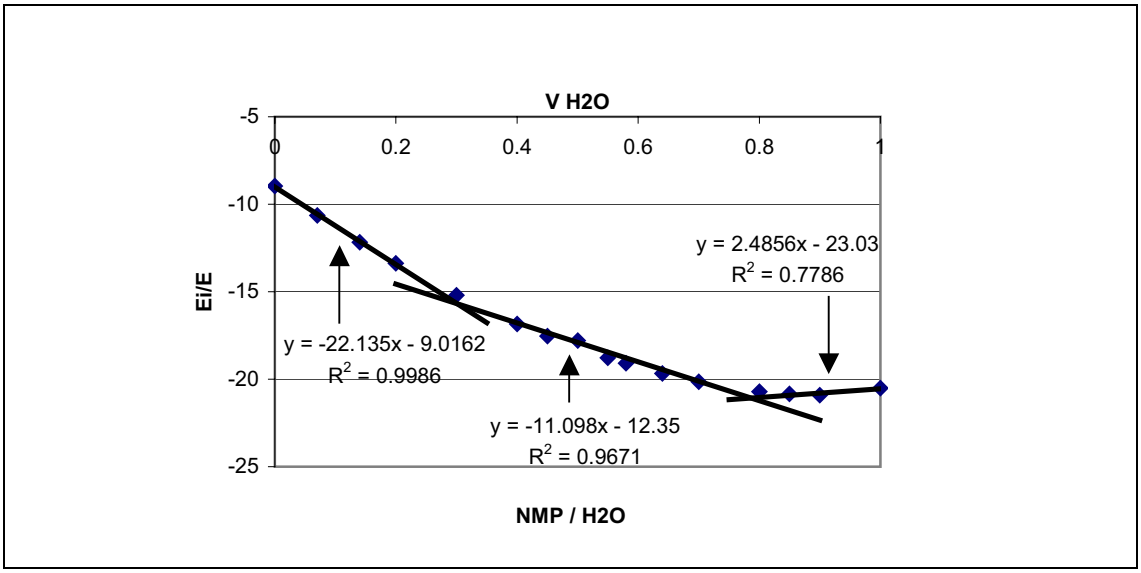

Figure 4.4: Ei/E values of the NMP-water binary mixtures at 25°C. The intersections are located at ca. 0.30 and 0.79 (Vwa/V).

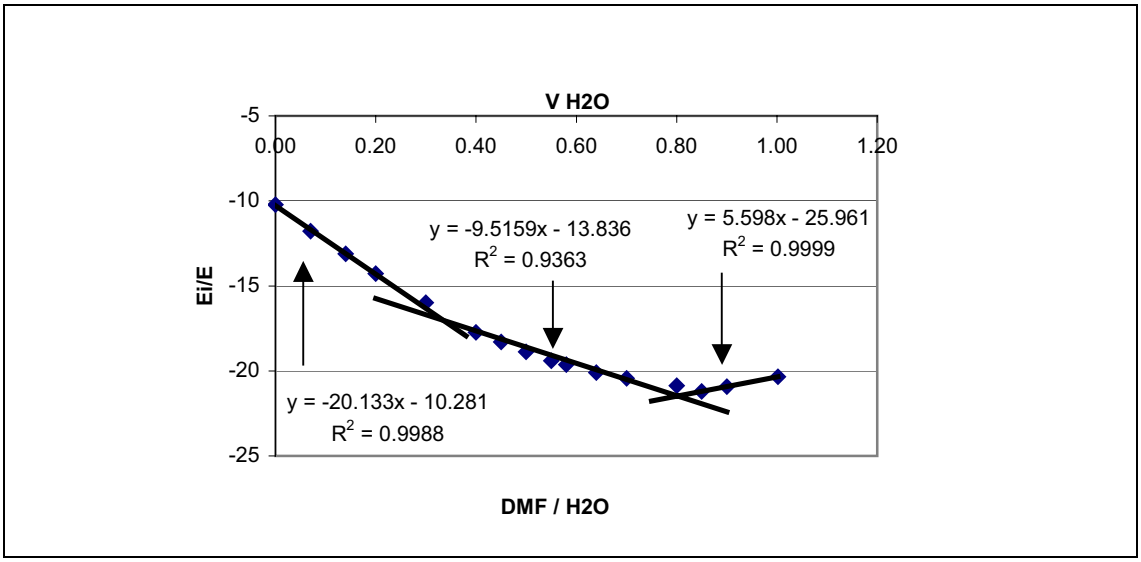

Figure 4.5: Ei/E values of the DMF-water binary mixtures at 25°C. The intersections are located at ca. 0.33 and 0.79 (Vwa/V).

It is interesting to compare the behavior of binary mixtures with1,4-dioxane and with water. In binary mixtures with 1,4-dioxaner there is only one percolation threshold observed which explains the concentration at which DMSO or its analogues start to form isolated cluster and it's no longer percolating in the system. This single percolation threshold is due to lack of dipoles in 1,4-

dioxane. These thresholds are detected at around 61% to 65% (V_{diox}/V). The results are presented in figures 4.6 – 4.9.

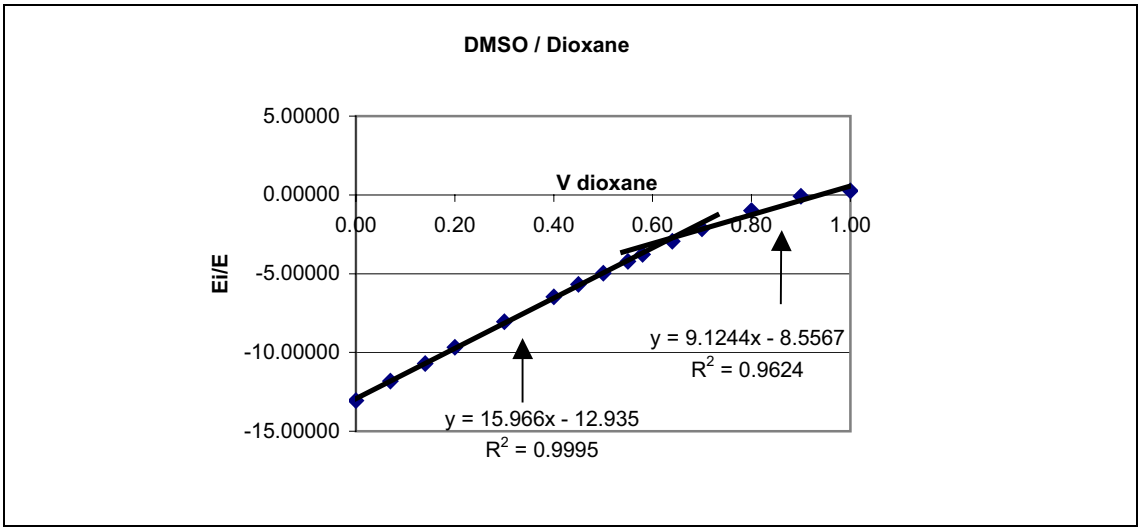

Figure 4.6: Ei/E values of the DMSO-1,4-dioxane binary mixtures at 25°C. The intersection is located at ca. 0.64 (Vwa/V)

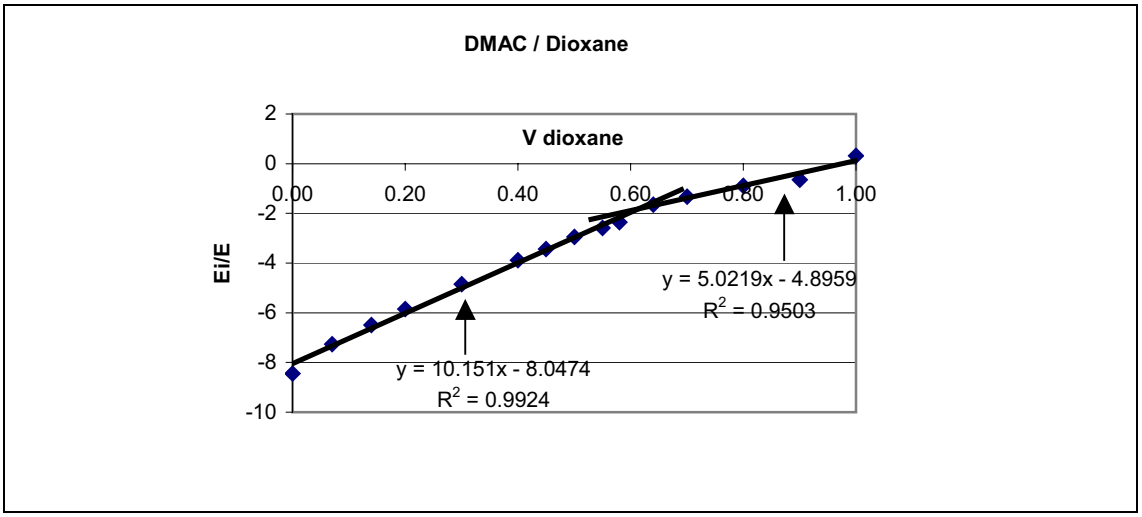

Figure 4.7: Ei/E values of the DMAC-1,4-dioxane binary mixtures at 25°C. The intersection is located at ca. 0.62 (Vwa/V)

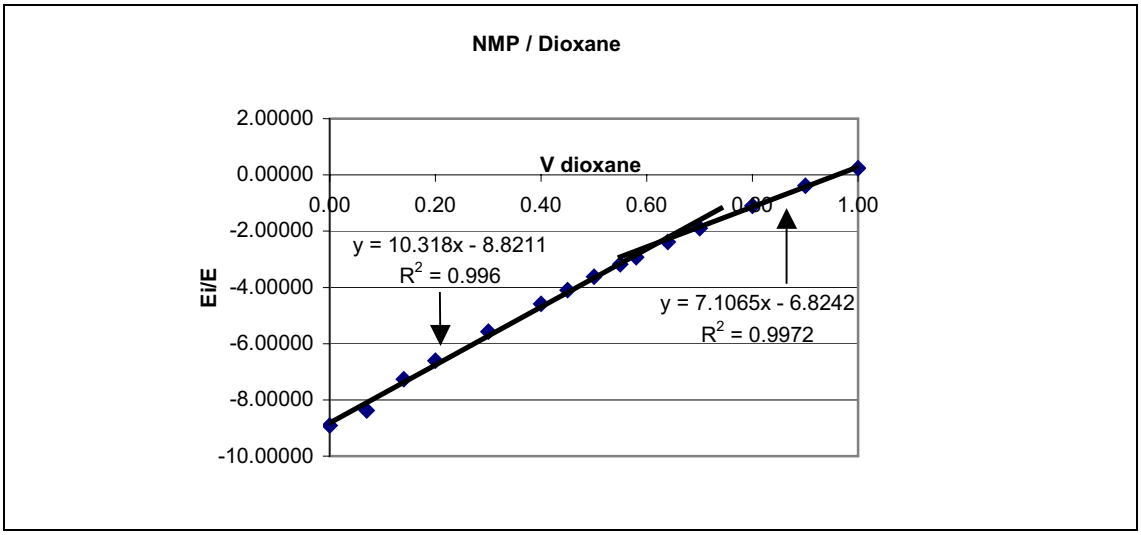

Figure 4.8: Ei/E values of the NMP-1,4-dioxane binary mixtures at 25°C. The intersection is located at ca. 0.62 (Vwa/V)

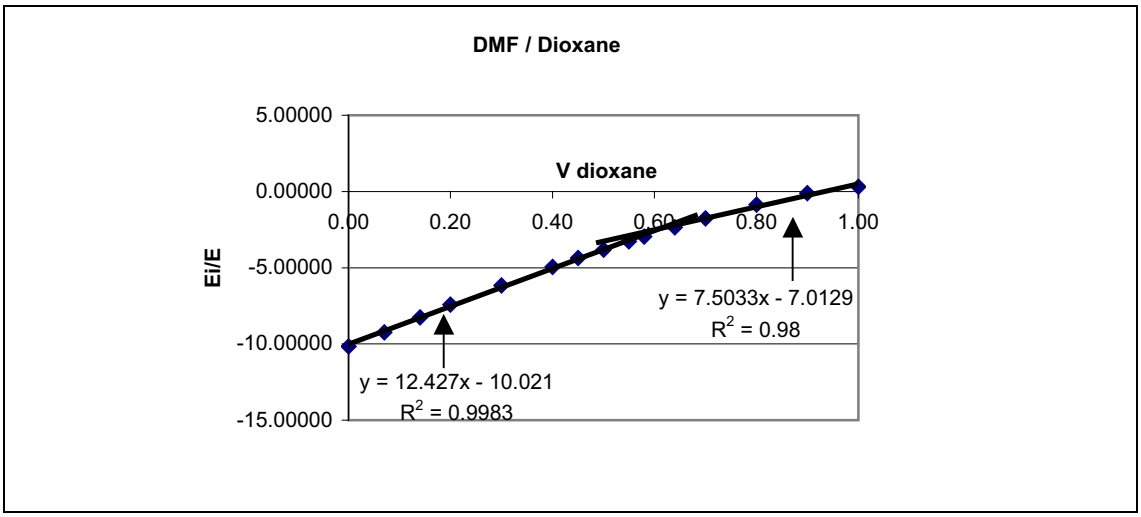

Figure 4.9: Ei/E values of the DMF-1,4-dioxane binary mixtures at 25°C. The intersection is located at ca. 0.61 (Vwa/V)

In 1,4-dioxane-water binary mixtures it is not possible to detect percolation threshold between 38% (V_{wa}/V) and 100% (V_{wa}/V). it is possible that water starts to percolate at ca 13% (V_{wa}/V), or that change of the "lattice structure" of the 1,4-dioxane-water system occurs. It can be shown that the water molecules form isolated island in a continuous phase of 1,4-dioxane as it is possible to get a better estimate of the dipole moment of water using the classical Debye equation for decreasing water concentration below 13% (V_{wa}/V). A second

critical concentration is observed at 38% (V_{wa}/V), which would correspond in fact to a percolation threshold of lattices with a coordination number close to 4 (diamond lattice). *(Hrenandez-perni, 2004).*

This as well explains the behavior of DMSO, DMAC, NMP and DMF binary mixtures in 1,4-dioxane, where only the percolation threshold of lattices with coordination number close to 4 where observed at around 40% ($V_{solvent}$/V).

In this context it has to be kept in mind that the structure of ice at normal pressure and close to 0°C corresponds to a tetrahedral configuration with the coordination number4.

According to the model of water described by a dynamic equilibrium of "nano-icebergs" which are formed and dissolve a coordination number of 4 can be adopted. The upper percolation threshold is not visible, which indicate that 1,4-dioxane fits well into the water as well as into DMSO and its analogues. It can be assumed that the volume of a single water cluster with 5 water units has a similar molar weight [mw = 90.10 gmol-1], and a similar volume as one 1,4-dioxane molecule [mw = 88.11 gmol-1]. *(Hrenandez-perni, 2004).*

With DMSO, DMAC, NMP and DMF-water binary mixtures both percolation threshold (respected solvent and water) can be detected: The lower one at ca. between 30% and 40% (V_{wa}/V) water and the upper one at between 74% and 82%(V_{wa}/V).

If the E_i/E values of the pure solvents are not taken into account the following percolation thresholds are obtained: for DMSO-water binary mixtures: the lower value at ca. 34% (V_{wa}/V), and the upper value at ca 66% (V_{wa}/V), for DMAC-water binary mixtures: the lower value at ca. 40% (V_{wa}/V), and the upper value at ca 78% (V_{wa}/V), for NMP-water binary mixtures: the lower value at ca. 32% (V_{wa}/V), and the upper value at ca 76% (V_{wa}/V) and for DMF-water binary mixtures: the lower value at ca. 43% (V_{wa}/V), and the upper value at ca 78%

(V_{wa}/V). If we consider our binary mixture being somehow structured it complies with the idea of having a critical concentration at between 32% (V_{wa}/V) and 43% (V_{wa}/V) for lower p_c respectively between 66%(V_{wa}/V) and 78%(V_{wa}/V) for the upper p_c, which corresponds to the percolation thresholds of a three dimentional lattice with a coordination number $z \approx 4$.

Thus, it can be concluded that DMSO and its analogues do not seem to induce a major disruption of the water structure. Btween the two percolation thresholds both components (solvent and water) percolate. Thus, more hydrophobic substances can be dissolved in the continuous phase of DMSO or its analogues. Thus, the special physiological properties of DMSO or its analogues with water mixtures may be related to the fact, that the water structure is not heavily modified.

It seems to be the case, that tetrahedral coordination remains intact *(Soper and Luzar, 1992)* within the whole range of DMSO or any of its analogues with water mixture. On the other hand, E_i/E decreases to a minimum at the upper percolation threshold indicating a higher local electric field E_i. This effect can be related to the high dipole moment of DMSO and its analogues. This dipole moment is also responsible for the different behavior of these solvents in water compare to mixtures with 1,4-dioxane.

In addition, we also studied THF and Sulfolane as standard example of binary mixtures with water which clearly posses a single percolation threshold. In case of THF, it clearly demonstrated that a single percolation treshold occurs at ca. 27% (V_{wa}/V) and in case of Sulfolane at ca. 79% (V_{wa}/V). Result is shown in Fig. 4.10.

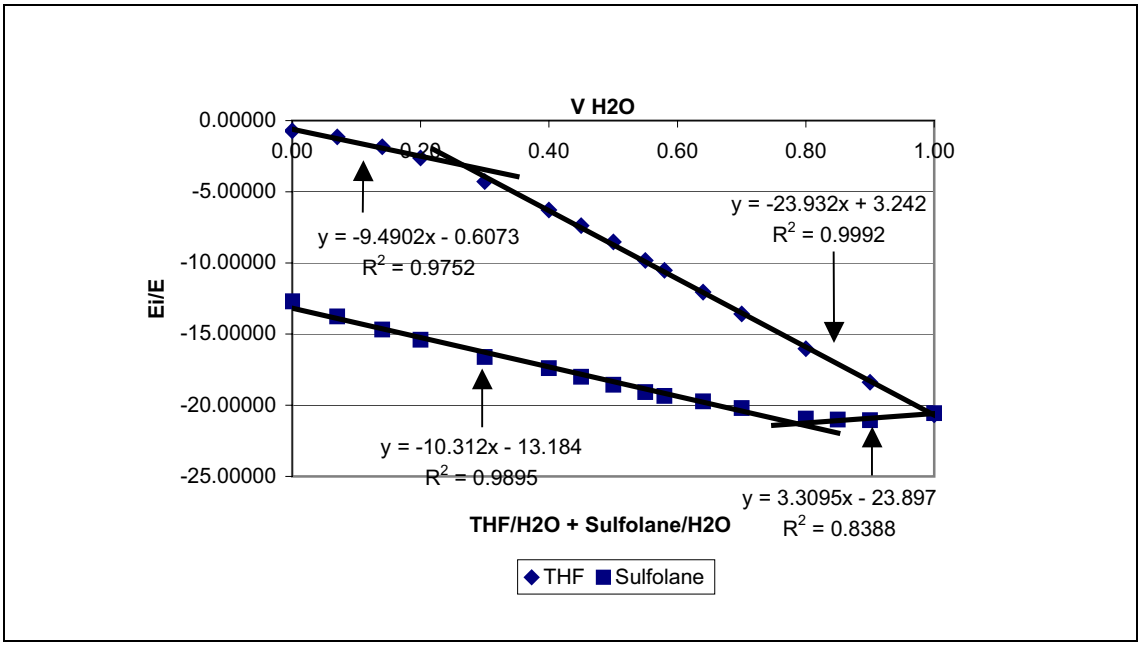

Figure 4.10: Ei/E values of the THF-water binary mixtures at 25°C. The intersection is located at ca. 0.27 (Vwa/V) and Ei/E values of the Sulfolane-water binary mixtures at 25°C. The intersection is located at ca. 0.79 (Vwa/V).

4.1.2. Percolation phenomena observed in the binary mixtures based on the results of g-values according to the Kirkwood-Fröhlich equation

The g-values for the binary mixtures of DMSO and its analogues with water at room temperature (25°C) are presented in figures 4.11 – 4.14. The curve can be subdivided into three linear segments. The intersections of the linear segments are located at ca. 35% (V_{wa}/V) and ca. 77% (V_{wa}/V) for DMSO-water mixtures, at ca. 37% (V_{wa}/V) and ca. 77% (V_{wa}/V) for DMAC-water mixtures, at ca.50% (V_{wa}/V) and ca. 78% (V_{wa}/V) for NMP-water mixtures and at ca. 36% (V_{wa}/V) and ca. 77% for DMF-water binary mixtures.

These findings are compatible with the findings of E_i/E at 4.1.1 for the lower and upper p_c as it is well known that the location of the critical concentrations may be influenced by the sensitivity of the parameter to be chosen to detect the p_c.

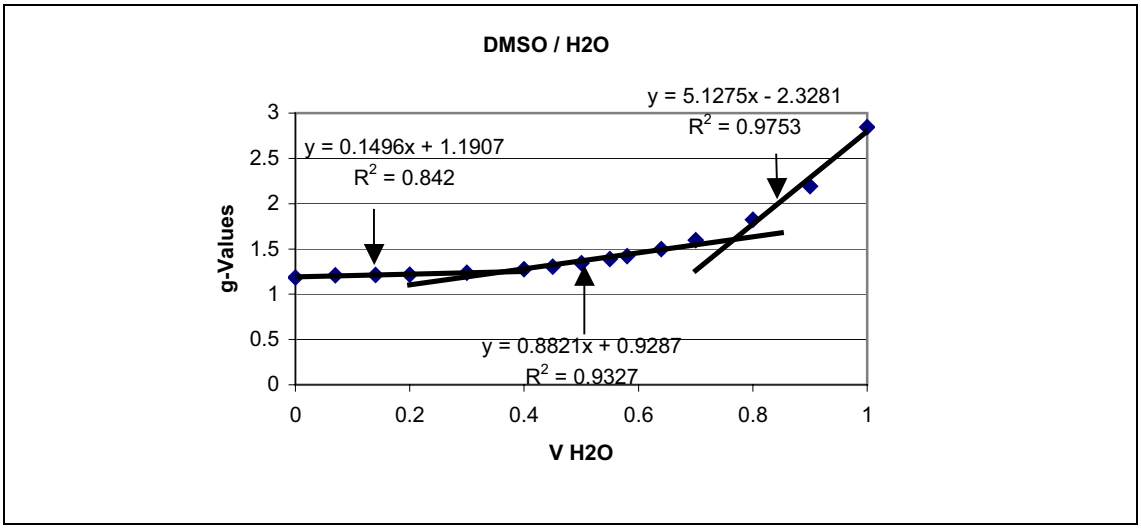

Figure 4.11: The values of the correlation factor g of the Kirkwood-Frölich Eq. For the binary mixture of DMSO-water with intersections at ca. 0.35 and 0.77 (Vwa/V) at 25°C.

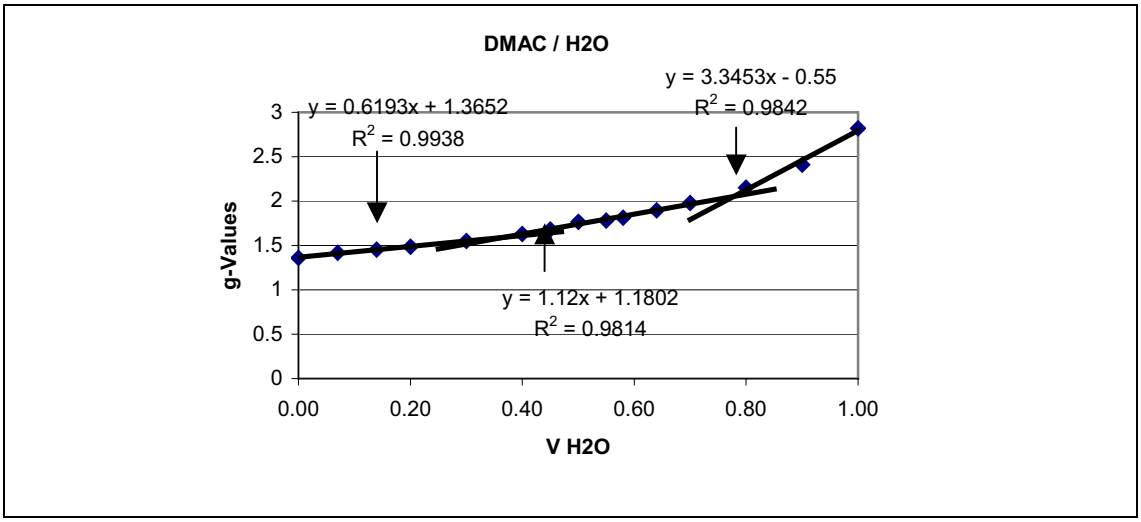

Figure 4.12: The values of the correlation factor g of the Kirkwood-Frölich Eq. For the binary mixture of DMAC-water with intersections at ca. 0.37 and 0.77 (Vwa/V) at 25°C.

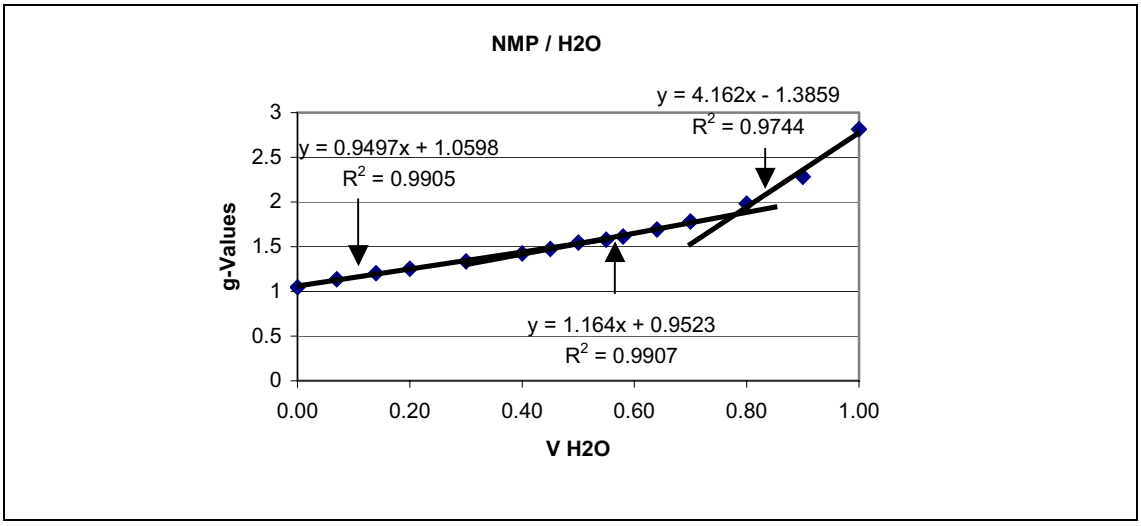

Figure 4.13: The values of the correlation factor g of the Kirkwood-Frölich Eq. For the binary mixture of NMP-water with intersections at ca. 0.50 and 0.78 (Vwa/V) at 25°C.

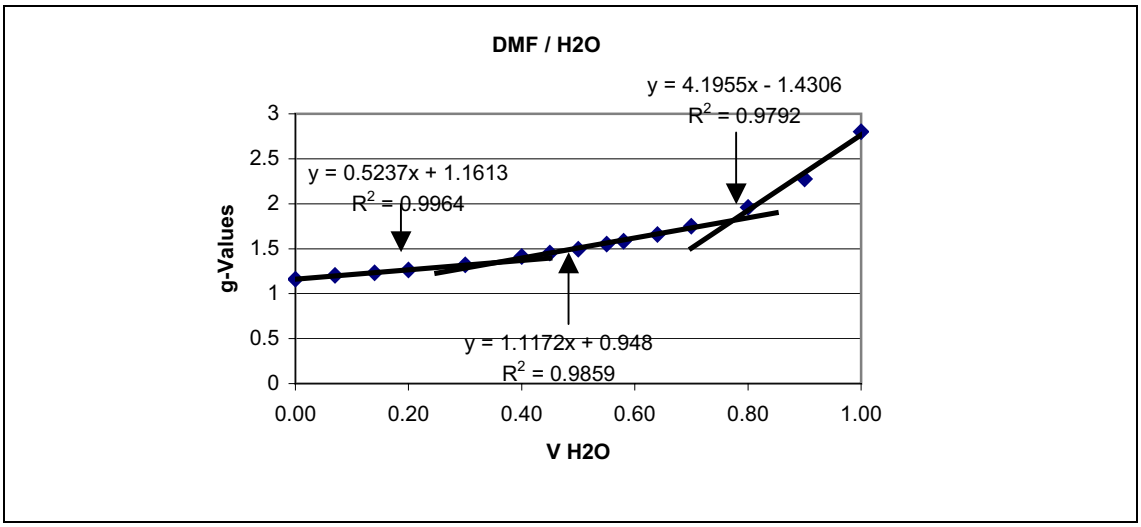

Figure 4.14: The values of the correlation factor g of the Kirkwood-Frölich Eq. For the binary mixture of DMF-water with intersections at ca. 0.36 and 0.77 (V_{wa}/V) at 25°C.

Unlike polar liquids capable of forming hydrogen bonds *(Stengele st al., 2002)* such as diglycerol in a mixture with water, the aprotic DMSO and its analogues behave differently with respect to the g-values (see figures 4.11 – 4.14). In case of DMSO and the analogues we find a region nearly constant to with g-values close to g ≈ 1 till around 35 % (V_{wa}/V) (differs slightly in 4 solvents). Thus, this finding confirms that there is no structural breaking effect of DMSO or any of the analogues structures by adding water. Below 35% (V_{wa}/V), i.e. below lower

percolation threshold the water molecules fit well into the solvent (DMSO, DMAC, NMP and DMF) structure of liquid. Due to the value of g ≈ 1 the water molecules are either randomly distributed in the solvent mixture or in an antiparallel alignment with the dipole moment of DMSO, DMAC, NMP or DMF.

Above the critical concentration of 35% (V_{wa}/V) the g-values are increasing i.e. the dipole moments of water and DMSO, DMAC, NMP or DMF assume more and more a parallel alignment. A parallel alignment of the dipole moments is being form due to the increase in the hydrogen bonding formation. From the point of view of percolation theory around 35% (V_{wa}/V) corresponds with the lower percolation threshold, where water starts to form infinite clusters, both water and the solvent (DMSO, DMAC, NMP and DMF) percolate the system up to around 77% (V_{wa}/V) where the second percolation threshold is found. From that point solvent (DMSO, DMAC, NMP and DMF) starts to form isolated clusters and is no longer percolating the system.

Like in 4.1.1 THF and Sulfolane binary mixtures with water were investigate. It shows 2 clear percolation thresholds in respect to g-values in case of THF-water mixtures, which showed a single threshold in respect to E_i/E. The lower threshold is at ca. 32% (V_{wa}/V) and upper at ca.67% (V_{wa}/V). For Sulfolane-water mixtures we still could detect only one percolation threshold in respect to g-values and it's located at ca. 76% (V_{wa}/V), same as in respect to E_i/E interpretation. Fig 4.15 demonstrates the results.

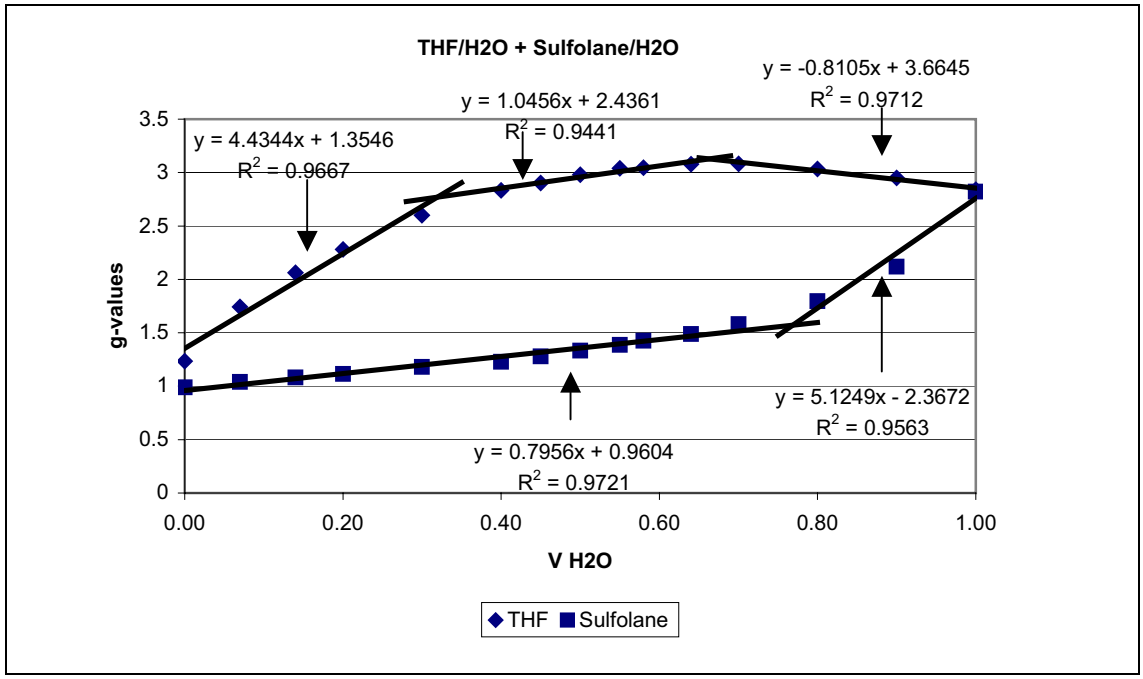

Figure 4.15: The values of the correlation factor g of the Kirkwood-Frölich Eq. For the binary mixture of THF-water with intersections at ca. 0.32 and 0.66 (Vwa/V) and for the binary mixture of Sulfolane-water with intersection at ca. 0.76 (Vwa/V) at 25°C.

4.1.3. Relaxation time according to the Debye equation for the complex dielectric permitivity ε^*

The Debye equation is able to characterize the whole range of DMSO or any of its analogues with water binary mixtures with $R^2 \geq 0.970$ showing with respect to the relaxation time (τ) a lower percolation threshold between ca. 24% (V_{wa}/V) (in case of DMAC-water mixtures) and 32% (V_{wa}/V) (in case of DMSO-water mixtures) and upper percolation threshold around ca. 73% (for DMSO, DMAC and NMP mixtures with water). Exception is DMF-water mixtures, which shows a single percolation threshold at ca. 34% (V_{wa}/V), upper threshold was not observed in this case. (See 4.2.3). Fig 4.16 shows these results in respect to relaxation time (τ).

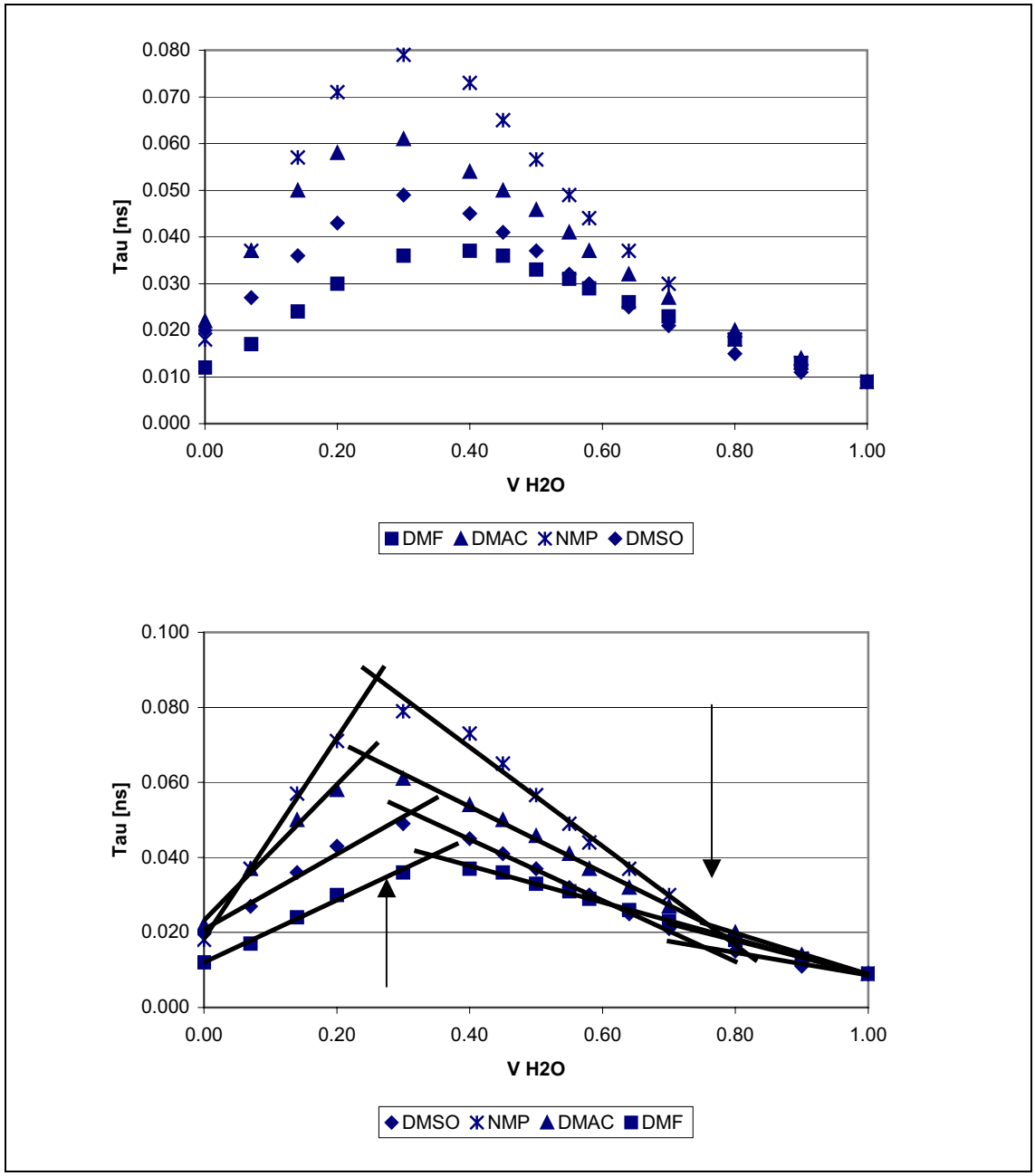

Figure 4.16: Relaxation behavior of the dipole of DMSO, DMAC, NMP and DMF in water mixtures as a function of the volume fraction of water (V_{wa}/V) with intersections at ca. 0.31 and 0.75 (V_{wa}/V) for DMSO mixtures, at ca. 0.24 and 0.76 (V_{wa}/V) for DMAC mixtures, at ca. 0.26 and 0.78 (V_{wa}/V) for NMP mixtures and at ca. 0.34 (V_{wa}/V) for DMF mixtures at 25°C which can be described by the Debye equation.

It is of interest to point out that in the case of the methanol-water mixtures the behavior of the relaxation time can be only described by a single Debye equation with a $R^2 \geq 0.997$ between 58%-100% (V_{wa}/V)*(Hernandez-Perni,*

2004). The fact that Debye equation is able todescribe the whole range of DMSO-water or its analogues with water mixtures is another strong evidence that the lattice type seems to remain intact. It is worth to realize that the percolation thresholds remain more or less at the same position independent of the choice of the parameters for their detection.

In case of mixtures with 1,4-dioxane, there are no clear threshold observed. This in fact shows the dominant of the solvents (DMSO, DMAC, NMP and DMF) in the whole concentration range. In the other hand, this also proves that the lack of dipoles in 1,4-dioxane is responsible for the different behavior of these solvents in water compare to mixtures with 1,4-dioxane. Fig 4.17 show the results.

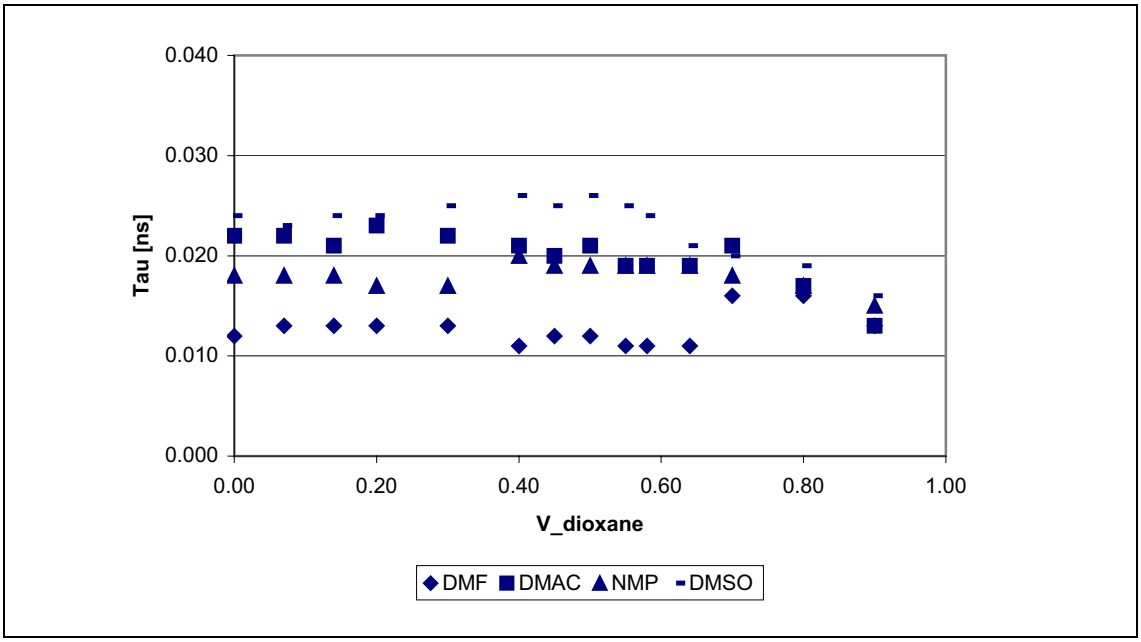

Figure 4.17: Relaxation behavior of the dipole of DMSO, DMAC, NMP and DMF in 1,4-dioxane mixtures as a function of the volume fraction of 1,4-dioxane (V_{diox}/V) at 25°C which can be described by the Debye equation.

THF and Sulfolane-water binary mixtures were also studied using simple Debye equation with mean $R^2 \geq 0.970$.The lower percolation threshold was detected at ca. 32% (V_{wa}/V) in case of THF-water mixtures. The upper percolation threshold

is at ca. 54% for THF-water mixtures and the single percolation threshold for Sulfolane-water mixtures is at ca. 76% for. Fig. 4.18 shows the results.

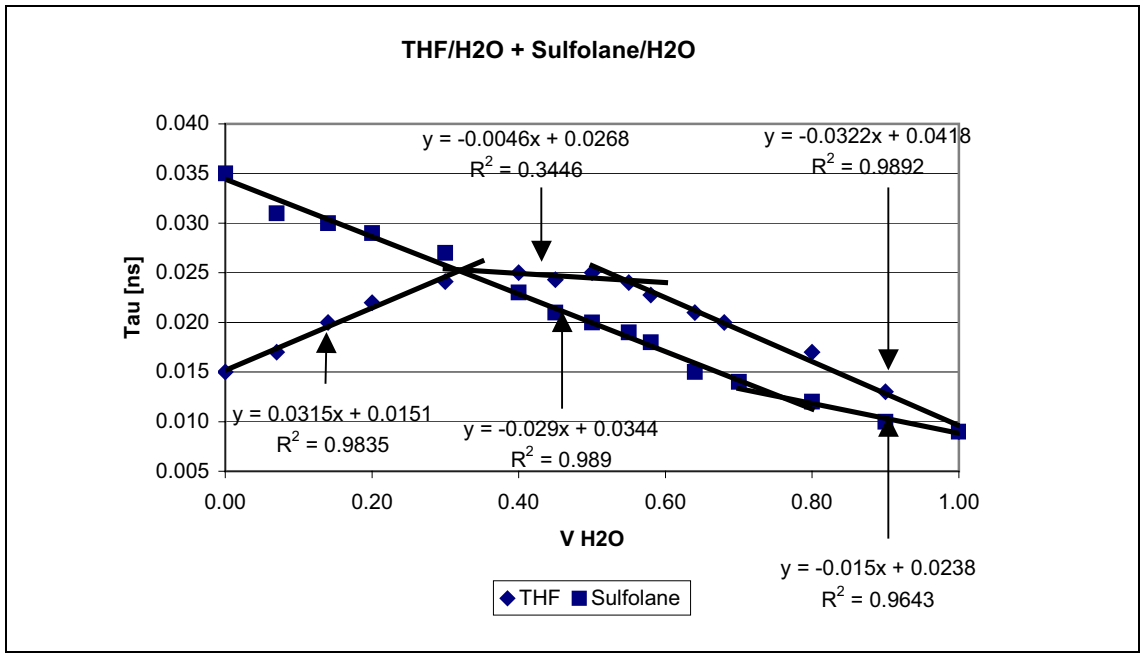

Figure 4.18: Relaxation behavior of the dipole of THF and Sulfolane in water mixtures as a function of the volume fraction of water (V_{wa}/V) with intersections at ca. 0.32 and 0.54 (V_{wa}/V) for THF mixtures and at ca. 0.76 (V_{wa}/V) for Sulfolane mixtures at 25°C which can be described by the Debye equation.

4.1.4. Conclusions

It is demonstrated the important role of the E_i/E parameter in the characterization of not only polar liquids able to form hydrogen bonds but also aprotic liquids being an easier measurable alternative parameter to describe the polarity of liquids.

The phenomenon of percolation could be well demonstrated in case of binary mixtures of DMSO, DMAC, NMP and DMF with water.

The value of E_i/E at room temperature in the binary mixtures can also be related to the viscosity changes, which was earlier shown by Peyrelasse et al., to be percolation phenomenon.

It was possible to clarify the maximum value of viscosity detected around 33% fraction in DMSO (34% (V_{wa}/V)) in the frame of percolation theory. This was possible by measuring the following parameters: E_i/E parameters obtained through the modified Clausius-Mossotti-Debye equation, g-values obtained from Kirkwood-Frölich equation, relaxation time using dielectric spectroscopy. The results are listed together with litreture data concerning the viscosity, adiabatic compressibility and freezing point of binary solvent mixtures. The values of the lower and upper percolation thresholds are comparable and it is of interest, that as a function of the parameter studied, only one or two percolation thresholds can be detected.

In Hernandez-Perni et al., we saw that for 1,4-dioxane-water binary mixtures, the upper percolation threshold is not visible, which indicates that 1,4-dioxane fits well into the water. With DMSO or any of its analogues binary mixtures with water both percolation thresholds can be detected. Nevertheless, it seems to be the case, that the tetrahedral coordination remains intact. For DMSO or any of its analogues binary mixtures with water we also observed that the value of E_i/E decrease to a minimun at the upper percolation thresholds indicating a higher local electric field E_i. This effect can be related to the high dipole moments of these solvents.

Unlike polar liquids capable of forming hydrogen bonds *(Stengele et al., 2002)* such as diglycerol in a mixture with water, the aprotic solvents (DMSO, DMAC, NMP and DMF) behave differently with respect to the g-values. Here we find a region nearly constant with g-values close to $g \approx 1$ till ca. around 35% (V_{wa}/V). Thus, there seems to be no structure breaking effect of the DMSO or any of its analogues structure by addind water. Below the lower percolation threshold the water molecules fit well into the DMSO or any of the analogues structure of the liquid. Due the value of $g \approx 1$ the water molecules are either randomly distributed in the solvent mixture or in an antiparallel alignment with dipole moments of the solvents (DMSO, DMAC, NMP and DMF). It can be concluded

that DMSO or any of its analogues and water have as a liquid similar lattice structure with a coordination number 4, which facilitates the complete miscibility and seem to be one of the reason for the special physiological behavior of DMSO-water mixtures and similarities can be seen with the aqueous binary mixtures of DMSO analogues.

As a final conclusion it is demonstrated that the use of percolation theory reveling percolation thresholds give insight into the “lattice structure” of DMSO or its analogues binary mixtures with water and contribute to lift a bit the mystery of the behavior of these binary mixtures. Nonetheless, it was clearly demonstrated that DMSO, DMAC, NMP and DMF behave very similarly in aqueous environment as well in 1,4-dioxane surroundings.

4.2. Investigation of Formamide and its mono & dimethylated form in water using dielectric spectroscopy

Formamide, also known as methanamide, is an amide derived from formic acid. It is a clear liquid which is miscible with water and has an ammonia-like odor. It is used primarily for manufacturing sulfa drugs and synthesizing vitamins and as a softener for paper and fiber. In its pure form, it dissolves many ionic compounds that are insoluble in water, so it is also used as a solvent. Formamide is also a constituent of cryoprotectant vitrification mixtures used for cryopreservation of tissues and organs. Formamide is also used as an RNA stabiliser in gel electrophoresis by deionizing RNA. Another use is to add it in sol-gel solutions in order to avoid cracking during sintering. *(www.wikipedia.com)*

Dimethylformamide (DMF, N,N-dimethylformamide) is a clear liquid, miscible with water and majority of organic solvents. It is a common solvent that is often used in chemical reactions. Pure dimethylformamide is odorless while technical grade or degraded dimethylformamide often has a fishy smell due to dimethylamine impurities. Its name is derived from the fact that it is formamide

(the amide of formic acid) with two methyl group substitutions, both of them on the N (nitrogen) atom. Dimethylformamide is a polar (hydrophilic) aprotic solvent with a high boiling point.

Dimethylformamide is synthesized from formic acid and dimethylamine. Dimethylformamide is not stable in the presence of strong bases like sodium hydroxide or strong acids like hydrochloric acid or sulfuric acid and is hydrolyzed back into formic acid and dimethylamine, especially at elevated temperatures. The primary use of dimethylformamide is as a solvent with low evaporation rate.

Dimethylformamide is used in the production of acrylic fibers and plastics. It is also used as a solvent in peptide coupling for pharmaceuticals, in the development and production of pesticides, and in the manufacture of adhesives, synthetic leathers, fibers, films, and surface coatings. It is used as a reagent in the Bouveault aldehyde synthesis and in the Vilsmeier-Haack reaction, another useful method of forming aldehydes.DMF penetrates most plastics and makes them swell. It therefore frequently occurs as a component of paint strippers.

N,methylformamide is a colorless toxic liquid, which is used as a polar solvent (e.g. Karl-Fischer method). It is an amide of the formic acid and has analogical properties to Formamide. *(www.wikipedia.com)*

N,methylformamide shows certain anti-tumor effect and is therefore object of actual medical research.

DMF has been linked to cancer in humans, and it is thought to cause birth defects. In some sectors of industry women are banned from working with DMF. For many reactions, it can be replaced with dimethyl sulfoxide.

We chose Formamide, N,methylformamide and N,N,dimethylformamide to investigate the effect of additions of methyl groups, and also to investigate the

percolation phenomenon on these molecules with relative high complex permittivity and their effect on the structure of water.

4.2.1. Percolation phenomena observed in the binary mixtures of Formamide and methylated forms (Mono and Dimethylated) based on the results of the modified Clausius-Mossotti-Debye equation

The Ei/E-values for the investigated Formamide-water, N,methylformamide-water and N,N,dimethylformamide-water binary mixtures at room temperature (25°C) are represented in figures 4.19-4.21. The Ei/E-values can be subdivided in three linear segments for DMF and in two linear segments for Formamide and N,methylformamide. The intersections clearly shows the lower and upper percolation threshold in case of DMF, while in Formamide and N,methylformamide only lower percolation threshold around that of DMF could be detected in respect to E_i/E values. As we said in 4.1.1 of this chapter, the lower intersection (single intersection in case of Formamide and N,methylformamide) can be interpreted as the percolation threshold of water. The second one can be assumed as upper percolation threshold, where DMF starts to form isolated clusters and is no longer percolating the system, which this could not be observed in case of the other two solvents by interpretation of the E_i/E values.

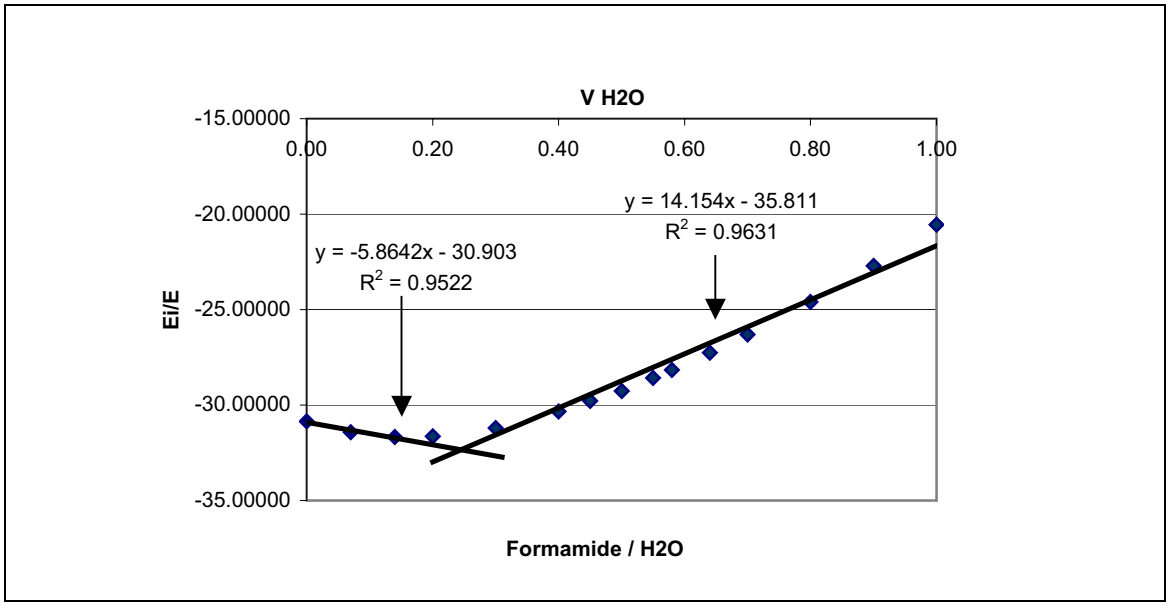

Figure 4.19: E_i/E values of the Formamide-water binary mixtures at 25°C. The intersection is located at ca. 0.24 (V_{wa}/V).

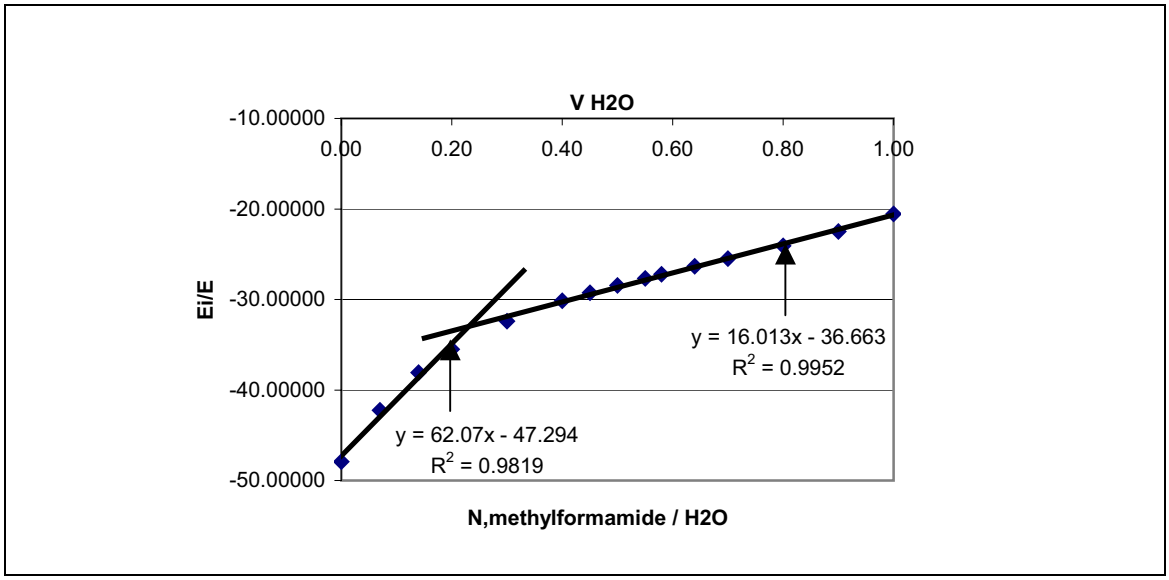

Figure 4.20: E_i/E values of the N,methylformamide-water binary mixtures at 25°C. The intersection is located at ca. 0.23 (V_{wa}/V).

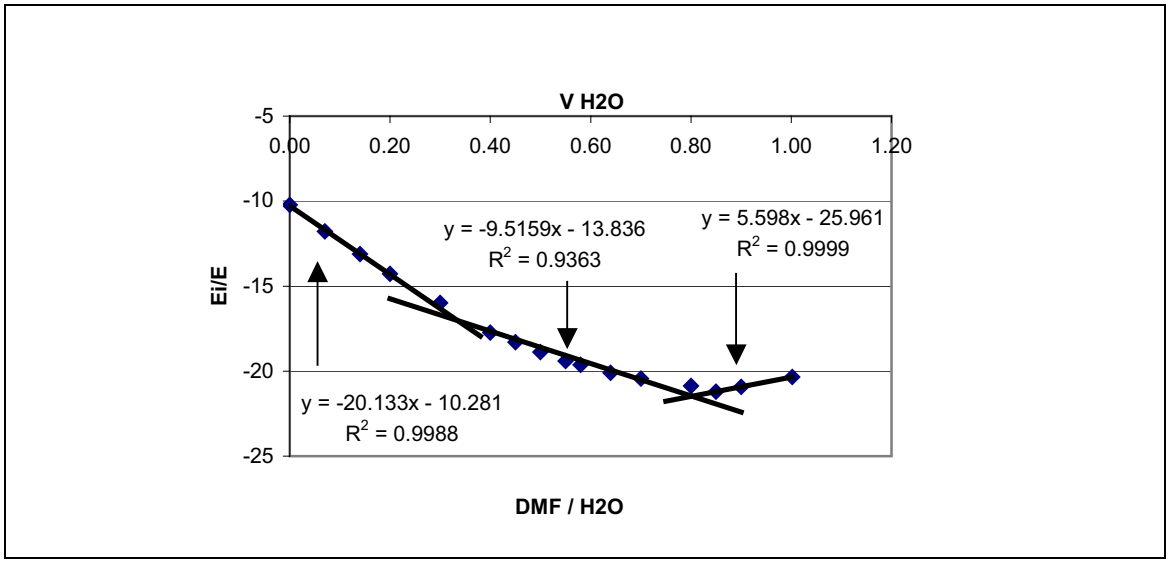

Figure 4.21: E_i/E values of the DMF-water binary mixtures at 25°C. The intersections are located at ca. 0.33 and 0.79 (V_{wa}/V).

These binary mixtures represent one of the more complicated binary systems, namely an associating component (water) plus a second component (Formamide, N,methylformamide and DMF) acting only as hydrogen bond acceptor as was assumed by *Luzar, 1990.*

These results clearly show that by addition of the first methyl group to the formamide structure an increase in dielectric constant ($\varepsilon_{formamide}$= 109.5, $\varepsilon_{N,methylformamide}$= 182.4) appears which will be hugely decreased by addition of the second methyl group to the structure (ε_{DMF}= 37). This phenomenon can be also observed by E_i/E-values, while by addition of the second methyl group to the structure the second percolation threshold (upper p_c) becomes visible and the solvent starts to form isolated clusters and is no longer percolating the system.

4.2.2. Percolation phenomena observed in the binary mixtures of Formamide and methylated forms based on the results of g-values according to the Kirkwood-Fröhlich equation

The g-values for the binary mixtures of Formamide-water, N,methylformamide-water and N,N,dimethylformamide-water at room temperature (25°C) are presented in figure 4.22-4.24. The curve can be subdivided into three linear segments. The intersections of the linear segments are located at ca. 43% (V_{wa}/V) and at ca. 77% (V_{wa}/V) for Formamide-water mixtures (one can assume that only the upper percolation threshold is visible using g-values), at ca. 23% (V_{wa}/V) and at 68% (V_{wa}/V) for N,methylformamide-water mixtures and at ca. 36% (V_{wa}/V) and ca.77% (V_{wa}/V) for DMF-water binary mixtures.

These findings are not compatible with the findings of E_i/E at 4.2.1 as it is well known that the location of the critical concentrations may be influenced by the sensitivity of the parameter to be chosen to detect the p_c and in this case the upper percolation threshold is clearly more detectable than the lower one in case of Formamide and DMF binary systems.

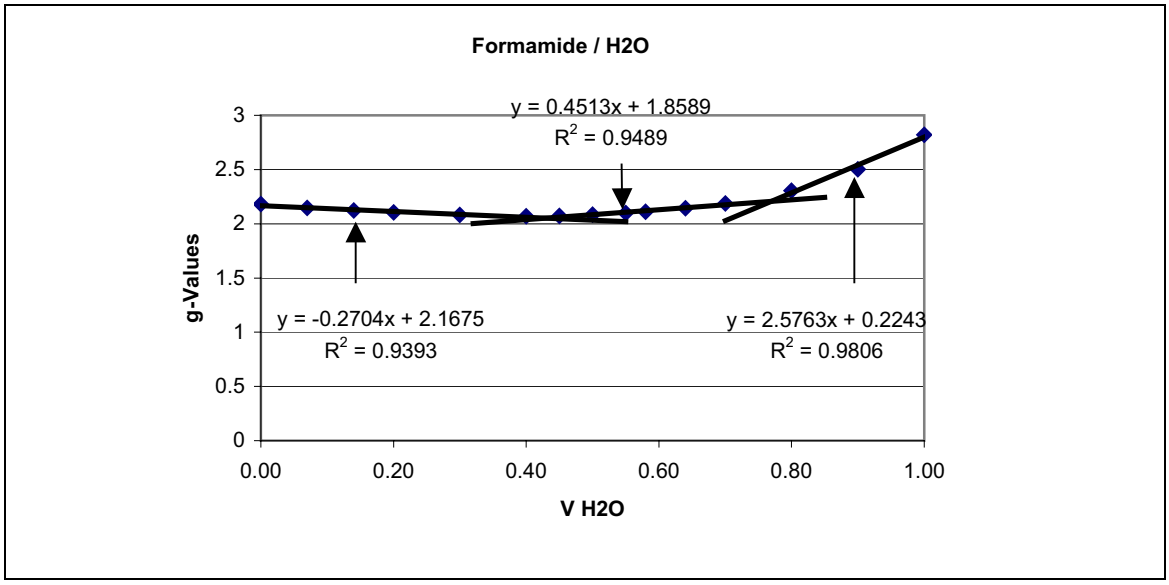

ıure 4.22: The values of the correlation factor g of the Kirkwood-Frölich Eq. For the binary mixture of rmamide-water with intersections at ca. 0.43 and 0.77 (V_{wa}/V) at 25°C.

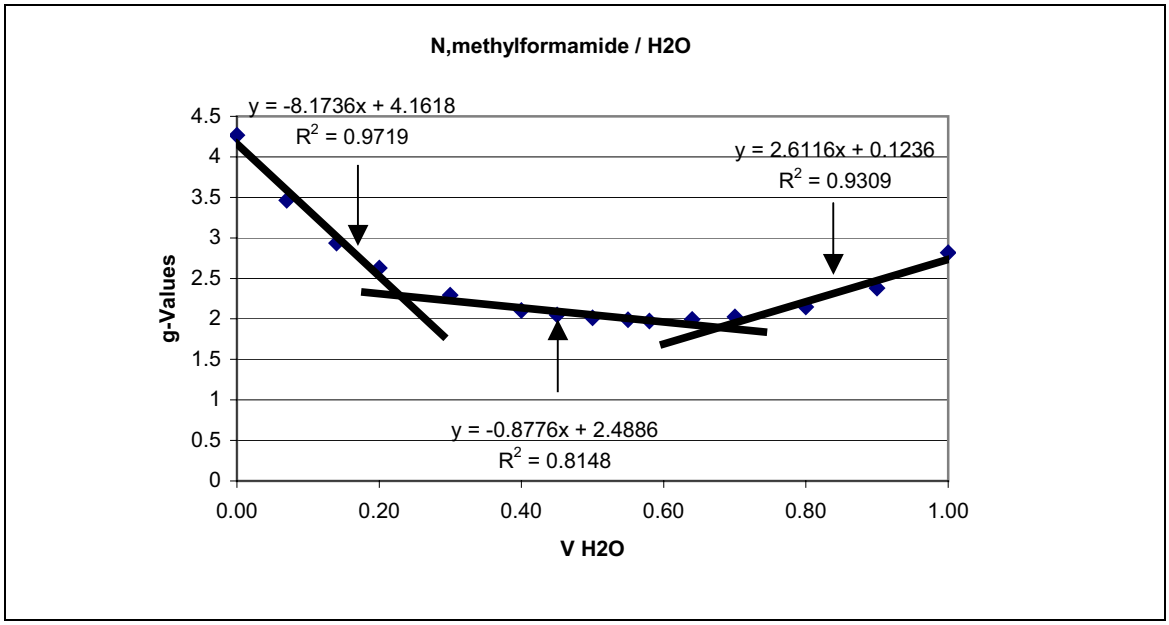

Figure 4.23: The values of the correlation factor g of the Kirkwood-Frölich Eq. For the binary mixture of N,methylformamide-water with intersections at ca. 0.23 and 0.68 (V_{wa}/V) at 25°C.

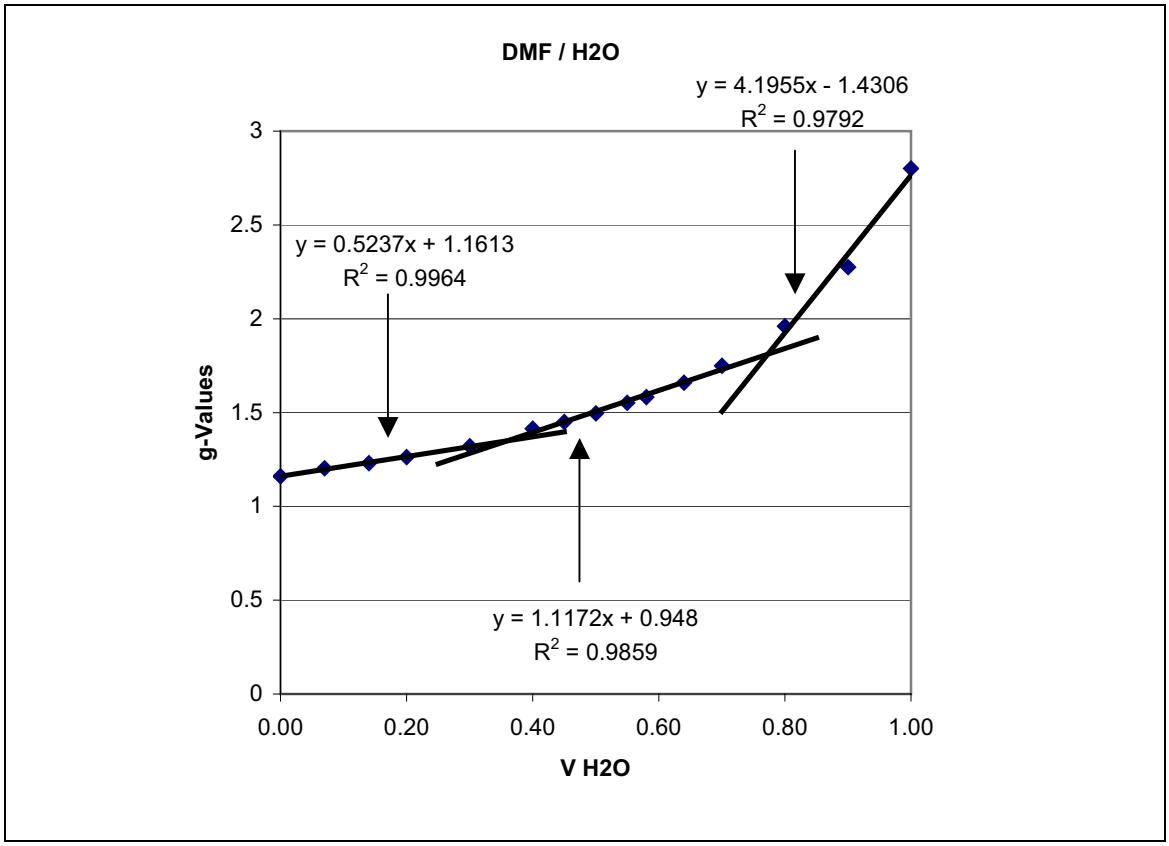

Figure 4.24: The values of the correlation factor g of the Kirkwood-Frölich Eq. For the binary mixture of DMF-water with intersections at ca. 0.36 and 0.77 (V_{wa}/V) at 25°C.

As it was mentioned before, g-values gives us information about the arrangements of the molecules. It can only be applied to polar molecules, as the calculation of g makes a division by μ_g necessary. Thus it leads to not defined values for $\mu_g = 0$ and suggests very high values for mixtures with a high content of a nonpolar liquid, such as 1,4-dioxane / water *(Stengele A. 2002).*

The increasing length of a linear chain leads to a higher preference of a parallel arrangement. This could be caused by molecules with longer nonpolar groups favouring a parallel alignment, as this allows both a separate grouping of the nonpolar and polar structures and a dense packing *(Stengele A. 2002)*.

This is also the case here with addition of a methyl group to the Formamide structure.

It can be concluded that g-values provides valuabale information about the arrangements of molecules, but it must be kept in mind that the resulting number is an overall average, meaning that strong effects can cancel each other out.

4.2.3. Relaxation time of Formamide and methylated forms according to the Debye equation for the complex dielectric permitivity ε*

The Debye equation is able to characterize the whole range of Formamide, N,methylformamide and DMF with water binary mixtures with $R^2 \geq 0.980$ showing with respect to the relaxation time (τ) one visible percolation threshold at around 34% (V_{wa}/V) for all three solvents (lower percolation threshold). Figure 4.25 shows the results in respect to the relaxation time (τ) [ns].

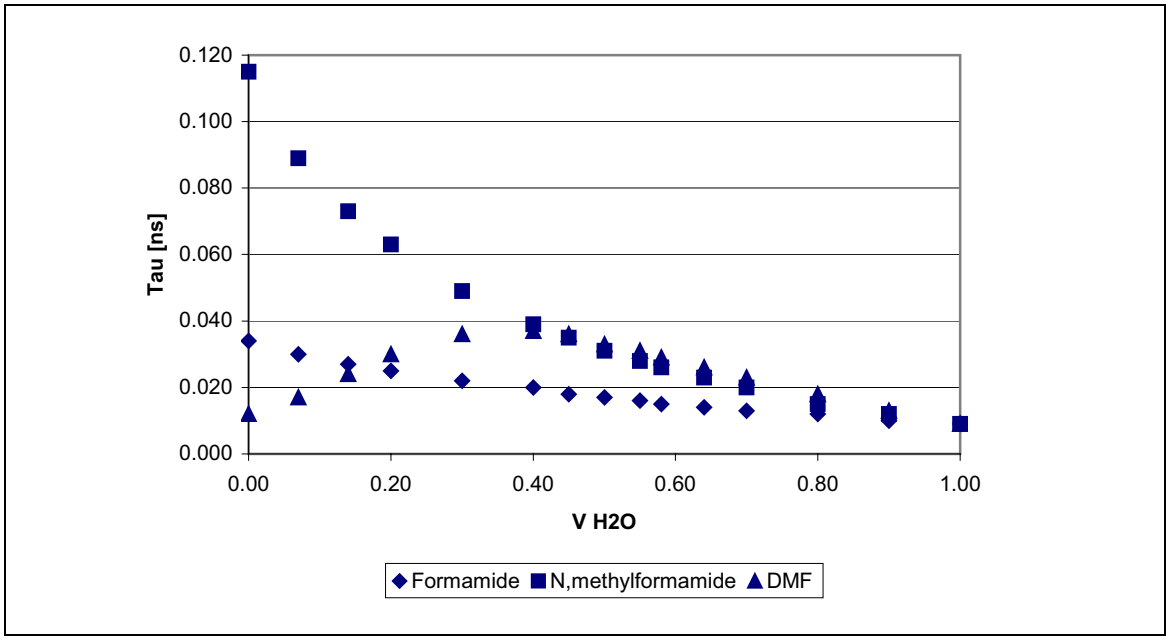

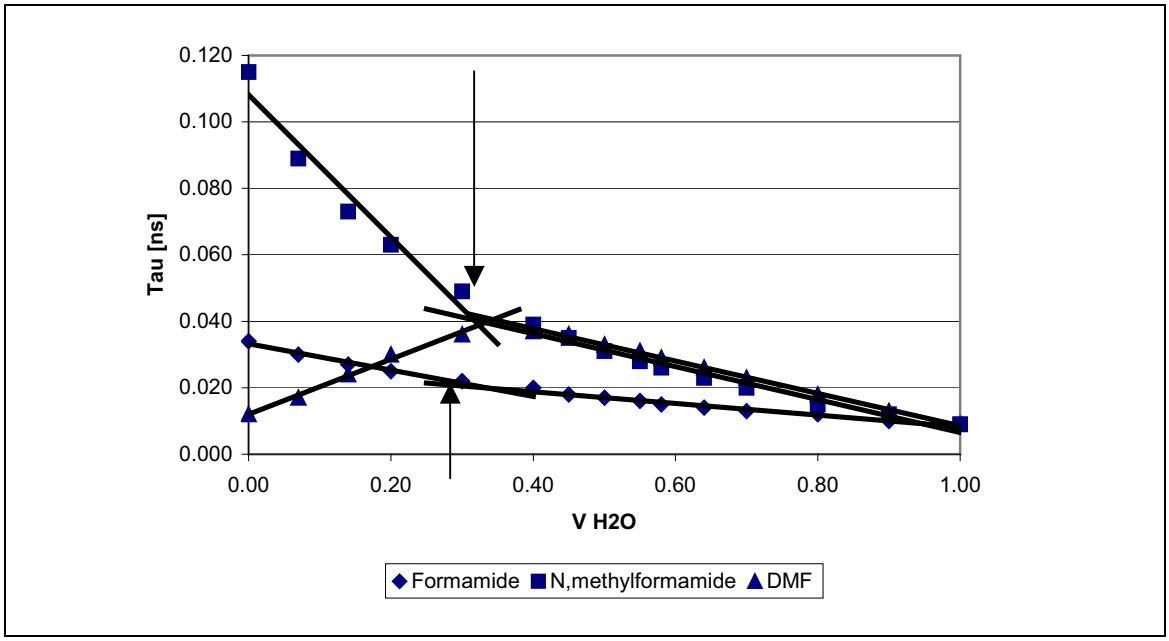

Figure 4.25: Relaxation behavior of the dipole of Formamide, N,methylformamide and DMF in water mixtures as a function of the volume fraction of water (V_{wa}/V) with intersection at ca. 0.34 (V_{wa}/V) for Formamide mixtures, at ca. 0.32 (V_{wa}/V) for N,methylformamide mixtures and at ca. 0.34 (V_{wa}/V) for DMF mixtures at 25°C which can be described by the Debye equation.

The fact that Debye equation is able to describe the whole range of Formamide or its mono and dimethylated form with water binary mixtures is another strong evidence that the lattice type seems to remain intact.

4.2.4. Conclusions

The phenomenon of percolation could be well demonstrated in case of binary mixtures of Formamide, N,methylformamide and N,N-dimetyhlformamide with water.

The critical concentration (lower p_c) was detected around ca. 34% (V_{wa}/V) in respect to relaxation time (τ) by Debye equation. E_i/E-values show a single p_c for Formamide-water binary system as well as its mono-methylated form with water (ca. 0.23 (V_{wa}/V)) (lower p_c), while a second (upper p_c) threshold was observed in case of N,N-dimethylformamide-water binary system (ca. 0.33 and ca. 0.79 (V_{wa}/V)). In respect to g-values, the upper percolation threshold was

clearly detectable between ca. 0.68 and ca. 0.77 (V_{wa}/V) and one can assume that the lower threshold is not clearly detectable in respect to g-values. It is well known that the location of the critical concentrations may be influenced by the sensitivity of the parameter to be chosen to detect the p_c and in case of g-values the upper percolation threshold is clearly more detectable than the lower one in case of Formamide and DMF binary systems.

It was also shown that by addition of the first methyl group to the Formamide structure there are no changes in behavior of the solvent molecule in Solvent-water binary system in respect to E_i/E-values, while adding the second methyl group show a lower and an upper threshold.

Nonetheless, all 3 solvents clearly demonstrate the same behavior in respect to relaxation time (τ) by Debye equation.

By looking at the g-values, it could certainly be seen that by adding each methylane group to Formamide structure, the alignment changes and first an increase by first addition and a decrease after second addition to the correlation factor g was observed. The increasing length of a linear chain leads to a higher preference of a parallel arrangement. This could be caused by molecules with longer nonpolar groups favouring a parallel alignment, as this allows both a separate grouping of the nonpolar and polar structures and a dense packing.

As a Final conclusion it is demonstrated that the use of percolation theory revealing percolation thresholds give insight into the changes of the “lattice structure” of this solvents in binary mixtures with water by addition of first and second methylane group.

4.3. Calculation of percolation threshold from experimental data using first and second derivatives

As it was mentioned in 3.2.6.3, we assume that the properties of a binary mixture should behave like the volume-wise addition of the properties of the pure liquids. If deviations from this theoretical assumption occur, the splitting up of the curve onto small number of segments leads to the distinction of percolation thresholds, critical volume fractions, and to a better description of properties of the system. The subdivision of data into a number of segments may be appropriate if the number of segments is small, the mathematical model describing the segments simple, via straight lines, and if there are sharp transitions between the segments.
(Belman et al., 1969), (Seber et al., 1989). For procedure please see 3.2.6.4 of part A of this work.

In many cases, to detect the percolation threshold is more convenient by using the plots of the first and second derivatives as in case of extremum, the first derivative is zero and second derivative is zero for the inflection point of a sigmoid curve (it is somewhat easier to find the zero crossing than it is to find the maximum).

By using first derivatives, its clear that at the inflection point (when the change from positive to negative value is observed) of the curve we have the first threshold as it can be compared with the experimental results.

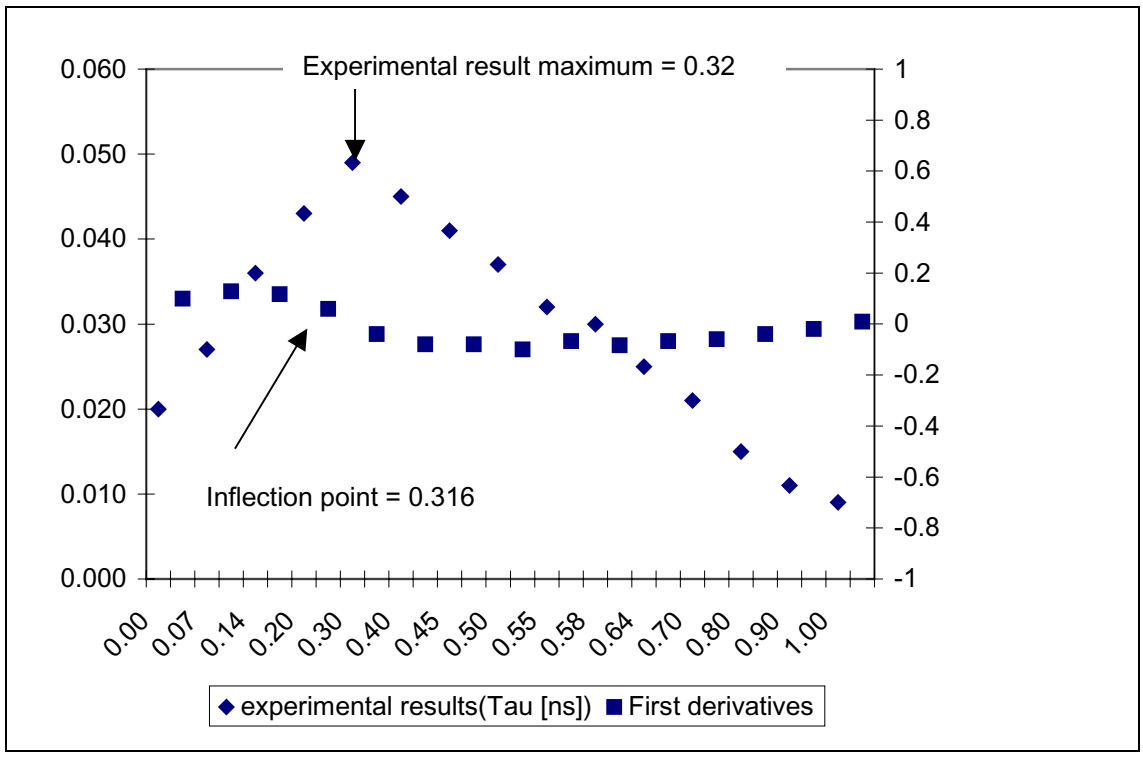

Figure 4.26: Comparison of the experimental results and first derivatives

By choosing the inflection area, and calculating the intersection of the first derivatives and x-axis (x=0), the percolation threshold is obtained by this method.

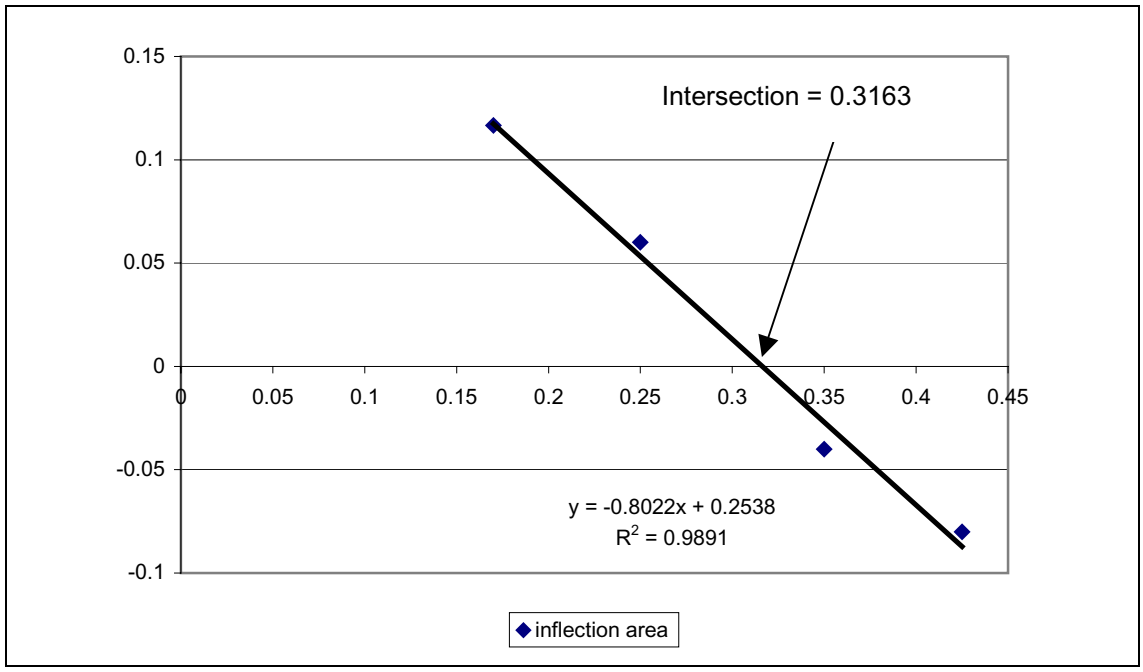

Figure 4.27: Percolation threshold obtained from first derivative of the experimental results

Using second derivatives gives an insight to the upper percolation threshold where the value get close to zero (sigmoid-like curve, inflection point) and its comparable with the result of the upper percolation threshold using old method discussed in 3.2.6.3 of part A of this work.

V H2O/ V	Tau [ns]	Mean V H2O/ V	first derivative	Second derivative
0.00	0.02	0.04	-	-
0.07	0.027	0.11	0.1	-
0.14	0.036	0.17	0.128571429	1.19047619
0.20	0.043	0.25	0.116666667	-1.416666667
0.30	0.049	0.35	0.06	-1.80144E+15
0.40	0.045	0.43	-0.04	0.8
0.45	0.041	0.48	-0.08	0
0.50	0.037	0.53	-0.08	-3.60288E+14
0.55	0.032	0.57	-0.1	-1.666666667
0.58	0.03	0.61	-0.066666667	-0.555555556
0.64	0.025	0.67	-0.083333333	-1.5012E+14
0.70	0.021	0.75	-0.066666667	0.166666667
0.80	0.015	0.85	-0.06	-1.80144E+14
0.90	0.011	0.95	-0.04	0
1.00	0.009	1.00	-0.02	-0.026363636

Table 4.2: Experimental result, first and second derivatives

None the less, it must be said by using this method, more number of data is needed, while by calculating first derivatives we loose one result point and by calculating second derivatives one further result point will be lost. Therefore, the second derivative method is not applicable in this work.

References

Agilent Technologies Inc., 1985. Materials Measurements: Measuring the dielectric constant of solids with the HP 8510 network analyzer: Product Note 8510-3, Agilent Technologies, Palo Alto. 1985

Agilent Technologies Inc., 1988. HP 4284A Precision LCR Meter Operation Manual, Agielnt Technologies, Palo Alto.

Agilent Technologies Inc., 1993. HP 85070M Dielectric Probe Measurement System / HP 85070B High-Temperature Dielectric Probe Kit: Technical Data, Agilent Technologies, Palo Alto.

Agilent Technologies Inc., 1994. The Impedance measurement Handbook: A guide to Measurement Technology and Techniques, Agilent Technologies, Palo Alto.

Alonso, M., Finn, E.J., 1992. Physics, Addison-Wesley, Reading.
Atkins, P.W., 1998. Physical Chemisrty. Oxford University Press, Oxford, Melbourne, Tokyo.

Barton, A.F.M., 1991. CRC Handbook of Solubility Parameters and Other Cohesion Parameters, 2nd Ed., CRC Press, Boca Raton.

Belman, R., Roth, R., 1969. Curve fitting by segmented straight lines. J. Am. Stat. Assoc, 64, 1079-1084.

Bottcher, C.J.F., 1973. Theory of Electric Polarization, Volumen I:Dielectrics in static fields, 2nd Ed., Elsevier, Amsterdam.

Burke, J., 1984.Solubility Parameters: Theory and Application. AIC Book and Paper Group Annual, Ed. Jensen C, Vol.3, 13-58.

Clausius, R.J.E., 1879. Die mechanische Waarmetheorie, Volume 2, Vieweg, Braunschweig.

Craig, DQ.M., 1995. Dielectric analysis of pharmaceutical systems, Taylor & Francis, London.

ChemDat, 2001. The Merck Chemical Databases, Darmstadt.
URL: http://www.merck.de/english/services/chemdat/english/index.htm

CRC Handbook of Chemistry and Physics, 1997. 77th edition, CRC Press Inc. Boca Raton.

Chen Danny, Song Di, Guillaume Wientjes M., Jessie L-S., 2003. Effect of dimethyl sulfoxide on bladder tissue penetration of interavesical Praclitaxel. Clin. Res., 9, 363-369.

Cowie, J.M.G., Toporowski, P.M., 1961. Association in the binary liquid system dimethyl sulfoxide-water. Can. J. Chem. 39, 2240-2243.

Debye, P., 1912. Einige Resultate einer kinetischen Theorie der Isolatoren. Phys. Z., 13, 97-100.

Decareau, R.V., Mudgett, R.E., 1985. Microwaves in the Food Processing Industry, Academic Press, Orlando.

Davis, R.S., Koch, W.F., 1992. Mass and Density Determinations. In: Rossiter, B.W., Baetzold, R.C. (Ed.): Physical Methods of Chemistry, Volume VI: Determination of Thermodynamic Properties, New York, pp. 59-62.

Fluka, Laborchemikalien und analytische Reagenzien, 2001/2002. Fluka Chemie GmbH, Buchs.

Frank, H.S., Wen, W.-Y., 1957. III. Ion-Solvent interaction. Structural Aspects of Ion-Solvent Interaction in Aqueous Solutions: A Suggested Pictzre of Water Structure. Disc. Farad. Soc., 24, 133-140.

Frohlich, H., 1958. Theory of dielectrics, Oxford University Press, Oxford.

Hasted, J.B., 1973. Aqueous dielectrics, Chapman and Hall, London, pp. 176-203.

Havemeyer, R.N., 1966. Freezing point curve of dimethyl sulfoxide-water solutions. J. Pharm. Sci. 55(8), 851-3.

Hernandez-Perni, G., Stengele, A., Leuenberger, H., 2004a. Towards a better understanding of the parameter E_i/E in the chracterization of polar liquids. Proceedings of the 5th Central European Symposium on Pharmaceutical Technology and Biotechnology, Ljubljana 2003. Int. J. Pharm.

Hernandez-Perni, G., Stengele, A., Leuenberger, H., 2004b. Detection of percolation phenomena in binary pola liquids by broadband dielectric spectroscopy. Proceedings of the 5th Central European Symposium on Pharmaceutical Technology and Biotechnology, Ljubljana 2003. Int. J. Pharm.

Jorjani, M., Rastegar, H., et al. 2003. Synthesis and Biological Evaluation of New 1,4-Dihydropyridines as Antihypertensive Agents in Rats. Iranian J. Pharm. Res. 43-46.

Kaatze, U., Brai, M., Scholle, F.D., Pottel, R., 1990. Ultrasonic absorption and sound velocity of dimethyl sulfoxide/water mixtures in the complete composition range. J. Mol. Liq. 44, 197-209.

Kirkpatrick, S., 1973. Percolation and conduction, Rev. Mod. Phys., 45, pp. 574-588.

Kirkwood, J.G., 1939. The dielectric polarization of polar liquids. J. Chem. Phys., 7, 911-919.

Kvakovszky, G. A Performance Profile of DMSO and its Analouges as a dipolar aprotic reaction solvents. Gaylord Chemical Co, annual report. Slidell, LA, USA.

Kuentz, M.T., 1999. Mechanical properties of pharmaceutical polymer tablets: modelling by taking into account the theory of percolation. PhD thesis, University of Basel, Switzerland.

Leuenberger, H., Rohera, B.D., Hass, C, 1987. phercolation theory: a novel approach to solid dosage form design. Int. J. Pharm. 38, 109-115.
Lorentz, H.A., 1909. Theory of electrons, Teubner, Leipzig.

Lower, St., 2001.
URL: http://www.cheml .com/acad/sci/aboutwater.html

Luzar, A. 1990. Dielectric behavior of DMSO-water mixtures: a hydrogen-bonding model. J. Mol. Liq. 46, 221-238.

Marshall, D.B., McHale, J. L., Carswell, S., Erne, D., 1987. Properties of nonideal binary solutions. An integrated physical chemistry experiment. J. Chem. Educ. 64(4), 369-370.

Mossotti, O.F., 1847. Recherches theoriques sur l'induction electrostatique, envisagee d'apres les idees de Faraday. Bibl. Univ. Modena, 6, 193-198.

Rangel, C., Niell, H., Miller, A., Cox, C. 1994. Taxol and taxotere in bladder cancer: *in vitro* activity and urine stability. Cancer Chemoth. Pharm., 33, 460-464.

Reichardt, C., 1994. Solvatochromic dyes as solvent polarity indicators. Chem. Rev. 94, 2319-2358.

Riddick, J.A., Bunger, W.B., 1970. Techniques of Chemistry, vol. 2, Third ed. Wiley, New York.

Roth, B. J., 1995. Preliminary experience with paclitaxel in advanced bladder cancer. Semin. Oncol., 22, 1-5.

Sahimi, M., 1994. Applications of percolation theory, Taylor & Francis, London.
Schoemaker, D.P., Garland, C.W., Nibler, J.W., 1989. Experiments in physical Chemistry, 5th Ed., McGraw-Hill, New York, pp. 402-418.

Siegmund, C, Leuenberger, H., 1999. Percolation theory, conductivity and dissolution of hydrophilic suppository bases (PEG-Systems), Int. J. Pharm., 189, 187-196.

Stauffer, D., Aharony, A., 1985. Introduction to percolation theory, 2nd Ed., Taylor & Francis, London.

Stengele, A., Rey, St., Leuenberger, H., 2001. A novel approach to the characterization of polar liquids. Part 1: pure liquids. Int. J. Pharm. 225, 123-134.

Stengele, A., Rey, St., Leuenberger, H., 2001. A novel approach to the characterization of polar liquids. Part 2: binary mixtures. Int. J. Pharm. 225, 123-134.

Stillinger, F.H., 1982. Low Frequency Dielectric Properties of Liquid and Solid Water. In: Montroll, E.W., Lebowitz, J.L. (Ed.): Studies in Statistical Mechanics, Volume VIII: The liquid State of Matter: Fluids, Simple and Complex, North-Holland, Amsterdam, pp.341-432.

Soper, A. K., Luzar, Alenka. 1992. A neutron-diffraction study of dimethyl sulfoxide-water mixtures. J. Chem. Phys. 97(2), 1320-31.

Tabor, D., 1991. Gases, liquids and soilds, 3rd Ed., Cambridge University Press, Cambridge, pp. 253-295.

Tommila, Pajunen, A., 1969. The dielectric constants and surface tensions of dimethyl sulfoxide-water mixtures. Suom. Kemistil. B 41, 172-176.

Wood, D.C., Wood, J., 1975. Pharmacologic and biochemical considerations of dimethyl sulfoxide, Ann. N.Y. Acad. Sci., 243, 7-18.

Part B:

Solubilized ferroelectric salts

Chapter 1

Introduction

The study of ferroelectricity is a branch of solid state physics which shown rapid growth during recent years. Ferroelectric materials exhibit unusual electric properties, which make them useful in modern (opto) electronic technology, especially display technology. These properties also make them important in other field on science, also in pharmaceutics as a material to be examined for better explanations of polymorphism and liquid crystals.

Ferroelectric and antiferroelectric liquid crystals, including also various polymer forms, are the hottest research topic today in liquid crystals. The field is at the very beginning of industrial exploitation – a sensitive phase in which a good reference work is needed and will have a broad spectrum of readers both at universities and in industry.

Ferroelectric liquid crystals are a novel state of matter, a very recent addition to the science of ferroelectrics which, in itself, is of relatively recent date. The phenomenon which was later called ferroelectricity was discovered in the solid state (on Rochelle salt) in 1920 by Joseph Valasek, then a PhD student at the University of Minnesota. His first paper on the subject had the title *Piezo-Electric and Allied Phenomena in Rochelle Salt.* This was at the time when solid-state physics was not a fashionable subject and it took several decades until the importance of the discovery was recognized. Valasek had then left the field. Later, however, the development of this branch of physics contributed considerably to our understanding of the electrical properties of matter, of polar materials in particular and of phase transitions and solid state physics in general. In fact, the science of ferroelectrics is today an intensely active field of research. Even though its technical and commercial importance is substantial, many breakthrough applications may still lie ahead of us. The relative importance of liquid crystals

within this broader area is also constantly growing. This is illustrated in Fig. 1.1, showing how the proportion of the new materials, which are liquid-crystalline, has steadily increased since the 1980s.

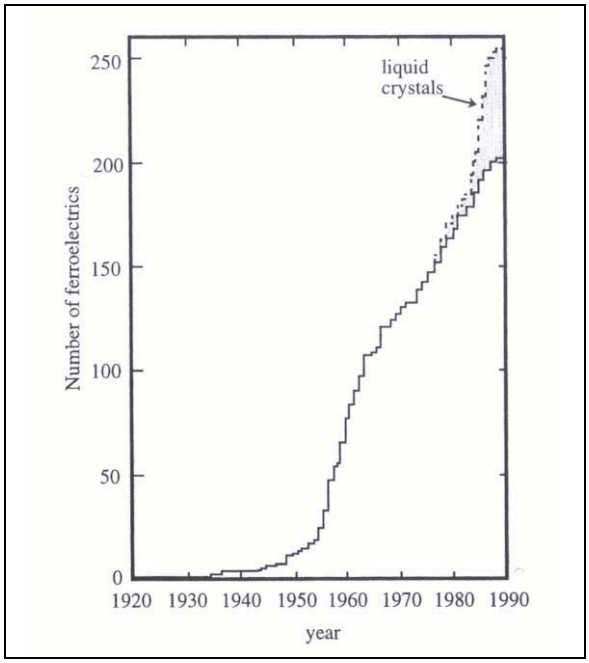

Fig. 1.1. Number of known ferroelectrics. Solid line: solid-state ferroelectrics, where each pure compound is counted as one. Dashed line: total number, including liquid crystal ferroelectrics, for which a group of homologs is counted as one. From about 1984, the proportion of liquid crystals has steadily grown which has been even more pronounced after 1990. (After Deguchi as cited by Fousek. J Fousek, Ferroelectrics 1991,113, 3 - 20.)

The general level of knowledge of ferroelectricity, even among physicists, is far lower than in the older and more classical subjects like ferromagnetism. It might therefore be worthwhile to discuss briefly the most important and characteristic features of solid ferroelectrics and polar materials, before turning to liquid crystals. This will facilitate the understanding and allow us to appreciate the striking similarities as well as distinctive differences in how polar phenomena appear in solids and how they appear in liquid crystals. One of the aims, of course, is also to make a bridge to existing knowledge. Those not aware of this important knowledge are apt to coin new words and concepts, which are bound to be in contradiction to already established concepts or even contradictory to themselves.

Concepts like piezoelectric, pyroelectric, ferroelectric, ferrielectric, antiferroelectric, paraelectric, electrostrictive, and several more, relate to distinct phenomena and are themselves interrelated. They are bound to appear in the description of liquid crystals and liquid crystal polymers, as they do in normal

polymers and crystalline solids. Presently, great confusion is created by the uncritical use of these terms. For example, in the latest edition of the Encyclopedia Britannica [4] it is stated that pyroelectricity was discovered in quartz in 1824. This is remarkable, because quartz is not pyroelectric at all and cannot be for symmetry reasons. To clarify such issues (and the confusion is no less in the area of liquid crystals), we will have to introduce some simple symmetry considerations that generally apply to all kinds of matter. In fact, symmetry considerations will be the basic guidelines and will probably play a more important role here than in any other area of liquid crystals. Chirality is a special property of dissymmetry with an equally special place in these considerations. It certainly plays a fundamental role for ferroelectric liquid crystals at least so far. Therefore we will have to check how exactly the appearance of polar properties in liquid crystals is related to chiral properties, and if chirality is dispensable, at least in principle. Finally, flexoelectricity is also a polar effect, and we will have to ask ourselves if this is included in the other polar effects or, if not, if there is an interrelation.

Can liquids in which the constituents are dipoles be ferroelectric? For instance, if we could make a colloidal solution of small particles of the ferroelectric $BaTiO_3$, would this liquid be ferroelectric? The answer is no, it would not. It is true that such a liquid would have a very high value of dielectric susceptibility and we might call it superparaelectric in analogy with the designation often used for a colloidal solution of ferromagnetic particles, which likewise does not show any collective behavior. An isotropic liquid cannot have polarization in any direction, because every possible rotation is a symmetry operation and this of course is independent of whether the liquid lacks a center of inversion, is chiral, or not. Hence we have at least to diminish the symmetry and go to anisotropic liquids, that is, to liquid crystals, in order to examine an eventual appearance of pyroelectricity or ferroelectricity. To search for ferroelectricity in an isotropic liquid would be futile, because a ferroelectric liquid cannot be isotropic. In order to have a bulk polarization, a medium must have a direction, the polarity of which cannot be reversed by any symmetry operation of the medium. On the

other hand, an isotropic liquid consisting of dipoles may show a polarization during flow, because a shear diminishes the symmetry and will partially order the dipoles, thus breaking the randomness. This order will be polar if the liquid is chiral. However, we would not consider such a liquid ferroelectric or pyro-electric - no more than we would consider a liquid showing flow birefringence to be a birefringent liquid. It is clear that there may be lots of interesting polar effects yet to be explored in flowing liquids, particularly in fluids of biological significance (which are very often chiral). Nevertheless, these effects should not be called "ferroelectric". They should not even be called piezoelectric, even if setting up shear flow in a liquid certainly bears some resemblance to setting up shear strain in a crystal. *(Ferroelectric and antiferroelectric Liquid Crystals, Sven T. Lagerwall, 1999).*

In Part B of this thesis we focus and try to find a relation between dielectric activities using the concepts of ferroelectricity and ferroelectric phenomena in preformation of crystals / liquid crystals and investigating the pre-polymorpic forms of compounds during crystallization using dielectric spectroscopy.

Chapter 2

Theory

2.1 Ferroelectric Terms

The term “ferroic” originates from a unification and generalization of the concepts “ferromagnetic”, “ferroelectric”, and “ferroelastic”. A ferroic crystal exhibits, in an attainable range of temperature and pressure, one or more of the following quantities: a magnetization, polarization or strain that is stable in the absence of any applied fields, whether magnetic, electric or mechanical stress. The application of these fields or combinations of them, one can switch the direction of the spontaneous magnetization, the spontaneous polarization or the spontaneous strain *(Institute of Electrical and Electronics Engineers, 1986)*.

Ferroelectricity was discovered in 1921 by J. Valasek during an investigation of the anomalous dielectric properties of Rochelle salt. A second ferroelectric material, KH_2PO_4 was found until 1935 and was followed by some of its isomorphs. An the third major substance, $BaTiO_3$, was reported in1944. Since then, this small group has been joined by 250 pure materials and many more mixed crystal systems *(Abrahams,1986)*.

The exact definitions of these terms are mentioned in the next sections.

2.1.1 Polar Axis

The polar axis is a direction that is parallel to the spontaneous polarization vector.

When a polar crystal is heated or cooled, the internal or external electrical conduction generally cannot provide enough current to compensate for the

change in polarization with temperature, and the crystal develops an electric charge on its surface. For this reason polar crystals are called pyroelectric *(Institute of Electrical and Electronics Engineers, 1986)*.

2.1.2 Pyroelectric Effect

The pyroelectric effect is the appearance of an electric charge at the surface of a polar material when uniform heating or cooling changes the polarization. If the polar material is electroded and an external resistance is connected between the electrodes, the current that flows is a pyroelectric current.

All pyroelectrics, are polar, ferroelectrics are a subgroup of the polar materials and they are both pyroelectric and piezoelectric. They differ form the pyroelectrics principally by the reversibility or reorientability of their spontaneous polarization *(Institute of Electrical and Electronics Engineers, 1986)*.

2.2 Ferroelectric Materials

A ferroelectric material is a material that exhibits, over some range of temperature, a spontaneous electric polarization that can be reoriented by application of an electric field.

The requierement of a nonvanishing spontaneous polarization P_s is a sufficient criterion for a ferroelectric phase. Materials belonging to nonpolar crystals classes at all temperatures, and in which a metastable polar state can be induced by an applied electric field, can also show reversible pyroelectric behavior.

The various possible stable orientatios of Ps for a given ferroelectric phase are designated as orientation states. A ferroelectric crystal has two or more such orientation states in the absence of an electric field, and it can be switched from one to another of these states by a relizable electric field *(Institute of Electrical and Electronics Engineers, 1986)*.

2.2.1 Polarization

Polarization is the electric dipole moment per unit volume *(Martin, 1993)*.
The Polarization *P* may be expressed as the bound surface change per unit area of a free surface normal to the direcction of *P (Institute of Electrical and Electronics Engineers, 1986)*.

2.2.2 Spontaneous Polarization

Spontaneous Polarization is defined as magnitude of the polarization within a single ferroelectric domain within a single ferroelectric domain in the absence of an external electric field.

This is an fundamental property of all pyroelectric crystals, although it is reversible or reorientable only in ferroelectrics.

The Spontaneous Polarization could be meaured by several methods:

Pyroelectric. Using charge integration as the crystal is heated to a temperature above the Curie point T_C.
Polarization reversal or switching, using either charge integration or integration of the area under switching current *i* versus time *t* curves *(Institute of Electrical and Electronics Engineers, 1986)*.

2.2.3 Permanent Dipole Moment of polar molecules

In a polar molecule, the separation of positively and negatively charged regions can be permanent, and the molecule will possess a permanent dipole moment, μ.

This is a nonionic phenomenon, and although regions of the molecule may possess charges, these charges should balance each other so the molecule as

a whole will have no net charge. The water molecule, for example, possesses a permanent dipole. The magnitude of the permanent dipole, is independent of any induced dipole from an electric field *(Martin, 1993)*.

It is defined as the vector sum of the individual charge moments within the molecule, including those from bonds and lone-pair electrons. The vectors depend on the distance of separation between the charges. The unit of μ, is the debye, with 1 debye equal to 10^{-18}esu (electrostatic unit) cm. This is derived from the charge on the electron (about 10^{-10} esu) multiplied by the average distance between charged centers on a molecule (about 10^{-8} esu) *(Martin, 1993)*.

In an electric field, molecules with permanent dipole moments can also have induced dipoles. The polar molecule, however tend to orient itself with its negatively charged centers closest to positively charged centers on other molecules before the electric field is applied, so that when the applied field is present, the orientation is in the direction of the field. Maximum dipole moment occurs when the molecules are oriented most perfectly. Absolutely perfect orientation can never occur owing to the thermal energy of the molecules, which contributes to agitation against the molecular alignment. The total molar polarization is the sum of induction and permanent dipole effects *(Martin, 1993)*.

In solution, the permanent dipole of a solvent such as water can strongly interact with the solute molecules. This interaction contributes to solvent effect and is associated, in the case of water, with the hydration of ions and molecules. The symmetry of the molecule can also be associated with its dipole moment *(Martin, 1993)*.

Permanent dipole moments can be correlated with biologic activities of certain molecules to obtain valuable information about the relationship of physical properties and charge separation in a class of compounds *(Martin, 1993)*.

2.2.4 Behavior of Dielectrics in Electric Fields: Classification of Polar Materials (Crystalse and liqiud crystals)

All dielectrics become polarized if we put them in an electric field. The polarization is linear in the field, $P \sim E$, which means that it changes sign if were reverse the sign of the field. When the field is reduced to zero, the polarization vanishees. For very strong fields we will observe saturation effects (and eventually dielectric breakdown of the material). The typical behavoir of a normal (nonpolar) dielectri is shown at the top of the Fig. 2.1. In a piezoelectric, an appropriate strain *s* will have a similar influence to the electric field for a normal dielectric. The effect is likewise linear around the origin and shows saturation at high strains. Conversley, we Can induce a strain $s \sim E$ by appling an external field. This is converse piezoelectric effect, which is used to produce ultrasound, wheras the direct effect is used to transform a mechanical strain into an electric signal, for instnace, in gramaphone *P* and *E* means that there is linearrity between *P* and *E*, that is, a nonpolar piezoelectric behaves dielectrically just like a normal dielectric.

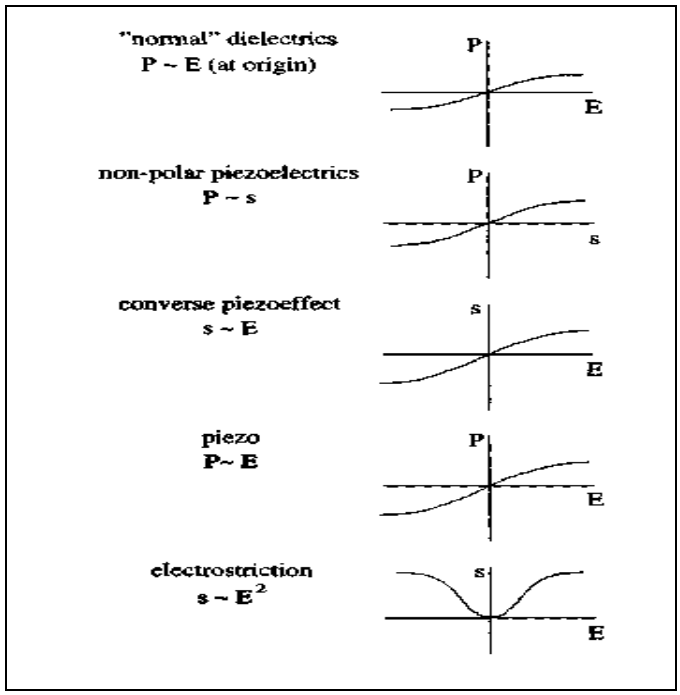

Fig. 2.1. Response of nonpolar dielectrics (which do not contain orientable local dipoles) to an applied electric field. Piezoelectric materials react both with polarization and distortaion and, because of the way these are related, they are alos polarized by a distirtion in the absence of an electric field.

In addition, all materials show the electrostrictive effect. This is normally a very small field-induced strain, which originates from the fact that the equilibrium distance between atoms and the distribution of dipoles are to some degree affected by an applied field. It corresponds to the small induced polarization and thus small dielectric constant typical for ordinary materials. The electrostrictive effect therefore has an entirely different charater; the strain itself is not related to any polarization so no converse effect exists (i.e, an electric field cannot be generated in ordinary materials simply by applying machanical pressure). The electrostrictive strain is always superposed on, but can be distinguished from, a pizoelectric strain by the fact that it is quadratic and not linear in the field, thus $s \sim E^2$. The linear and quadratic dependence, respectivly, of piezoelectric and electrostrictive strain, of course applies near the origin for small fields. In the more general case, the effect is called piezoelectric if it is an odd function of *E*, and electrostrative if it is an even function. The piezoelectric effect can only be present in noncentrosymmetric materialy. If we apply a field to a material with center of symmetry, the resultant strain must be independent of the field direction, hence

$$s^e = \alpha E^2 + \alpha' E^4 + \ldots \qquad (2.1)$$

whereas the field reversibility of teh piezoeffect will only admit odd powers

$$s^p = \beta E + \beta' E^3 + \ldots \qquad (2.2)$$

Sometimes care has to be taken not to confuse the two effects. If, for some reason, the sample has been subjected to a static field E, and the a small ac signal Eac is applied, the electrostractive strain will be

$$s^e = a (E_0 + E_{ac})^2 \approx a E_0^2 + 2aE_0E_{ac} \qquad (2.3)$$

giving a linear response with the same frequency as the applied field. An aligning field E_0 may, for instance, be applied to a liquid crystal polymer, for which the electrostrative coefficient is often particularly large and the signal coming form this so-called biased electrostriction ma yeasily be mistaken for piezoelectricity. Therefore, in the search for piezoelectricity, which would indicate the lack of a center of symmetry in a material, the direct piezoeffect should be measured, whenever possible, and not the converse effect.

In Fig. 2.2 we have in the same way illustrated how polar materials may behave in response to an external electric field *E*.

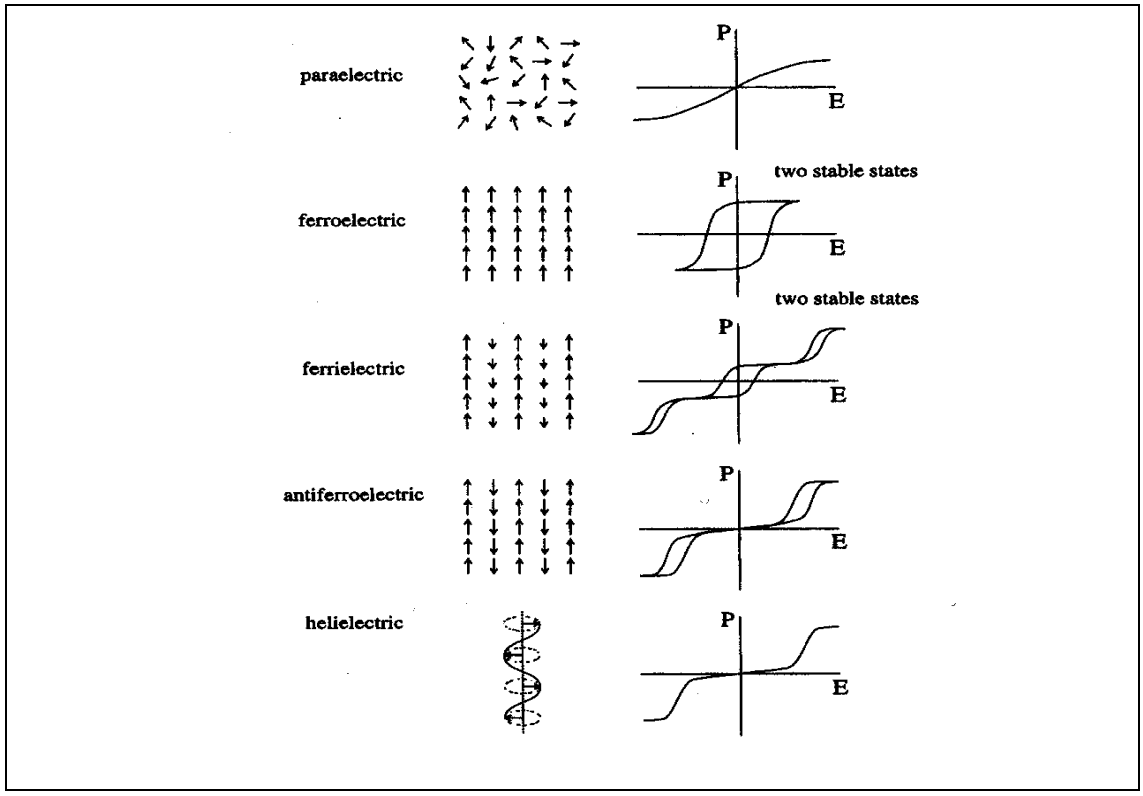

Fig. 2.2. Response of polar dielectrics (containing local permanent dipoles) to an applied electric field; from top to bottom: paraelectric, ferroelectric, ferrielectric, antiferroelectric, and helielectric (helical antiferroelectric). A pyroelectric in the strict sense hardly responds to a field at all. A paraelectric, antiferroelectric, or helieletric phase shows normal, i.e., linear dielectric behavior and has only one stable, i.e., equilibrium, state for E=0. A ferroelectric as well as a ferrielectric (a subclass of ferroelectric) phase shows the peculiarity of two stable states. These states are polarized in opposite directions *(±P)* in the absence of an applied field (E = 0). The property in a material of having two stable states is called bistability. A single substance may exhibit several of these phases and temperature changes will provoke observable phase transitions between phases with different polar characteristics.

The *P* – *E* tarce is fingerprint of the category that is charactristic of the technologocal potential. At the top there is the normal dielectric response with *P* increasing linearly to a saturation value at high fields. In principle this behavior is the same whether have local dipoles or not, except that with local dipoles the saturation value will high and strongly temperature-dependent. If the molecules lack permanent dipole the induced local polarization is always along the field and temperature-independent. Dipolar molecules may, on the other hand, align spontaneously at a certain temperature (Curie temperature) to a state of homogeneous polarization. On approach such a temperature the susceptibility

takes on very high values and is strongly temperature-dependent. We will describe this state - which is unpolarized in absence of a field, but with a high and strongly temperature-dependent value of dielectric susceptibility - as paraelectric, independent of whether there actually transition to an ordered state or not. It should be noted from the previous figure 2.1 a piezoelectric material has the same shape as the *P-E* curve of a normal dielectric, but it often shows paraelectric behavior with a large and even diverging susceptibility.

Next, the contrasting, very strongly nonlinear response of a ferroelectric is shown in Fig. 2.2. The two stable states *(+P, -P)* at zero field are the most characteristic feature of this hysteresis curve, which also illustrates the threshold (coercive force) the external field has to overcome in order to flip over from one state to the other. In the solid state this behavior may be represented by $BaTi0_3$.

The response of an antiferroelectric is shown two diagrams below. The initial macroscopic polarization is zero; just as in a normal dielectric and the *P-E* relation is linear at the beginning until, at a certain threshold, one lattice polarization flips over to the direction of the other (the external field is supposed to be applied along one of the sublattice polar directions). This is the field-induced transition to the so-called ferroelectric state of the antiferroelectric. (Not ferroelectric phase, as often written the phase is of course antiferroelectric. Transitions between different thermodynamic phases by definition only occur on a change of temperature, pressure, or composition, that is, the variables of a phase diagram.) The very characteristic double-hysteresis loop reveals the existence of two sublattices as opposed to a random distribution of dipoles in a paraelectric. From the solid state we may take $NaNb0_3$ as representative of this behavior. It is not without interest to note that the structure of $NaNb0_3$ is isomorphous with $BaTi0_3$. The fact that the latter is ferroelectric whereas the former is antiferroelectric gives a hint of the subtleties that determine the character of polar order in a lattice.

At the limit where the hysteresis loops shrink to thin lines; as in the diagram at the bottom, we get the response from a material where the dipoles are ordered in a

helical fashion. Thus this state is ordered but has no macroscopic polarization and therefore belongs to the category of antiferroelectrics. It is called helical antiferroelectric or heliectric for short. If an electric field is applied perpendicular to the helical axis, the helix will be deformed as dipoles with a direction almost along the field start to line up, and the response *P-E* is linear. As in the normal antiferroelectric case, the induced *P* value will be relatively modest until we approach a certain value of *E* at which complete unwinding of the helix takes place rather rapidly. Although the helielectric is a very special case, it shares the two characteristics of normal antiferroelectrics: to have an ordered distribution of dipoles (in contrast to random) and a threshold where the linear response becomes strongly nonlinear (see Fig. 2). In the solid state this behavior is found in $NaN0_2$.

In the middle diagram of Fig. 3 we have also traced the *P-E* response for the modification of an antiferroelectric, which we get in the case where the two sublattices have a different polarization size. This phase is designated ferrielectric. Because we have, in this case, a macroscopic polarization, ferrielectrics are a subclass of ferro-electrics. It also has two stable states, as it should, although the spontaneous macroscopic polarization is only a fraction of that which can be induced. If the polarization values of the sublattices are P_1 and $P_2<P_1$, the bistable states have the values $\pm(P_1-P_2)$, whereas the saturation polarization after sublattice reversal is $\pm(P_1+P_2)$.

The presence of two stable states indicates that a ferroelectric material basically has memory properties, just like a ferromagnetic material. Any of these two states can prevail when the acting external field has been removed *(E = 0).* In the virgin state, the ferroelectric tries to minimize its own external field by the creation of macroscopic domains of opposite polarization, which is an important characteristic in identifying the state as ferroelectric. In all the other materials mentioned, including pyroelectrics and antiferroelectrics, we have no spontaneous polarization domains, i.e., polarization up and polarization down domains appearing in the field-free state. The fact that it has not yet been possible to develop solid state

ferroelectric memory devices is related to the very involved interactions with charge carriers and to the fact that switching between the two states is normally coupled to a change in the lattice distortion, which may eventually cause a total breakdown of the lattice (crystal fatigue). If the same or analogous memory property could be found in a liquid, this might be an attractive way to rule out at least the second problem. This is one of the facts that make ferroelectric liquid crystals very promising. As a result of these inherent problems, solid state ferroelectrics have, strangely enough, not been used for their ferroelectric properties, but rather for their superior pyroelectric (heat detectors), piezoelectric, and dielectric (very high ε) properties. In addition, they are the dominating electrooptic materials as Pockels modulators as well as for nonlinear optics (NLO), e.g., for second-harmonic generation.

The hierarchy of dielectric materials is shown in Fig.2.3. All are of course dielectrics in a broad sense. To distinguish between them we limit the sense, and then a dielectric without special properties is simply called a dielectric; if it has piezoelectric properties it is called a piezoelectric, if it further has pyroelectric but not ferroelectric properties it is called a pyroelectric, etc. A ferroelectric is always pyroelectric and piezoelectric, a pyroelectric always piezoelectric, but the reverse is not true. Knowing the crystal symmetry we can decide whether a material is piezoelectric or pyroelectric, but not whether it is ferroelectric. A pyroelectric must possess a so-called polar axis (which admits no inversion). If in addition this axis can be reversed by the application of an electric field, i.e., if the polarization can be reversed by the reversal of an applied field, the material is called ferroelectric. Hence a ferroelectric must have two stable states in which it can be permanently polarized *(Ferroelectric and antiferroelectric Liquid Crystals, Sven T. Lagerwall, 1999)*.

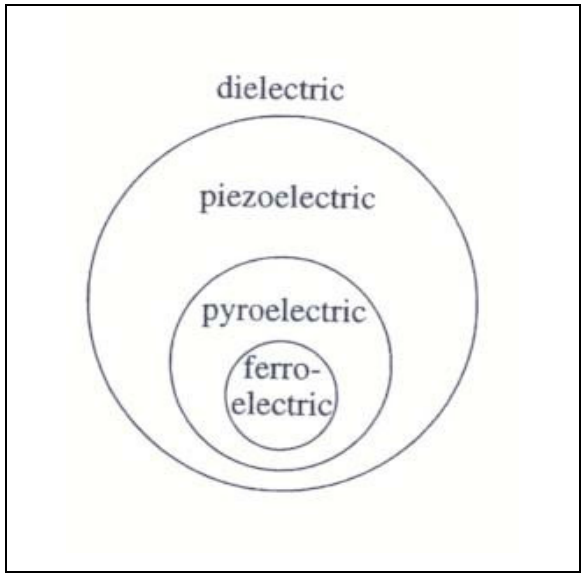

Fig. 2.3. The hierarchy of dielectric materials.

2.2.5 Ferroelectric Domains

A ferroelectric domain is a region of a ferroelectric crystal exhibiting homogeneous and uniform spontaneous polarization.

An unpoled ferroelectric material may exhibit a complex domain structure consisting of many domains, each with a different polarization orientation. The direction of the sponatneous polarization within each domain is constrained to a small number of equivalent directions dictated by the symetry of the prototype. The boundary region between two ferroelectric domains is called a domain wall. Domains can usually be observed by pyroelectric, optical, powder decoration, or electrooptic means *(Institute of Electrical and Electronics Engineers, 1986)*.

2.2.6 Phase Transition

The phase transition of a ferroelectric material is defined as a change in the crystal structure, usually occurring at a well-defined temperature, which alters the orientation or magnitude, ot both ot the electris polarization *(Institute of Electrical and Electronics Engineers, 1986)*.

2.2.7 Ferroelectric Curie Point T_C

The ferroelectric Curie Point, is defined as temperature at which a ferroelectric material undergoes a structural phase transition to a state where spontaneous polarization vanishes.

At the Curie point, the small signal permittivity and the piezoelectric coefficients usually exhibit a peak. As a rule, the low temperature phase is ferroelectric and the high temperature phase paraelectric. In some materials, however, the high temperature phase may be a polar phase of higher symmetry that the ferroelectric phase *(Institute of Electrical and Electronics Engineers, 1986)*.

2.2.8 Curie-Weiss Temperature

The Curie-Weiss temperature of a ferroelectric material is defined as the intercept θ of the linear portion of the plot of $1/\kappa$ versus T, in the region above the ferroelectric Curie point, where κ is the small-signal relative dielectric permittivity measured at zero bias field along the polar axis, and T is the absolute Temperature. In many ferroelectrics κ follows the Curie-Weiss relation:

$$\kappa = \varepsilon/\varepsilon_0 = C/(T - \theta) \qquad (2.4)$$

where:

ε = small signal absolute permittivity
ε_0 = permittivity of free space (8.854 *1012 coulomb/voltmeter)
C = Curie constant
θ = Curie- Weiss temperature

The Curie-Weiss temperature θ is always less than or equal to the Curie point T_C and generally within a few degrees of T_C (Institute of Electrical and Electronics Engineers, 1986).

2.2.9 Paraelectric Phase

The paraelectric phase encompasses the range of temperature or pressure over which the permittivity exhibits Curie-Weiss behavior.

A ferroelectric material is said to be paraelectric at temperatures above the Curie point T_C if the small-signal relative dielectric permittivity κ is characterized by a Curie-Weiss behavior. *(Institute of Electrical and Electronics Engineers, 1986)*.

2.3 Dielectric Constant

A molecule can maintain a separation of electric charge either through induction by an external electric field or by a permanent charge separation within a polar molecule. To understand the concepts it is necessary to understand the concept of the dielectric constant *(Martin, 1993)*.

Consider two parallel conducting plates, such as the plates of an electric condenser, which are separated by some medium across a distance r, as shown in Figure 1, by apply a potential across the plates. Electricity will flow from the left plate to the right plate through the battery until the potential difference of the plates equals that of the battery supplying the initial potential difference. The capacitance, C (in farads), is equal to the quantity of electric charge, q (in coulombs), stored on the plates, divided by the potential difference, V (in volts), between the plates:

$$C = q/V \qquad (2.5)$$

The capacitance of the condenser in the Figure 2.4 depends on the type of medium separating the plates as well as on the thickness *r*. When a vacuum fills the space between the plates, the capacitance is C_0. This value is used as a reference to compare capacitances when other substances fill the space. If water fills the space, the capacitance is increased, since the water molecule can orientate itself so that its negative end lies nearest the positive condenser plate and its positive end lies nearest the negative plate. This alignement provides additional movement of charge because of the increased ease with which electrons can flow between the plates. Thus additional charge can be placed on the plates per unit of applied voltage *(Martin, 1993)*.

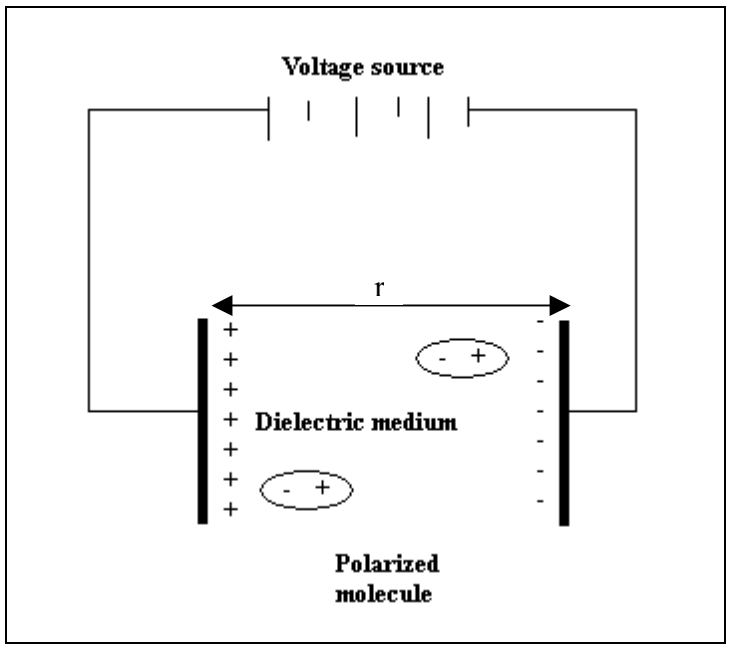

Fig. 2.4. Parallel plate condenser.

The capacitance of the condenser filled with some material, Cx, divided by the refence standard C0, is referred to as the dielectric constant, ε:

$$\varepsilon = C_x / C_0 \qquad (2.6)$$

The dielectric constant ordinarily has no dimensions, since it is the ratio of two capacitances.

The dielectric constant is dependent on the polarizability of the dielectric. As the polarizability increases, the dielectric constant increases with it *(Martin, 1993)*.

The dielectric constant is also frequency dependent (Figure 2.5). The response of normal materials to external fields generally depends on the frequency of the field. This frequency dependence reflects the fact that a material's polarization does not respond instantaneously to an applied field. Depending on the frequency, different polarization types of the dielectric can be observed *(Martin, 1993)*.

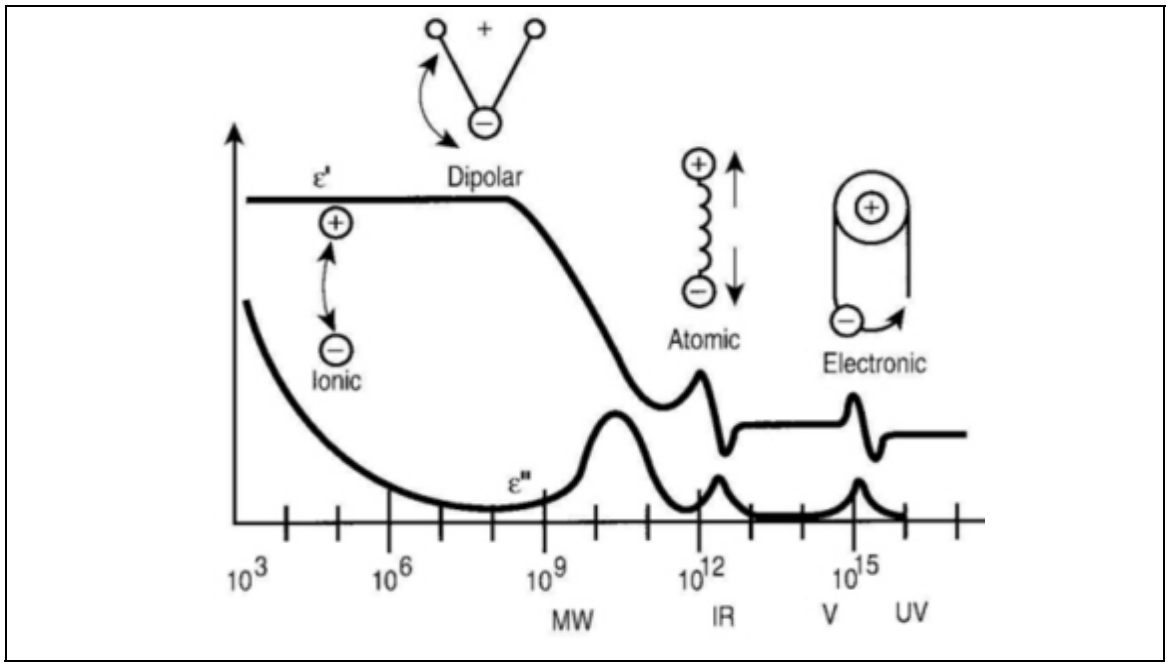

Fig. 2.5. A dielectric permittivity spectrum over a wide range of frequencies, are represented the real and the imaginary part of the dielectric function. Various processes are labeled on the image: ionic and dipolar relaxation, and atomic and electronic resonances at higher energies. http://en.wikipedia.org/wiki/Permittivity

Dielectric constant measured at low frequencies is called static or differential permittivity, at high frequencies complex permittivity.

2.3.1 Complex Permitivity

Permittivity is defined as the incremental change in electric displacement per unit electric field when the magnitude of the measuring field is very small compared to the coercive electric field. The small signal relative permittivity, κ, is equal to the ratio of the absolute permittivity ε to the permittivity of free space ε_0, that is $\kappa = \varepsilon/\varepsilon_0$.

The value of the small-signal permittivity may depend on the remanent polarization, electric field, mechanical stress or frequency of the measuring field.
Macroscopically ε is found by measuring the capacitance.

The complex permittivity is commonly referred to as ε∞.

The frequency at which the phase shift becomes noticeable depends on temperature and the details of the medium. For moderate fields strength (E_0), D and E remain proportional, and

$$\hat{\varepsilon} = \frac{D_0}{E_0} e^{i\delta} = |\varepsilon| e^{i\delta}. \tag{2.7}$$

Since the response of materials to alternating fields is characterized by a complex permittivity, it is natural to separate its real and imaginary parts, which is done by:

$$\hat{\varepsilon}(\omega) = \varepsilon'(\omega) + i\varepsilon''(\omega) = \frac{D_0}{E_0} (\cos\delta + i \sin\delta). \tag{2.8}$$

In the equation, ε" is the imaginary part of the permittivity, which is related to the rate at which energy is absorbed by the medium (converted into thermal energy, etc.). The real part of the permittivity is ε'.

2.3.2 Static or Differential Permittivity

The slope of the hysteresis loop (electric displacement versus electric field) at any point.

Differential permittivity is usually measured at low frequency (60Hz) due to the self-heating produced on cycling through a hysteresis loop. The value of differential permittivity is often different from the small-signal permittivity measured under equivalent bias conditions *(Institute of Electrical and Electronics Engineers, 1986)*.

2.4 Dielectric Spectroscopy

Dielectric spectroscopy involves the study or response of material to an applied electric field. By appropriate interpretarion of the data, it is possible to obtain structural information on a range of samples using this technique. While the use of dielectric spectroscopy technique has previously been largely confined to the field of physics, the generality of dielectric behavior has led to the technique being used in more diverse fields such as colloid science, polymer sience and, more recently, the pharmaceutical sciences *(Craig,1995)*.

Most pharmaceutical systems may be described as dielectrics, which contain dipoles. In principle, therefore the majority of such materials may be studied using this technique.

The use of the information obtained may be broadly divided into two categories:

1. Dielectric data may be used as fingerprint with which to compare samples prepared under different conditions; this therefore has implications for the use of dielectric spectroscopy as a quality control.

2. Each spectrum may be interpreted in terms of the structure and behavior of the sample, therefore leading to more specific information in the sample under study.

Both approaches are useful and obviously require different levels of understanding regarding the theory the technique.

As with any technique, there are associated advantages and disadvantages.

The advantages are:

- The sample preparation is generally very simple.
- Samples with a range of sizes and shapes may therefore studied; solid compacts, powders, gels or liquids may be esily measured.
- The method and conditions of measurement may be varied. For example, the sample may be examined under a range of tempeeratures, humidities, pressures, etc. *(Craig,1995)*.

The principal disadvantages of the technique with respect to pharmaceutical uses are

1. Not all samples may be usefully analyzed, a fault which is common to all analytincal methods.
2. The second disadvantage lies with the general inaccessibility of the dielectrics literature to pharmaceutical sciences. This has arisen largely for historical reasons, as most of the dielectric literature has been written on the (hitherto) reasonable assumption that any reader interested in the subject will already have a prior knowledge of dielectrics (or at least physics) *(Craig, 1995)*.

2.5 Polymorphism

Polymorphism is the ability of a solid material to exist in more than one form or crystal structure. Polymorphism can potentially be found in any crystalline

material including polymers and metals and is related to allotropy which refers to elemental solids *(Martin, 1993)*.

2.5.1 Polymorphism in pharmaceuticals

Polymorphism is important in the development of pharmaceutical ingredients. Many drugs are receiving regulatory approval for only a single crystal form or polymorph.

Polymorphs generally have different melting poitns, x-ray diffraction patterns, and solubilities, even though they are chemicall identical.

Nearlly all long-chain organic compounds exhibit polymorphism. In fatty acids, this results from different types of attachment between the carboxyl groups of adjacent molecules, which in turn modifiy the angle of the titl of the chains in the crystal *(Martin, 1993)*.

It is difficult to determine the crystal structure and molecular confirmations of different polymorphs of a single drug, and the reports of such work are not common.

Behme et al. reviewed the principles of polymorphism with emphasis on the changes that the polymorphic forms may undergo. When the change from one form to another is reversible, it is said to be enantiotropic. When the transition takes place in one direction only for example, from a metastable to a stable form the change is said to be monotropic. Enantiotropism and monotropism are important properties of polymorphs *(Martin, 1993)*.

The transition temperature in polymorphism is important because it helps to characterize the system and determine the more stable form at low temperatures.

At their transition temperatures, polymorphs have the same free energy, identical solubilities in a particular solvent, and identical vapor pressures. Accordingly, plots of logarithmic solubility of two polymorphic forms against 1/T provide the transition temperature at the intersection of the extrapolated curves. For dilute solutions, the logarithm of the solubility ratios of two polymorphs can be plotted against 1/T, and the intersection at a ratio equal to unity gives the transition temperature. This temperature can also be obtained from the phase diagram of pressure versus temperature and by using differential scanning calorimetry *(Martin, 1993)*.

Amorphus Solids. Amorphus solids may be considered as supercooled liquids in which the molecules are arranged in a random manner somewhat as in the liquid state. Substancess such as glass, pitch, and many synthetic plastics are amorphous solids. They differ from crystalline solids in that they tend to flow when subjected to sufficient pressure over a period of time, and they do not have definite melting points *(Martin, 1993)*.

Amorphus substances, as well as cubic crystals, are usually isotropic, that is, they exhibit similar properties in all directions. Crystals other than cubic are anistropic, showing different characteristics (electric conductance, refractive index, rate of solubility) in varios directions along the crystal *(Martin, 1993)*.

It is not always possible to determine by casual observation whether a substance is crystalline or amorphus. Beeswax and paraffin, although they appear to be amorphous, assume crystalline arrangements when heated and then allowed to cool slowly. It's affect directly its therapeutic activity *(Martin, 1993)*.

2.6 Water

See "Part A, 2.1" of this work.

2.7 Rochelle Salt (Sodium Potassium tartrate $NaK(C_4H_4O_6)4H_2O$)

2.7.1 The Rochelle Salt Period

Rochelle salt ($NaK(C_4H_4O_6)4H_2O$) was first synthesized in 1655 by the pharmacist Pierre Seignette in La Rochelle (France). Therefore the name Seignette salt is in use in the literature (Sodium potassium tartrate tetrahydrate (Rochelle Salt) was used for over 200 years for its mild purgative medicinal properties. Although it enjoyed a rapid distribution for medical and chemical purposes from the beginning, its unusual physical properties, especially the large piezoelectric coefficient, were discovered in the late 18th century only *(Cross and Newnham, 1987)*.

Brewster had observed the phenomenon of pyroelectricity in various crystals, among which was Rochelle Salt, but perhaps the first systematic studies were those of the brothers Pierre and Paul-Jacques Curie in 1880. This classic work established unequivocally the existence of the piezoelectric effect and correctly identified Rochelle Salt and a number of other crystals as being piezoelectric *(Cross and Newnham, 1987)*.

Walter Cady contributed to the unique way which led to the development of the piezoelectrically stabilized resonator. His massive contribution to the science of piezoelectricity is in his book *Piezoelectricity*, published in 1946. Early observations on Rochelle Salt by Cady and coworkers included measurements of elastic properties, dielectric constant, piezoelectric effects (including the first observation of the Curie point at 23°C), and the anomalously high d_{14} in this crystal *(Cross and Newnham, 1987)*.

Another major contributor to the knowledge of Rochelle Salt was Joseph Valasek. He began a systematic study of the analogy between the magnetic properties of ferromagnetics and the dielectric properties of Rochelle Salt.

These studies were to lead later to the firm establishment of the term *ferroelectricity* to describe this set of phenomena. His ballistic galvanometer studies of the charge and discharge of carefully prepared X-cut Rochelle Salt crystals clearly demonstrated for the first time the hysteretic nature of the polarization and its marked dependence on temperature *(Cross and Newnham, 1987)*.

Its extraordinary ferroelectric properties along the crystallographic a-axis were revealed by Valasek who transferred the terminology of magnetic phase transitions (Curie temperature) into the physics of dielectric materials. In his work he found two second-order phase transition temperatures at 297 K=24°C and 255 K=-18°C which indicate a narrow temperature range where ferroelectric (FE) order exists *(Cross and Newnham, 1987)*.

Mueller, for the first time distinguished the three possible origins for proper ferroelectricity in Rochelle Salt, namely the possibility of a dielectric-, an elastic-, or piezoelectric- dominated instability and, from the experimental information, showed that the driving force in Rochelle Salt was softening of the clamped dielectric stiffness X_{11} *(Cross and Newnham, 1987)*.

Some of the major difficulties which Rochelle Salt presented to the studies are *(Cross and Newnham, 1987)*:

- Rochelle salt is not stable against dehydration either in vacuum or in dry air. It is thus a difficult material to electrode for reliable electrical measurement.
- The crystal symmetry, based on morphological assessments, was incorrectly assigned. The occurrence of spontaneous polarization was a fearsome violation of the by-then sacred Neumann's principle, and it was not until Jaffe's suggestion of the necessary occurrence of phase change at T_C that this seeming conflict was resolved.

- The very marked structural complexity. With 112 atoms unit cell, it was not until 1941 made the first X-ray structure analysis and it was not until 1954 that the detailed neutron diffraction data of Fraser was finally able to pin down the troublesome water molecules.
- The strong ferroelastic bias in most small crystals made them almost always unipolar and ever the larger samples were often spontaneously biased.
- Rochelle Salt remains one of the few ferroelectric crystals with such a limited ferroelectric range and two clear Curie points.

2.7.2 Crystal Structure of Rochelle Salt (NaK $(C_4H_4O_6)4H_2O$)

Depending on their geometry, crystals are commonly classified into seven systems: triclinic (the least symmetrical), monoclinic, orthorhombic, tetragonal, trigonal, hexagonal, and cubic *(Institute of Electrical and Electronics Engineers, 1986)*.

The crystal structure of the non-polar phases of pure NaK-tartrate was determined to be orthorhombic. The structure of the polar phase was found to be monoclinic. Despite numerous theoretical approaches there is no overall consensus concerning the explanation of the strange re-entrant behavior. *(Schneider, et al., 1999)*.

The seven systems that were mentioned above are divided into point groups (crystal classes) according to their symmetry with respect to a point *(Institute of Electrical and Electronics Engineers, 1986)*.

The crystal symmetry is that of class 222, except that between about -16°C and 24°C there is a minute departure from orthorhombic symmetry to monoclinic, class 2 *(Mueller 1935, 1940)*.

The *a* axis of the orthorhombic crystal becomes the unique diad axis of the monoclinic crystal. Figure 6 shows a Rochelle Salt crystal with the polar axis marked *(Wooster, 1953)*.

For an orthorhombic crystal of class 222 the three relevant piezoelectric module are d_{14}, d_{25} and d_{36}. Of these d_{25} and d_{36} have normal values in Rochelle Salt and show no remarkable change with temperature. Modulus d_{14} however is anomalous. Below -16°C it is small but at this temperature it rises at first gradually and then rapidly up to about 3 x 10^{-4} which is roughly 10^4 times as large as the principal modulus for α-quartz. Beyond 22.5°C the modulus d_{14} falls rapidly until at 30°C the conductivity becomes too great for further measurements *(Wooster, 1953)*.

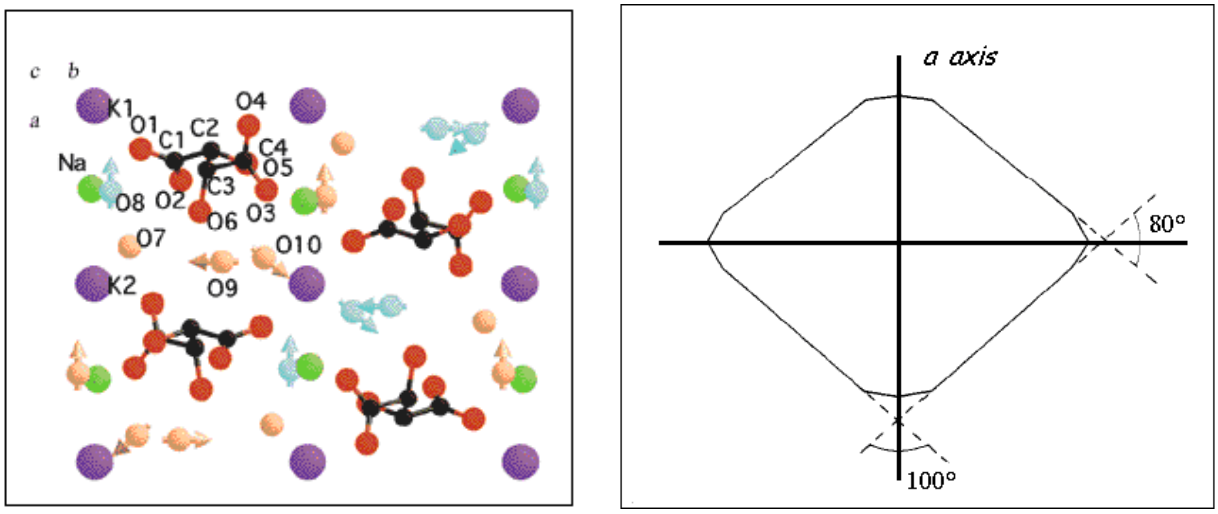

Fig. 2.6. Section through Rochelle Salt crystal, showing the polar *a* axis.

2.7.3 Polymorphism of Rochelle Salt

The polymorphic transition of Rochelle Salt is of a very unusual type.

According to the X-ray evidence it does not involve any marked structural changes, it has no latent heat of transition and it is not accompanied by a sudden change of the optical properties. It is a transition of the second kind

which the specific heat and the temperature gradient of the birefringence have a discontinuity at the Curie point. Especial significant is the fact that one can produce artificially, at temperatures above the Curie point, the same type of polymorphic transition which occurs spontaneously below the Curie point. This can be accomplished by applying either an electric field in the direction of the *a* axis or a shearing strain in the *b, c,* plane. In either case the angle between the *b* and *c* axes is slightly changed, the optical properties are altered and the crystal becomes pyroelectric. To realize that the latter statement is true in this experiment they recall the above the Curie point the dielectric and piezoelectric constants show a large temperature variation. Hence if a constant field or stress is applied the electric polarization of the crystal varies with temperature *(Mueller,1940)*.

Mueller, has shown that the relation between the spontaneous polarization and the change of birefringence is the same as between dielectric polarization above the Curie point *(Mueller,1940)*.

The polymorphic transition is simply a spontaneously occurring elastic deformation. It can be explained on the basis of the dipole theory: The spontaneous deformation is the inverse piezoelectric effect produced by the spontaneous polarization *(Mueller,1940)*.

At the Curie points the orthorhombic lattice of Rochelle Salt becomes unstable against elastic deformations, i.e., an elastic anomaly is the intrinsic cause of the abnormal properties *(Mueller,1940)*.

Some of the experimental results imply indeed, since the crystal gets a shearing strain without a stress being applied, that the elastic modulus becomes infinitely large at the Curie point the lattice has two elastically stable states. An alternating field can force it to flop from one position into the other, hence the hysteresis loops *(Mueller,1940)*.

If this interpretation the final solution of the problem of Rochelle Salt must be found in its lattice structure and the lattice forces, and not in the dipole-dipole interaction.

2.8 Potassium dihydrogen phosphate (KDP)

Systematic experimental research, based on a theoretical model have lead us to a new substance with a temperature variation of the dielectric constant similar to Rochelle salt. This is the primary potassium phosphate (KH_2P0_4) crystallizing with tetragonal-scalenoedric symmetry, but containing no crystal water. The principal dielectric constant ε_{33}, measured parallel to the crystallographic c-axes is of special interest. Figure 2.7 shows its temperature-variation as a result of measurements with 50 cycles a.c. at a field strength of 1000 V/cm. At room temperature ε_{33} has a value of 30 approximately, then rises steeply, reaches a maximal value of 155 at –130°C and stays approximately constant down to –190°C. Below –200°C ε_{33} drops again to 7 approximately. Like Rochelle salt KH_2P0_4 exhibits two Curie points θ_1 *(*T_1*)* and θ_2 *(*T_2*)* at –130°C and –195°C respectively. Although the absolute values of the dielectric constant are much lower than for Rochelle salt, the typical temperature variation is the same. *(A new Seignette-Electrics substances, G. Busch and P. Scherrer. Ferroelectrics, 1987, Vol. 71, pp.15-16).*

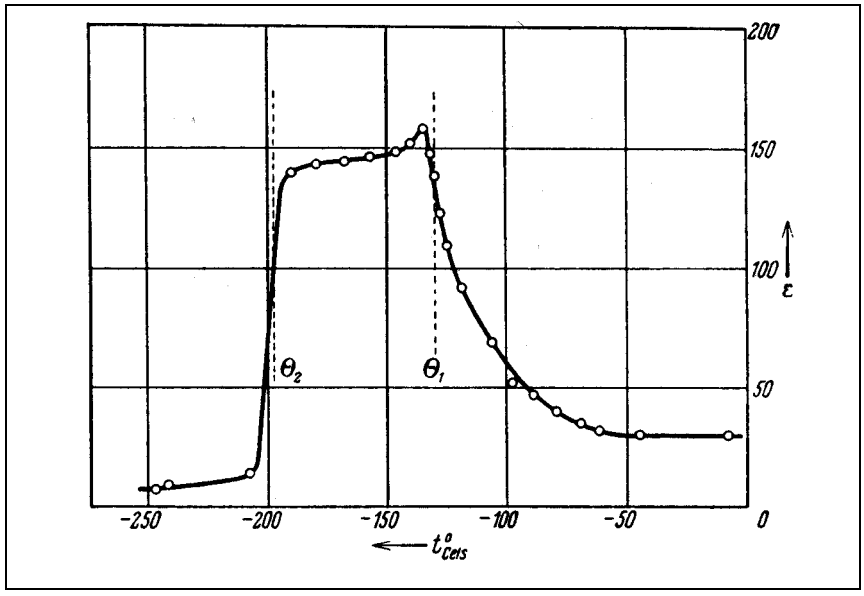

Fig. 2.7. Temperature variation of the dielectric constant ε_{33} of KH2P04

KH_2P0_4 exhibits a dielectric constant of 31, which is unusually high. In contrast K_3PO_4 and K_2HP0_4 show normal values. The assumption that the primary potassium phosphate contains dipoles seems plausible, therefore. This conjecture is supported by the existence of H_2 in this salt and the possibility of an interaction of H_2 with an oxygen atom.

In table 2.1 ε is the dielectric constant, *d* the density, *M* the molecular weight and the expression (ε – 1)*M* / *d* the molecular dielectric constant. *(The dielectric constant of some potassium salts and alkali halides, Gert Steulmann, Ferroelectrics, 1987, vol. 71, pp. 11-13).*

Salt	ε	*d*	*M*	(ε – 1)*M* / *d*
$KClO_4$	5.9	2.52	138.60	269.5
KCN	6.15	1.52	65.10	221.0
KCNS	7.9	1.886	97.10	355.5
$KbrO_3$	7.3	3.24	167.00	325.8
KJO_3	16.85	3.89	214.0	872.0
K_3PO_4	7.75	-	212.3	-
K_2HPO_4	9.05	-	174.2	-
KH_2PO_4	31	2.338	136.1	1745
KH_2AsO_4	>31	2.86	140.9	-

Table 2.1. Properties of some Potassium salts. (The dielectric constant of some potassium salts and alkali halides, Gert Steulmann, Ferroelectrics, 1987, vol. 71, pp. 11-13).

For comparison the values of the potassium salts are listed in Table 2.2.

Salt	ε	*d*	*M*	(ε – 1)*M* / *d*
KCl	4.51	1.98	74.6	132
KBr	4.6	2.75	119.0	155.8
KJ	5.2	3.115	166.0	221.5
K_2CO_3	4.96	2.29	138.2	239
K_2SO_4	6.4	2.666	174.2	361
KNO_3	4.37	2.109	101.1	161.7
$KClO_3$	5.1	2.344	122.6	214.2

Table 2.2. Properties of some Potassium salts for comparison. (The dielectric constant of some potassium salts and alkali halides, Gert Steulmann, Ferroelectrics, 1987, vol. 71, pp. 11-13).

The principal dielectric constants ε_a and ε_c were measured on crystal plates oriented perpendicular to the *a* and *c* axis of the crystals at frequency of 800 Hz and a fieldstrength of 200 V/cm. The results are shown in figure 2.8.

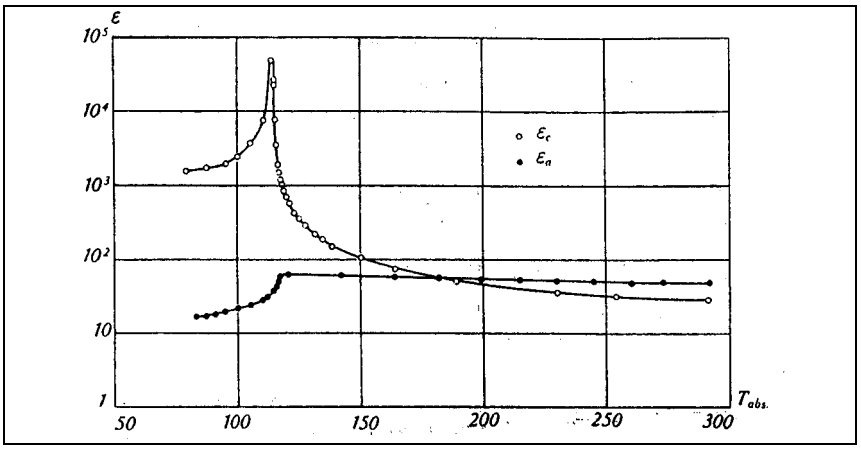

Fig. 2.8. Dielectric Constants ε_a and ε_c of KH_2PO_4 as a function of temperature. E = 200 Volt cm^{-1}, n = 800 Hz

KH_2PO_4 $\varepsilon_c = 29$ at $T = 273$ K and rises to a maximum of 47500 at $T = 114$ K. Up to these temperatures the dielectric constant is independent of the frequency and the fieldstrength. For lower temperatures ε_c decreases again and depends strongly on frequency and fieldstrength. Because of the onset of harmonics it is impossible to bring the measuring bridge to equilibrium.

Plotting the reciprocal susceptibility $1/\chi_c = 4\pi /(\varepsilon_c - 1)$ we obtain the diagram shown in figure 2.9. Extrapolating the curve to $1/\chi_c = 0$, according to a Curie-

Weiss relation $1/\chi_c = c\,(T - \theta)$, we find the Curie point of $\theta = 115$ K for KH_2PO_4. However, as can be seen, the measured points do not lie on a straight line, which means that the Curie-Weiss law is not strictly fulfilled in a wide temperature range. A fit between measured and calculated values of χ can be obtained by modifying the Langevin-Weiss theory.

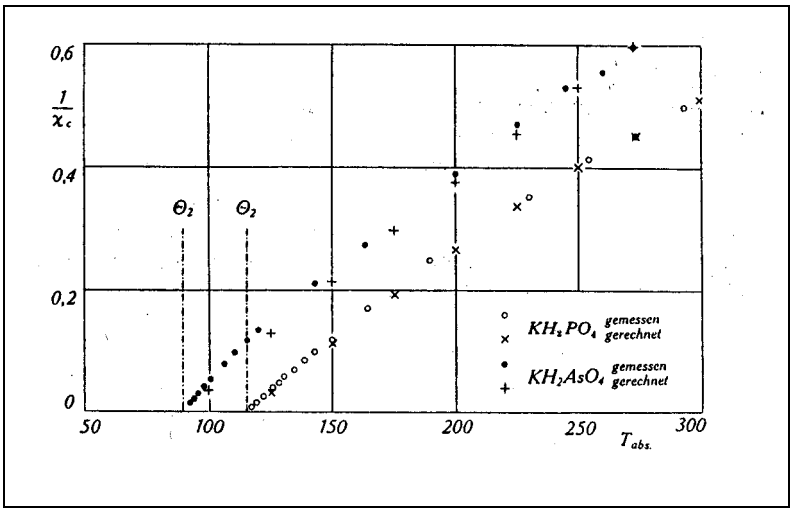

Fig. 2.9. Reciprocal Susceptibility χ_c of KH_2PO_4 and KH_2AsO_4 for comparison as a function of temperature.

For KH_2PO_4 the temperature variation of the dielectric constant ε_a, perpendicular to siegnette electric axis is remarkable, as can be seen in Figure 2.10. (At room temperature $\varepsilon_a = 47.8$). These value rise up to 62 at 120 K. In contrast to ε_c the dielectric constants in the *a*-direction are independent of the frequency and the fieldstrength. In both cases ε_a and ε_c drop sharply below the Curie temperature.

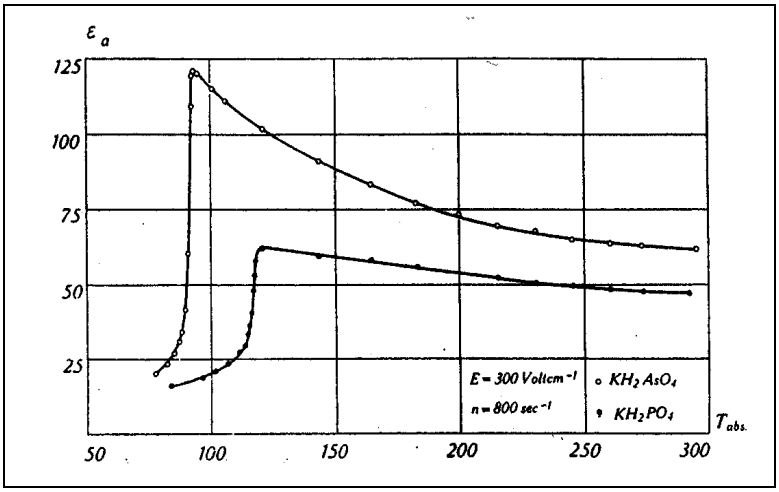

Fig. 2.10. Dielectric Constant ε_a of KH_2PO_4 and KH_2AsO_4 for comparison as a function of temperature.

Since in the *a*-direction no spontaneous polarization and no signs of siegnette electricity show up, the high values of 50 to 60 are surprising and difficult to understand.

The polarization *P* was measured by means of a ballistic galvanometer at d.c. fieldstrengths up to 50 V/cm. For temperature below the Curie temperature θ the polarization increases approximately with the square of the fieldstrength; for T > θ the relation is linear. At these low fields the polarization and the dielectric constant show the typical sharp peaks at the Curie points.

For higher field strengths, up to 3000 V/cm a circuit indicated by Valasek was applied. The voltage can be changed in steps of 30 Volts up to 300 Volts, back to 0, to –300 Volts and again back to 0.the induced charges were measured again with ballistic galvanometer. The results are typical hysteresis curves shown in Figure 2.11 at a temperature of 78.5 K. Saturation is reached at about 2000 V/cm and the respective charge density is $3.6*10^{-6}$ Coul/cm^2. These values are about 25 times higher than those found for Rochelle salt. With increasing temperature the hysteresis loops become narrower and disappear completely at the Curie point. In the *a*-direction of the crystals no hysteresis was observed.

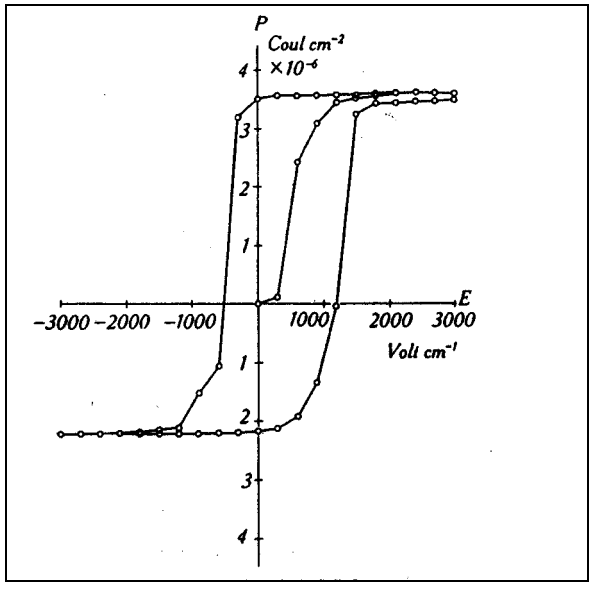

Fig. 2.11. Hysteresis of KH_2PO_4 at *T* = 78.5 K.

From ac-measurements by means of Sawyer and Tower's method the variation of the polarization at saturation with temperature was obtained. The result is shown in Figure 2.12. Below the Curie point the polarization rises much faster than would be expected according to a Langevin-Weiss type model of dipole orientation.

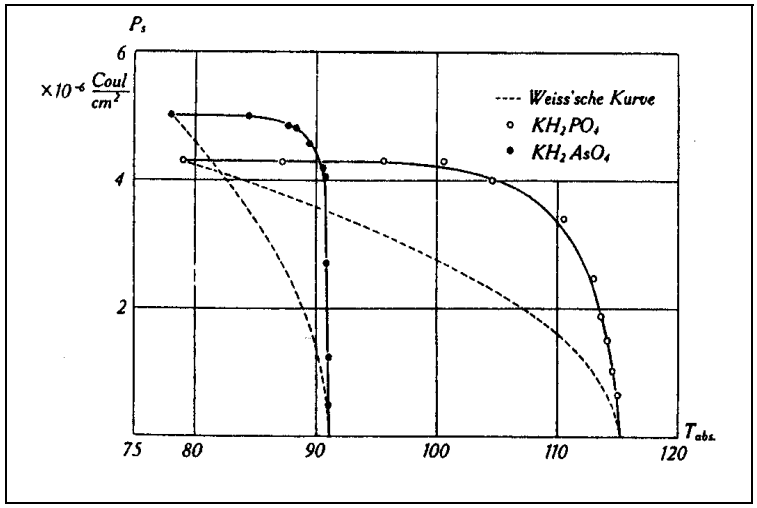

Fig. 2.12. Polarization at saturation of KH_2PO_4 and KH_2AsO_4 for comparison as a function of temperature.

Although the nature of the dipoles is unknown, water molecules as their carriers can be excluded. According to West's X-ray analysis no water molecules do exist in KH_2PO_4. However, O—H groups or O—H•••O groups might generate dipolemoments. The latter group represents the hydrogen bonding, found in KH_2PO_4 by West. This type of bonding was discussed especially by Bernal and Megaw. *(New Seignette-Electrics, G. Busch, Ferroelectrics, 1987, Vol 71, pp. 17-24).*

Some solubility parameters of KH_2PO_4 in different temperatures is shown in Figure 2.13. *(Guohui Li et al.: Rapid growth of KDP crystal from aqueous solutions).*

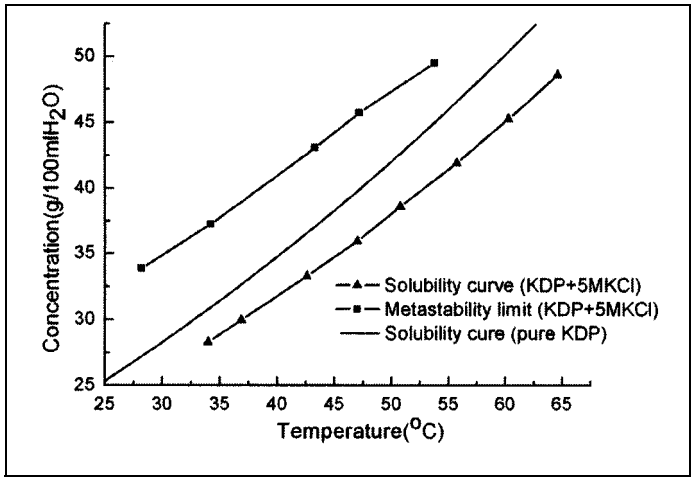

Fig. 2.13. Solubility parameters of KH_2PO_4.

2.9 Amonium dihydrogen phosphate (ADP)

At room temperature the $NH_4H_2PO_4$ shows properties very similar to those of potassium salts. Mearsurements of the dielectric constants as a function of temperature by G. Busch are shown in Figure 2.14. In contrast to potassium salts ε_c is smaller than ε_a. With falling temperature both quantities show a rapid rise, but at a critical temperature the crystals disintegrate into small pieces due to a structural transition apparently. A low temperature structural transition seems to occur in these crystals. *(New Seignette-Electrics, G. Busch, Ferroelectircs, 1987, VOL. 71, pp. 17-24).*

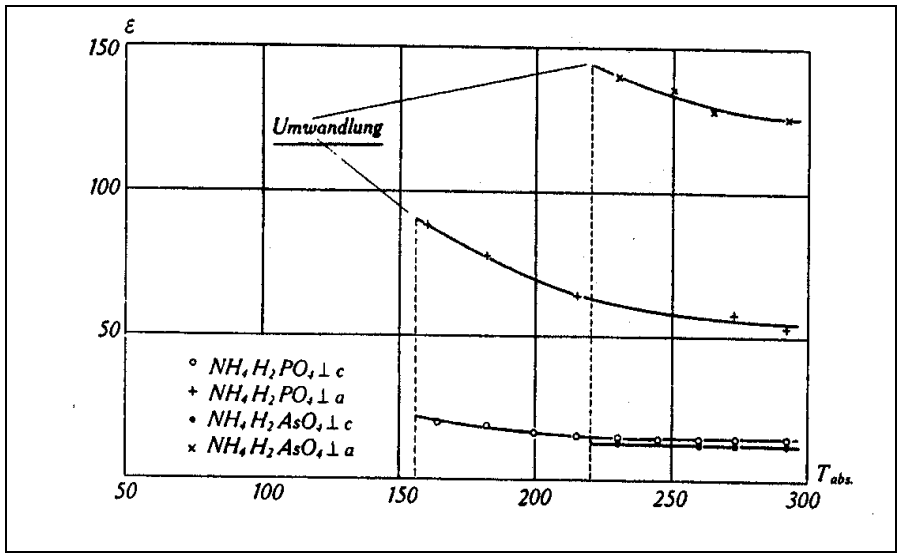

Fig. 2.14. Dielectric constants of $NH_4H_2PO_4$ and $NH_4H_2AsO_4$ as a function of temperature.

Some properties of $NH_4H_2PO_4$ can be compared to KH_2PO_4 in Table 2.3.

Propertiey	KH_2PO_4	$NH_4H_2PO_4$
Molecular weight	136.14	158.98
Density	2.338	1.803 – 1.799
Number molecules/ cm^3	10.3×10^{21}	8.73×10^{21}
Melting point	96°C	Decomp
Symmetry	Tetrag.	Tetrag.
Space group	V_d^{12}	V_d^{12}
Lattice constants	7.43×10^{-8} 6.97	7.51×10^{-8} 7.53
Refractive index n_a	1.5095	1.5246
Refractive index n_c	1.4684	1.4792
Piezoelectricity	-	Pos.
Average Diel. Const.	31 17.93	- -

Table 2.3. Properties of KH2PO4 & NH4H2PO4. (New Seignette-Electrics, G. Busch, Ferroelectircs, 1987, VOL. 71, pp. 17-24).

Chapter 3

Materials and Methods

3.1. Materials

3.1.1. Sodium Potassium tartrate, known as Seignette salt or Rochelle salt

Sigma-Aldrich Laborchemikalien GmbH. D-30926 Seelze

Article number 25508

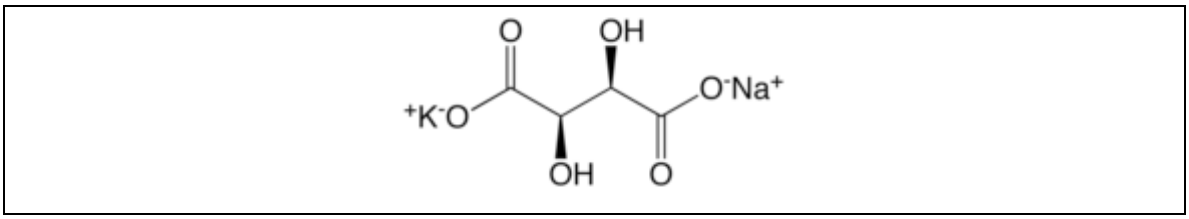

Molecular formula	$NaK(C_4H_4O_6)4H_2O$
Molecular weight mw (g/mol)	282.22
Density (g/ml)	1.79
Solubility	Slightly soluble in alcohol Completely soluble in water
Melting point	55.65 °C

Seignette salt as was mentioned is a ferroelectric substance which has a Curie temperature at -18°C and 24°C to investigate its their ferroelectric and structural properties change in a binary system as well as in a ternary system.

3.1.2. 1,4-Dioxane

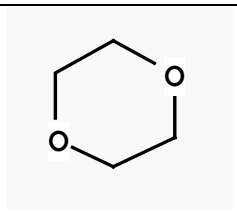

Molecular formula	$C_4H_8O_2$
Molecular weight mw (g/mol)	88.11
Density (g/ml)	1.02797
Static permittivity	2.21
Dipole moment	0.00
Melting point	11.8 °C
Boiling point	101.1 °C

1,4-Dioxane is a cyclic flexible diether, possesses through its symmetry no overall dipole moment, but it is miscible with water due to hydrogen bonding to the exposed oxygen atoms.

3.1.3. Potasium dihydrogen phosphate (KDP)

Fluka Chemie GmbH CH-9471 Buchs

Article number 60230

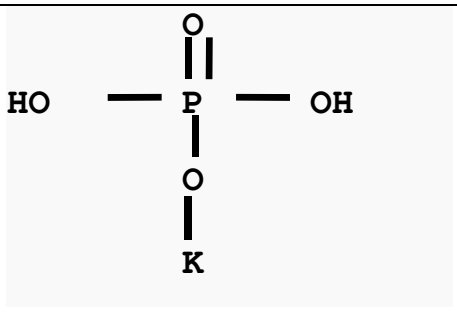

Molecular formula	KH_2PO_4
Molecular weight mw (g/mol)	136.09
Density (g/ml)	2.338
Melting point	253.8 °C
Solubility	Slightly soluble in alcohol Completely soluble in water

3.1.4. Amonium dihydrogem phosphate (ADP)

Fluka Chemie GmbH CH-9471 Buchs

Article number 09708

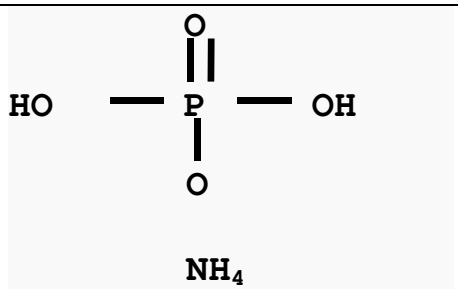

Molecular formula	$NH_4H_2PO_4$
Molecular weight mw (g/mol)	115.03
Density (g/ml)	1.803
Melting point	190 °C
Boiling point	87.4 °C
Solubility	Slightly soluble in alcohol Completely soluble in water

Water

Freshly prepared by means of Büchi Fontavapor 285

For physicochemical properties and structure see “Part A, 2.1” of this work.

Substance	1,4-dioxane	Potassium sodium tartrate tetrahydrate	Potassium dihydrogeh phosphate	Ammonium dihydrogen phosphate	Water
	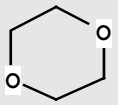	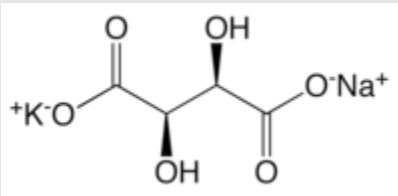	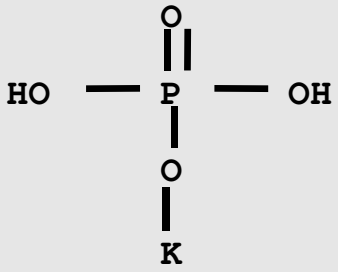	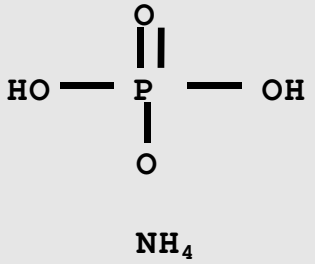	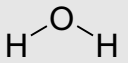
CA registry number	123-91-1	304-59-6	7778-77-0	7722-76-1	7732-18-5
Molecular formula	$C_4H_8O_2$	$NaK(C_4H_4O_6)4H_2O$	KH_2PO_4	$NH_4H_2PO_4$	H_2O
Molecular weight mw [g/mol]	88.11	282.22	136.09	115.03	18.02
Density ρ [kg/m^3]	1.02797	1.79	2.338	1.803	0.99705
Melting point [°C]	11.8	55.65	253	190	1
Boling point [°C]	101.1	200	-	87.4	100
Solubility	Completely miscible with water	Completely soluble in water Slightly soluble in alcohols	Completely soluble in water Slightly soluble in alcohols	Completely soluble in water Slightly soluble in alcohols	Completely miscible with alcohols

Table 3. Literature values of some physical properties of the measured solvents and salts at 298.2 K [Barton, 1991], [CRC Handbook of Chemistry and Physics, 1997], [Fluka, 2006], [ChmDAT, 2001], [Merck Index, 1983], [Purohit et al., 1991]

3.2. Apparatus

The following apparatus were used for sample preparation and analysis:

- **Analytic Balance**
  Mettler-Toledo AG CH-8606 Greifensee
  AT 460 Delta Range; 1115330561

- **Bidistilling Apparatus**
  Büchi AG CH-9230 Flawil
  Fontavapor 285; 499982

- **Stirrer**
  VarioMag Magnetic stirrer
  Electronichührer Multipoint HP 6
  Speed range 100-750 rpm

- **Network Analyser**
  Agilent Technologies Inc. USA-Palo Alto CA 94304-1185
  HP 8720D 50 MHz – 20GHz

- **Slim Form Probe**

Frequency range	500 MHz to 50GHz
Finish Nickel	100 µinches

Operating temp.	0-125°C
Outside diameter of tip (approximate)	2.2 mm
Immersable length (approximate)	200 mm
Connector	2.4 mm male
Repeatability and resolution	two to four times better than accuracy
Material under test assumumptions	Liquid of soft semi-solid. Material is “infinite” in size, non-magnetic (μr=1) Isotropic (uniform orientation), and homogeneous (uniform composition)
Sample requirements	Diameter: Minimum 5mm insertion and 5mm around tip of probe.
Accuracy	Dielectric constant εr: ±5% of |εr| Loss tangent, tan d, εr”/ εr’: ±0.05

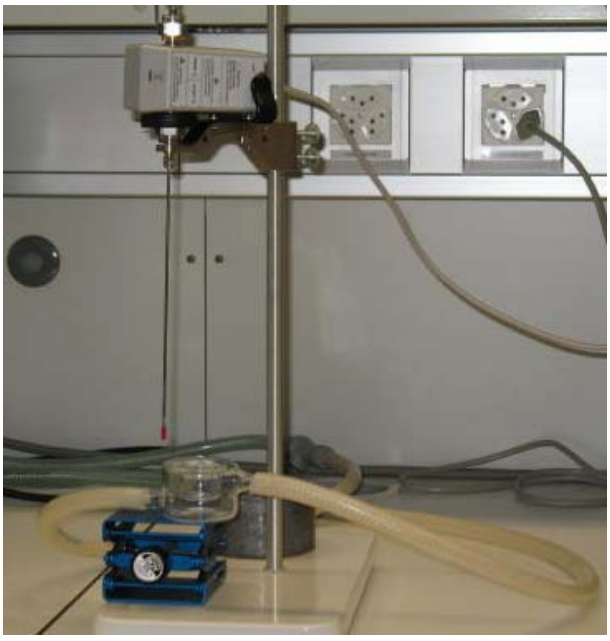

- **ECal module**

Model number N4691-60004

Connector type 3.5mm

Operating Frequency 300 kHz to 26.5 GHz

- **Connecting cable**

High Temperature 20 GHz Cable

Type-N female 1250-1743

2.4 mm male 11901D

- **Thermostat / circulating water bath**

B. Braun Biotech International GmbH D-34209 Melsungen

Thermomiux UB; 852 042/9; 90120498

Frigomix U-1; 852 042/0; 8836 004

Temperature control of $\pm$0.1°C

- **Measuring Vessel**

Pyrex-Glass

Diammeter 25 mm

Height 25 mm

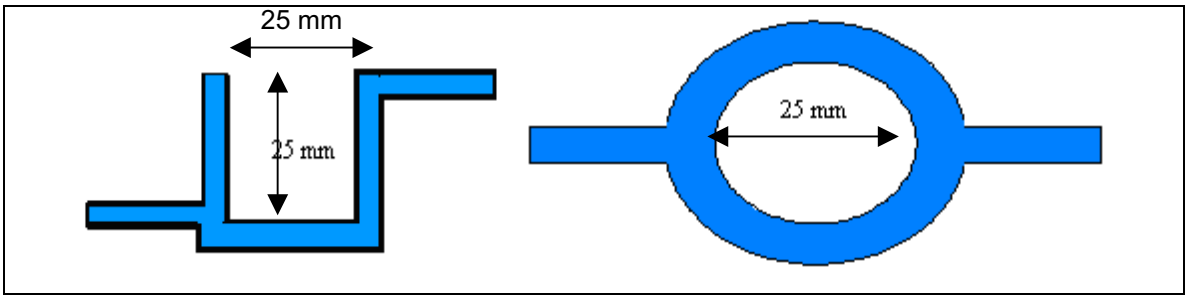

- **Digital Thermometer**

Haake GmbH D-76227 Karlsruhe

DT 10

Pt. 100 platinum resistance thermometer

- **Infrared Thermometer**

Fluke 66 Ir Thermometer

3.3. Computer Software

- **HP 85070 Software Program**

Agilent Technologies Inc.

And for the data analysis:

- **Excel**

Microsoft Corp. USA-Redmond W A 98052-6399

Version 2000

- **SYSTAT for Windows**

SPSS Inc. USA-Chicago IL 60606-6307
Version 7.0

3.4. Methods

3.4.1. Sample Preparation

Samples were prepared by weighing each amount of salt: 5, 10, 20, 30 and 35 g, with the necessary amount of distilled water into 50 ml volumetric flasks.

A pure solid salt sample was also measured.

The samples were stirred at 750 rpm using a magnetic stirrer until complete dissolution.

3.4.2. Measurement of Dielectric Constant ε

3.4.2.1. Measuring principle

The sample was poured into the measuring vessel which is connected to the Thermostat (control +0.1C) with the required temperatures (10, 20, 25, 30, 40, 50, 60 and 70°C).

The temperature of the samples was checked by means of Digital Thermometer (+0.1C). For the pure solid salt sample the temperature was checked by the Infrared Thermometer.
The temperature of the probe was also checked using the Infrared Thermometer.

The measurements were made by means of a personal computer connected to the Network Analyzer, using software HP 85070 (Agilent Technologies).

3.4.3. Measuring procedure

Measurements were made between 0.5-20.05 GHz at 351 points.

The slim probe was calibrated by air, calibration short block and bidistilled water.

The slim probe was recalibrated by using the ECal module before every measurement

Measurements are made by immersing the probe into the sample, which was brought to the required temperature. Special attention has to be paid to avoid the bubbles on the measuring surface of the probe. The samples were measured 3 times at each temperature.
This procedure was also done for the bidistilled water at each temperature.

The measuring system consists of a dielectric probe and an Ecalmodule were connected to a network analyzer by means of a high temperature 20GHz cable. The probe transmits an electromagnetic signal into the material under test (MUT) via cable.

ECal module recalibrates the system automatically, in seconds, just before each measurement is made. This virtually eliminates cable instability and system drift errors.

Processes can be monitored over long time periods, including tests that vary MUT temperature, and pressure over time.

This ECal module is connected in line between the probe and the network analyzer test port cable. The ECal module communication port is connected either to the PNA Series network analyzer running the 85070E software. The software guides the user through a normal “three standard” calibration, (open, short, water), performed at the end of the probe. This calibration is then transferred to

the ECal module. The ECal module remains in line and a complete ECal calibration is automatically performed before each measurement. Errors due to test port cable movement or temperature change are removed by the new calibration.

3.4.4. Data analyses

For investigating the ferroelectric activities, we took a look at the changes of the real and imaginary parts of complex permittivity $(\varepsilon', \varepsilon'')$ in different temperatures to see if there is any sudden increase / decrease observed.

Furthermore we investigated the relaxation time (τ) in all volume fractions and at all measured temperatures. (For more information about relaxation time and its explanation please see “Part A, 2.3.6).

Chapter 4

Results and Discussion

4.1 Investigation of ferroelectric activity in pure Seignette Salt and its binary and ternary mixtures of H2O and H2O/Dioxane in different temperatures

The pure Seignette salt was examined at the temperature range of 10-88.5°C to investigate the influence of the temperature on its ferroelectric behavior.

Pure Water and Pure 1,4-Dioxane were studied at the temperature range of 10-70°C in order to investigated the influence of the temperature on the structural properties as well as their Dielectric behaviour.

Additionally, we studied the binary mixture of Seignette salt-Water and the ternary mixture of Seignette salt-Water-Dioxan, at the temperature range of 10-70°C in order to investigate the influence of the temperature, and volume fractions on the ferroelectric properties of the Seignette salt.

In this chapter, we discuss the real part of dielectric constant and the imaginary part is shown in the figures.

4.1.1 Influence of temperature on Pure Seignette Salt, Pure Water and Pure Dioxan

Pure Seignette Salt (Melted & Relative measurement)

4.1.1.1 Pure Seignette Salt, Melted measurement

In order to find out more information about the ferroelectric properties, the dielectric constant of the pure Seignette salt was measured. This results help to interpretate the measurements of binary and ternary mixtures.

As it was mentioned in section 1.8, Seignette salt is a ferroelectric substance that has two Curie temperature of -18°C and 24°C and above the Curie temperature, the Seignette salt loses its ferroelectric ability and the salt present a Paraelectric behaviour.

The dielectric constant of the pure salt was measured at the frequency range of 500 MHz – 20.05 GHz. The salt was placed in the measuring vessel, the crystals begin to melt and a transparent gel like liquid was obtained. Then the temperature was increased until 88.5°C. Finally the sample was coold down until 10°C. The salt recrystalices from its gelatinus like solution to a white solid state. The results are shown in the Table 4.1.

In this study, we can observe that the dielectric constant shows a temperature dependence behaviour. When the temperature was increased the dielectric constant shows a small rise (see Figure 4.1). We can not observe the transition of ferroelectric to paraelectric mentioned above. This maybe due to the result of different recrystalization or change in its polymorphic form.

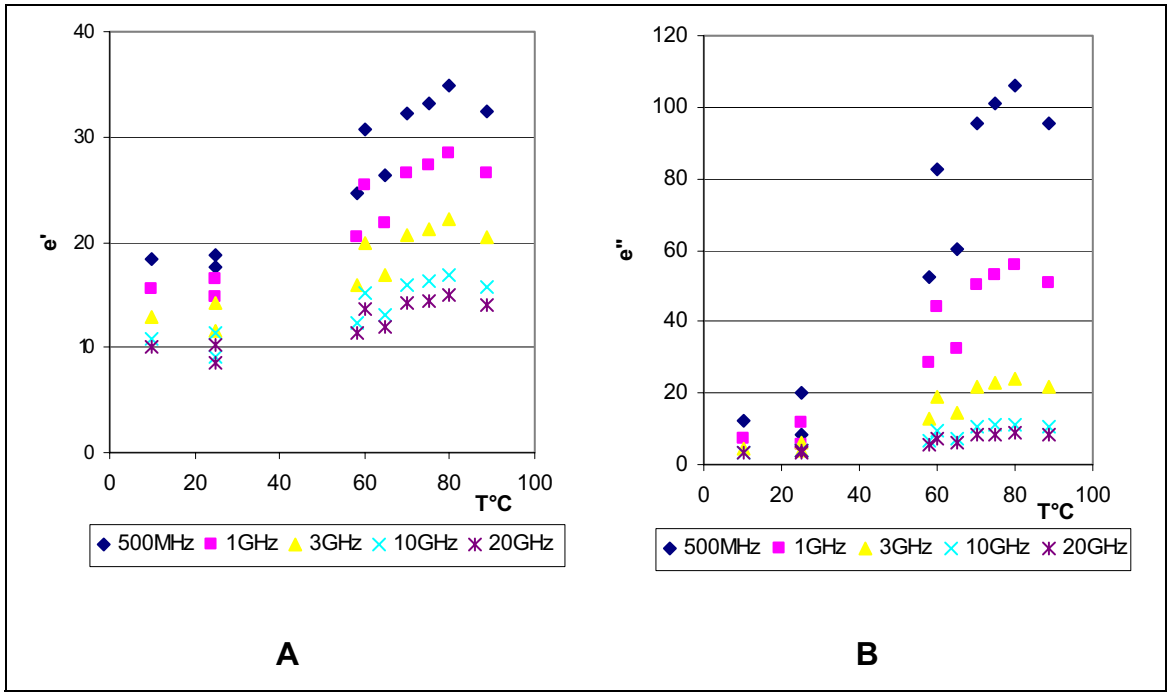

Figure 4.1. A) Real and B) Imaginary part of complex permittivity for Pure Seignette salt measured at temperatures between 10 and 88.5°C.

Temperature °C	500 MHz e'	1 GHz e'	3 GHz e'	10 GHz e'	20 GHz e'
10	18.3609	15.4890	12.9614	10.7895	10.0973
25	17.7110	14.7909	11.6467	9.1714	8.5893
58	24.5871	20.4312	15.9056	12.3761	11.2874
60	30.7923	25.4153	19.8489	15.1923	13.6126
65	26.3057	21.7352	16.9213	13.1132	11.9148
70	32.2333	26.5119	20.7078	15.8385	14.1411
75	33.2154	27.2472	21.2263	16.2319	14.4756
80	34.9312	28.5193	22.1140	16.8574	15.0646
88.5	32.4671	26.4683	20.4821	15.7113	14.1038

Table 4.1. Dielectric Constant of Pure melted Seignette Salt measured at different temperatures at frequencies: 500 MHz, 1GHz, 3GHz, 10GHz and 20GHz.

4.1.1.2 Pure Seignette Salt Relative measurement

The dielectric constant of the Seignette salt crystals was measured at the frequency range of 500 MHz – 20 GHz. The crystals were placed into the

measuring vessel. In order to find the ferro – paraelectric behaviour the temperature was gradually increased from 15 to 35°C. The results are shown on the Table 4.2.

The contact between the measuring surface of the probe and crystals are always constant (There were no change to the contact surface between crystals and probe). The sample was brought to the require temperature and then the probe was inserted into the sample.
We could not observe the ferro to paralectric behaviour. (see Figure 4.2).

Temperature °C	500 MHz e'	1 GHz e'	3 GHz e'	10 GHz e'	20 GHz e'
15	1.8914	1.9902	1.9081	1.8836	1.9799
20	3.1220	3.1878	2.9015	2.8613	2.9877
22	2.7212	2.8247	2.5934	2.5696	2.6295
23	2.8365	2.7287	2.7451	2.6413	2.7588
23.5	2.9706	3.0066	2.8494	3.0691	2.8845
24	3.0624	3.2106	2.9897	3.0473	3.0910
24.5	2.9992	3.0287	2.9351	2.7312	2.8936
25	3.0209	2.9750	2.8258	2.8186	2.9539
26	2.3097	2.3172	2.2260	2.1866	2.3064
27	3.8445	3.7848	3.5923	3.4886	3.6412
28	3.7441	3.6945	3.4180	3.2596	3.4237
29	3.3229	3.3304	3.1379	3.0335	3.2318
30	3.5677	3.5412	3.3516	3.2424	3.4205
31	3.1519	3.1363	2.9218	2.8395	2.9856
32	3.8041	3.7258	3.5136	3.4197	3.6438
33	3.3970	3.4011	3.2145	3.1204	3.3123
35	4.1509	4.0515	3.8371	3.7541	3.9964

Table 4.2. Dielectric Constant of Pure Seignette Salt measured at different temperatures at frequencies: 500 MHz, 1GHz, 3GHz, 10GHz and 20GHz.

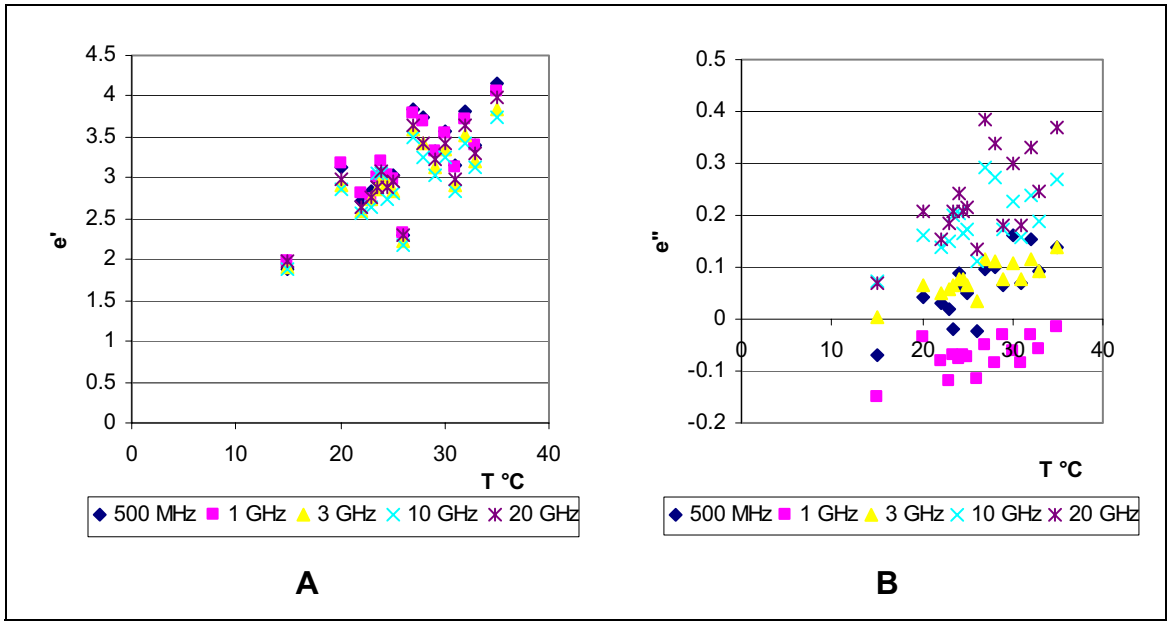

Figure 4.2. A) Real and B) Imaginary part of complex permittivity for single Seignette crystals measured at temperatures between 10 and 35°C.

4.1.2 Pure Water

Water presents a high polarizability, dipole moment and the ability to act as a proton acceptor and donor. One of its unusual properties is that water presents a high dielectric constant of 78.39 at room temperature.

The dielectric constant of the pure water was measured at the temperature range varies between 10 and 70°C. The results are shown in the Table 4.3. The Figures 4.3 – 4.5 show the dielectric constant versus the frequency.

We can observe that when we increased the temperature the dielectric constant decrease in frequencies below 10GHz. Due to higher temperature, the molecular movement increases and the intermolecular forces, caused by dipole-dipole interactions and hydrogen bonds are reduced. The temperature is an important factor in determining the structure of water in aqueous solutions.

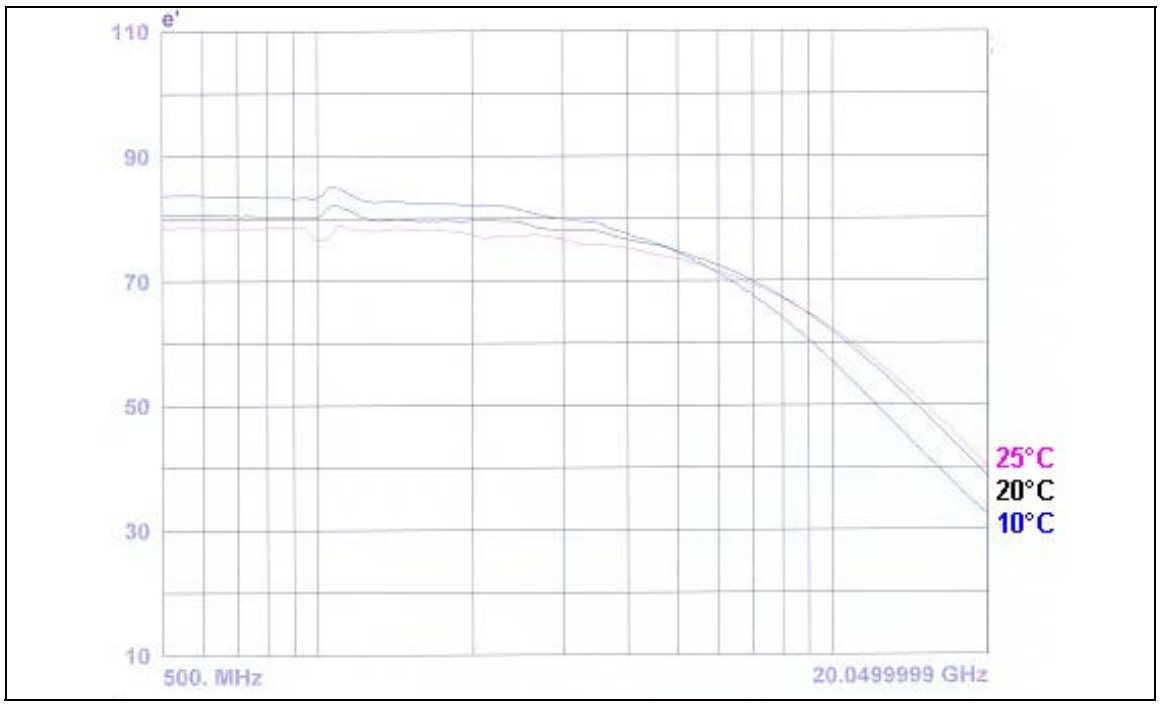

Figure 4.3. Dielectric Constant of Pure Water measured at temperatures 10, 20 and 25°C.

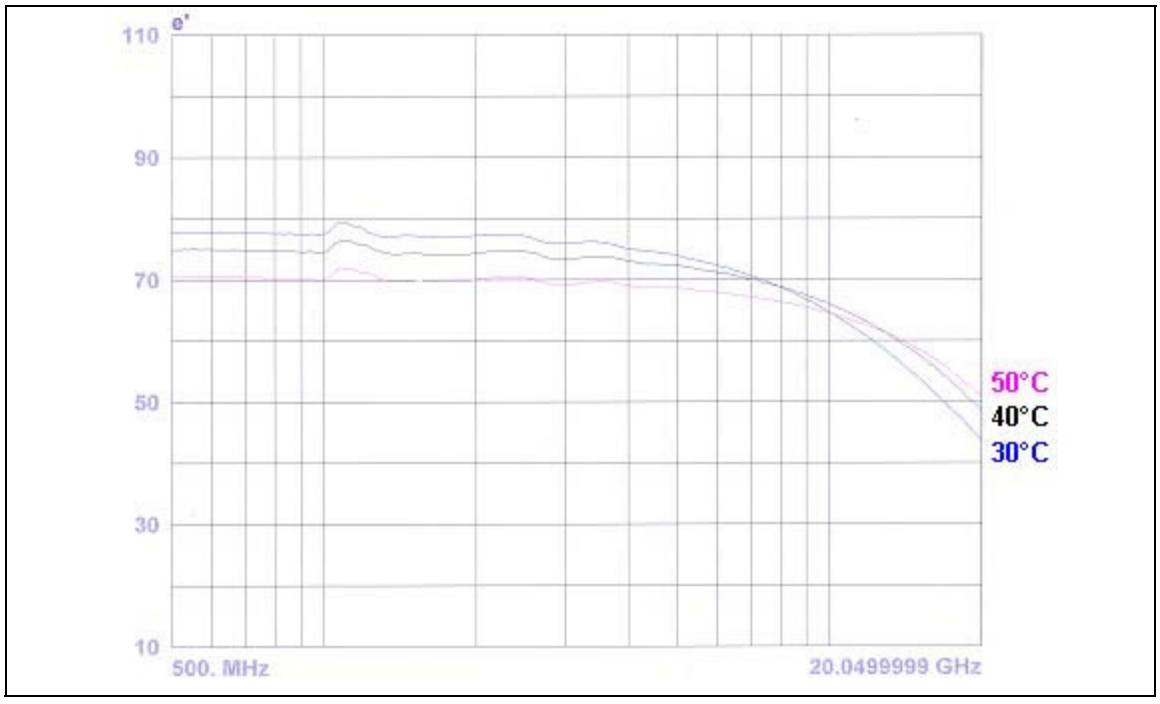

Figure 4.4. Dielectric Constant of Pure Water measured at temperatures 30, 40 and 50°C.

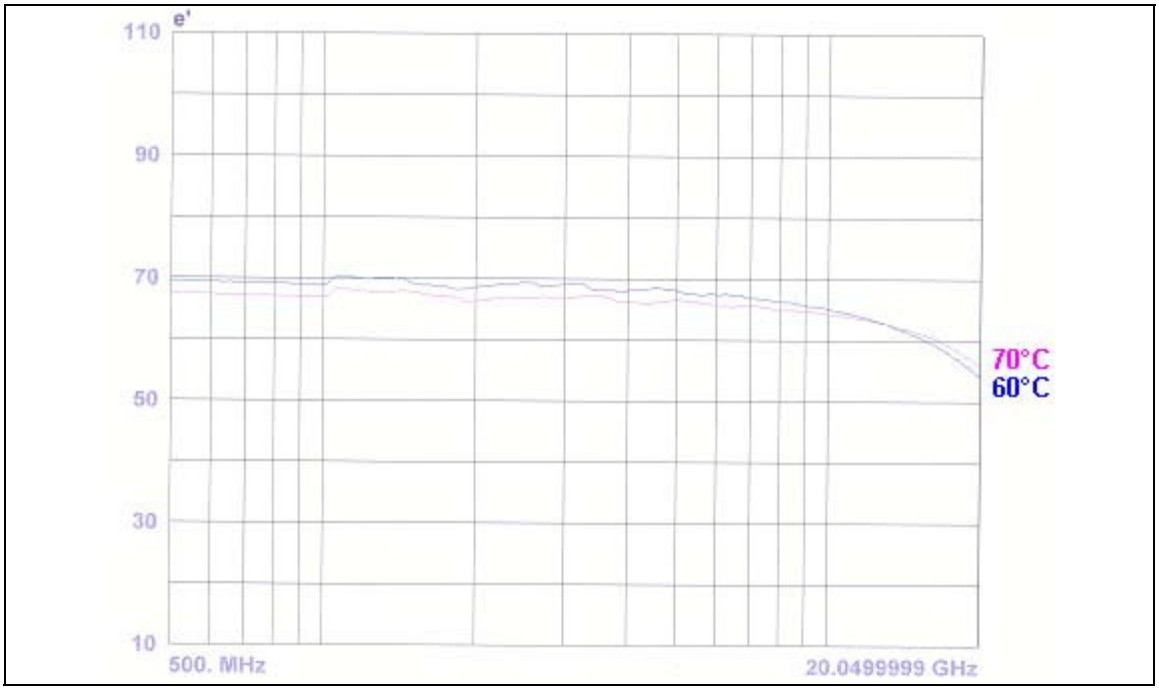

Figure 4.5. Dielectric Constant of Pure Water measured at temperatures 60 and 70°C.

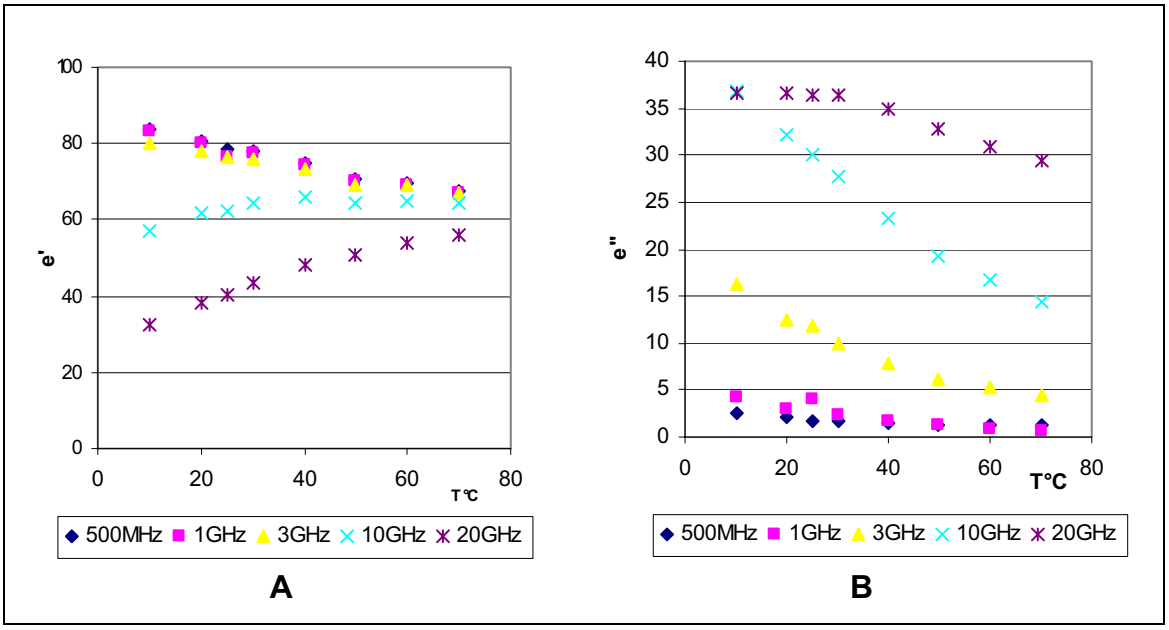

Figure 4.6. A) Real and B) Imaginary part of complex permittivity for Pure Water measured at temperatures between 10 and 70°C

Temperature °C	500 MHz e'	1 GHz e'	3 GHz e'	10 GHz e'	20 GHz e'
10	83.7055	83.3222	79.9164	56.8472	32.2892
20	80.4504	80.2549	78.0896	61.7271	38.4418
25	78.5514	76.6586	76.5922	62.2023	40.0873
30	77.8285	77.5232	75.9639	64.5883	43.6901
40	74.9422	74.5834	73.341	65.901	48.3343
50	70.5707	70.1693	69.096	64.5385	50.7856
60	69.4406	68.8939	69.0978	65.1555	54.1875
70	67.4669	66.8793	66.8525	64.3405	56.1086

Table 4.3. Dielectric Constant of Pure Water measured at different temperatures at frequencies: 500 MHz, 1GHz, 3GHz, 10GHz and 20GHz.

4.1.3 Pure 1,4-Dioxane

1,4-Dioxane it is a non polar solvent with zero dipole moment and on the literature it presents a low dielectric constant of 2.2 at room temepreature.
The dielectric constant of the pure 1,4-Dioxane was measured. The datas are shown in the Table 4.4. The Figure 4.7 show the dielectric constant versus the temperature range of 10-70°C.

We can observe a very small change on the dielectric constant when the temperature increase.

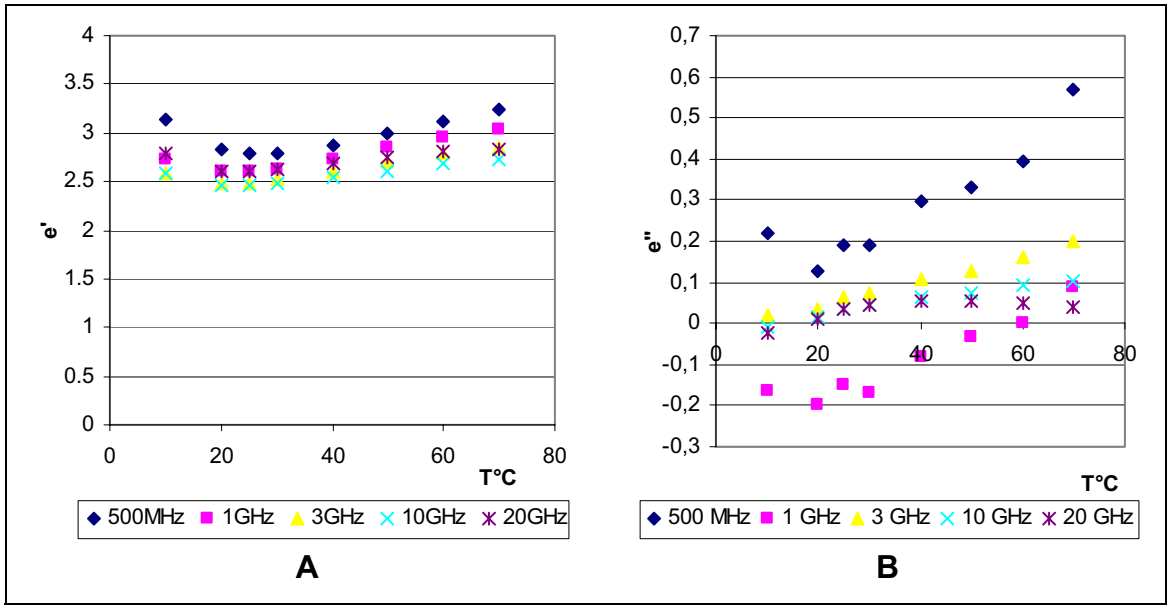

Figure 4.7.A) Real and B) Imaginary part of complex permittivity for Pure 1,4-Dioxane measured at temperatures between 10 and 70°C.

Temperature °C	500 MHz e'	1 GHz e'	3 GHz e'	10 GHz e'	20 GHz e'
10	3.1322	2.7203	2.5806	2.5817	2.7796
20	2.8306	2.5983	2.4812	2.4546	2.6153
25	2.7836	2.5989	2.4896	2.4555	2.6053
30	2.7963	2.6310	2.5274	2.4742	2.6225
40	2.8726	2.7333	2.6132	2.5373	2.6820
50	2.9924	2.8534	2.6995	2.6067	2.7522
60	3.1222	2.9459	2.7924	2.6784	2.8106
70	3.2316	3.0431	2.8534	2.7226	2.8288

Table 4.4.Dielectric Constant of Pure 1,4-Dioxane measured at different temperatures at frequencies: 500 MHz, 1GHz, 3GHz, 10GHz and 20GHz.

4.1.4 Influence of the volume fraction on the ferroelectric properties of the Seignette Salt-Water solutions

In order to study the influence of the volume fraction on the ferroelectric properties, the dielectric constant of the binary Seignette Salt-Water solutions were measured. In each volume fraction complete disolution of salt was

observed. The solutions were measured at the temperature range of 10-70°C. The results for the investigated solutions are reported below (see Figures 4.7 – 4.11).

The volume fractions of water 1, 0.94, 0.88, 0.77, 0.66, 0.6 were studied.

In solution with high volume fraction of water (0.77-1) the results show that when a very small amount of salt is added, smalls changes on the dilectric constant were observed.

In the volume fractions of water 0.66 and 0.6, the solutions are concentrated and the dielectric constant decrease.

It could be said, when the volume fraction of water was increased the dielectric constant increased.

This may be due to that, in diluted solutions the salt is dissolved completely, the quantity of ions in the medium are higher and the structure of the salt is not preserved and it loses the ferroelectric properties. The transition from ferro to paraelectric due to temperature was not observed in these binary solutions.

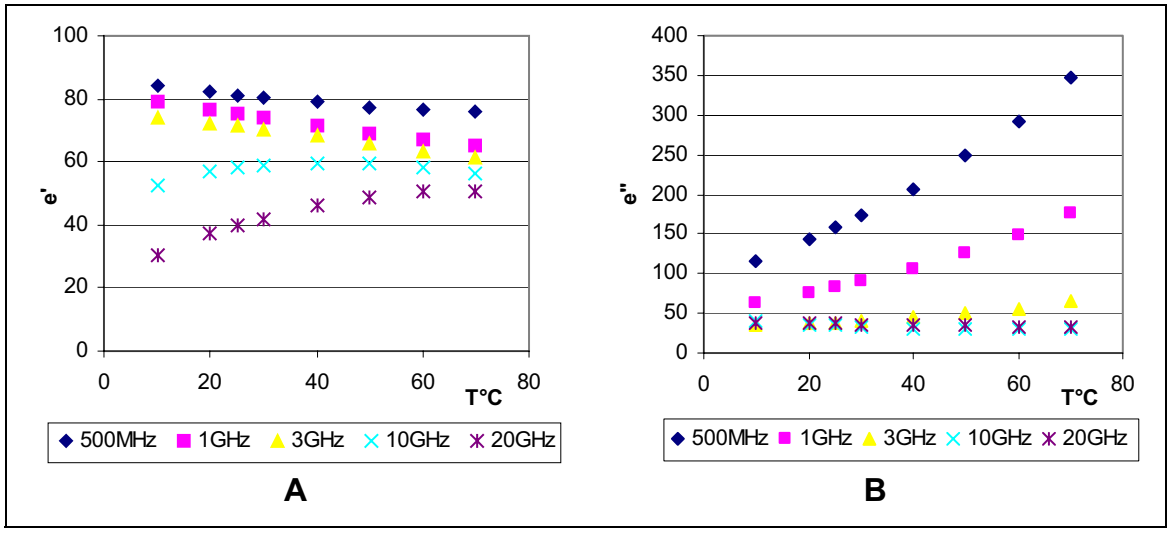

Figure 4.7. A) Real and B) Imaginary part of complex permittivity versus temperature for V_{H2O} =0.9441 measured at different frequencies.

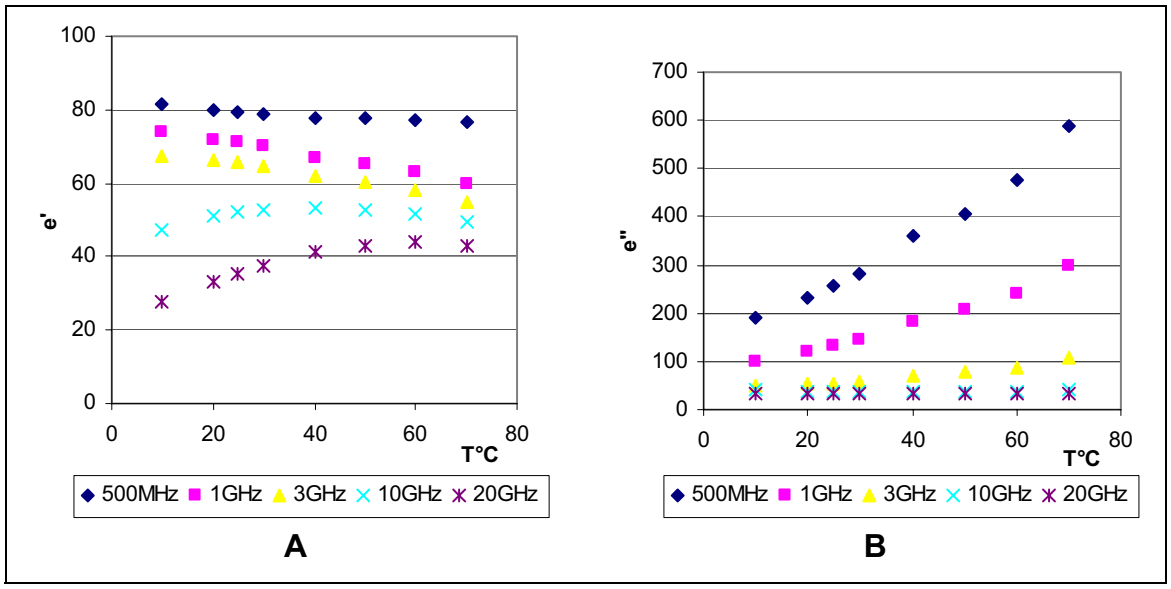

Figure 4.8. A) Real and B) Imaginary part of complex permittivity versus temperature for V_{H2O} =0.88 measured at different frequencies.

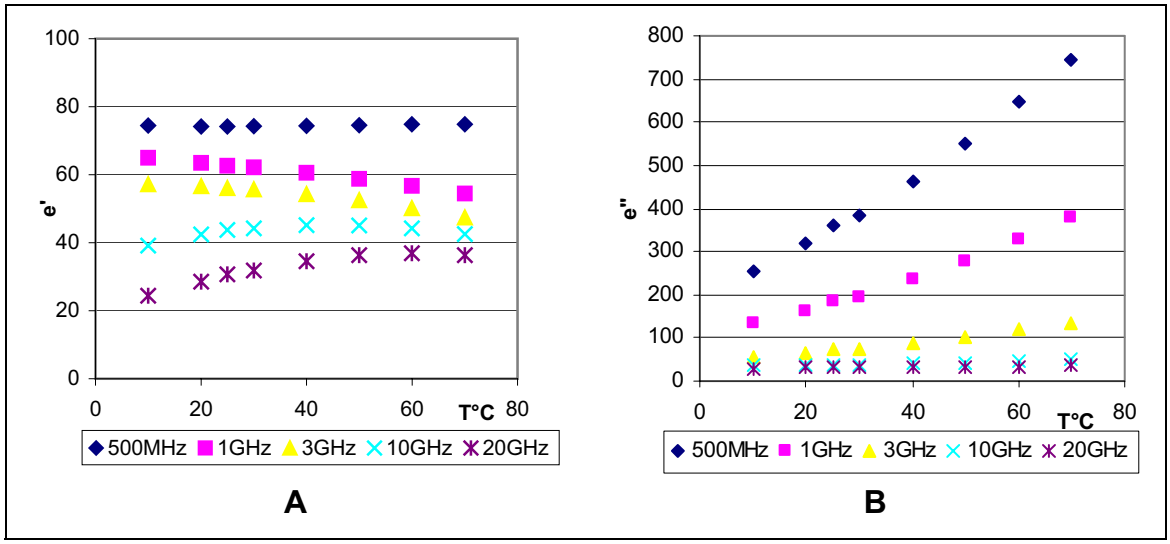

Figure 4.9. A) Real and B) Imaginary part of complex permittivity versus temperature for V_{H2O} =0.77 measured at different frequencies.

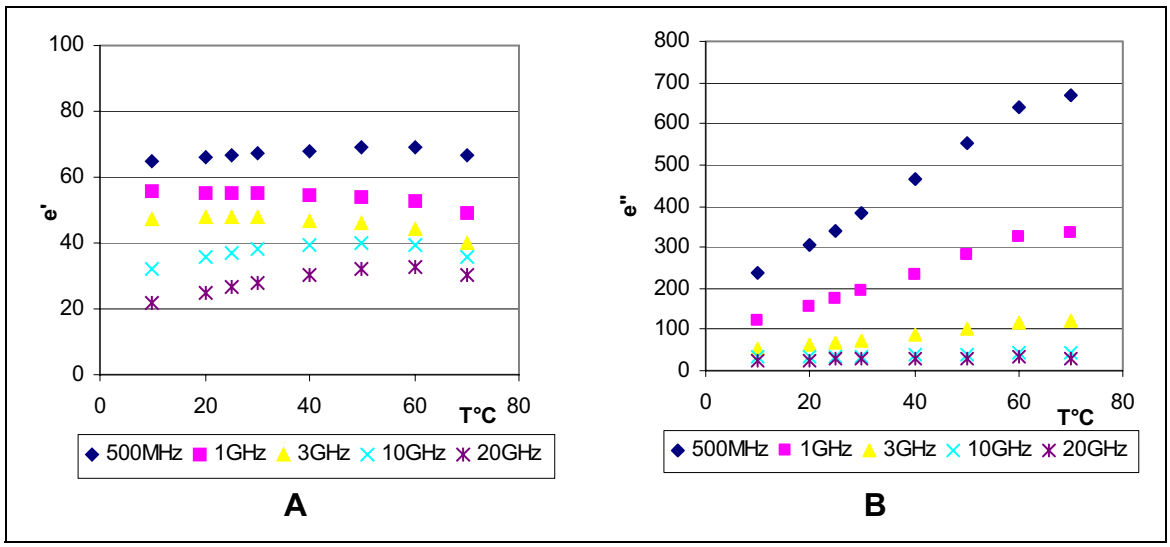

Figure 4.10. A) Real and B) Imaginary part of complex permittivity versus temperature for V_{H2O} =0.664 measured at different frequencies.

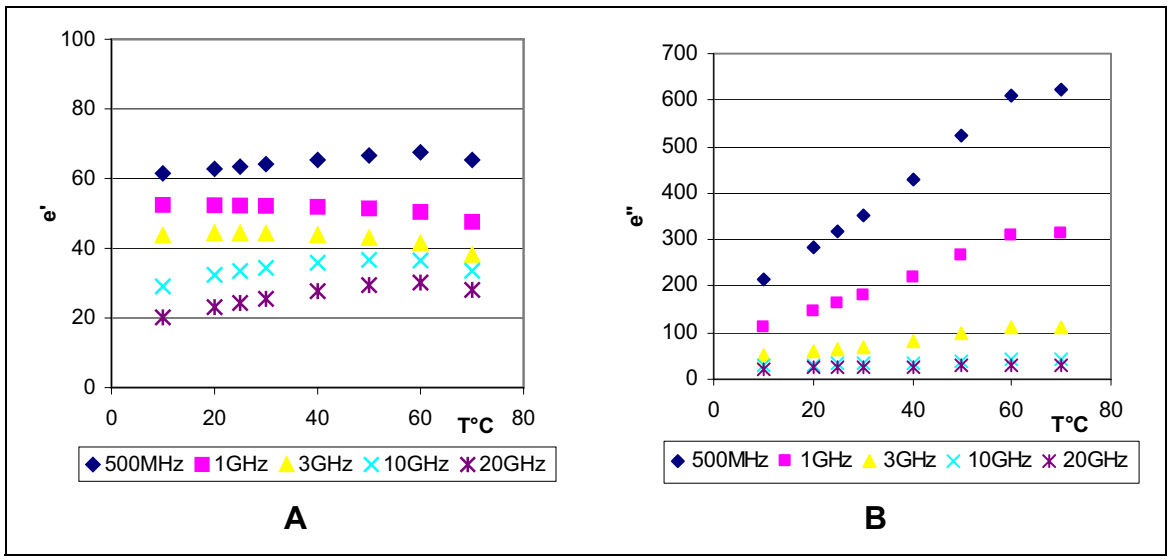

Figure 4.11. A) Real and B) Imaginary part of complex permittivity versus temperature for V_{H2O} =0.61 measured at different frequencies.

4.1.5 Influence of the temperature on the ferroelectric properties of the Seignette salt-Water solutions

The influence of the temperature on the properties of the binary Seignette salt-Water solutions was studied. The Figures 4.12 - 4.16 represent the complex permittivity (real and imaginary part) versus the volume fraction of water, measured at the frequencies: 500 MHz, 1 GHz, 3 GHz, 10 GHz and 20 GHz.

As it can be seen, in each of the volume fractions measured, the dielectric constant (real part) shows a very small change when the temperature increase.This is due to increase in inner molecular movements and probably the reduction of close interaction forces.

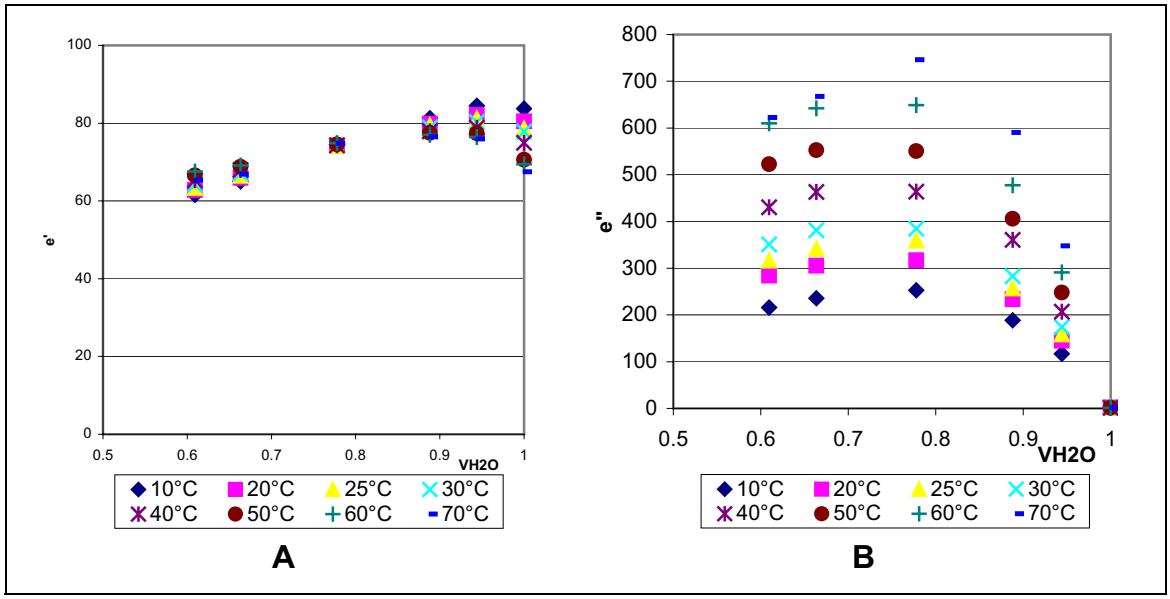

Figure 4.12. A) Real and B) Imaginary part of complex permittivity versus V_{H2O} at different temperatures at measured frequency of 500 MHz.

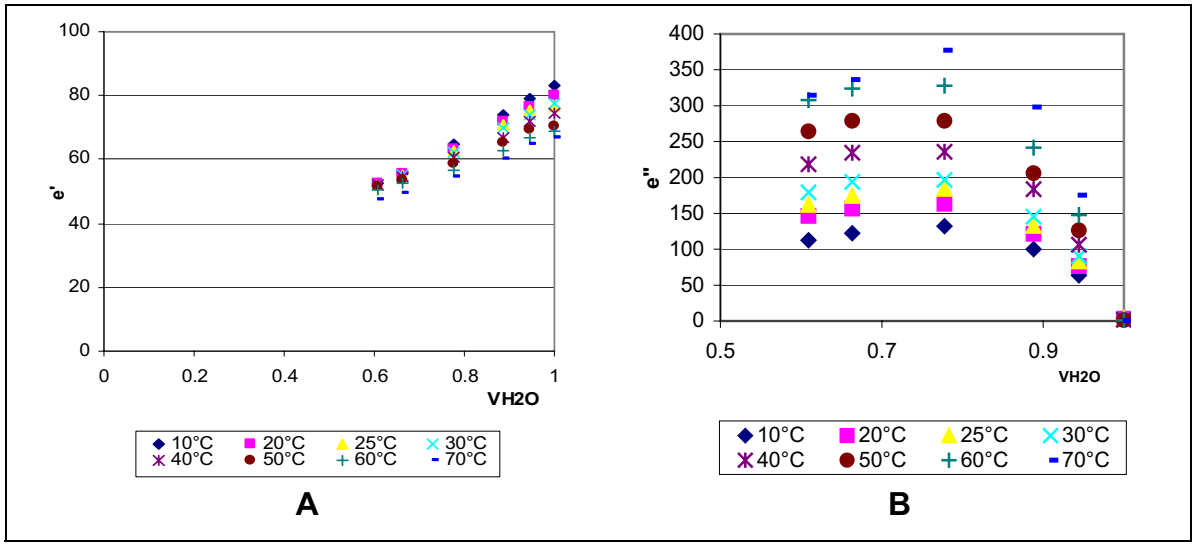

Figure 4.13. A) Real and B) Imaginary part of complex permittivity versus V_{H2O} at different temperatures at measured frequency of 1 GHz.

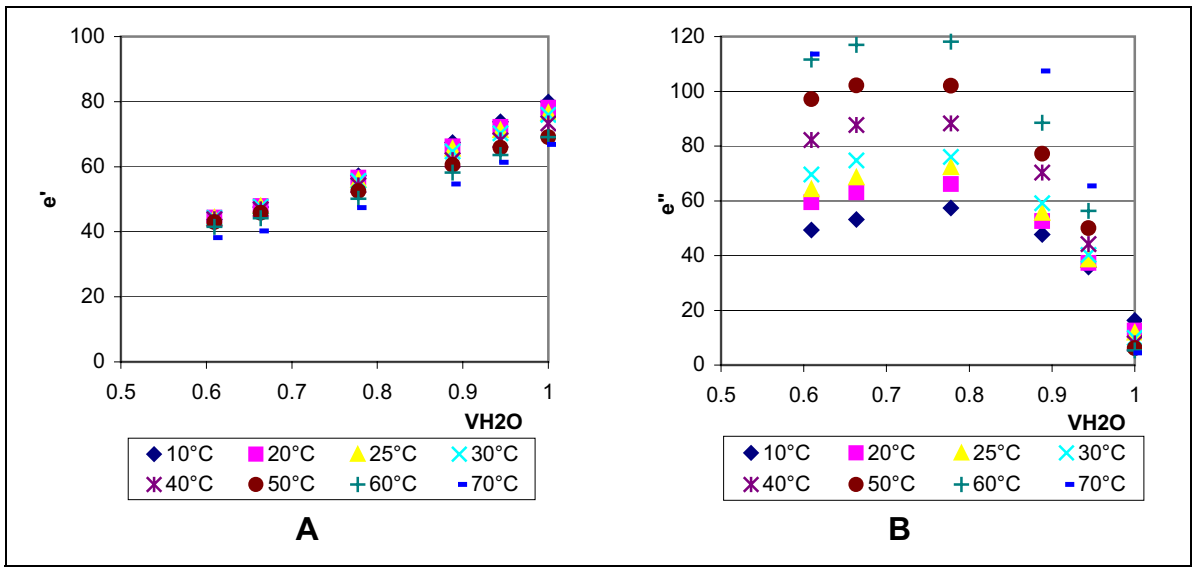

Figure 4.14. A) Real and B) Imaginary part of complex permittivity versus V_{H2O} at different temperatures at measured frequency of 3 GHz.

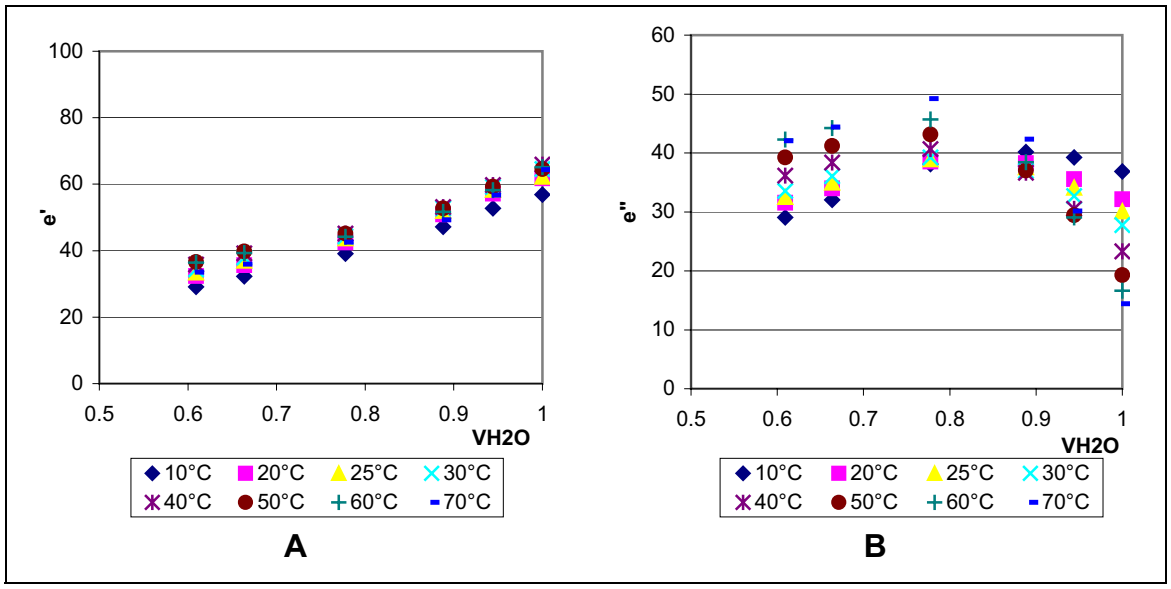

Figure 4.15. A) Real and B) Imaginary part of complex permittivity versus V_{H2O} at different temperatures at measured frequency of 10 GHz.

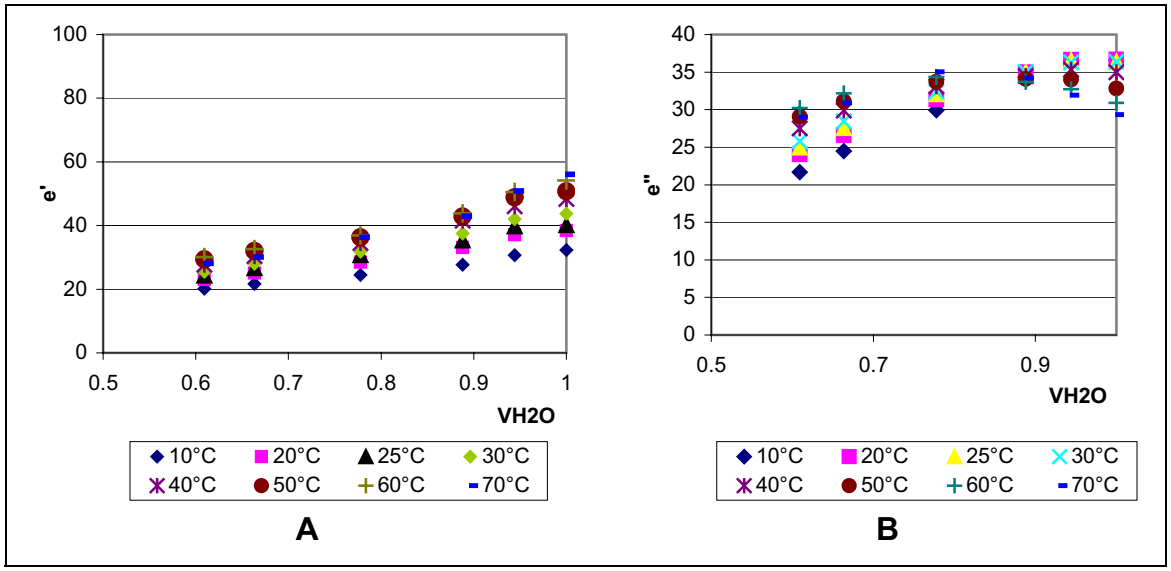

Figure 4.16. A) Real and B) Imaginary part of complex permittivity versus V_{H2O} at different temperatures at measured frequency of 20GHz.

4.1.6 Ternary Seignette Salt-Water-1,4-Dioxane solutions

The influence of increased in volume fraction of 1,4-Dioxane and the temperature on the properties of the ternary Seignette salt-Water-1,4-Dioxane solutions was studied.

In last section the properties of binary mixtures were investigated. In this section, we investigate the binary Water-1,4-Dioxane and 1,4-Dioxane-Seignette salt solutions, in order to know more about the behavior of these systems. The results help to interpretation of the ternary systems. Figure 4.17 represents the mixtures investigated.

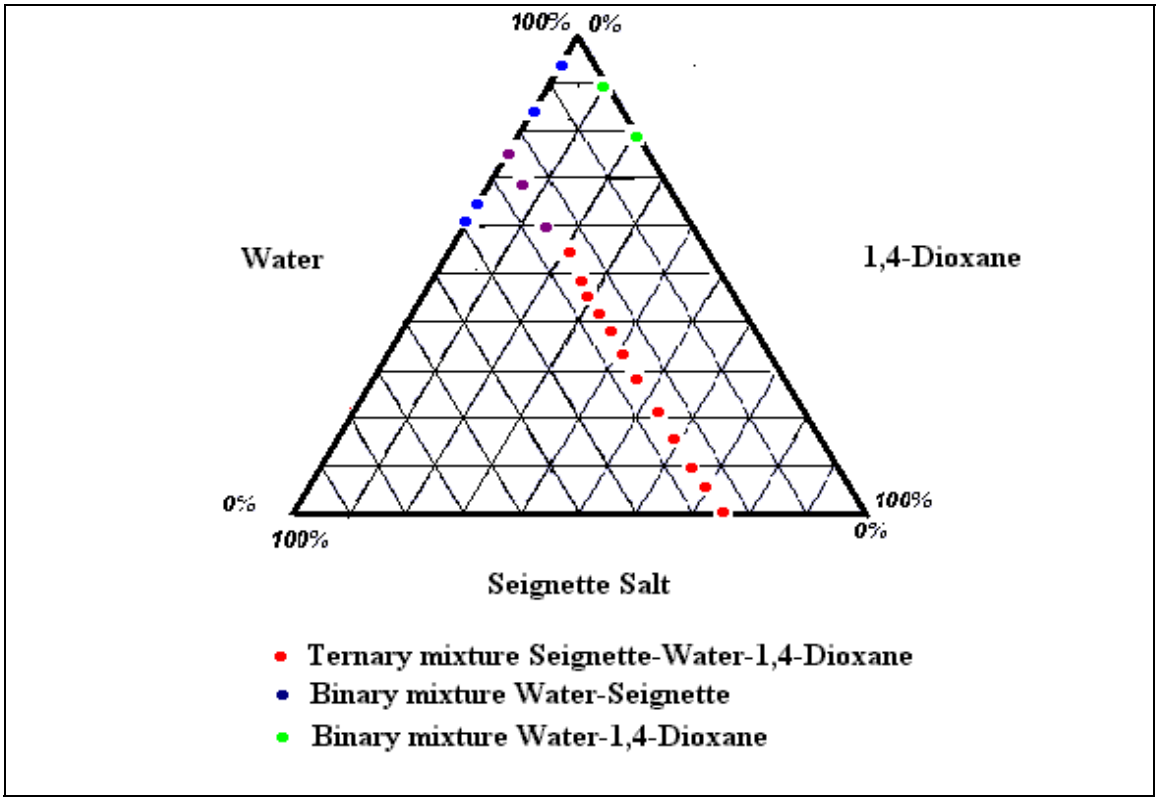

Figure 4.17. Binary and Ternary mixtures at %w/w of Seignette Salt, Water and 1,4-Dioxane .

4.1.6.1 Water-1,4-Dioxane solutions

In order to know more about the differences between polar and non-polar solvents, these mixtures were investigated.

The volume fractions of the water 0.8 and 0.9 were studied. The Figures 4.18 and 4.19 show the results obtained. It can be observed that the dielectric constant decrease when the temperature increase.

When the volume fraction of water was higher the dielectric constant of the solution rise (see Figure 4.20). As it was mentioned in previous section the 1,4-Dioxane is a non polar solvent, but miscible with water, due to hydrogen bonding to the exposed oxygen atoms. It can be assumed that, the 1,4-Dioxane molecules are only on the surface of the water cluster attached through hydrogen bonding. And pure water clusters dominate the system.
These show agreement with the previous results obtained by Ketani, D., 2002.

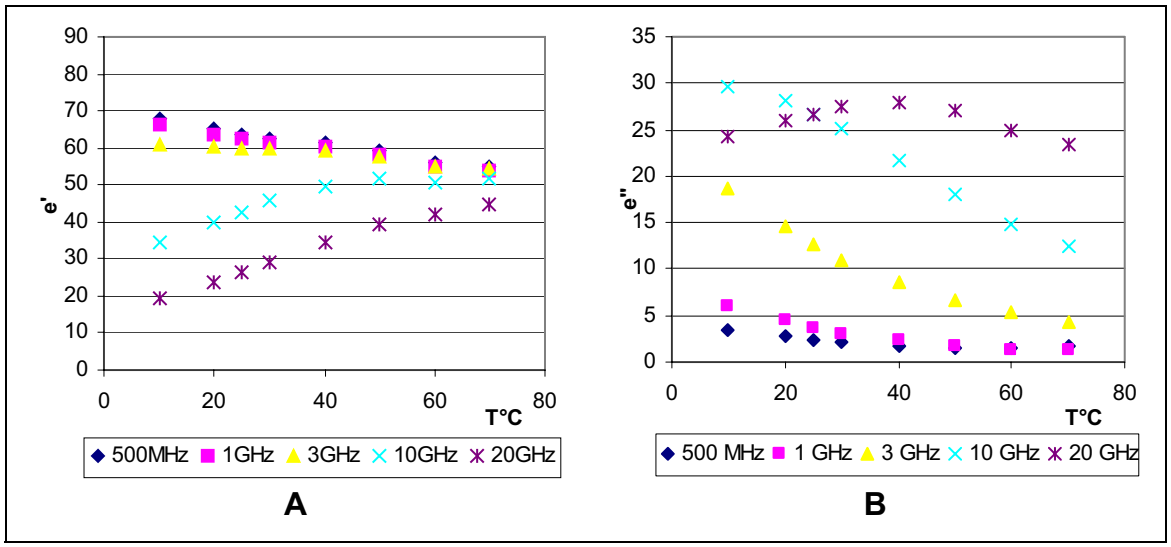

Figure 4.18. A) Real and B) Imaginary part of complex permittivity measured at different temperatures for V_{H2O}=0.8 in binary mixture of Water-1,4-Dioxane.

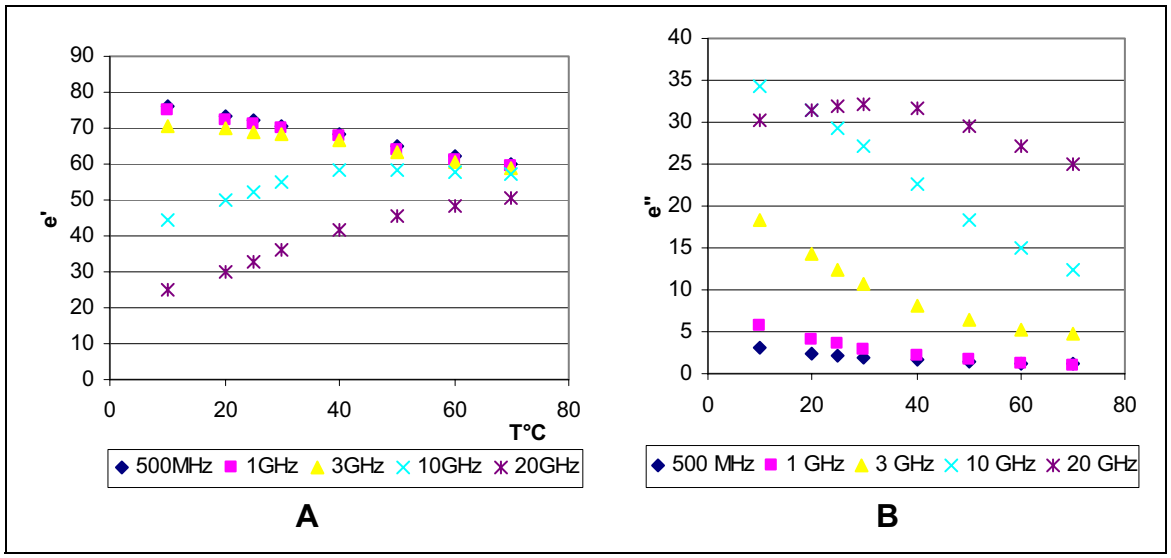

Figure 4.19. A) Real and B) Imaginary part of complex permittivity measured at different temperatures for V_{H2O}=0.9 in binary mixture of Water-1,4-Dioxane.

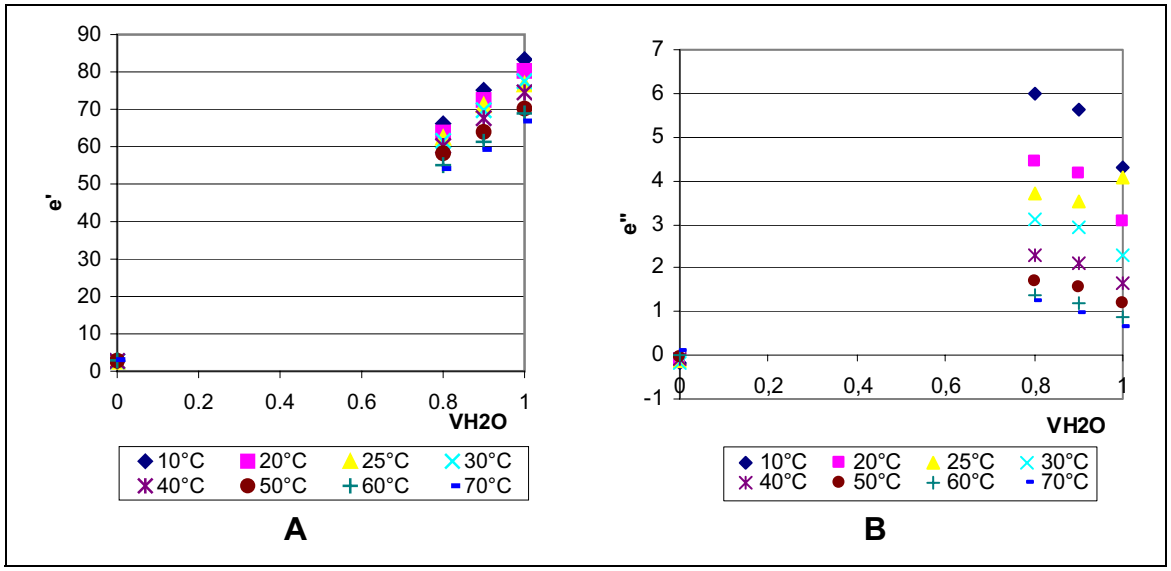

Figure 4.20. A) Real and B) Imaginary part of complex permittivity versus V_{H2O} at different temperatures for ternary Dioxane- Water solution at measured frequency of 1GHz.

4.1.6.2 1,4-Dioxane-Seignette salt solutions

The 1,4-Dioxane-Seignette salt solution was investigated, in order to know the influence of a non-polar solvent on the ferroelectric properties of the Seignette salt. We should note that Seignette salt is poorly soluble in 1,4-Dioxane.

The pure 1,4-Dioxane was saturated with Seignette salt. The mixture was filtered with simply filter paper. Figure 4.21 shows the results obtained.

It can be observed that the solution presents a very low dielectric constant and a very small rise when the temperature increases. The same behavior was obtained when the pure 1,4-Dioxane was measured.

We can say that there is no effect of 1,4-Dioxane on the ferroelectric properties of the Seignette salt. The 1,4-Dioxane dominates the system.

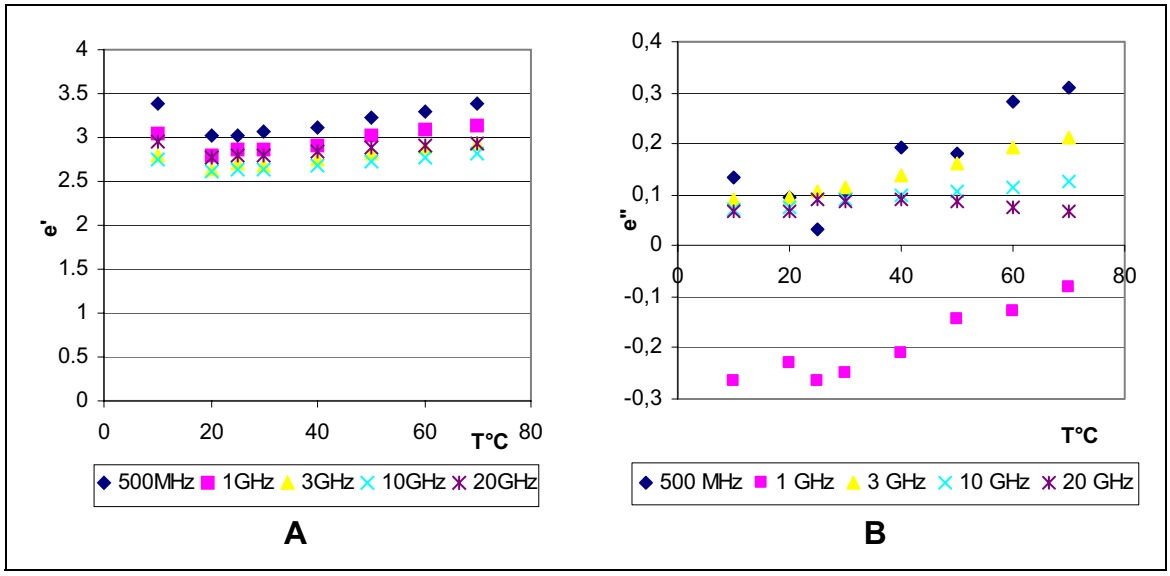

Figure 4.21. A) Real and B) Imaginary part of complex permittivity measured at different temperatures for the binary mixture of 1,4-Dioxane-Seignette Salt.

4.1.6.3 Ternary Seignette salt-Water-1,4-Dioxane solutions

Figures 4.22 – 4.25 represent the complex permittivity (real and imaginary part) versus the temperature measured at frequencies: 500 MHz, 1 GHz, 3 GHz, 10 GHz and 20 GHz.
The volume fractions of water 0.8, 0.9 and 1 were studied.

For each volume fraction studied, it can be seen that the dielectric constant presents a very small change when the temperature was increased.

The dielectric constant increases when the volume fraction of water increased (see Figure 4.25).

This is due the salt can not dissociate in 1,4-Dioxane due to its low dielectric constant, and therefore no ion migration can take place. As it was studied before there is no influence from 1,4-Dioxane.

The dielectric constant depends on the water molecules in the system (water molecules dominate the system).

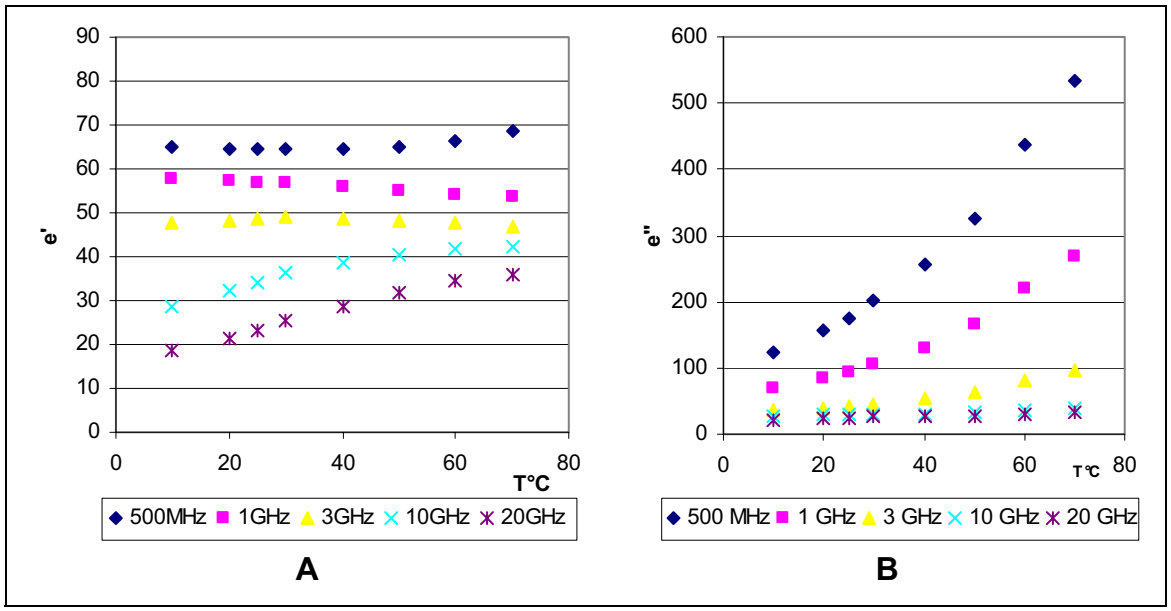

Figure 4.22. A) Real and B) Imaginary part of complex permittivity versus temperature for V_{H2O}=0.8 in ternary Seignette salt- Water -1,4-Dioxane solution.

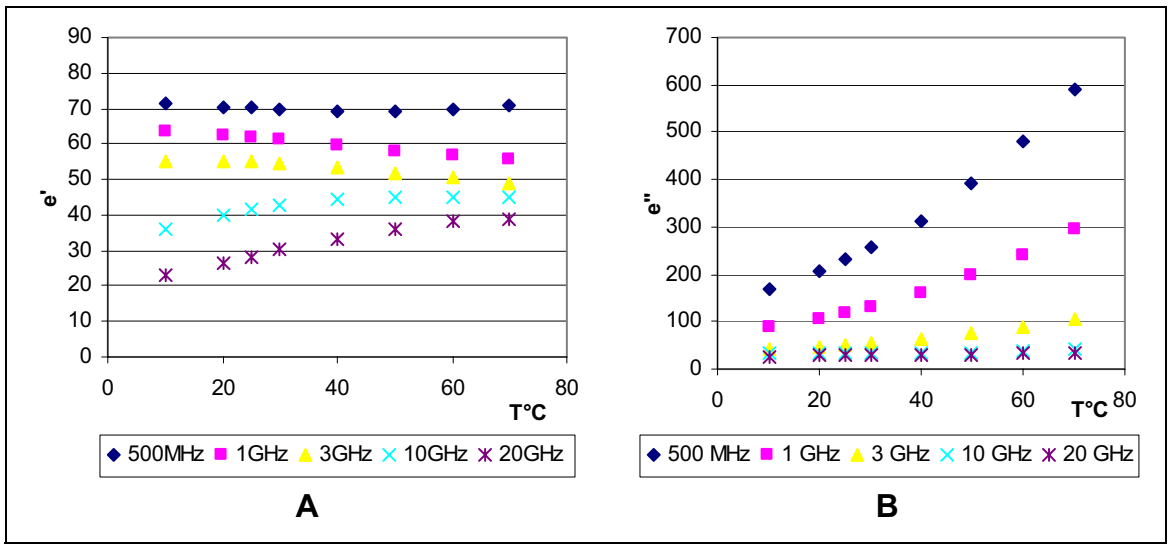

Figure 4.23. A) Real and B) Imaginary part of complex permittivity versus temperature for V_{H2O}=0.9 in ternary Seignette salt-Water-1,4-Dioxane solution.

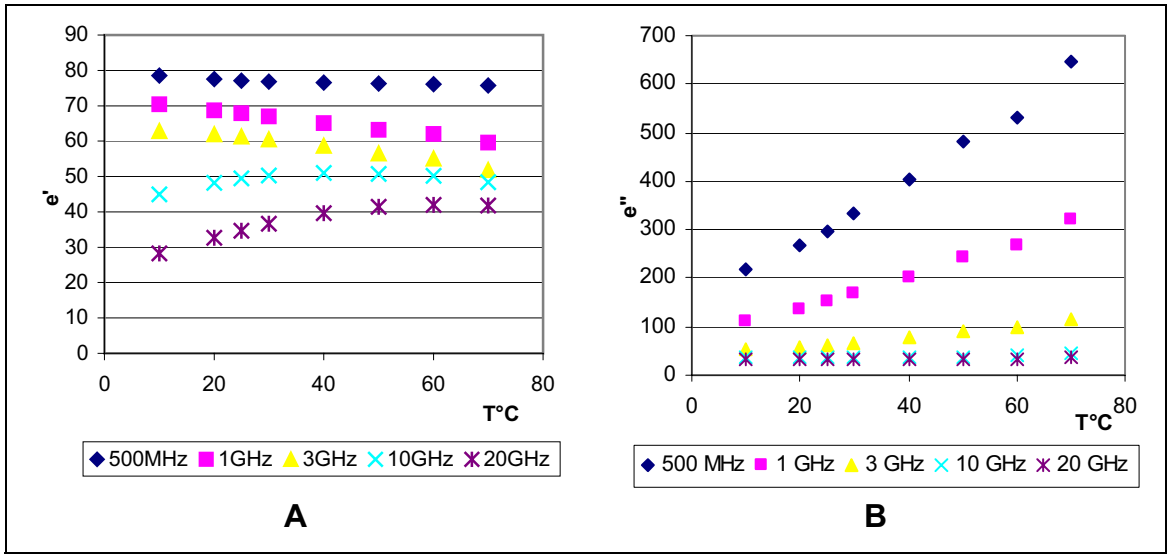

Figure 4.24. A) Real and B) Imaginary part of complex permittivity versus temperature for V_{H2O}=1.0 in ternary Seignette salt-Water -1,4-Dioxane solution.

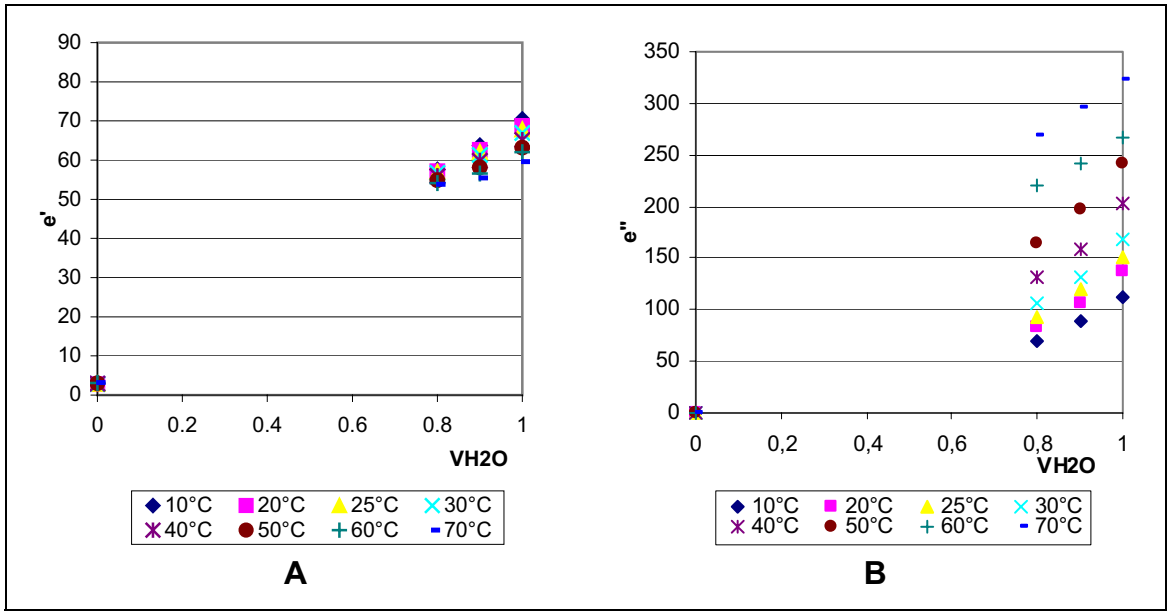

Figure 4.25. A) Real and B) Imaginary part of complex permittivity versus V_{H2O} at different temperatures of ternary Seignette salt-Water-1,4-Dioxane solution at measured frequency of 1GHz.

A stock solution with volume fraction of water 0.89 was also studied. 1,4-Dioxane was added in order to obtain different volume fractions (see Figure 4.26). The ternary solutions were measured at room temperature.

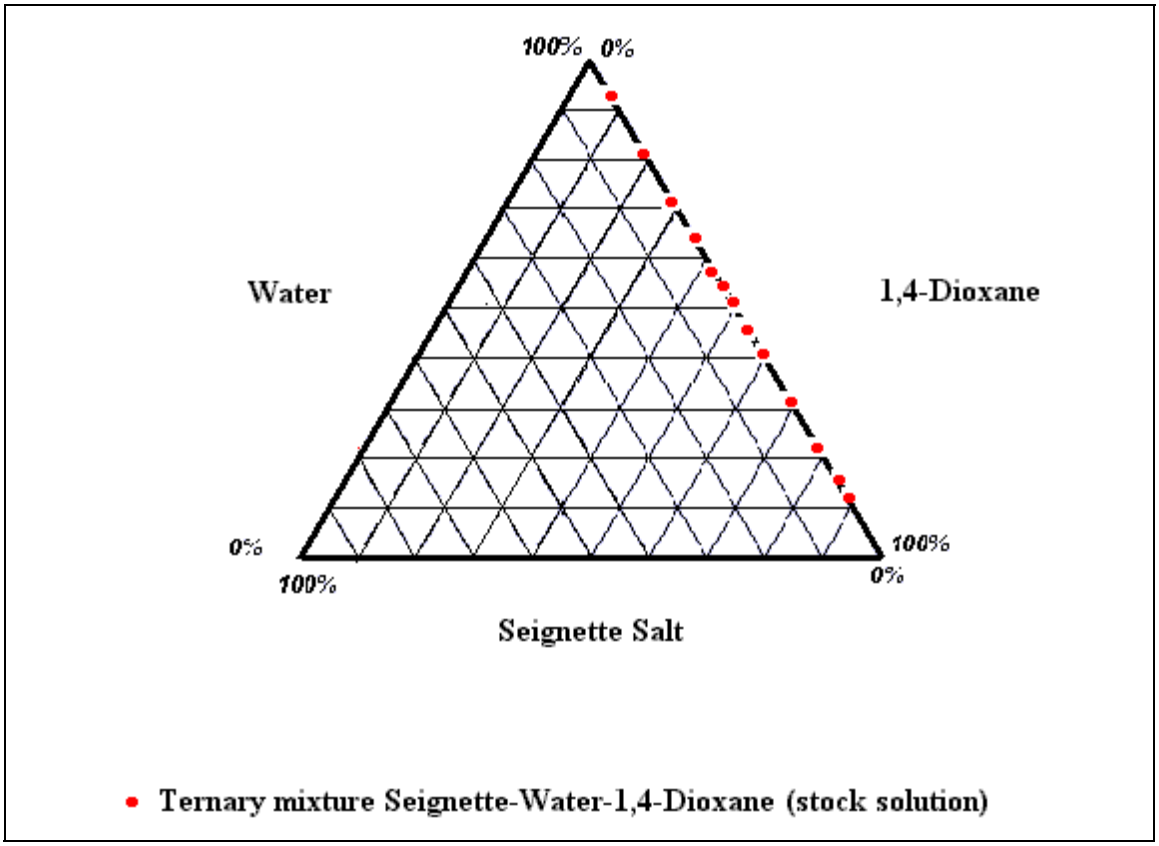

Figure 4.26. Stock solution investigated at %w/w of the components Seignette Salt, Water and 1,4-Dioxane.

Figure 4.27 shows the results obtained. It can be observed that the dielectric constant increases when the volume fraction of water increased. No effect of 1,4-Dioxane could be observed.

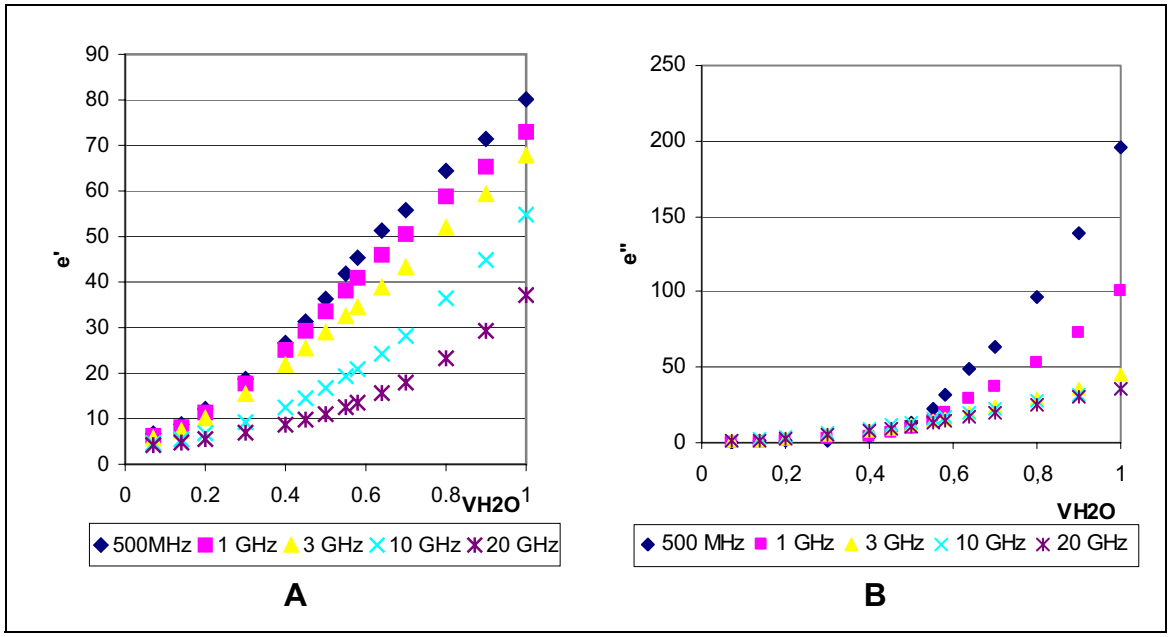

Figure 4.27. A) Real and B) Imaginary part of complex permittivity measured for different volume fractions of the ternary mixtures Seignette salt- Water-1,4-Dioxane at 25°C.

4.1.7 Relaxation behavior of pure Seignette salt and the binary mixtures of Seignette salt / H2O

The Debye relaxation equation (see Section A, 2.3.3 – 2.3.6.1) is based on the assumption of a molecule in the gas form or highly diluted in a nonpolar liquid *(Chelkowski, 1980).* The position of the molecule depends only on the initial orientational polarization P_0 at t = 0 and on the relaxation time τ, an inherent property of the molecule. Intermolecular interactions occurring in nonideal gases or in liquids are expresses implicitly through their influence on the relaxation times and on their distributions.

It can be assumed that small spheric molecules possess small relaxation times of little or no distribution (β≈1), as this shape should allow for a fast reorientation. Big, linear molecules would possess, due to their inertia, long relaxation times with broad distribution. If only the polar groups reorient, and not the whole molecule, a short relaxation time τ_0 will result and values for β close to 1. A rule of thumb could be: the more polar, hydrogen bonding groups a

molecule possesses, the larger τ_0 will be – as these interactions have to be broken up – and the broader the relaxation times will be distributed.

All the investigated polar liquids were examined with regards to the above outlined hypotheses. (*Stengele 2002.)*

For calculation of relaxation times the 1-Debye equation was chosen due to the simplicity of the methods and low number of free parameters (see Section A, 3.2.6.2).

Figure 4.28 shows the results of relaxation times of pure water at different temperatures.

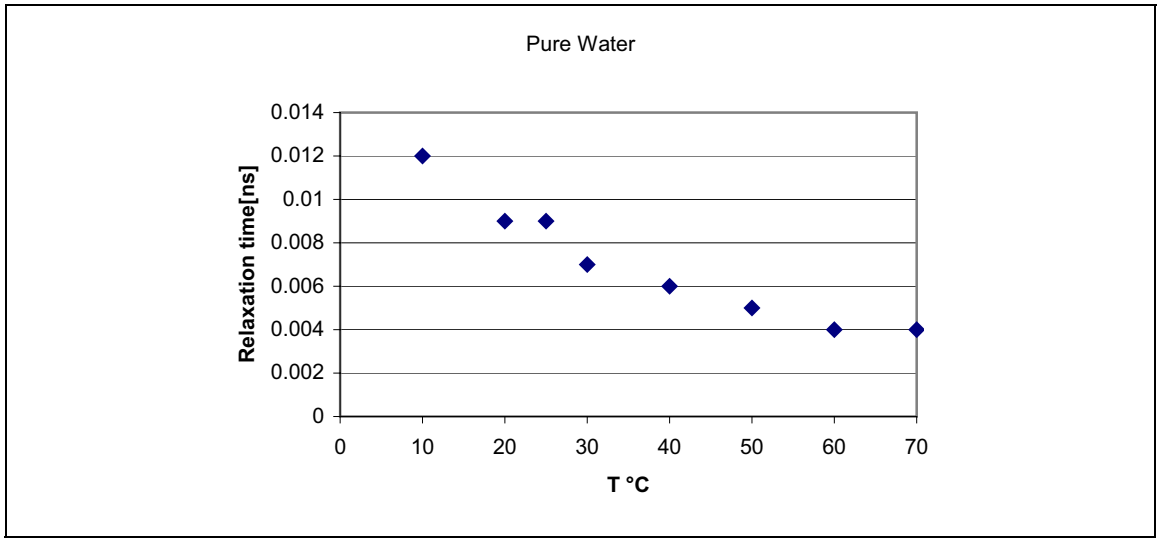

Figure 4.28. Relaxation times of pure water at different temperatures.

As it can be seen above, the relaxation time decrease by increasing the temperature in case of pure water.

Figure 4.29 shows the relaxation time versus temperature at different volume fractions.

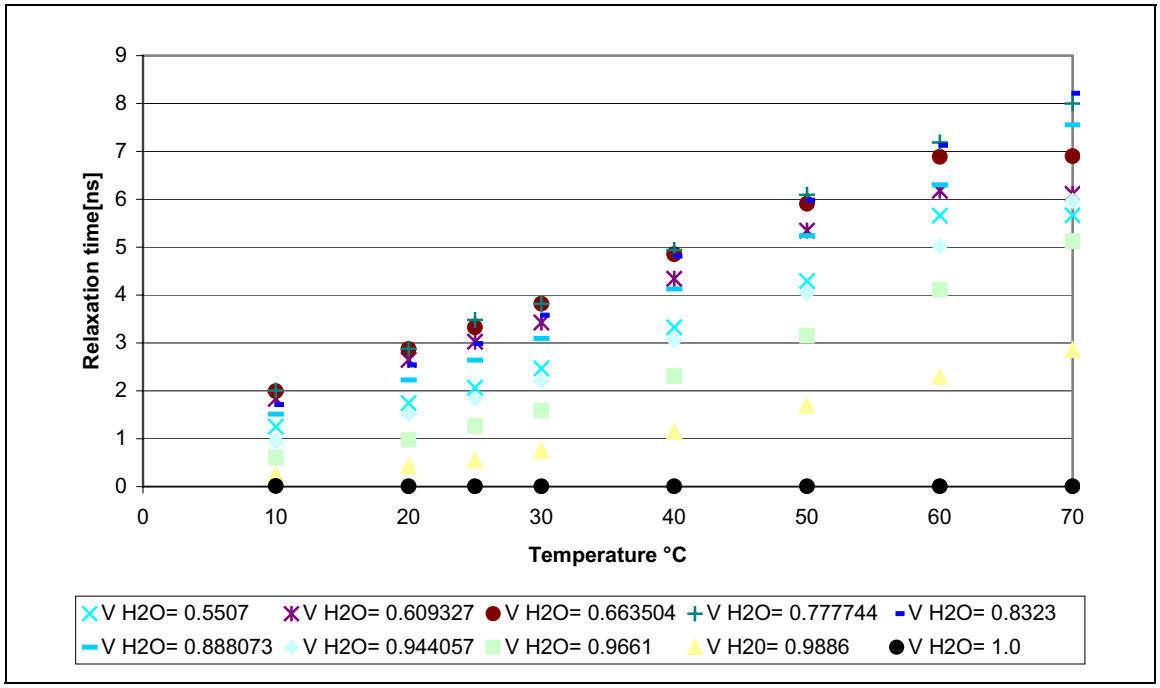

Figure 4.29. Relaxation times versus temperature at different volume fractions.

As it can be seen on figure 4.29, in case of addition of Seignette salt in any volume fraction the behavior of relaxation times changes and it increase by increasing the temperature. The relaxation time increases by increasing the V_{H2O} till the V_{H2O} = 0.83 and then starts to decrease by increasing the V_{H2O}. The significant interpretation from this figure is the huge increase of relaxation times by just adding small amount of salt to the system (V_{H2O} = 0.9886).

Table 4.5 shows the results obtained using single Debye model for different V_{H2O} at different temperature.

Tau [ns]								
V H20	**10°C**	**20°C**	**25°C**	**30°C**	**40°C**	**50°C**	**60°C**	**70°C**
1	0.012	0.009	0.009	0.007	0.006	0.005	0.004	0.004
0.988	0.248	0.424	0.546	0.745	1.146	1.691	2.295	2.853
0.966	0.606	0.982	1.264	1.585	2.305	3.153	4.113	5.129
0.944	0.954	1.52	1.836	2.209	3.054	4.042	5.021	5.966
0.888	1.512	2.225	2.64	3.096	4.127	5.238	6.303	7.551
0.832	1.711	2.539	2.988	3.58	4.811	5.979	7.124	8.212
0.777	2.006	2.882	3.483	3.819	4.937	6.093	7.187	8
0.663	1.991	2.872	3.326	3.818	4.856	5.909	6.886	6.898
0.609	1.832	2.647	3.024	3.426	4.343	5.344	6.179	6.114
0.550	1.255	1.75	2.07	2.467	3.326	4.293	5.661	5.668

Table 4.5 Relaxation times [ns] obtained for different V_{H2O} at different temperatures.

When we plot the relaxation times versus V_{H2O}, we can observe a pick at the V_{H2O} = 0.77 which this pick is only shifted to V_{H2O} = 0.83 at 70°C. Figure 4.30 shows the results of relaxation times versus V_{H2O}.

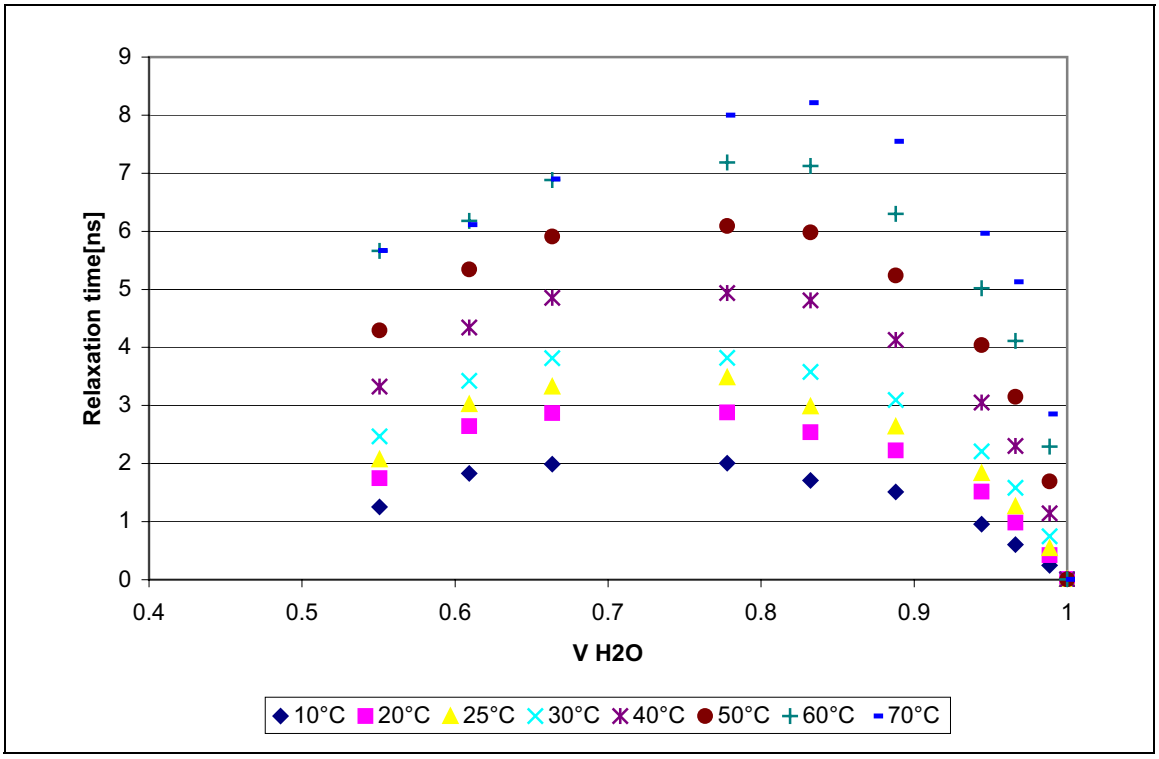

Figure 4.30. Relaxation times versus V_{H2O} at different temperatures.

Figure 4.30 shows also a single percolation threshold in respect to relaxation time (τ) at V_{H2O} = 0.77 which is shifted to V_{H2O} = 0.83 at 70°C.

For showing the reliability of the method the R^2 values are plotted versus volume fractions at different temperatures. Results are show in table 4.6 and the plots are shown in figure 4.31 and 4.32.

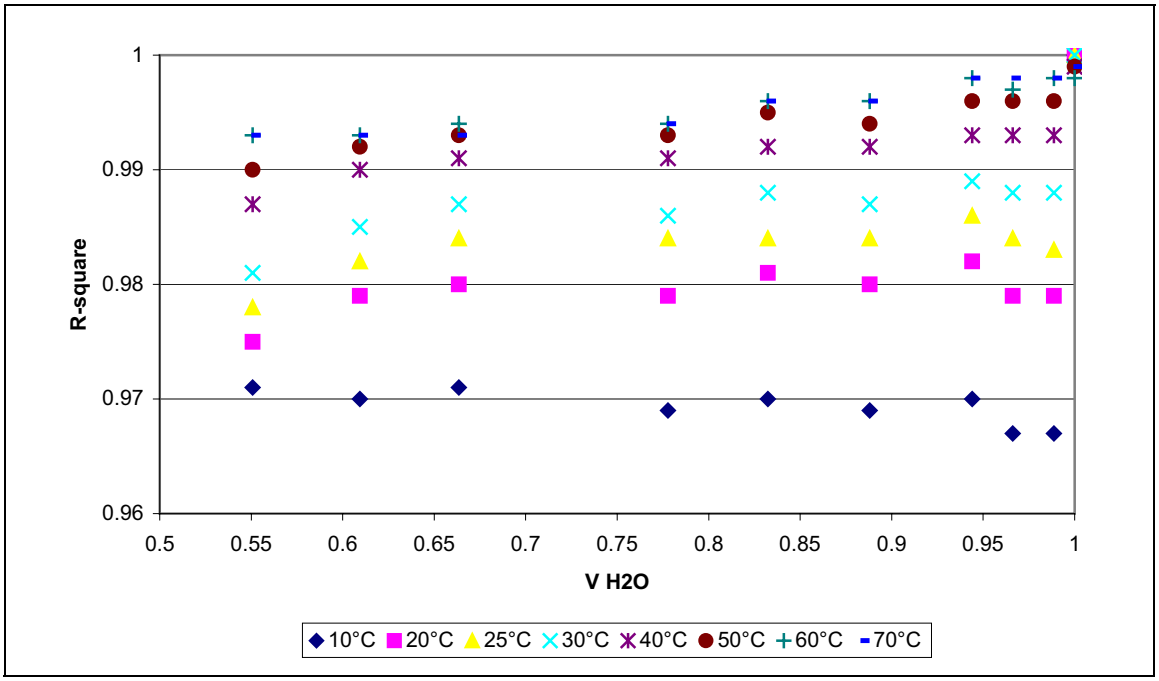

Figure 4.31. Correlation coefficient (R^2) versus V_{H2O}.

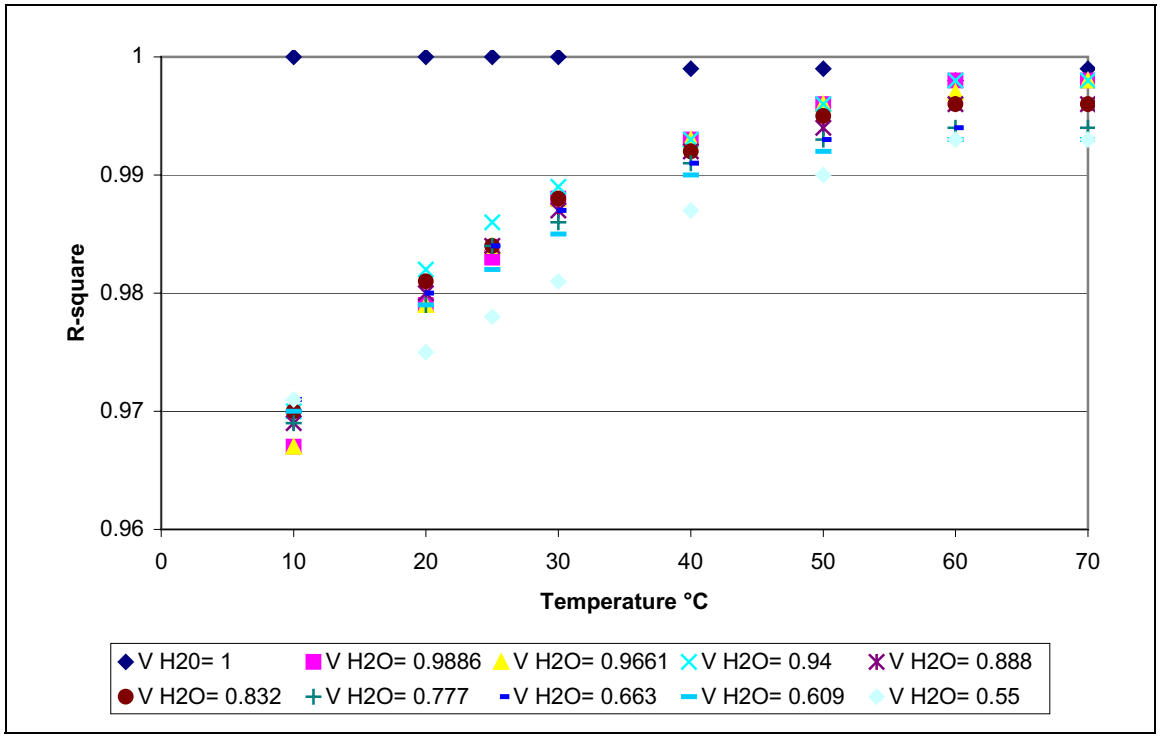

Figure 4.32. Correlation coefficient (R^2) versus temperature °C.

	(R^2)									
T°C	V_{H2O}= 1.00	V_{H2O}= 0.988	V_{H2O}= 0.966	V_{H2O}= 0.944	V_{H2O}= 0.888	V_{H2O}= 0.832	V_{H2O}= 0.777	V_{H2O}= 0.663	V_{H2O}= 0.609	V_{H2O}= 0.550
10	1	0.967	0.967	0.97	0.969	0.97	0.969	0.971	0.97	0.971
20	1	0.979	0.979	0.982	0.98	0.981	0.979	0.98	0.979	0.975
25	1	0.983	0.984	0.986	0.984	0.984	0.984	0.984	0.982	0.978
30	1	0.988	0.988	0.989	0.987	0.988	0.986	0.987	0.985	0.981
40	0.999	0.993	0.993	0.993	0.992	0.992	0.991	0.991	0.99	0.987
50	0.999	0.996	0.996	0.996	0.994	0.995	0.993	0.993	0.992	0.99
60	0.998	0.998	0.997	0.998	0.996	0.996	0.994	0.994	0.993	0.993
70	0.999	0.998	0.998	0.998	0.996	0.996	0.994	0.993	0.993	0.993

Table 4.6. Correlation coefficient (R^2) obtained for different V_{H2O} at different temperature.

4.2 Discussion

Dielectric Spectroscopy is a good technique to investigate physical properties of materials as well as their structural behavior, because of its accuracy and reproducibility.

Some works, like binary aqueous solutions have been done using Dielectric Spectroscopy in order to characterize and investigate the behavior as well as the changes that occur on the properties of the system. Applying the concepts of the Percolation Theory, the percolation thresholds of different binary systems, have been found using the dielectric spectroscopy.

Another application of Dielectric Spectroscopy is the study of ferroelectric properties of substances. In this case the ferroelectric properties of pure Seignette salt (not single crystal, relative measurement), 1) as a powder, studying the behavior as a function of increasing temperature 2) pure Seignette salt after melting as a function of further increase in temperature and subsequently as a function of decreasing temperature 3) its binary and 4) ternary mixtures with Water and 1,4-Dioxane, was investigated using the high frequency network analyzer.

The results demonstrate that the specific ferroelectric properties of a single crystal of Seignette salt, could not be observed on the temperature range of 10-70°C at frequency range of 500MHz - 20GHz as our experiment is in other order than a crystal (Liquid and molted salt).

On the other hand an increase of the real part of the dielectric constant was measured as a function of increasing temperature at high frequencies and a slight decrease at low frequencies in the range of 10-70°C.

In case of binary and ternary systems, it could not be possible to observe the change from Ferro to paraelectric behavior typical for a solid single Seignette crystal because of different order of the matter.

It shows definitely that in solution the Seignette salt has a different “order” than in a solid crystal. Thus Seignette salt is not influencing the binary or ternary mixtures. In other words the dominant factors are that of Water.

The absence of a “ferroelectric” behavior in solution and as a powder could be also due to an “anti-ferroelectric” arrangement of the polarized particles of the powder or the polarized water clusters islands with dissolved Seignette salt in a continuous phase of a polar 1,4-Dioxane. As it has been said in theory part, the ferroelecrtic activity in a single crystal depends very much on the axis of the crystal on which the excitation (mechanical or electrical) happens. In liquid crystals or in preformed crystalline structure this axis does not exist yet and this may result in absence of “ferroelectric” behavior.

The finding that water can be described using the Debye relaxation equation is well documented *(e.g. Böttcher et al. 1978; c; Kaatze, 1989)*. This result is surprising, because the Debye relaxation theory had been developed for the gaseous form or for solutions highly diluted in nonpolar liquids, where hardly any intermolecular interactions occur.

The single Debye equation is also able to characterize the whole range of Seignette salt-water mixtures at all temperatures with $R^2 \geq 0.982$ showing with respect to the relaxation time (τ), a percolation threshold in all temperatures between V_{H2O}= 0.77 and V_{H2O}= 0.83 (Fig. 4.31). This may be due to preformation of a crystalline lattice around these concentrations.

It may be of interest to study other polar substances, which are well soluble in water but not in 1,4-Dioxane in order to see whether a “crystalline preformation” in solution exists, close to the saturation concentration and/or as un supersaturated condition, which influences the final crystalline structure after precipitation. This could be of special interest for drugs showing a polymorphic crystalline behavior.

4.2.1 Investigation of ferroelectric activity in KDP/water binary mixtures using dielectric spectriscopy at temperature range between 10 and 70

In this part, we investigate KDP/water binary mixtures in temperature range between 10 and 70°C to see, if any, ferroelectric activity could be observed.

Measurement of pure salt was not possible due to high melting point of salt. As this salt also has very low Curie temperature (T_c = -150°C), investigation around T_c was not possible. Please see Appendix for complete table of results.

4.2.2 Influence of the volume fraction on the dielectric properties of the KDP/water solutions

In order to study the influence of the volume fraction on the ferroelectric properties, the dielectric constant of the binary KDP/water solutions were measured. In each volume fraction complete dissolution of salt was observed. The solutions were measured at the temperature range between 10 and 70°C. The results for the investigated solutions are reported below (see Figures 4.33 – 4.40).

The volume fractions of water 1, 0.995, 0.983, 0.966, 0.948, 0.931, 0.914, 0.897 and 0.871 were studied.

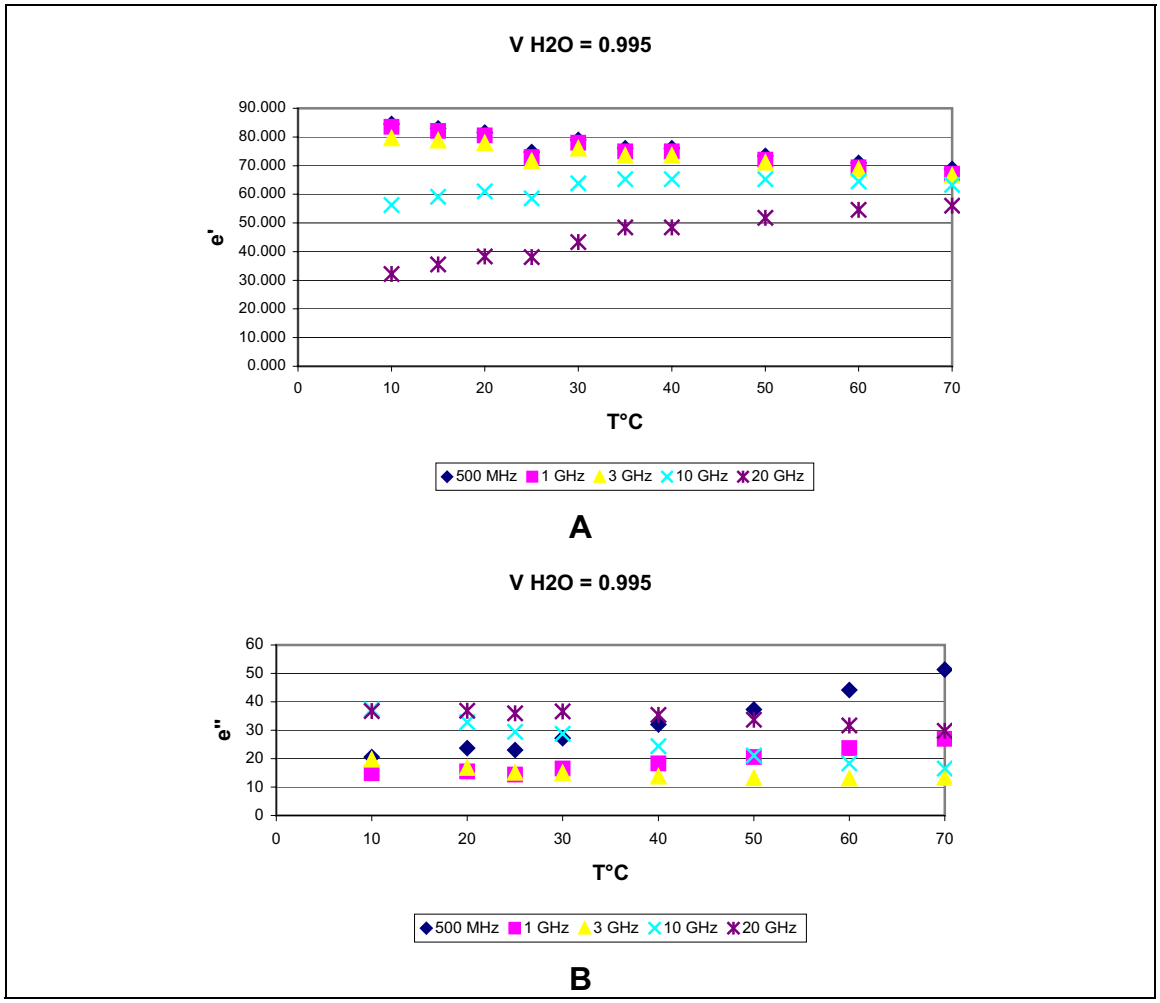

Figure 4.33. A) Real and B) Imaginary part of complex permittivity versus temperature for V_{H2O} =0.995 measured at different frequencies.

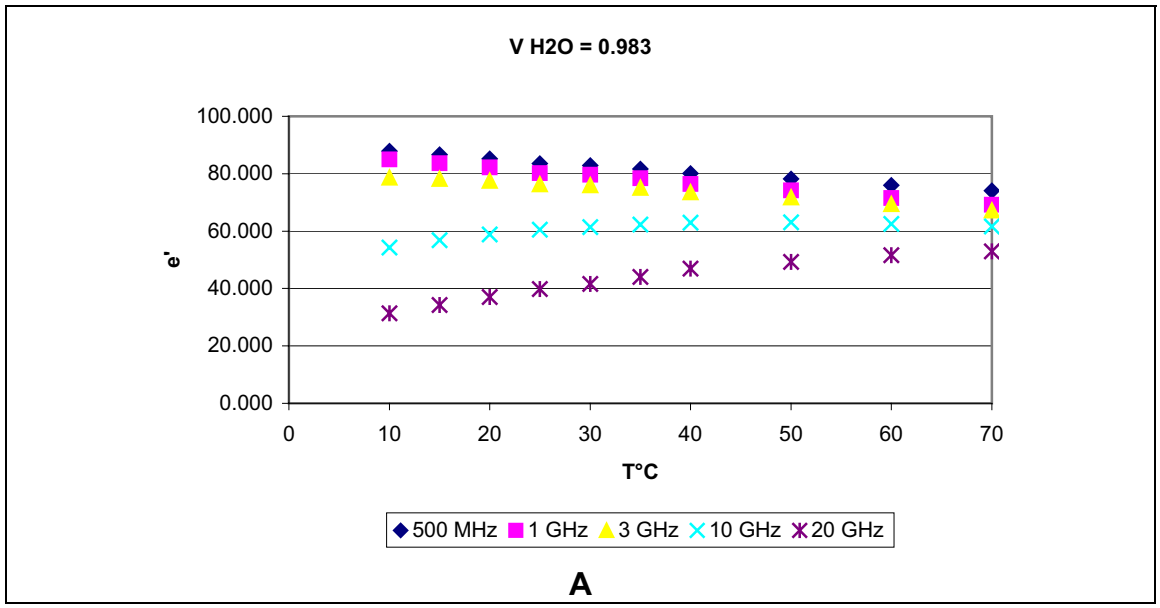

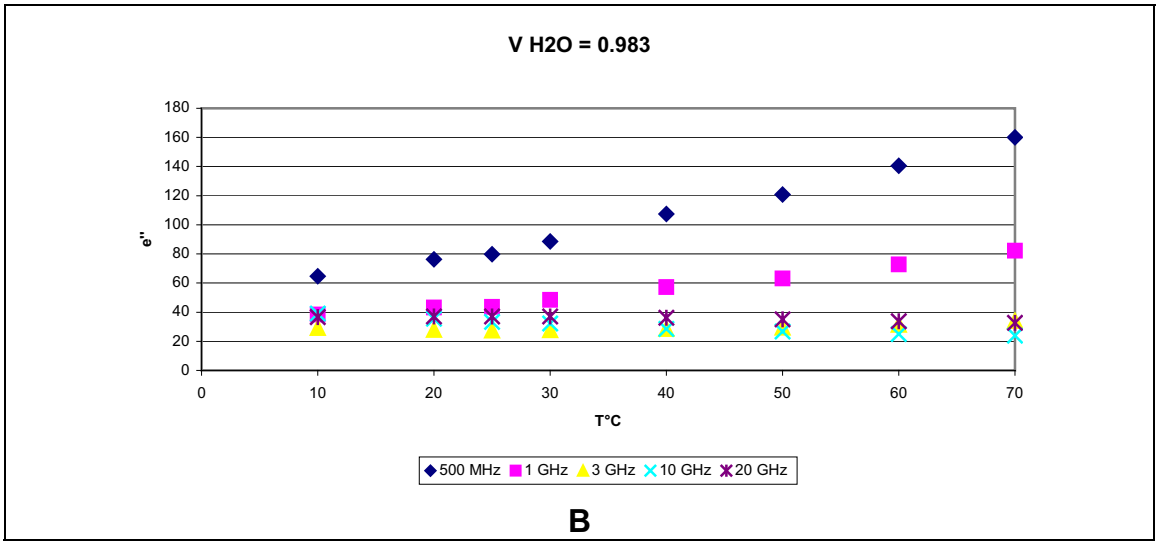

Figure 4.34. A) Real and B) Imaginary part of complex permittivity versus temperature for V_{H2O} =0.983 measured at different frequencies.

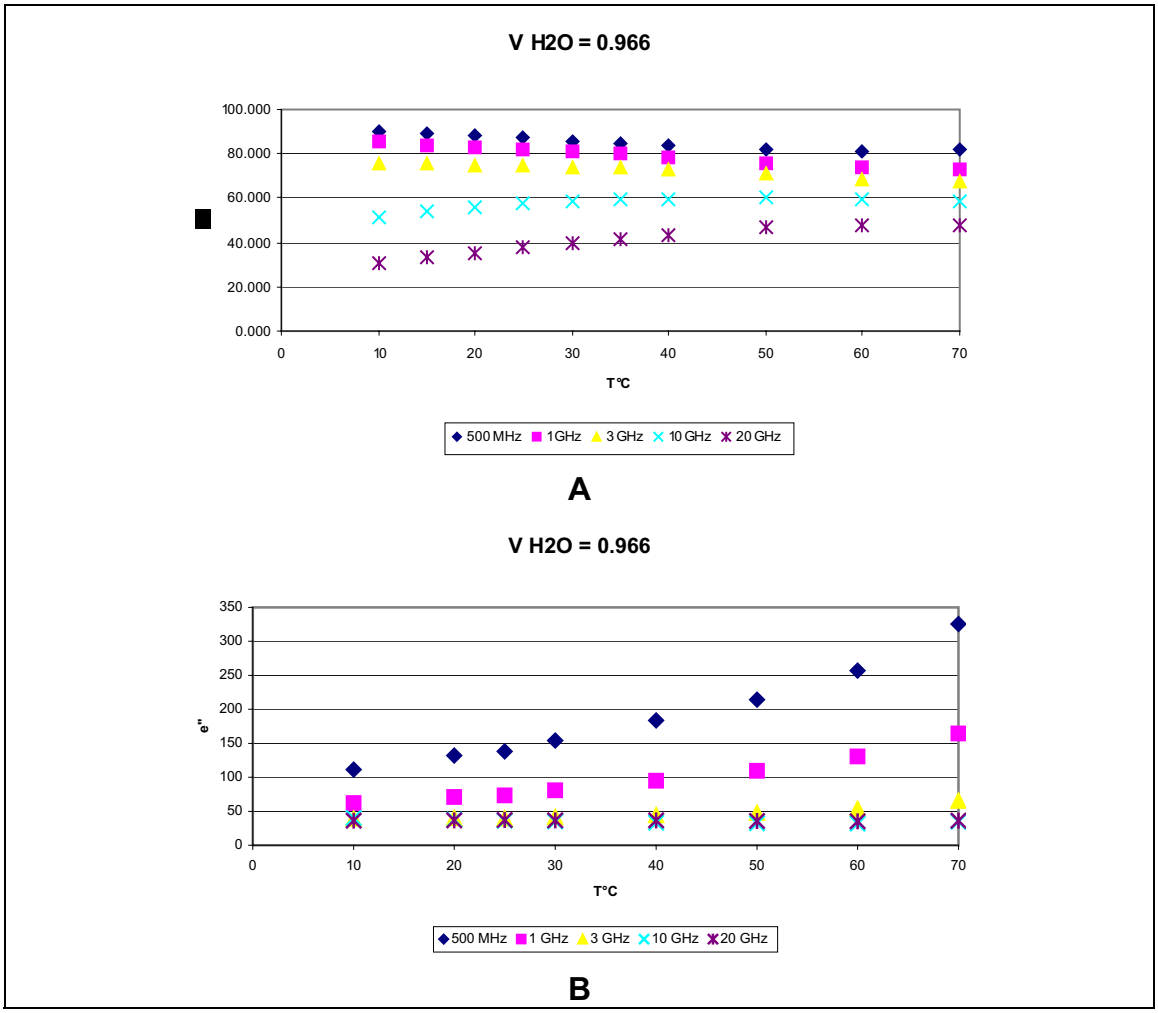

Figure 4.35. A) Real and B) Imaginary part of complex permittivity versus temperature for V_{H2O} =0.966 measured at different frequencies.

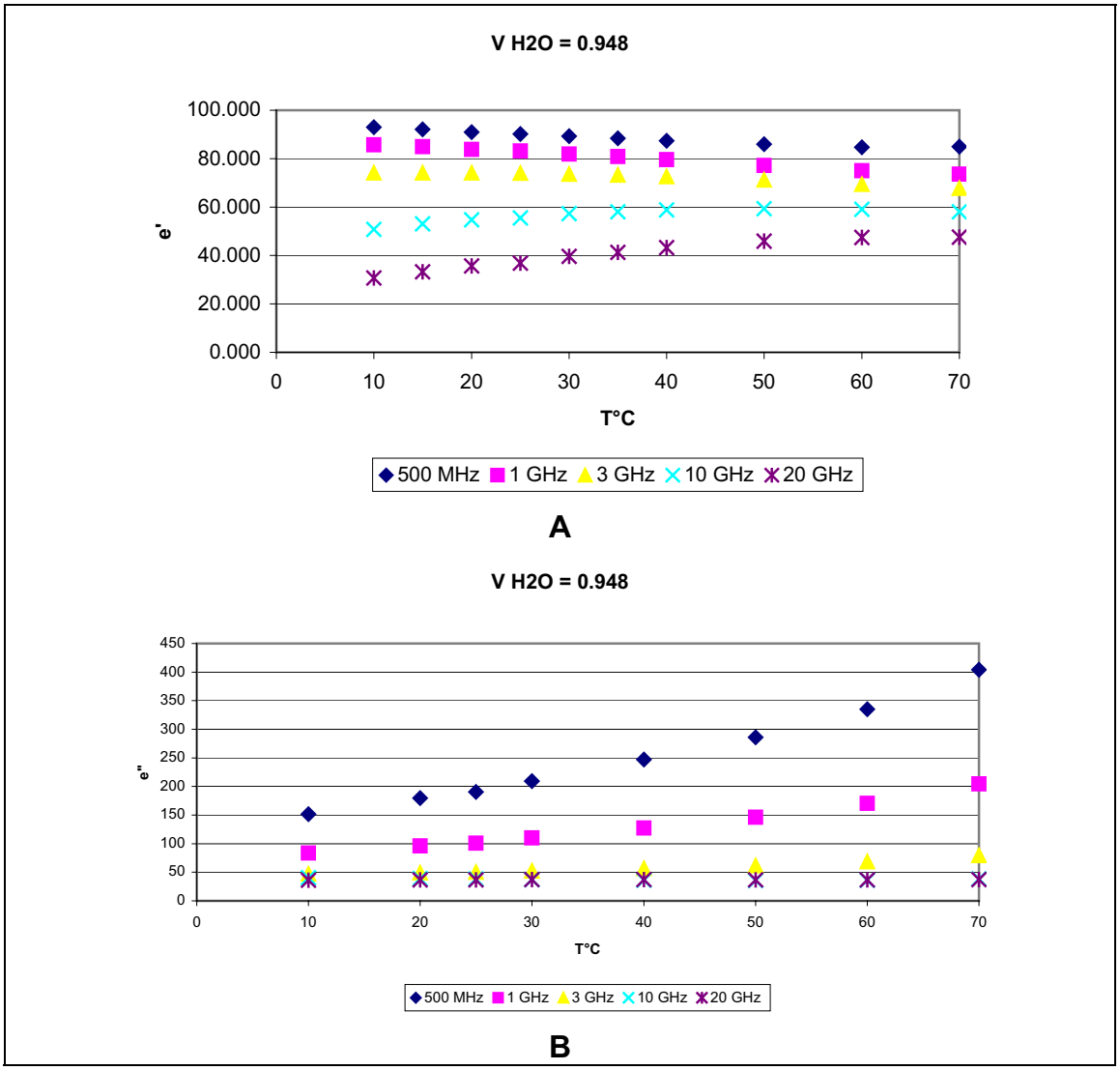

Figure 4.36. A) Real and B) Imaginary part of complex permittivity versus temperature for V_{H2O} =0.948 measured at different frequencies.

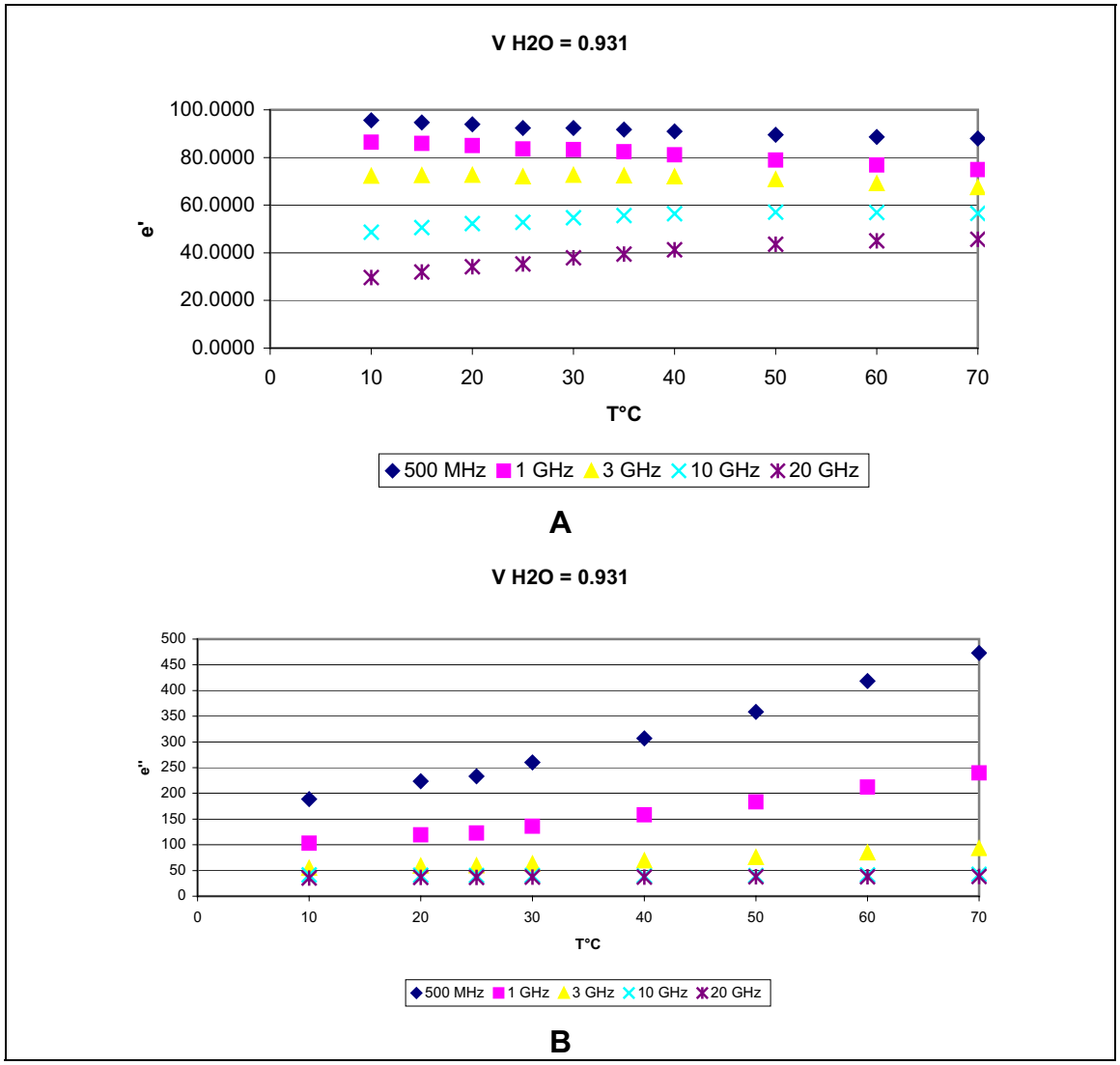

Figure 4.37. A) Real and B) Imaginary part of complex permittivity versus temperature for V_{H2O} =0.931 measured at different frequencies.

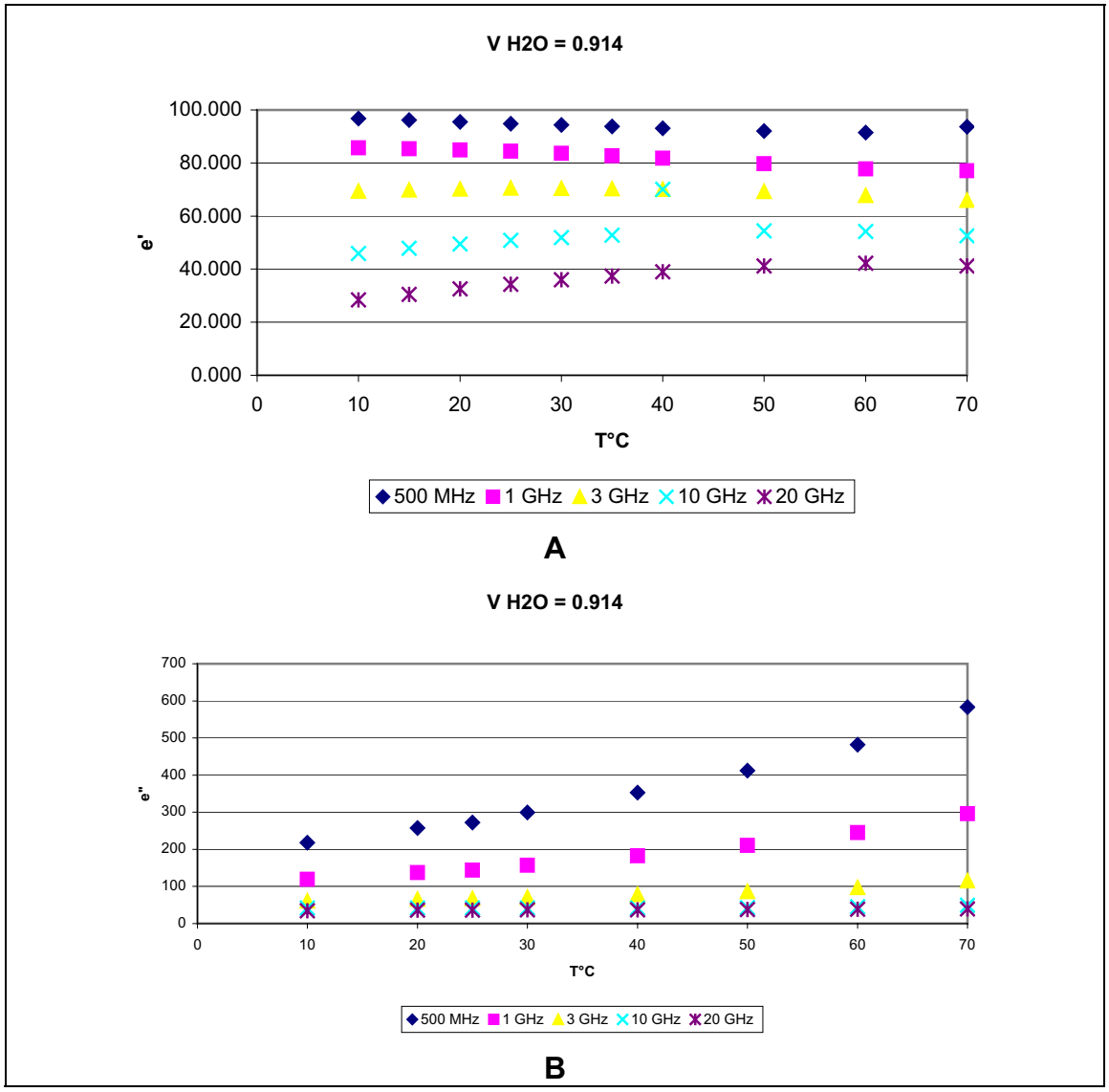

Figure 4.38. A) Real and B) Imaginary part of complex permittivity versus temperature for V_{H2O} =0.914 measured at different frequencies.

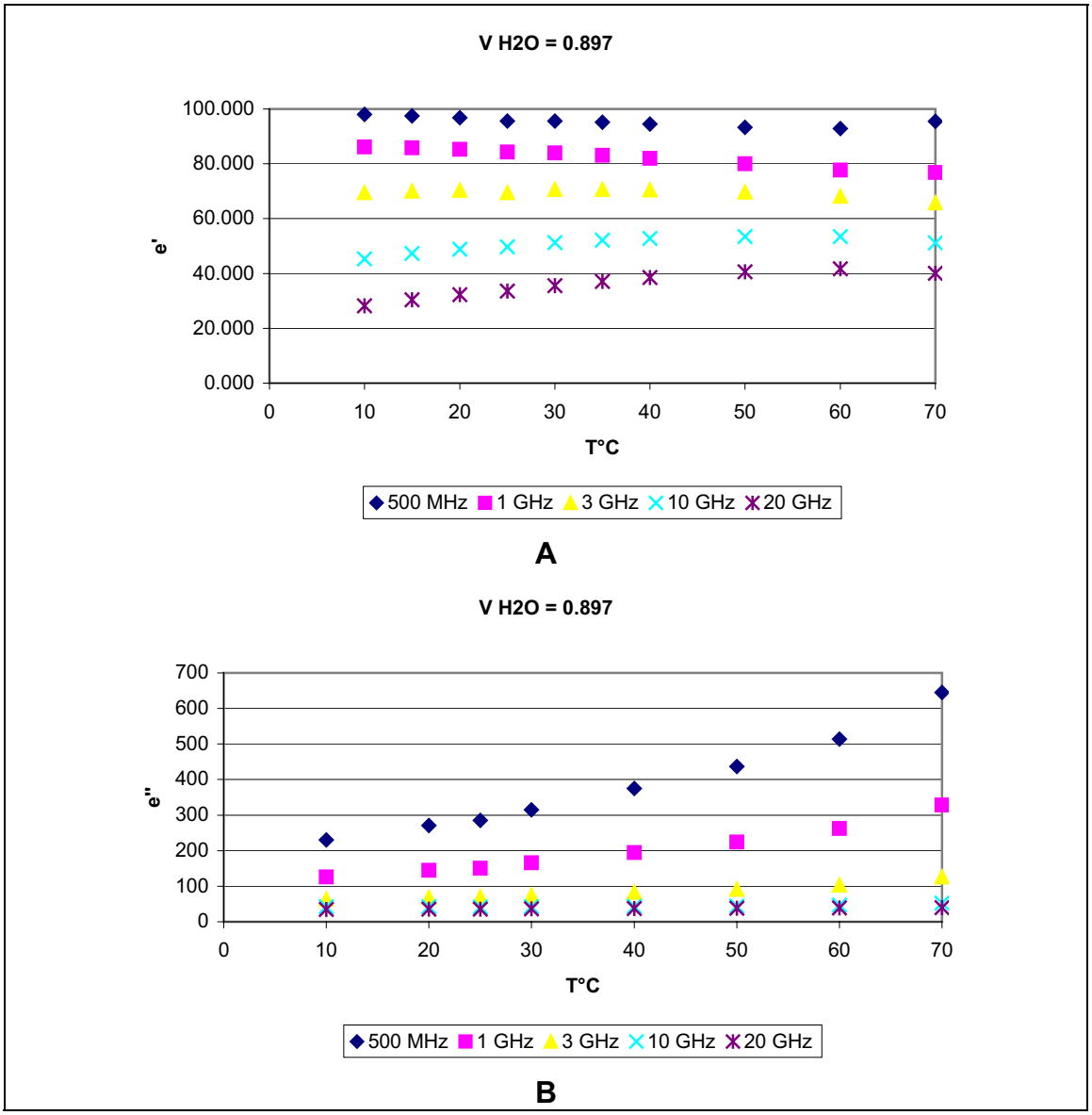

Figure 4.39. A) Real and B) Imaginary part of complex permittivity versus temperature for V_{H2O} =0.897 measured at different frequencies.

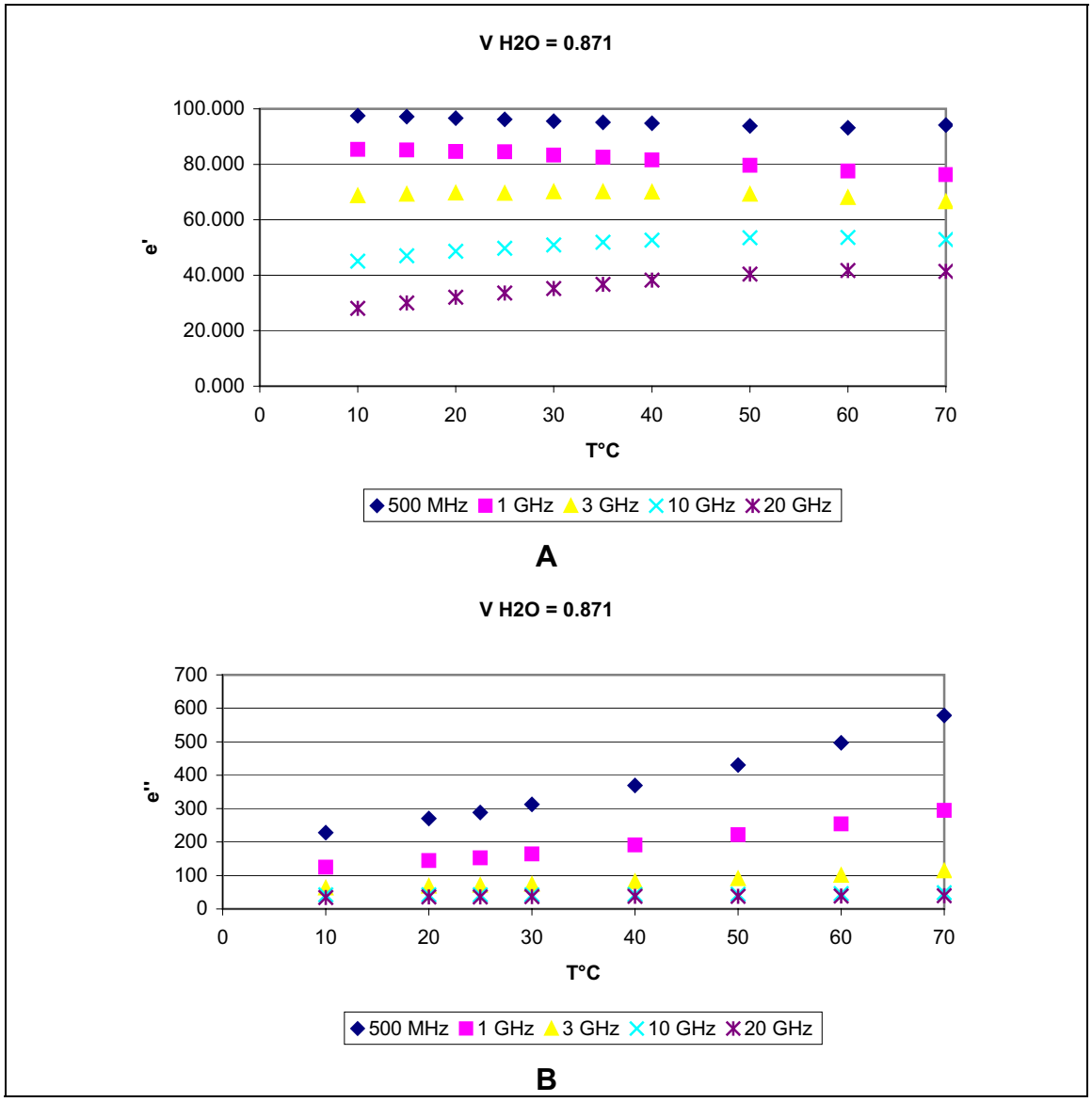

Figure 4.40. A) Real and B) Imaginary part of complex permittivity versus temperature for V_{H2O} =0.871 measured at different frequencies.

In solutions with higher volume fraction of water, the results show that when a very small amount of salt is added, small increase on the dielectric constant were observed compared to pure water. With increasing the amount of salt this increase starts to get larger, in other words more salt higher the dielectric properties.

This change is reverse to that of observed by Seignette salt. It could be said, when the volume fraction of water was increased the dielectric constant decreased.

This also may be due to that, in diluted solutions the salt is dissolved completely, the quantity of ions in the medium are higher and the structure of salt is not preserved and it shows lower dielectric constant than those with higher amount of salt. In other hand, it could be assumed that by increase the amount of salt the probability of preformation of crystals and liquid crystals are much higher and will result in increase of electric properties.

Due to very low T_c the investigation of ferroelectric activity and the transition from ferro to paraelectric due to temperature changes was not possible, but a small change in dielectric properties was observed. For example, pure water shows the value of around 78 at room temperature (25°C) and in measured frequency of 500 MHz for the real part of complex permittivity, while by addition of salt (V_{H2O} = 0.87) this value increases to about 96. Although these changes may not be significant, but it certainly shows an increase in probability of crystals preformation.

4.2.3 Influence of the temperature on the dielectric properties of the KDP/water solutions

The influence of the temperature on the properties of the binary KDP salt-Water solutions was studied. The Figures 4.41 - 4.45 represent the complex permittivity (real and imaginary part) versus the volume fraction of water, measured at the frequencies: 500 MHz, 1 GHz, 3 GHz, 10 GHz and 20 GHz.

As it can be seen, in each of the volume fractions measured, the dielectric constant (real part) shows a very small change when the temperature increases. At low frequencies (500 MHz, 1 GHz and 3 GHz) these values decreases slightly by increasing temperature, where at higher frequencies (10

GHz and 20 GHz) this effect is reversed. This is due to increase in inner molecular movements and probably the reduction of close interaction forces.

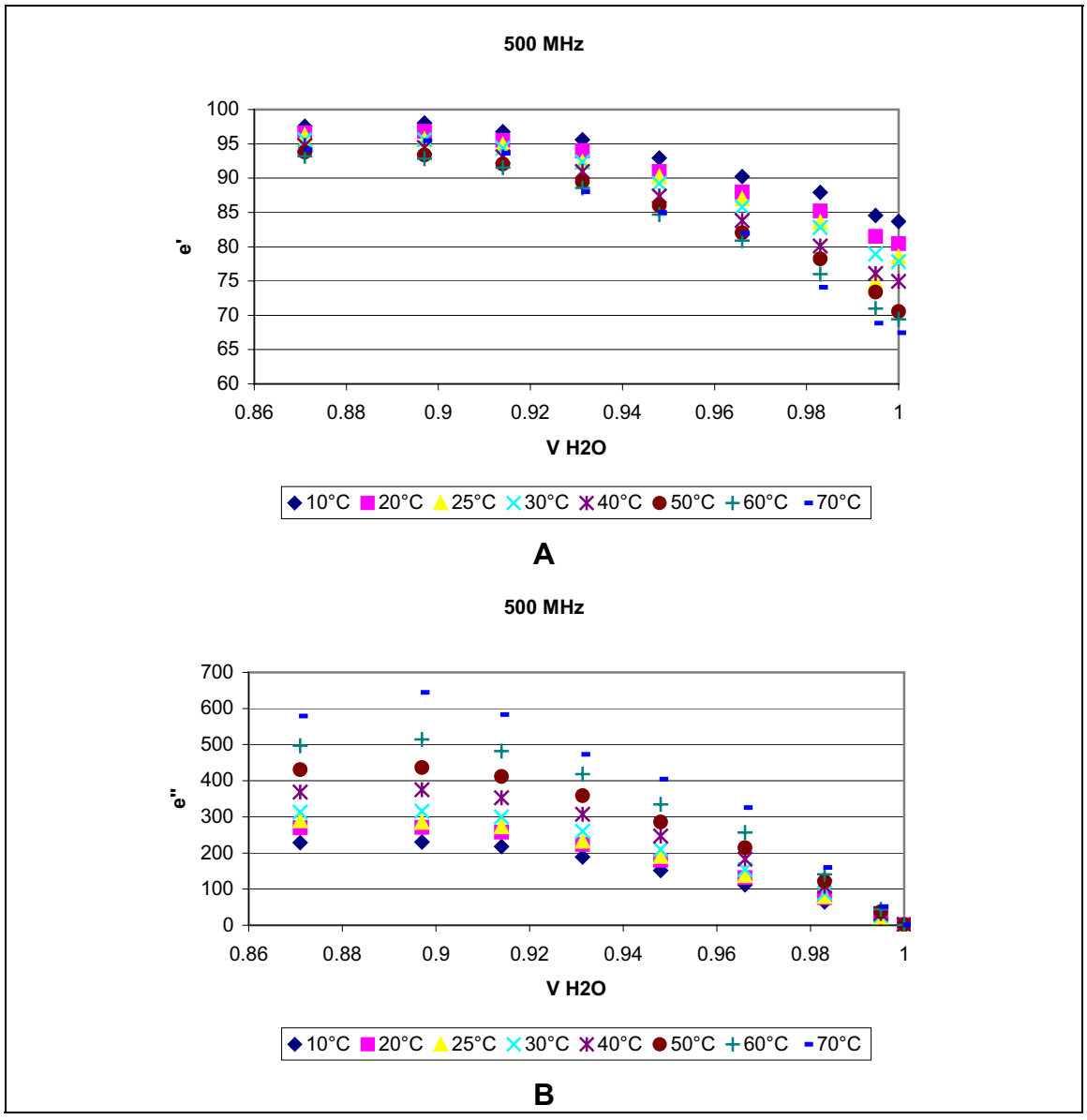

Figure 4.41. A) Real and B) Imaginary part of complex permittivity versus V_{H2O} at different temperatures at measured frequency of 500 MHz.

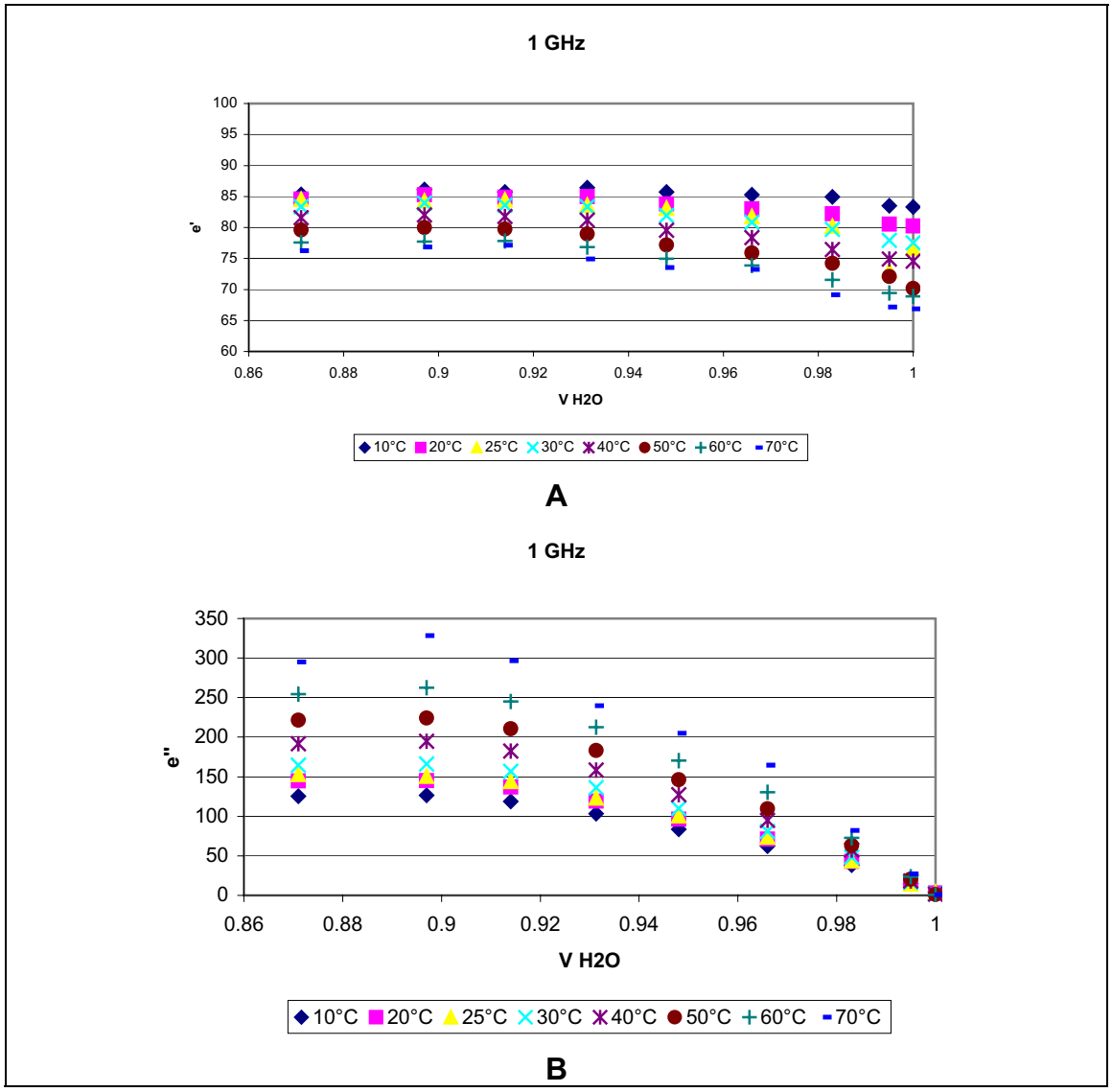

Figure 4.42. A) Real and B) Imaginary part of complex permittivity versus V_{H2O} at different temperatures at measured frequency of 1 GHz.

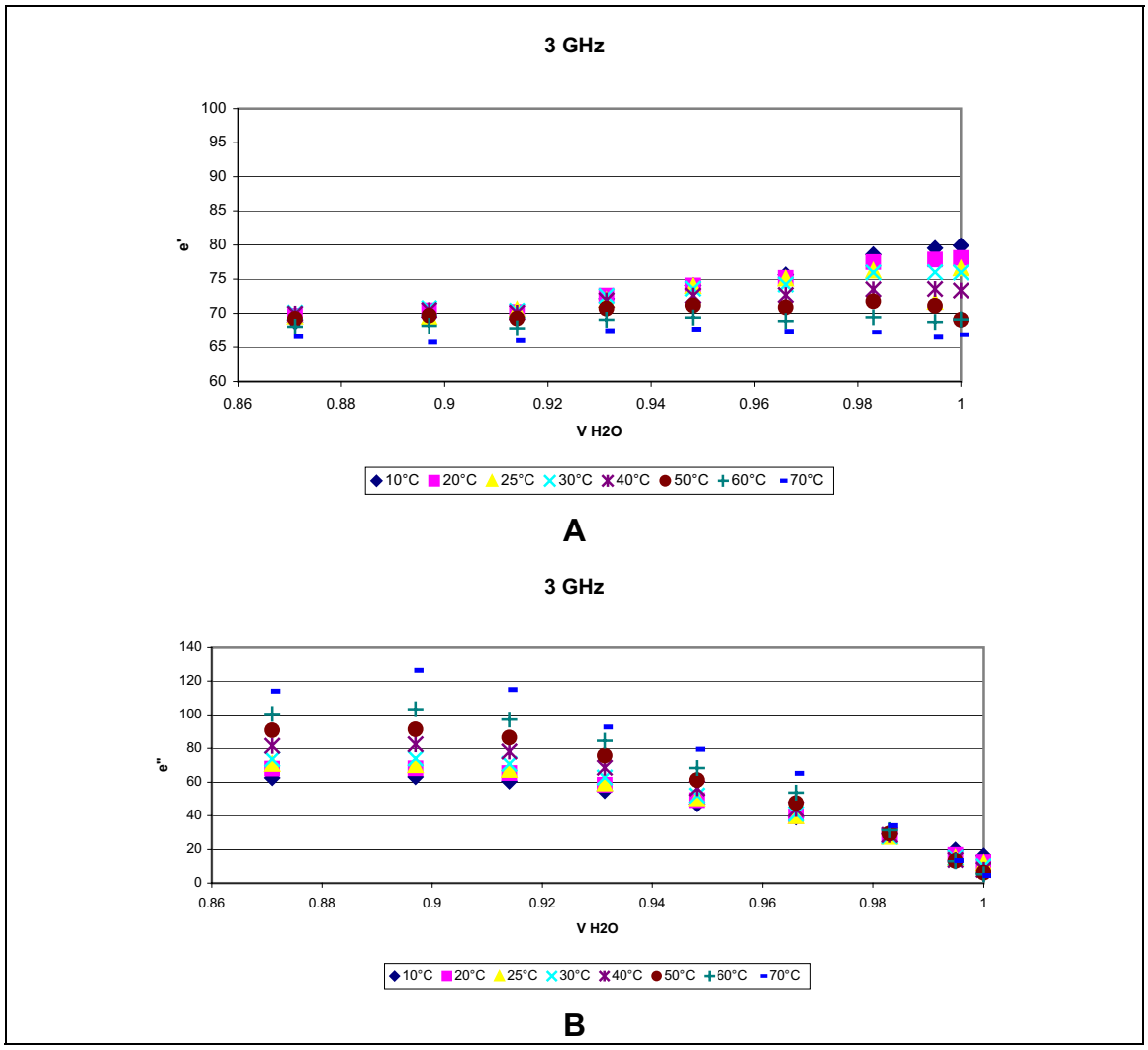

Figure 4.43. A) Real and B) Imaginary part of complex permittivity versus V_{H2O} at different temperatures at measured frequency of 3 GHz.

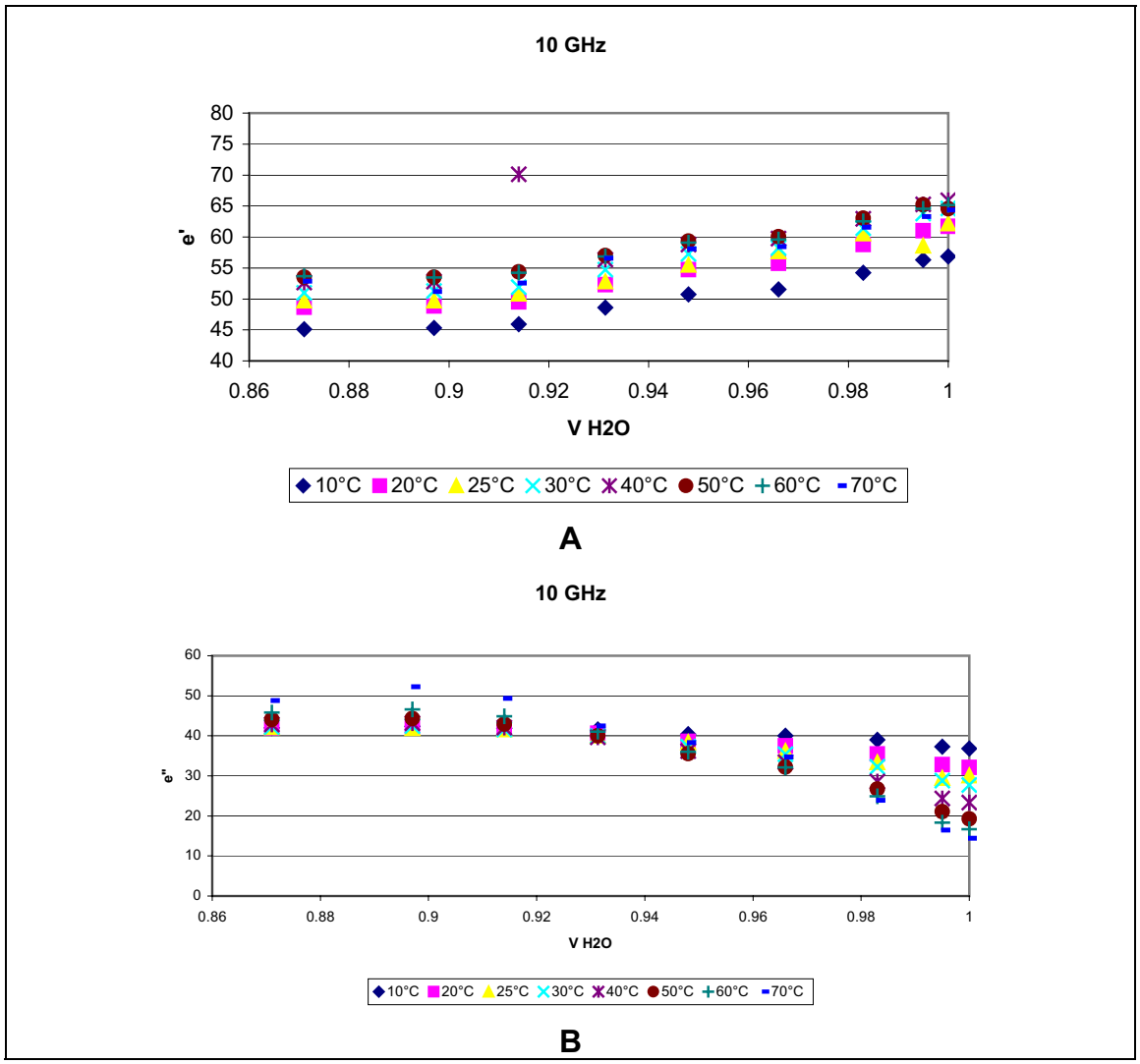

Figure 4.44. A) Real and B) Imaginary part of complex permittivity versus V_{H2O} at different temperatures at m
easured frequency of 10 GHz.

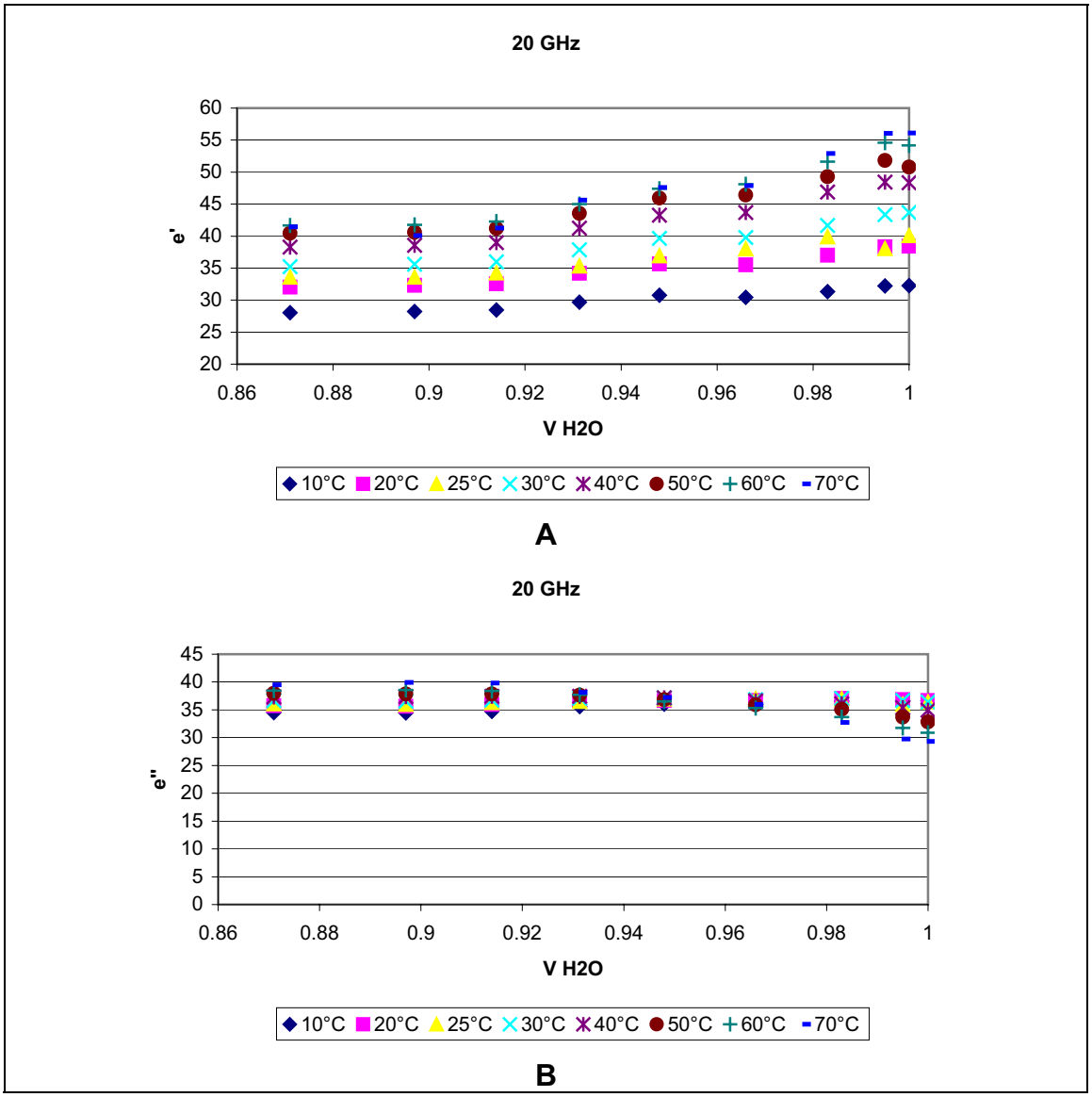

Figure 4.45. A) Real and B) Imaginary part of complex permittivity versus V_{H2O} at different temperatures at measured frequency of 20 GHz.

4.2.4 Relaxation behavior of KDP/water solutions

As it has been said before, The Debye relaxation equation (see Section A, 2.3.3 – 2.3.6.1) is based on the assumption of a molecule in the gas form or highly diluted in a nonpolar liquid *(Chelkowski, 1980)*.

All the investigated polar liquids were examined with regards to the outlined hypotheses mentioned in 4.1.5.

For calculation of relaxation time the 1-Debye equation was chosen due to the simplicity of the model and low number of free parameters (see Section A, 3.2.6.2).

Figure 4.46 shows the relaxation time versus temperature at different volume fractions.

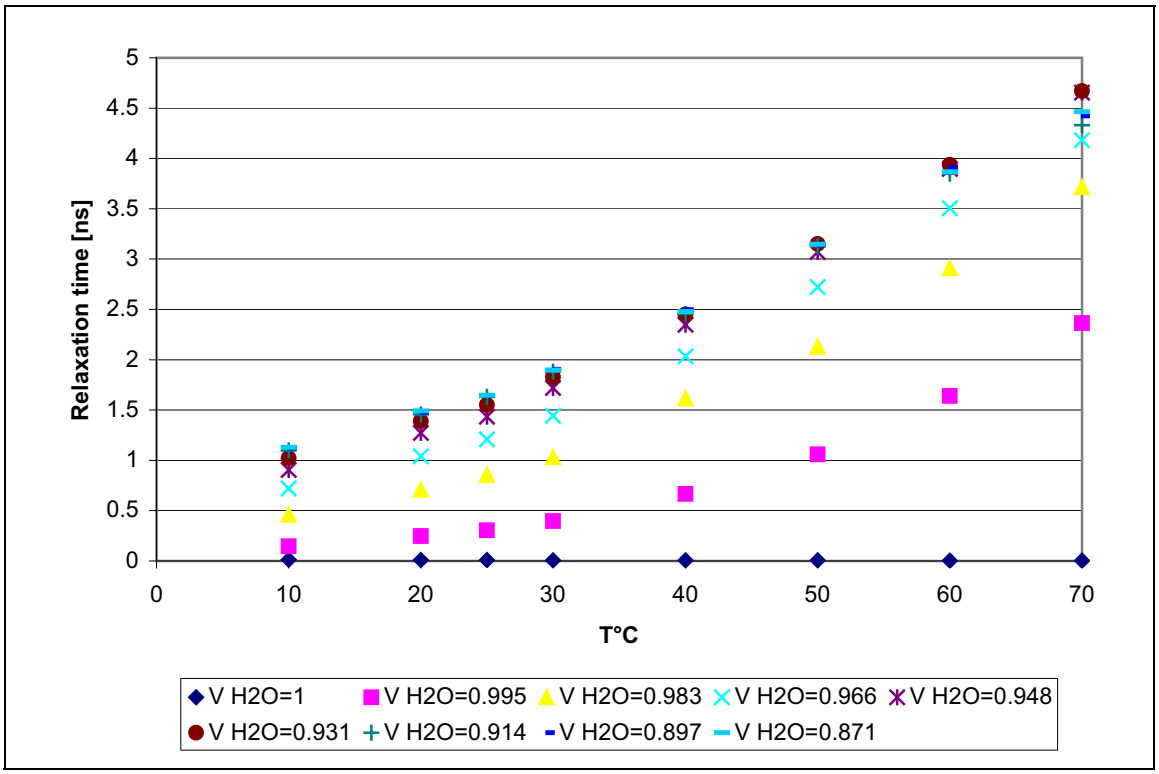

Figure 4.46. Relaxation times versus temperature at different volume fractions.

As it can be seen above, the relaxation times increase by increasing the amount of KDP in the binary solutions. An increase in relaxation time by increasing the temperature has been also observed.

These increased get smaller as the $V_{H2O} < 0.931$. This might be due to increase of pre-formed crystalline structure in the mixture.

Table 4.7 shows the results obtained using 1-Debye model for different V_{H2O} at different temperatures.

	τ [ns]							
V H20	**10°C**	**20°C**	**25°C**	**30°C**	**40°C**	**50°C**	**60°C**	**70°C**
1	0.012	0.009	0.009	0.007	0.006	0.005	0.004	0.004
0.995	0.146	0.246	0.303	0.395	0.665	1.059	1.64	2.363
0.983	0.461	0.707	0.858	1.03	1.614	2.13	2.909	3.715
0.966	0.719	1.04	1.208	1.445	2.033	2.721	3.505	4.183
0.948	0.904	1.273	1.434	1.72	2.349	3.07	3.897	4.653
0.931	1.02	1.389	1.551	1.827	2.448	3.151	3.938	4.671
0.914	1.097	1.457	1.631	1.88	2.457	3.129	3.847	4.329
0.897	1.123	1.48	1.644	1.902	2.498	3.142	3.904	4.423
0.871	1.131	1.491	1.646	1.898	2.478	3.146	3.866	4.464

Table 4.7. Relaxation times [ns] obtained for different V_{H2O} at different temperatures.

When the relaxation times are plotted against V_{H2O}, we can observe a maximum at the V_{H2O} = 0.931, and a platue is reached from this volume fraction. Figure 4.47 shows this behavior.

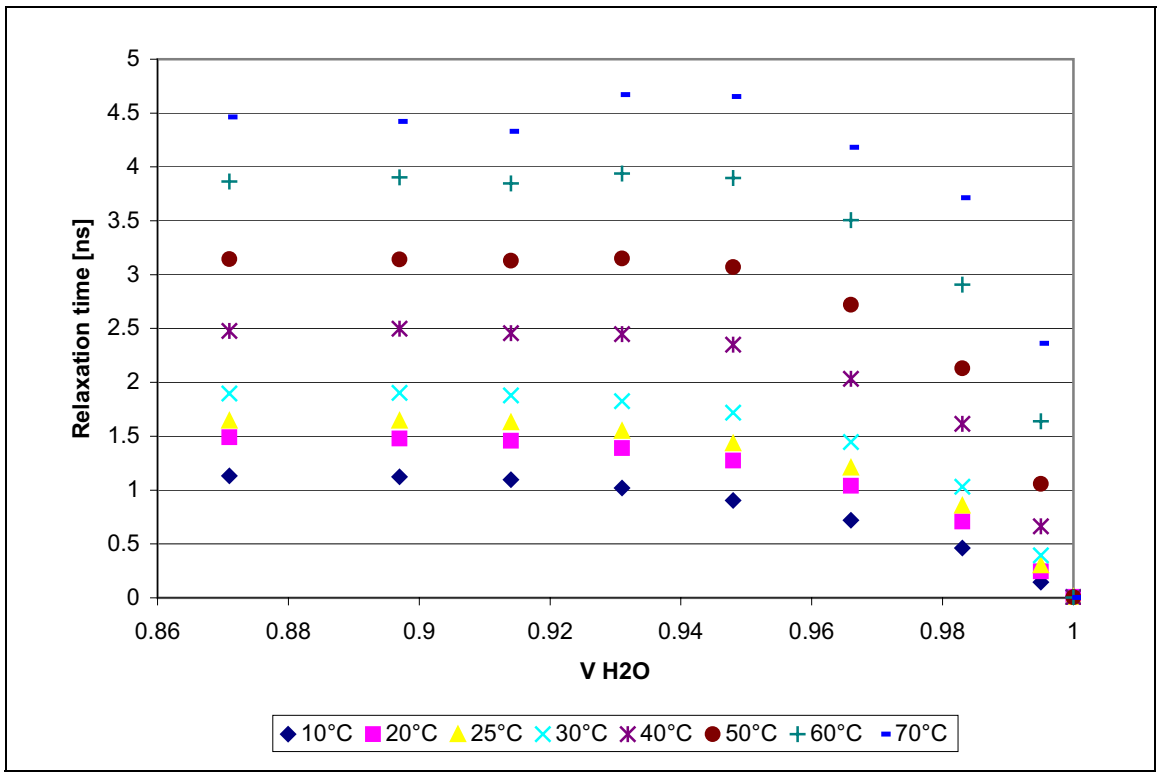

Figure 4.47. Relaxation times versus V_{H2O} at different temperatures.

This figure also shows a percolation threshold in respect to relaxation time(τ) at V_{H2O} = 0.931 which stays the same at all volume fractions (no shift like in case of Signette salt were observed).

To show the reliability of the method, the R^2 values are plotted against volume fraction at different temperatures and visa-versa. Results are shown in table 4.8 and the plots in figures 4.48 and 4.49.

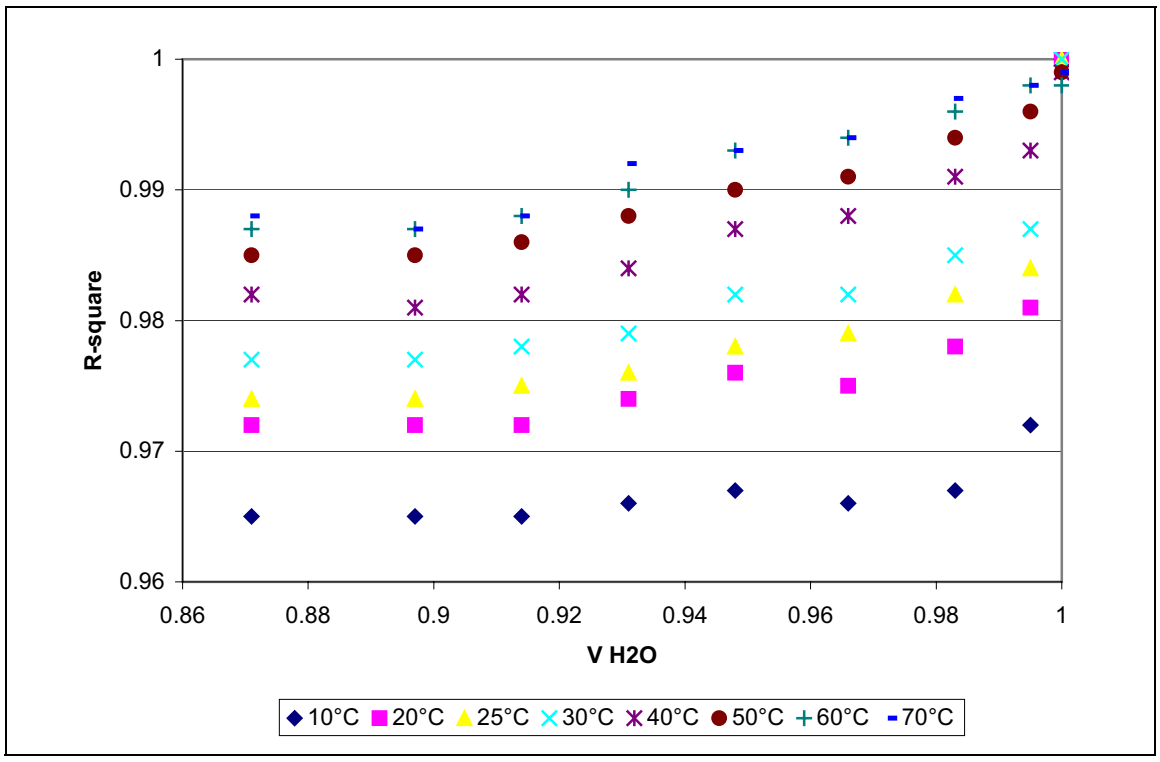

Figure 4.48. Correlation coefficient (R^2) versus V_{H2O}.

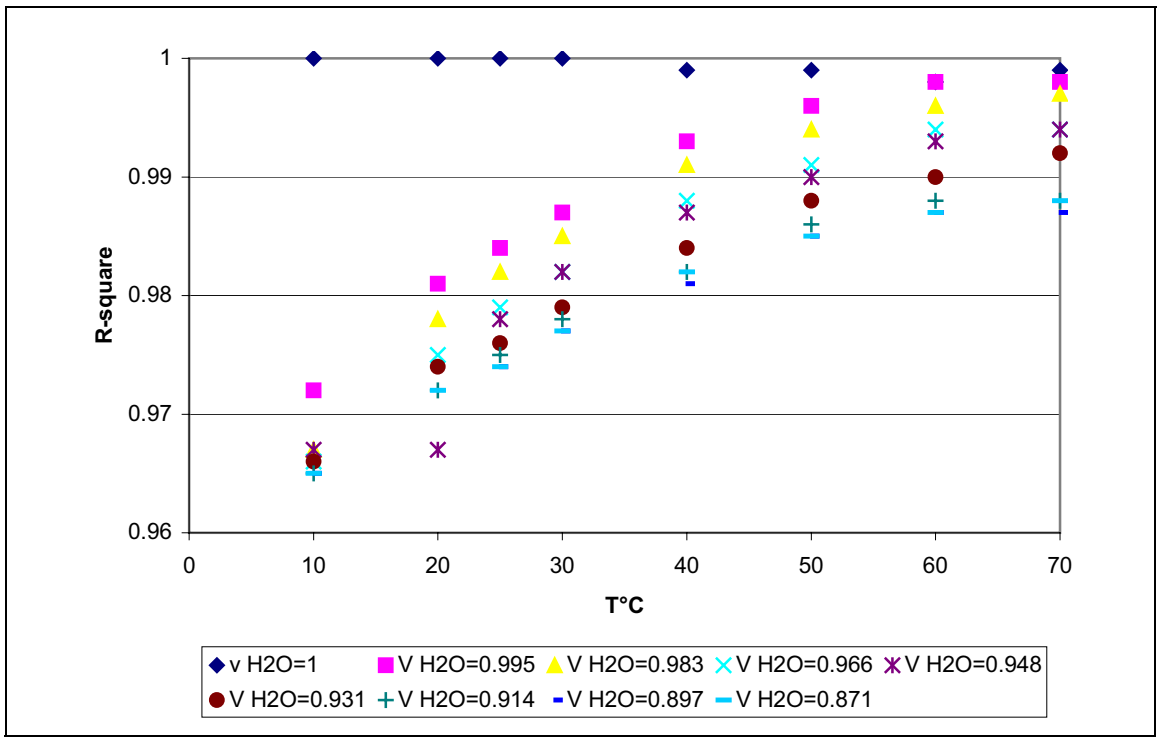

Figure 4.49. Correlation coefficient (R^2) versus temperature °C.

	R^2								
T°C	V_{H2O}= 1.00	V_{H2O}= 0.995	V_{H2O}= 0.983	V_{H2O}= 0.966	V_{H2O}= 0.948	V_{H2O}= 0.931	V_{H2O}= 0.914	V_{H2O}= 0.897	V_{H2O}= 0.871
10	1	0.972	0.967	0.966	0.967	0.966	0.965	0.965	0.965
20	1	0.981	0.978	0.975	0.967	0.974	0.972	0.672	0.972
25	1	0.984	0.982	0.979	0.978	0.976	0.975	0.974	0.974
30	1	0.987	0.985	0.982	0.982	0.979	0.978	0.977	0.977
40	0.999	0.993	0.991	0.988	0.987	0.984	0.982	0.981	0.982
50	0.999	0.996	0.994	0.991	0.99	0.988	0.986	0.985	0.985
60	0.998	0.998	0.996	0.994	0.993	0.99	0.988	0.987	0.987
70	0.999	0.998	0.997	0.994	0.994	0.992	0.988	0.987	0.988

Table 4.8. Correlation coefficient (R^2) obtained for different V_{H2O} at different temperature.

4.2.5 Discussion

As we mentioned in 4.1.6 of this Section, Another application of Dielectric Spectroscopy is the study of ferroelectric properties of substances. In this case the ferroelectric properties of KDP salt were investigated. The behavior of its binary mixtures with water as a function of increasing temperature was investigated using the high frequency network analyzer.

The results demonstrate that the specific ferroelectric properties of these mixtures could not be observed in measured temperatures between 10 and 70 at frequencies between 500 MHz and 20 GHz. In other words, it could not be possible to observe the change from Ferro to paraelectric typical for a single solid crystal as a result of difference in their “order” of the matter.

It shows definitely that in solution the KDP salt has a different “order” than in a solid crystal. Thus KDP salt is not influencing the binary mixtures, meaning, the dominant factor is that of water.

The absence of a “ferroelectric” behavior in binary solutions could be also due to an “anti-ferroelectric” arrangement of the polarized particles of the KDP or the polarized water clusters islands with dissolved KDP salt in a continuous phase. As it has been said in theory part, the ferroelecrtic activity in a single crystal depends very much on the axis of the crystal on which the excitation (mechanical or electrical) happens. In liquid crystals or in preformed crystalline structure this axis does not exist yet and this may result in absence of “ferroelectric” behavior.

The finding that water can be described using the Debye relaxation equation is well documented *(e.g. Böttcher et al. 1978; c ; Kaatze, 1989)*. This result is surprising, because the Debye relaxation theory had been developed for the gaseous form or for solutions highly diluted in nonpolar liquids, where hardly any intermolecular interactions occur.

The single Debye equation is also able to characterize the whole range of KDP salt-water mixtures at all temperatures with average $R^2 \geq 0.985$ showing with respect to the relaxation time (τ), one percolation threshold in all temperatures at $V_{H2O}= 0.931$(Fig. 4.47).

As mentioned before, It may be of interest to study other polar substances, which are well soluble in water in order to see whether a “crystalline preformation” in solution exists, close to the saturation concentration and/or as un supersaturated condition, which influences the final crystalline structure after precipitation. This could be of special interest for drugs showing a polymorphic crystalline behavior.

4.3 Investigation of ferroelectric activity in ADP/water binary mixtures using dielectric spectriscopy at temperature range between 10 and 70

In this part, we investigate ADP/water binary mixtures in temperature range between 10 and 70°C to see, if any, ferroelectric activity could be observed.

Measurement of pure salt was not possible due to decomposition of salt during melting process. As this salt also has very low Curie temperature (T_c = -125°C), investigation around T_c was not possible. Please see Appendix for complete table of results.

4.3.1 Influence of the volume fraction on the dielectric properties of the ADP/water solutions

In order to study the influence of the volume fraction on the ferroelectric properties, the dielectric constant of the binary ADP/water solutions were measured. In each volume fraction complete dissolution of salt was observed. The solutions were measured at the temperature range between 10 and 70°C. The results for the investigated solutions are reported below (see Figures 4.50 – 4.57).

The volume fractions of water 1, 0.993, 0.973, 0.946, 0.920, 0.894, 0.868, 0.817 and 0.790 were studied.

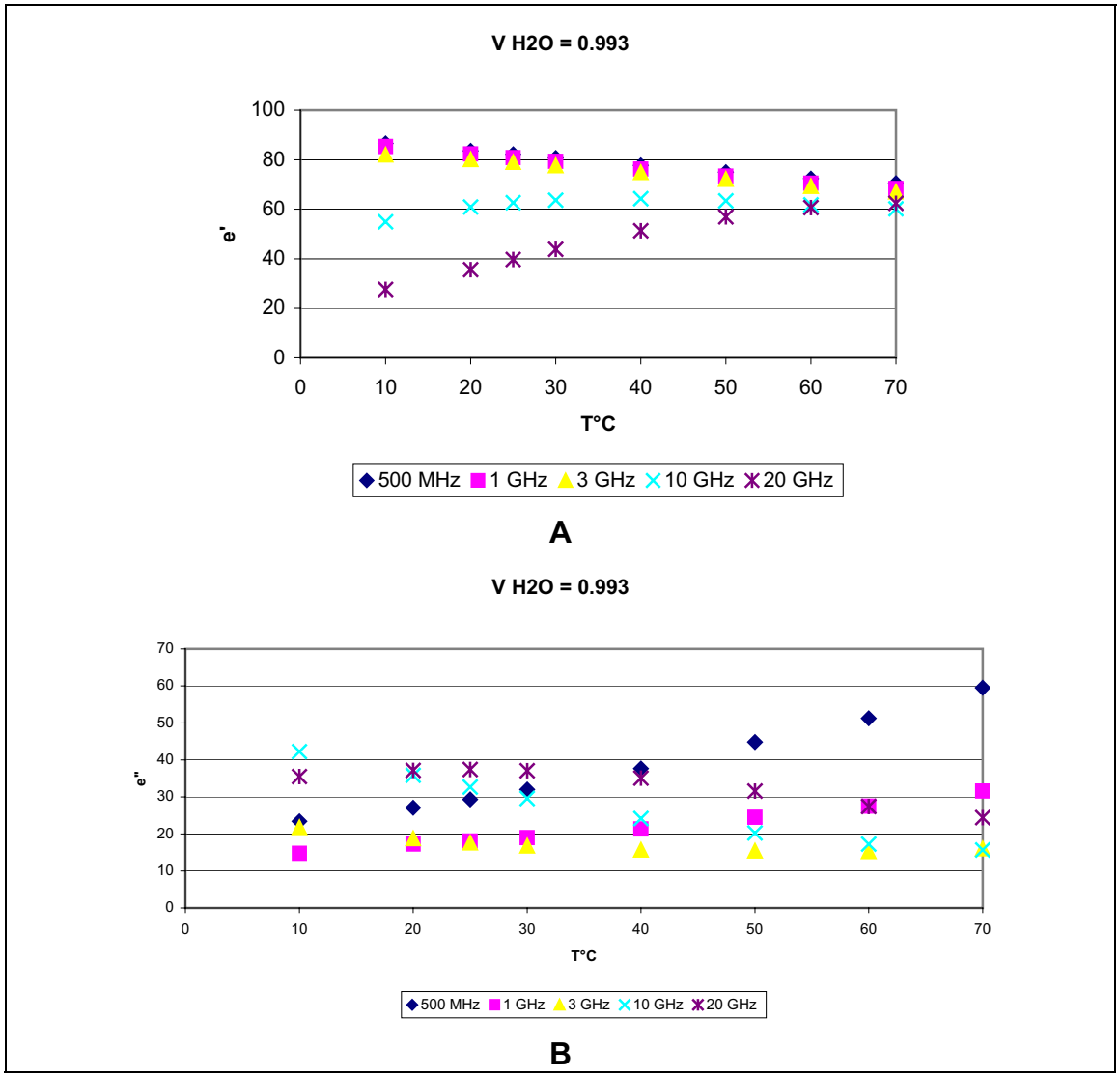

Figure 4.50. A) Real and B) Imaginary part of complex permittivity versus temperature for V_{H2O} =0.993 measured at different frequencies.

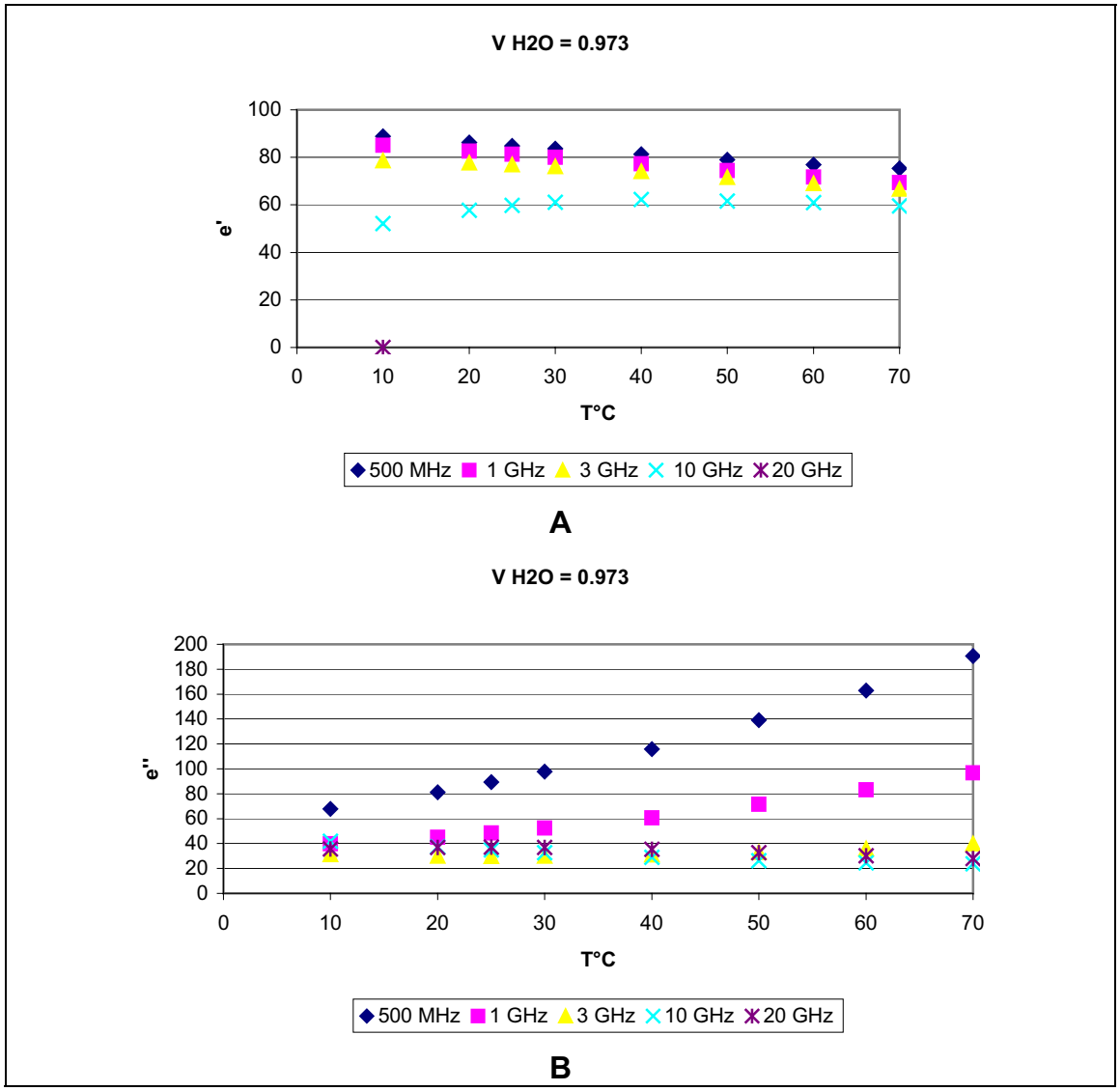

Figure 4.51. A) Real and B) Imaginary part of complex permittivity versus temperature for V_{H2O} =0.973 measured at different frequencies.

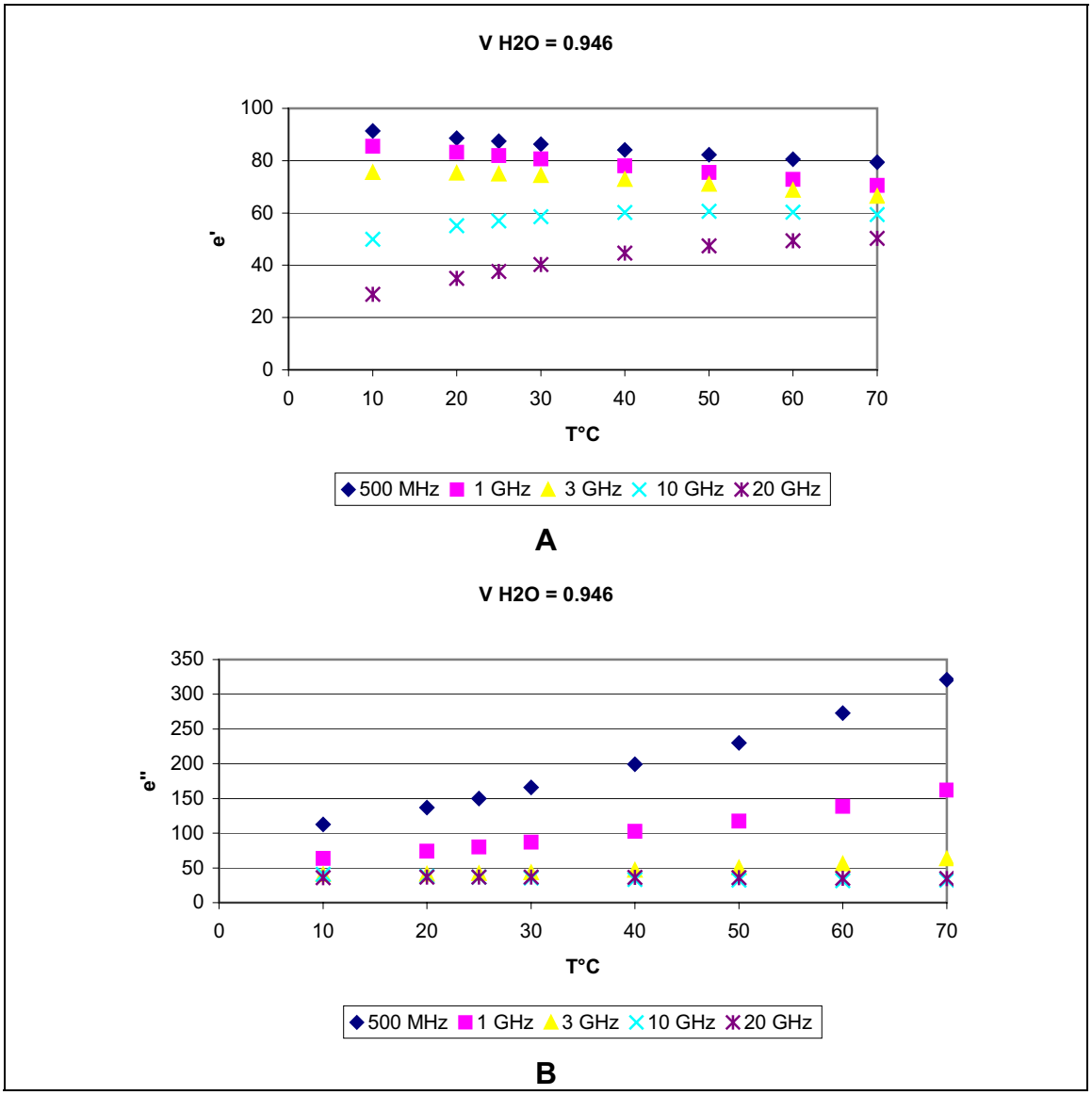

Figure 4.52. A) Real and B) Imaginary part of complex permittivity versus temperature for V_{H2O} =0.946 measured at different frequencies.

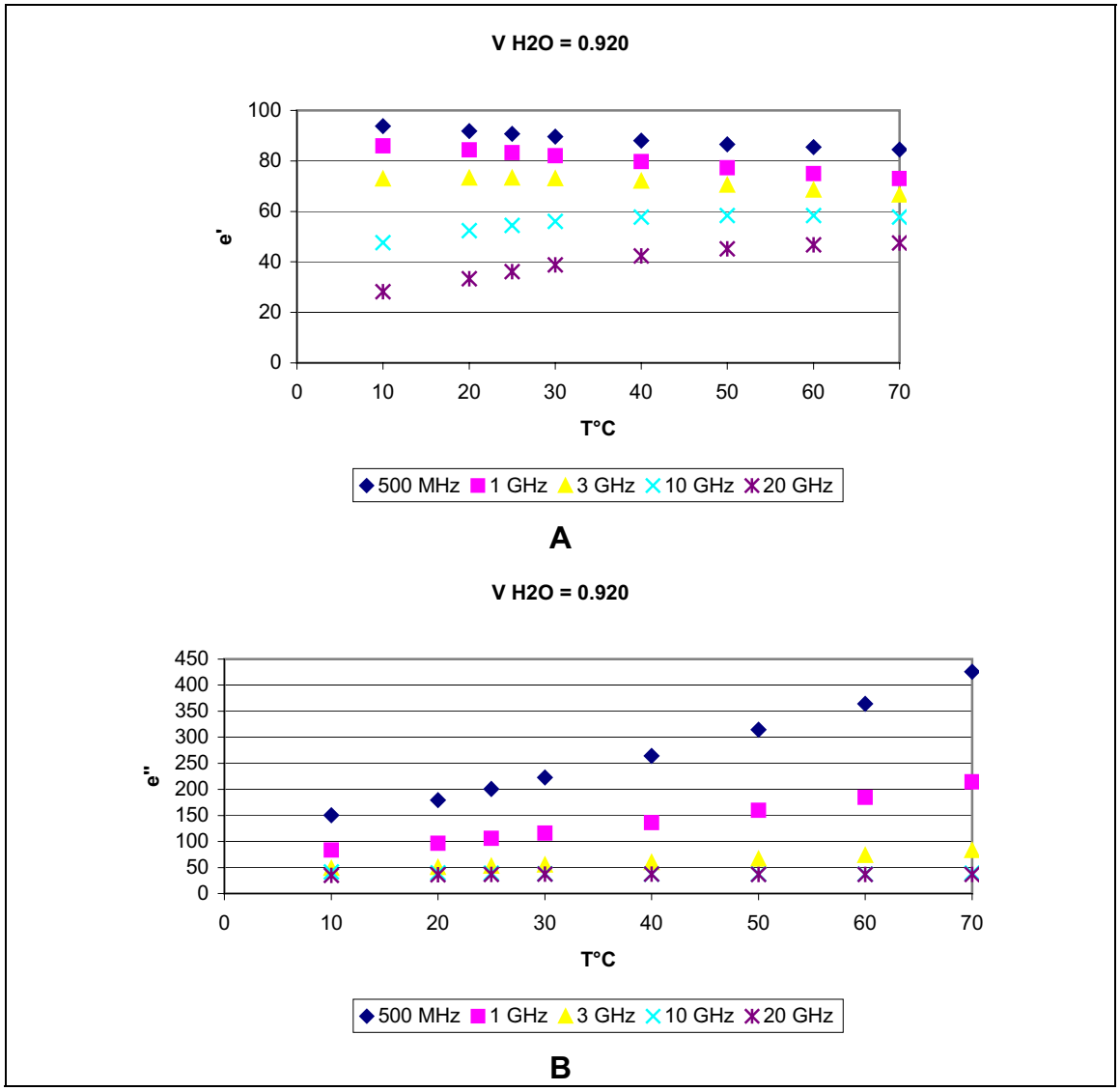

Figure 4.53. A) Real and B) Imaginary part of complex permittivity versus temperature for V_{H2O} =0.920 measured at different frequencies.

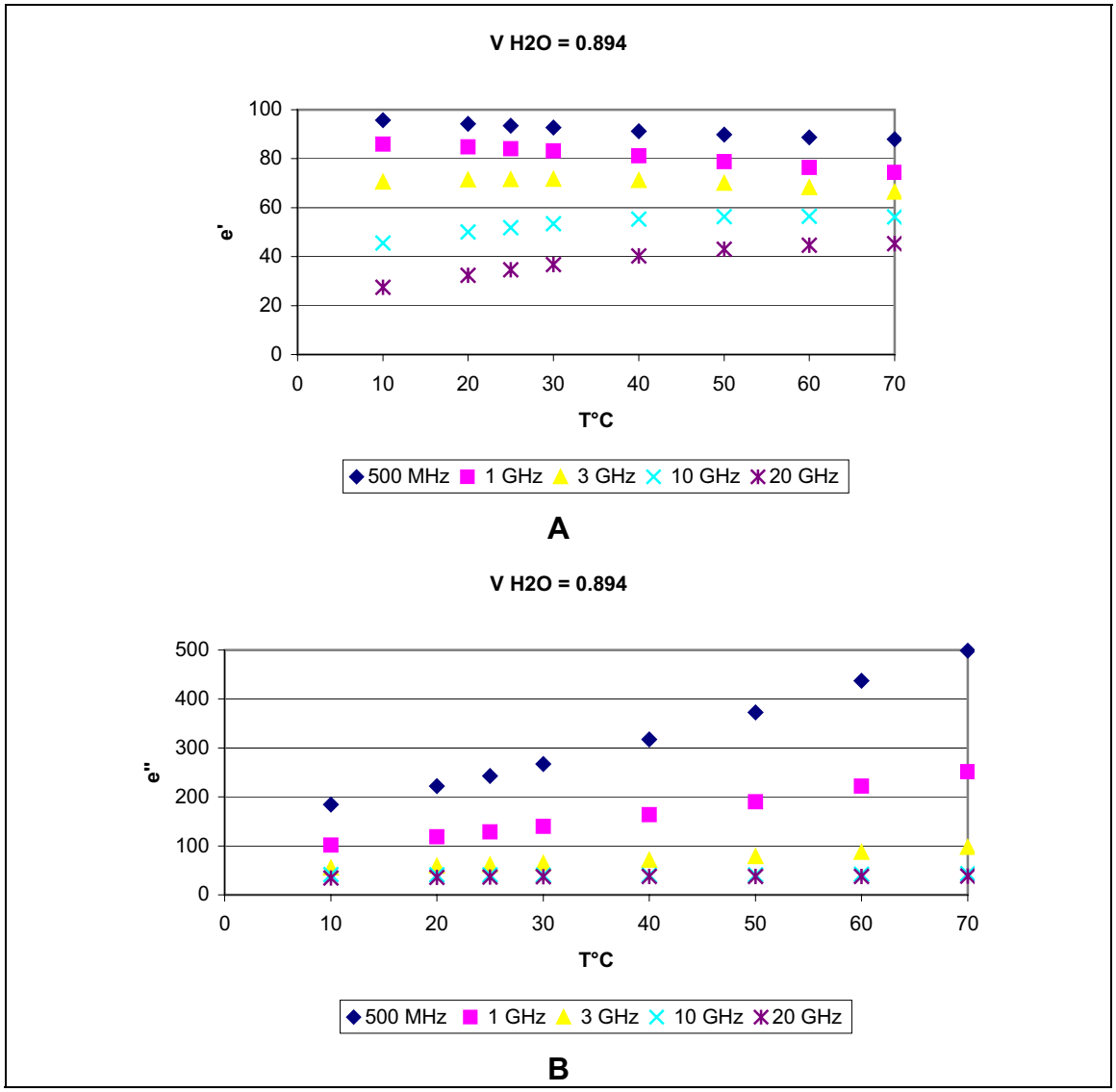

Figure 4.54. A) Real and B) Imaginary part of complex permittivity versus temperature for V_{H2O} =0.894 measured at different frequencies.

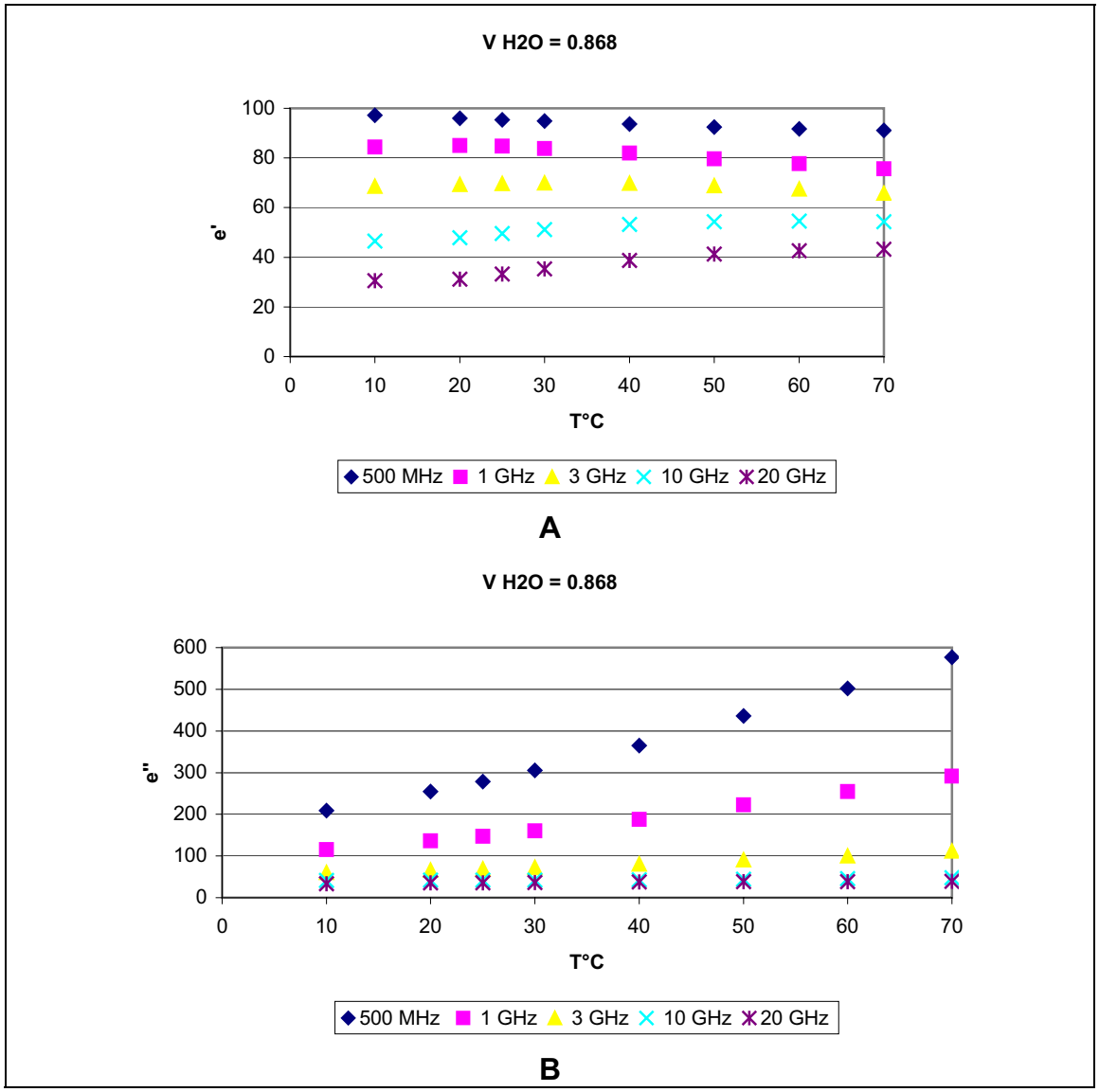

Figure 4.55. A) Real and B) Imaginary part of complex permittivity versus temperature for V_{H2O} =0.868 measured at different frequencies.

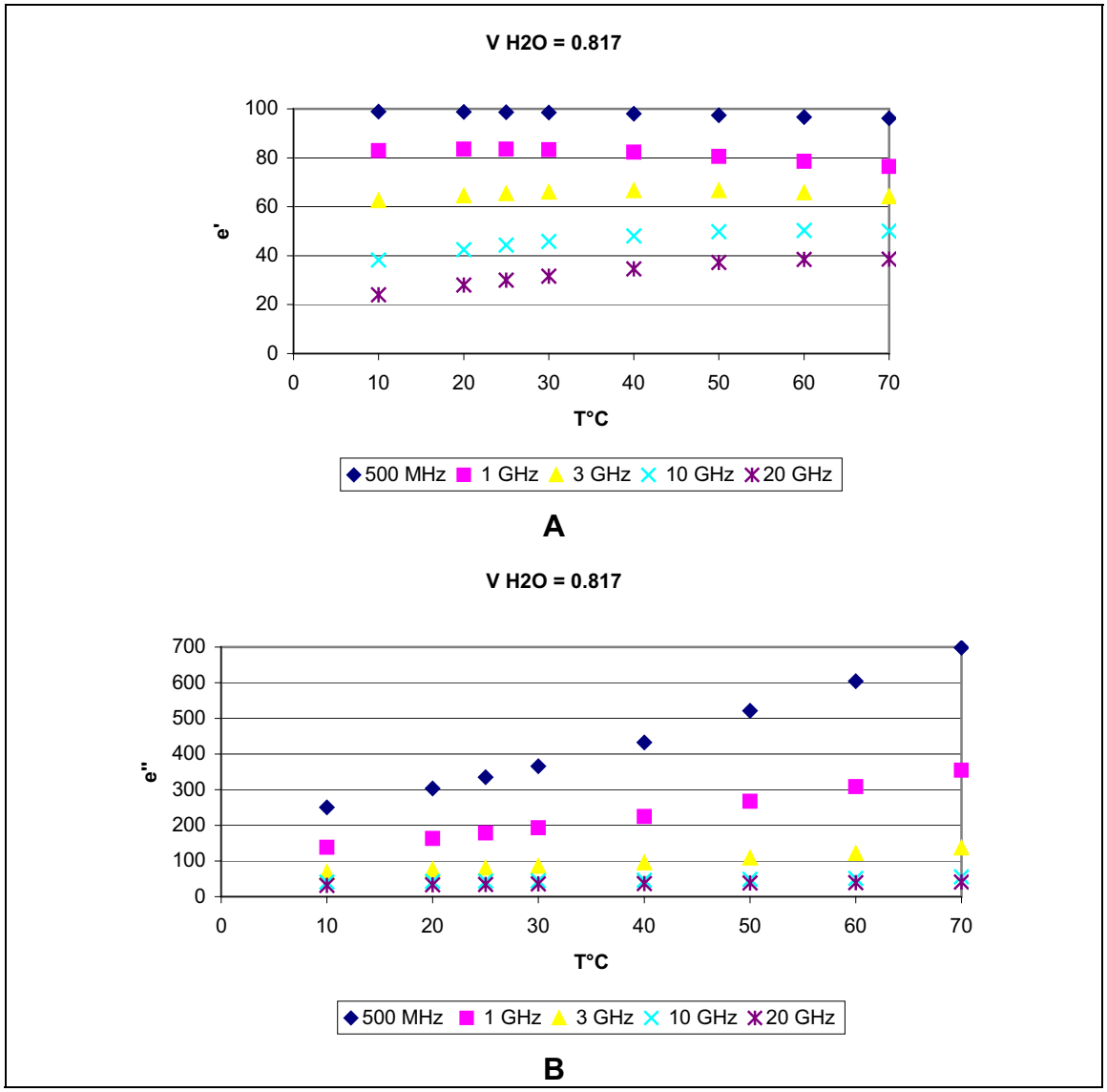

Figure 4.56. A) Real and B) Imaginary part of complex permittivity versus temperature for V_{H2O} =0.817 measured at different frequencies.

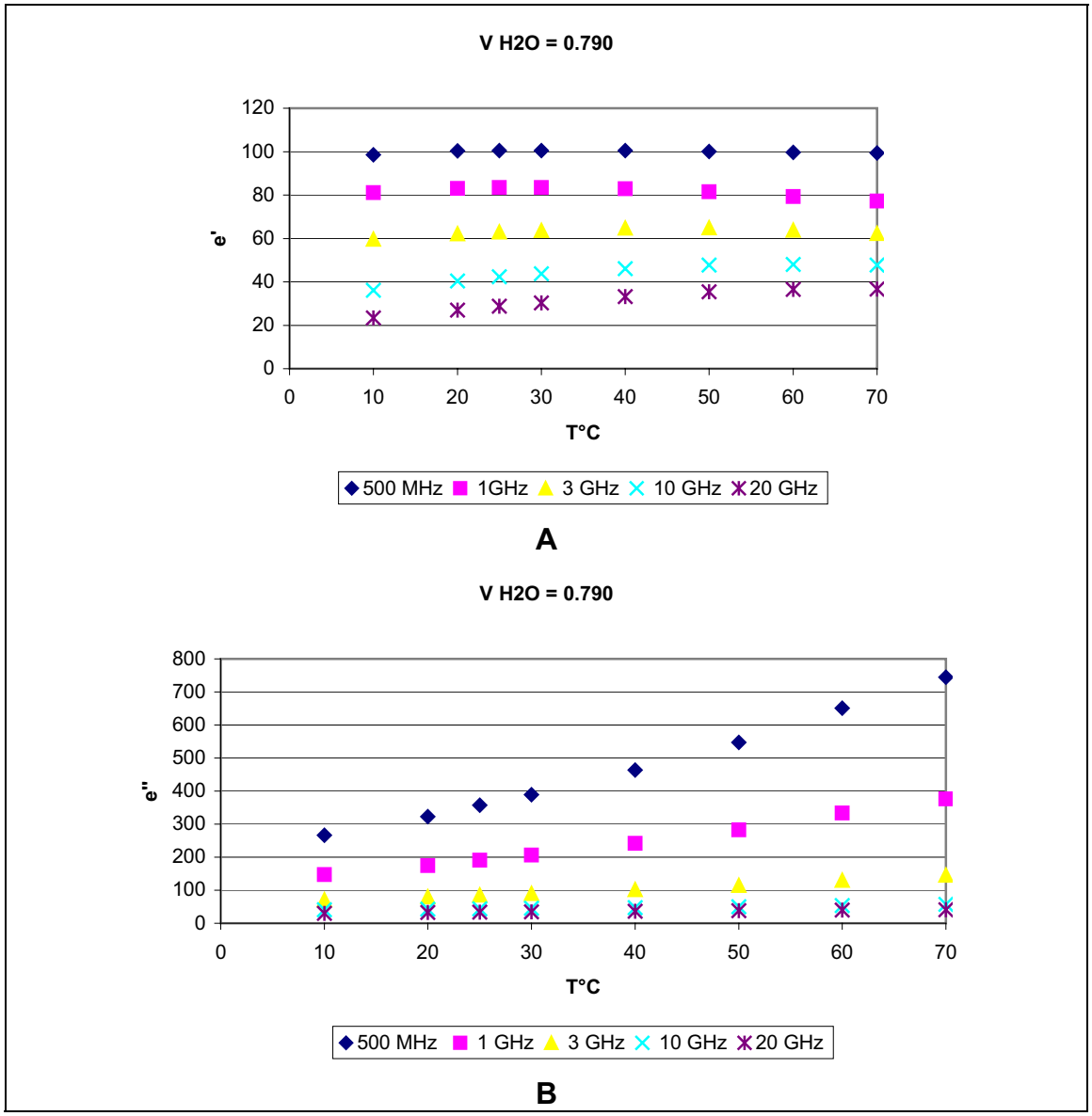

Figure 4.57. A) Real and B) Imaginary part of complex permittivity versus temperature for V_{H2O} =0.790 measured at different frequencies.

In solutions with higher volume fraction of water, the results show that when a very small amount of salt is added, small increase on the dielectric constant were observed compare to pure water. With increasing the amount of salt this increase starts to get larger, in oder word more salt higher the dielectric properties.

This change is reverse to that of observed by Seignette salt but shows similarities with KDP results. It could be said, when the volume fraction of water was increased the dielectric constant decreased.

This also may be due to that, in diluted solutions the salt is dissolved completely, the quantity of ions in the medium are higher and the structure of salt is not preserved and it shows lower dielectric constant than those with higher amount of salt. In other hand, it could be assumed that by increase the amount of salt the probability of preformation of crystals and liquid crystals are much higher and will result in increase of electric properties.

Due to very low T_c the investigation of ferroelectric activity and the transition from ferro to paraelectric due to temperature changes was not possible, but a small change in dielectric properties was observed. For example, pure water shows the value of around 78 at room temperature (25°C) and in measured frequency of 500 MHz for the real part of complex permittivity, while by addition of salt (V_{H2O} = 0.87) this value increases to about 100.5. Although these changes may not be significant, but it certainly shows an increase in probability of crystal preformation.

4.3.2 Influence of the temperature on the dielectric properties of the ADP/water solutions

The influence of the temperature on the properties of the binary ADP -Water solutions was studied. The Figures 4.58 - 4.62 represent the complex permittivity (real and imaginary part) versus the volume fraction of water, measured at the frequencies: 500 MHz, 1 GHz, 3 GHz, 10 GHz and 20 GHz.

As it can be seen, in each measured volume fractions, the dielectric constant (real part) shows a very small change when the temperature increases. This changes are more significant at those solutions with higher V_{H2O}. At low frequencies (500 MHz, 1 GHz and 3 GHz) these values decreases slightly by

increasing temperature, where at higher frequencies (10 GHz and 20 GHz) this effect is reversed (same observation as in case of KDP solutions). This is due to increase in inner molecular movements and probably the reduction of close interaction forces.

It can be also seen that at lower frequency this plots show an exponential increase by decreasing V_{H2O}, while this effect is reversed at higher frequencies.

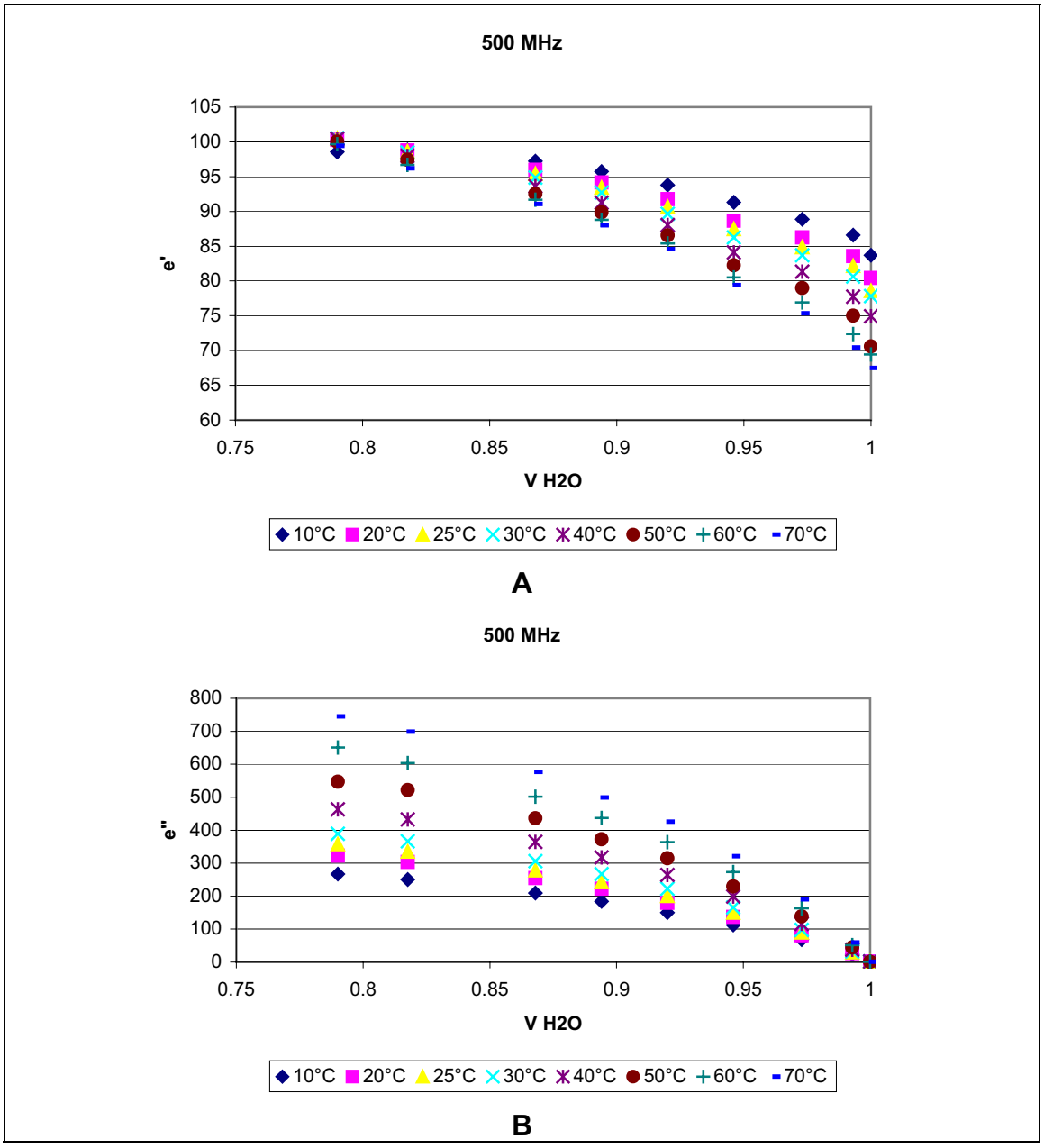

Figure 4.58. A) Real and B) Imaginary part of complex permittivity versus V_{H2O} at different temperatures at measured frequency of 500 MHz.

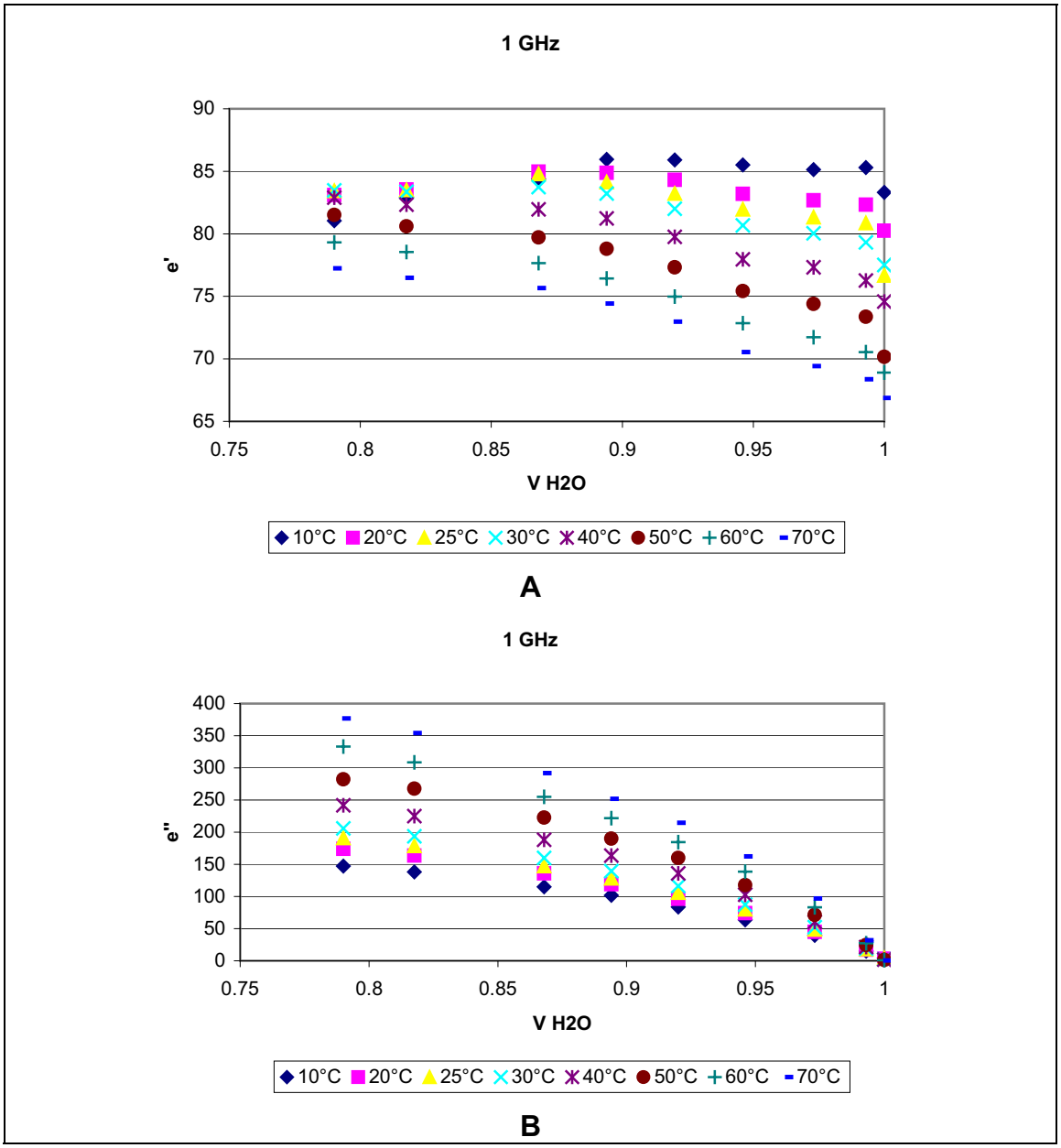

Figure 4.59. A) Real and B) Imaginary part of complex permittivity versus V_{H2O} at different temperatures at measured frequency of 1 GHz.

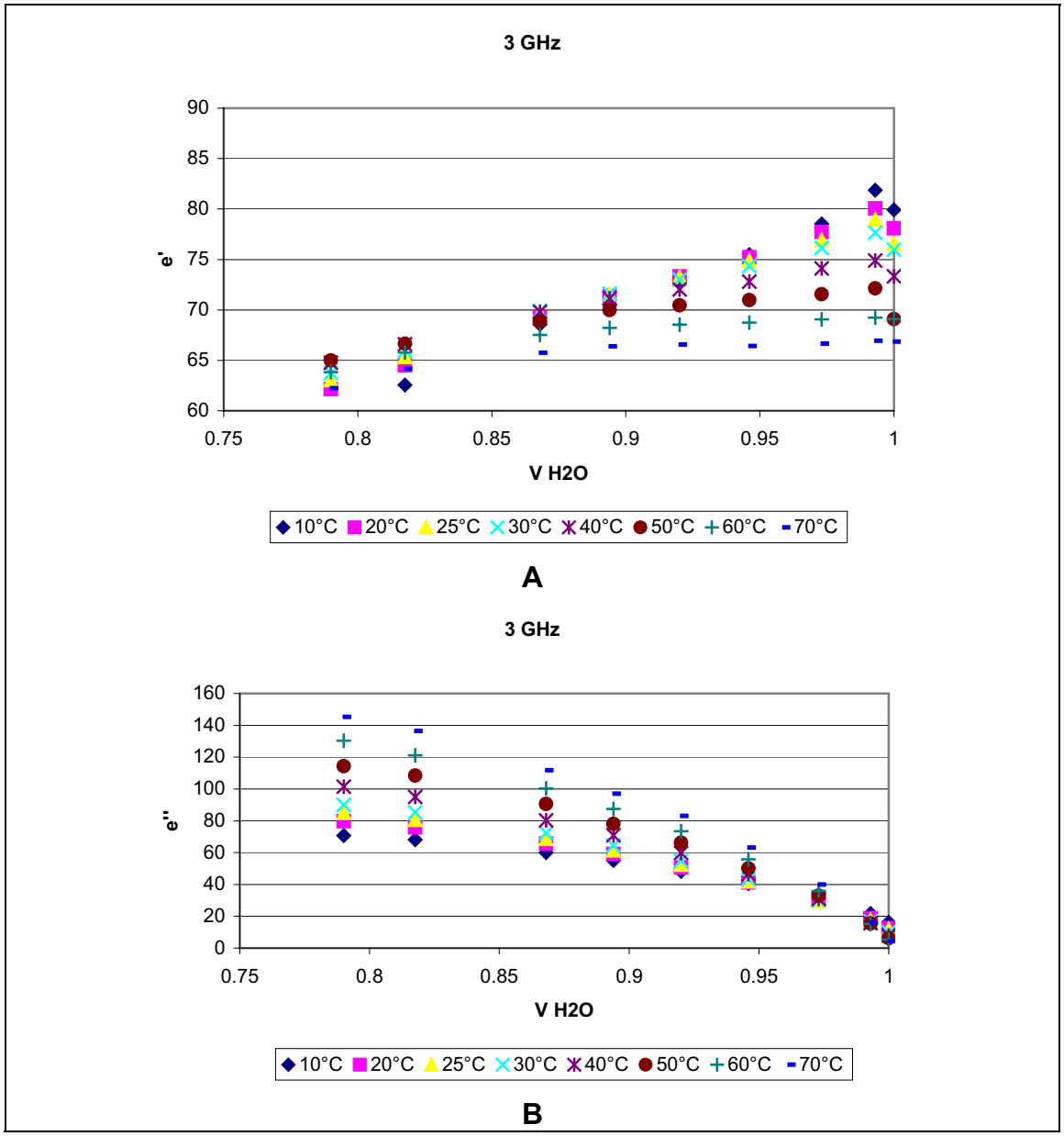

Figure 4.60. A) Real and B) Imaginary part of complex permittivity versus V_{H2O} at different temperatures at measured frequency of 3 GHz.

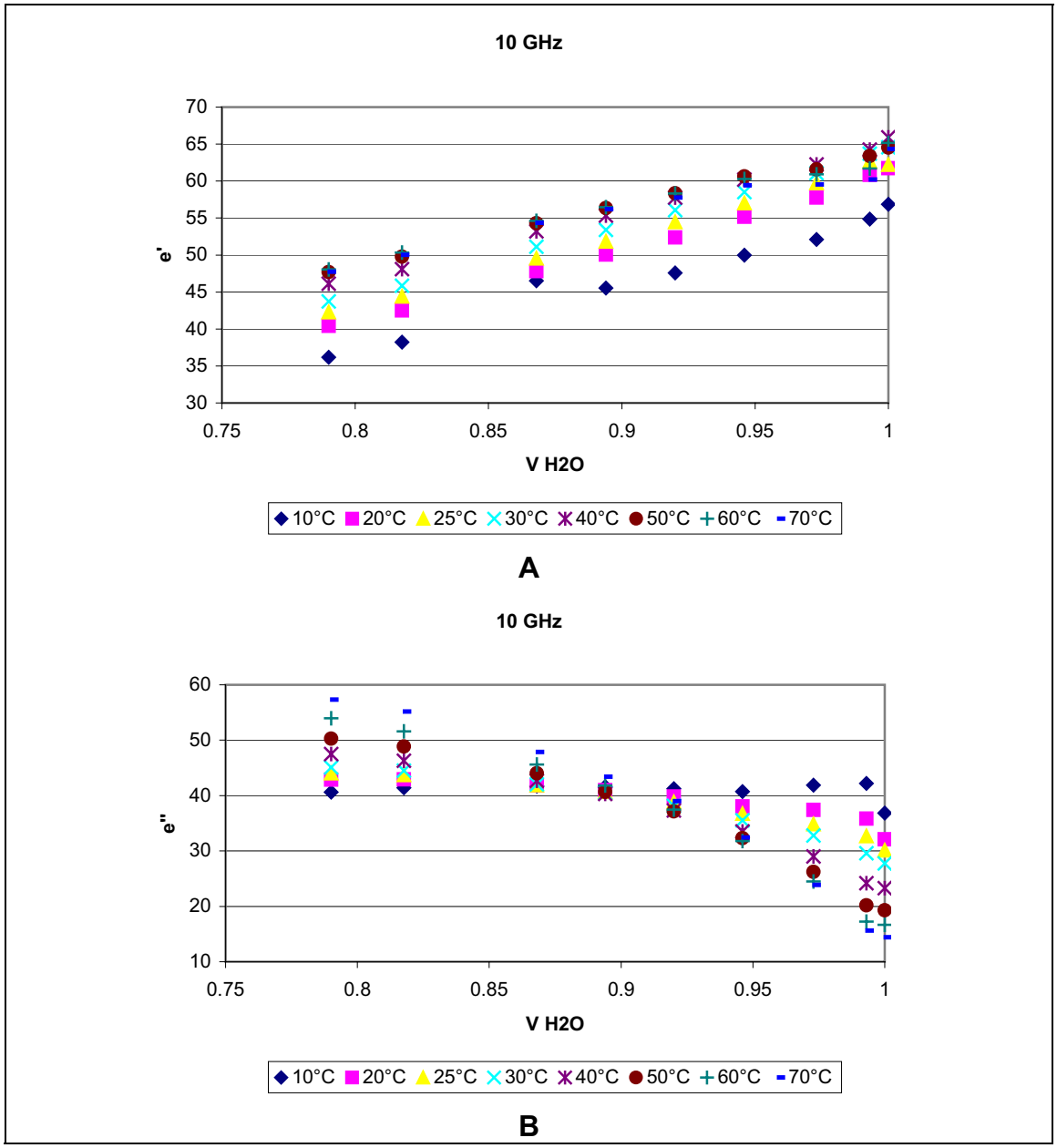

Figure 4.61. A) Real and B) Imaginary part of complex permittivity versus V_{H2O} at different temperatures at measured frequency of 10 GHz.

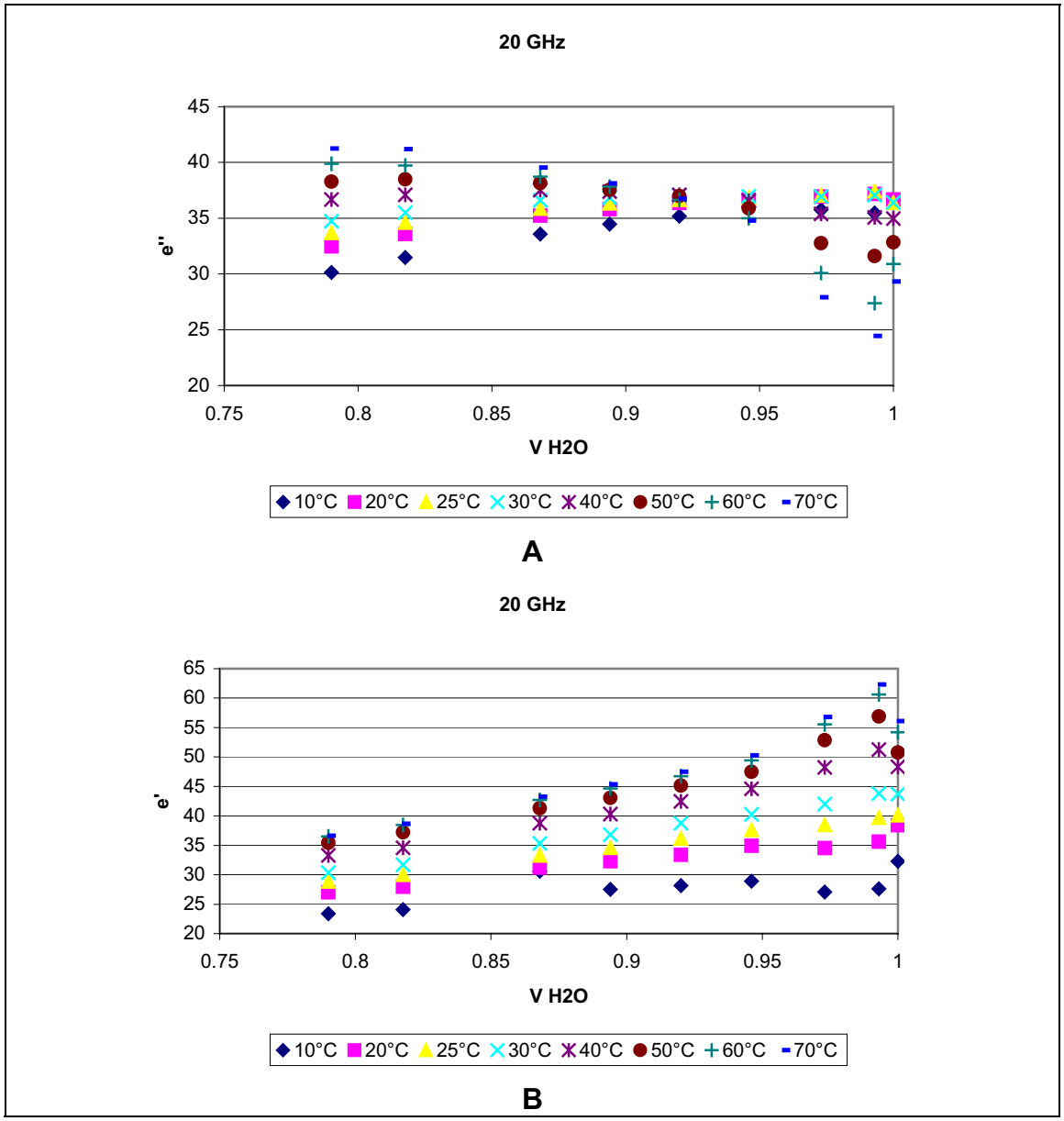

Figure 4.62. A) Real and B) Imaginary part of complex permittivity versus V_{H2O} at different temperatures at measured frequency of 20 GHz.

4.3.3 Relaxation behavior of ADP/water solutions

As it has been said before, The Debye relaxation equation (see Section A, 2.3.3 – 2.3.6.1) is based on the assumption of a molecule in the gas form or highly diluted in a nonpolar liquid *(Chelkowski, 1980)*.

All the investigated polar liquids were examined with regards to the outlined hypotheses mentioned in 4.1.5.

For calculation of relaxation time the 1-Debye equation was chosen due to the simplicity of the model and low number of free parameters (see Section A, 3.2.6.2).

Figure 4.63 shows the relaxation time versus temperature at different volume fractions.

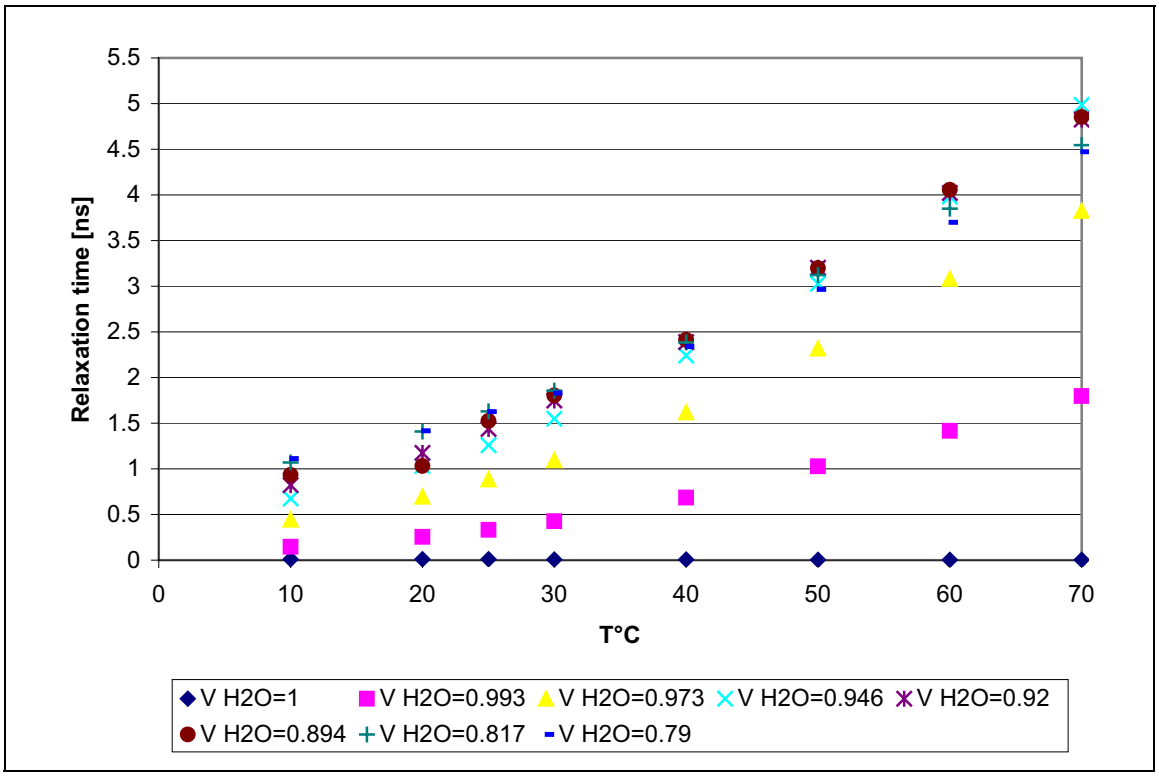

Figure 4.63. Relaxation times versus temperature at different volume fractions.

As it can be seen above, the relaxation times increase by increasing the amount of ADP in the binary solutions. An increase in relaxation time by increasing the temperature has been also observed.

These increased get smaller as the $V_{H2O} < 0.946$. This might be due to increase of pre-formed crystalline structure in the mixture.

Table 4.9 shows the results obtained using 1-Debye model for different V_{H2O} at different temperatures.

	τ [ns]							
V H20	**10°C**	**20°C**	**25°C**	**30°C**	**40°C**	**50°C**	**60°C**	**70°C**
1	0.012	0.009	0.009	0.007	0.006	0.005	0.004	0.004
0.993	0.148	0.255	0.331	0.427	0.686	1.028	1.417	1.797
0.971	0.443	0.697	0.884	1.094	1.618	2.317	3.08	3.826
0.946	0.676	1.03	1.258	1.548	2.24	3.027	3.982	4.987
0.920	0.821	1.175	1.437	1.747	2.389	3.202	4.02	4.824
0.894	0.933	1.0302	1.525	1.804	2.413	3.2	4.057	4.854
0.868	0.989	1.369	1.588	1.857	2.484	3.273	4.042	4.858
0.817	1.071	1.41	1.631	1.856	2.383	3.124	3.849	4.544
0.790	1.112	1.415	1.627	1.83	2.34	2.965	3.699	4.471

Table 4.9. Relaxation times [ns] obtained for different V_{H2O} at different temperatures.

When the relaxation times are plotted against V_{H2O}, unlike KDP no exact maximum for all volume fraction were observed, but a single percolation threshold around V_{H2O}= 0.95 and V_{H2O}= 0.91 was shown.

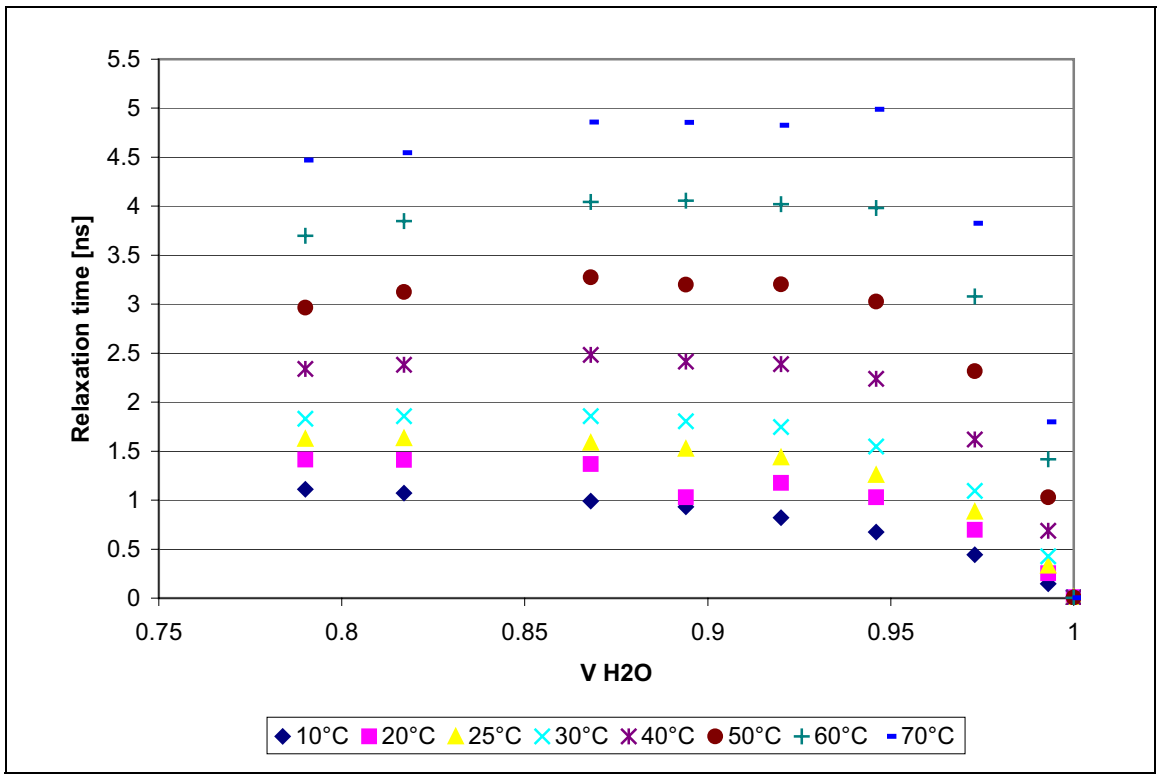

Figure 4.64. Relaxation times versus V_{H2O} at different temperatures.

To show the reliability of the method the R^2 values are plotted against volume fraction at different temperatures and visa-versa. Results are shown in table 4.10 and the plots in figures 4.65 and 4.66.

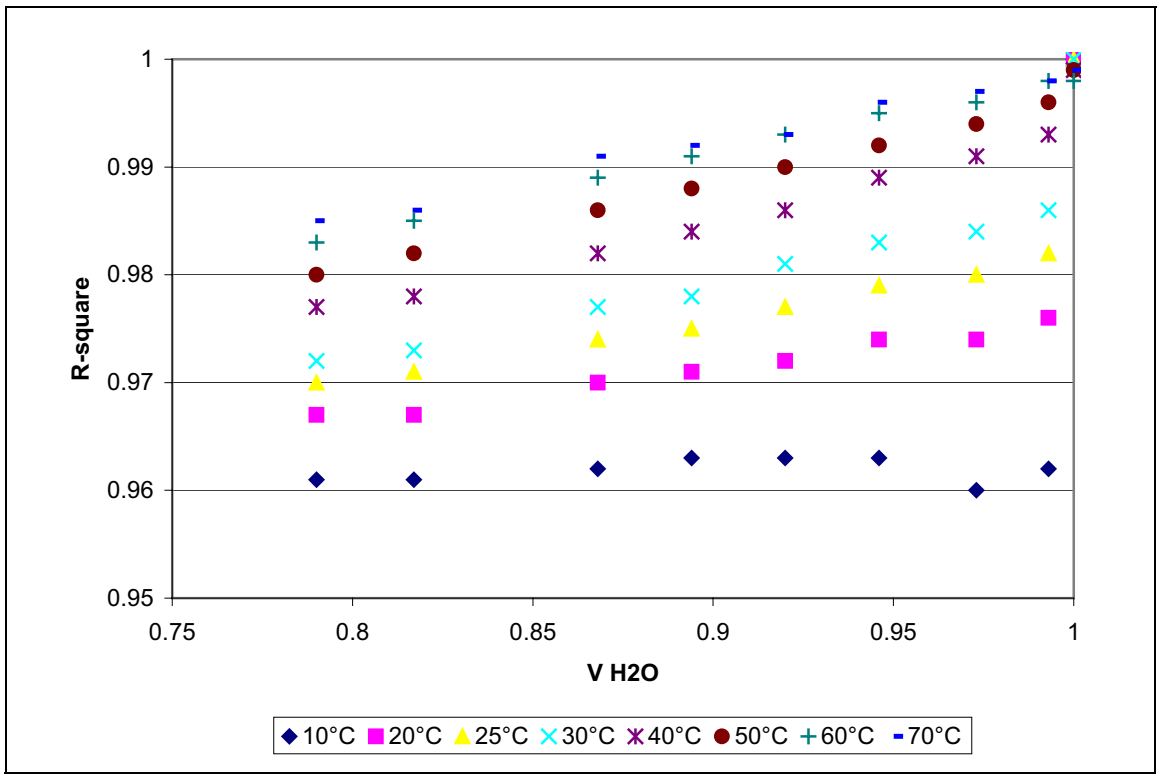

Figure 4.65. Correlation coefficient (R^2) versus V_{H2O}.

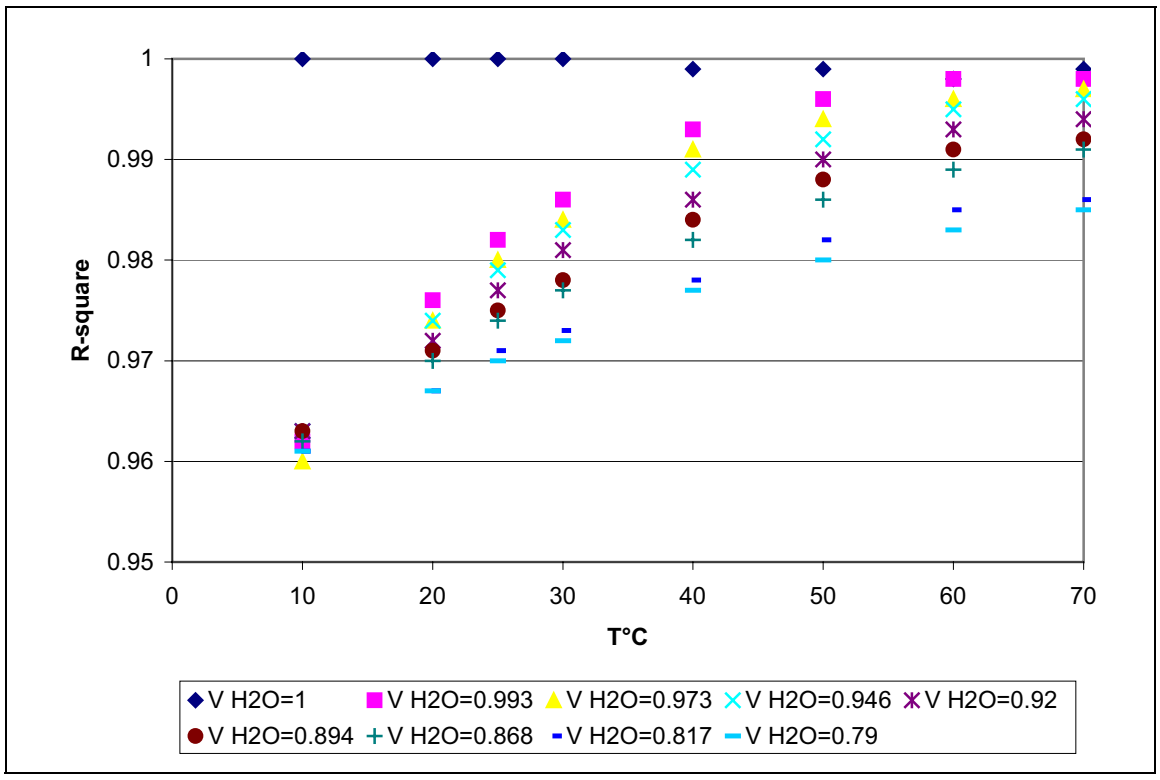

Figure 4.66. Correlation coefficient (R^2) versus temperature °C.

	R^2								
T°C	V_{H2O}= 1.00	V_{H2O}= 0.993	V_{H2O}= 0.973	V_{H2O}= 0.946	V_{H2O}= 0.920	V_{H2O}= 0.894	V_{H2O}= 0.0.868	V_{H2O}= 0.817	V_{H2O}= 0.790
10	1	0.962	0.96	0.963	0.963	0.963	0.962	0.961	0.961
20	1	0.976	0.974	0.974	0.972	0.971	0.97	0.967	0.967
25	1	0.982	0.98	0.979	0.977	0.975	0.974	0.971	0.97
30	1	0.986	0.984	0.983	0.981	0.978	0.977	0.973	0.972
40	0.999	0.993	0.991	0.989	0.986	0.984	0.982	0.978	0.977
50	0.999	0.996	0.994	0.992	0.99	0.988	0.986	0.982	0.98
60	0.998	0.998	0.996	0.995	0.993	0.991	0.989	0.985	0.983
70	0.999	0.998	0.997	0.996	0.994	0.992	0.991	0.986	0.985

Table 4.10. Correlation coefficient (R^2) obtained for different V_{H2O} at different temperature.

4.3.4 Discussion

As we mentioned in 4.1.6 of this Section, Another application of Dielectric Spectroscopy is the study of ferroelectric properties of substances. In this case the ferroelectric properties of ADP salt were investigated. The behavior of its binary mixtures with water as a function of increasing temperature was investigated using the high frequency network analyzer.

The results demonstrate that the specific ferroelectric properties of these mixtures could not be observed in measured temperatures between 10 and 70 at frequencies between 500 MHz and 20 GHz. In other words, it could not be possible to observe the change from ferro to paraelectric typical for a single solid crystal as a result of difference in their “order” of the matter.

It definitely shows that in solution, the ADP salt has a different “order” than in a solid crystal. Thus ADP salt is not influencing the binary mixtures, meaning, the dominant factor is that of water.

The absence of a “ferroelectric” behavior in binary solutions could be also due to an “anti-ferroelectric” arrangement of the polarized particles of the ADP or the

polarized water clusters islands with dissolved ADP salt in a continuous phase. As it has been said in theory part, the ferroelecrtic activity in a single crystal depends very much on the axis of the crystal on which the excitation (mechanical or electrical) happens. In liquid crystals or in preformed crystalline structure this axis does not exist yet and this may result in absence of “ferroelectric” behavior.

The finding that water can be described using the Debye relaxation equation is well documented *(e.g. Böttcher et al. 1978; c; Kaatze, 1989)*. This result is surprising, because the Debye relaxation theory had been developed for the gaseous form or for solutions highly diluted in nonpolar liquids, where hardly any intermolecular interactions occur.

The single Debye equation is also able to characterize the whole range of ADP salt-water mixtures at all temperatures with average $R^2 \geq 0.983$ and a percolation threshold around $V_{H2O}= 0.95$ and $V_{H2O}= 0.91$ was observed.

It may be of interest to study other polar substances, which are well soluble in water in order to see whether a “crystalline preformation” in solution exists, close to the saturation concentration and/or as un supersaturated condition, which influences the final crystalline structure after precipitation. This could be of special interest for drugs showing a polymorphic crystalline behavior as mentioned before.

4.4 Conclusions

Dielectric Spectroscopy is a good technique to investigate physical properties of materials as well as their structural behavior, because of its accuracy and reproducibility.

It shows definitely that in solution the Seignette salt, KDP and ADP have a different “order” than in a single solid crystal. Thus these salts are not

influencing the binary or ternary mixtures. In other words the dominant factors are that of Water.

The absence of a “ferroelectric” behavior in solution could be also due to an “anti-ferroelectric” arrangement of the polarized particles of the powder or the polarized water clusters islands with dissolved salt in a continuous phase of a polar 1,4-Dioxane or water. As it has been said in theory part, the ferroelecrtic activity in a single crystal depends very much on the axis of the crystal on which the excitation (mechanical or electrical) happens. In liquid crystals or in preformed crystalline structure this axis does not exist yet and this may result in absence of “ferroelectric” behavior.

The single Debye equation is also able to characterize the whole range of salt-water binary mixtures at all temperatures with average $R^2 \geq 0.95$ showing with respect to the relaxation time (τ), a percolation threshold in all temperatures at $V_{H2O}= 0.931$ for KDP, around $V_{H2O}= 0.77$ and $V_{H2O}= 0.83$ for Seignette salt and around $V_{H2O}= 0.95$ and $V_{H2O}= 0.91$ in case of ADP.

It may be of interest to study other polar substances, which are well soluble in water in order to see whether a “crystalline preformation” in solution exists, close to the saturation concentration and/or as un supersaturated condition, which influences the final crystalline structure after precipitation (determining the formation of different polymorphic form of a substance). This could be of special interest for drugs showing a polymorphic crystalline behavior.

References

Bacon, G. E. The First Studies of KH_2PO_4 By Neutron Diffraction. Ferroelectrics, 1987, Vol. 71, pp. 77-87.

Beresnev, L.A., Pikin, S.A., Hasse, W. Ferroelectric polymers. Condensed Matter News, Vol. 1, NO. 8, 1992.

Blinc, R. Solid and Liquid Crystalline, Ferroelectrics and Antiferroelectrrics. Condensed Matter News, Vol. 1, NO. 1, 1991.

Bornarel, J. Domains in KH_2PO_4. Ferroelectrics, 1987, Vol. 71, pp. 255-268.

Busch, G. Early History Of Ferroelectricity. Ferroelectrics, 1987, Vol. 74, pp.267-284.

Busch, G. A New Seignette-Electrics. Ferroelectrics, 1987, Vol. 71, pp. 17-24.

Endo. S., Deguchi, K., Tokunaga, M., 2002. Vanishing of T_c and appearance of quantum paraelectricity in KD_2PO_4 and KH_2PO_4 under high pressure. J. Phys.: Condens. Matter 14 (2002) 11275-11283.

Fukami, T., 1993. Phase Transition of the Aqueous Solution of the Rochelle Salt. IL NUOVO CIMENTO, Vol. 15D, N.5, 771-773.

Hans von R., Jaffer, 1936. Polymorphism of Rochelle salt. Physical Review, Vol. 51, 43-47.

Lang, S. B. Piezoelectric and Pyroelectric Effects in the KDP-Family. Ferroelectrics, 1987, Vol. 71, pp. 225-245.

Lagerwall, S. T. Ferroelectric and Antiferroelectric Liquid Crystals. ISBN 3-527-29831-2, 1999.

Mielke, A., Timofte, A.M., 2005. Modelling and Analytical Study For Ferroelectric Material. 2nd ECCOMAS Thematic Conference on Smart Structures and Materials, Lisbon, Portugal, July 2005.

R.H. Chen., Chen-Chieh Yen., C. S. Shern., Fukami, T., 2005. Studies of high-temperature phase transition, electrical conductivity, and dielectric relaxation in $(NH_4)H_2PO_4$. Journal of Applied Physics 98, 044104 (2005).

Sandy, F., Jones, V., 1968. Dielectric Relaxation of Rochelle Salt. Physical Review, Vol. 168, Number 2, 481-493.

Slater, J. C. Theory of the Transition in KH_2PO_4. Ferroelectrics, 1987, Vol. 71, pp. 25-42.

Steulmann, G. The Dielectric Constant of Some Potassium Salts and Alkali Halides. Ferroelectrics, 1987, Vol. 71, pp. 11-13.

Valasek, J., 1920. Piezo-Electric and Allied Phenomena in Rochelle Salt. Presented at the meeting of the American Physical Society in Washington DC.

Valasek, J.,1922. Properties of Rochelle Salt Related to the Piezo-Electric Effect. Phys. Rev., XIX., 478, 639-664, 1922.

** Please note that, all the references in part A were also used in Part B.*

Part C:

Paraffin-based derivatives

EFFECT OF PEG NUMBER ON DIELECTRIC PROPERTIES OF PARAFFIN BASE-PEG POLYMERS AT MICROWAVE FREQUENCIES

Yoko Yamada Pittini[(1)], Dana Daneshvari[(2)], Susanne Leparoux[(1)], Sébastian Vaucher[(1)], Axel Ritter[(3)], Lukas Rohr[(1)], Hans Leuenberger[(4)]

[(1)] Swiss Federal Institute for Materials Research and Testing, EMPA, Feuerwerkerstrasse 39, CH-3602 Thun, Switzerland
[(2)] Institute of Pharmaceutical Technology, Pharmacenter University of Basel, Klingelbergstrasse 50, CH-4056 Basel, Switzerland
[(3)] Swiss Federal Institute for Materials Research and Testing, EMPA, Lerchenfeldstrasse 5, CH-9014 St. Gallen, Switzerland
[(4)] Institute of Pharmaceutical Technology, Pharmacenter University of Basel, Klingelbergstrasse 50, CH-4056 Basel, Switzerland /
Institute for Innovation in Industrial Pharmacy, CH-4148 Pfeffingen , Switzerland

ABSTRACT. Dielectric constant studies of paraffin base PEG (Poly ethylene glycol) polymers were carried out at temperatures above the melting point. The measured frequency region was situated between 0.4 and 20 GHz. The chemical structure of the polymers is expressed as $H(CH_2)_n$–$(OCH_2CH_2)_mOH$. The number of PEG units, *m*, was varied from 0 to 80 to investigate the effect of the PEG chain length on the dielectric properties of the whole polymer. With the existence of a dipole moment on PEG but not on pure paraffin, the dielectric constants become larger with increasing chain length of PEG. PEG 3000 showed the highest dielectric constant in the measured frequency range. The effect of PEG chain length can be explained well by introducing the fraction of molecular weight of PEG divided by the molecular weight of the whole polymer (we call this fraction 'Mw fraction of PEG'.). Both, real and imaginary part of the dielectric permittivity exhibit a cubic dependence of the molecular weight fraction, and the loss tangent exhibits a linear dependence. These relationships make it possible to predict the dependency of the microwave heating of the polymer on the PEG chain length, carbon chain length and microwave frequency.

INTRODUCTION

Microwave technology has been widely used to accelerate chemical reactions [1-3]. In contrast to conventional heating, microwave assisted or hybrid heating yields a rapid heating and direct heating of the selected components of materials [4, 5]. Microwave active polymers accomplish heating and pyrolysis processes with high-energy efficiency and contributes making progress the process for industrial usage.

PEG is also a microwave active polymer because of the existence of a dipole moment in its molecular structure. Several attempts to study the configuration of PEG and PEO (Poly ethylene oxide) have been made by measuring the dielectric permittivity [6-11]. PEG and PEO are also known as nonionic surfactants by chemically bonding with hydrophobic molecules like hydrocarbon. The PEG bonded hydrocarbon is an attractive polymer for industrial applications that, after been used as a surfactant, this polymer is expected to be removed easily and rapidly by applying microwave.

In the present investigation, we focus on the microwave activity of the PEG bonded hydrocarbon. Paraffin with carbon length of 18 and 22 were chosen because it can be extracted from naturally existing resources and is generally employed for ordinary use. Hydrogen bonded at the end of the carbon chain was substituted by PEG chains to

produce paraffin based PEG polymers. The dielectric permittivity of these polymers was measured with different PEG chain length. The effect of PEG chain length on the dielectric permittivity of the whole compounds was analyzed by introducing the fraction of molecular weight of PEG part divided by molecular weight of whole polymer (Mw fraction of PEG). This Mw fraction of PEG gives better relationship with polymer's dielectric permittivity than the value of PEG chain length number. Furthermore, by analyzing the dielectric behaviors using linear-fit technique, we succeeded to predict the contribution of the PEG chain length to the polymer's loss tangent.

EXPERIMENTAL METHOD

Materials

Paraffin base-PEG polymers ($H(CH_2)_n$–$(OCH_2CH_2)_mOH$) were prepared by Zschimmer & Schwarz GmbH & Co. KG in Germany (n=18 or n=22). The PEG chain length, m, was varied between 1 and 80. Their chemical structures, molecular weight and melting point are shown in Table 1. The melting point was determined by DSC measurement (Mettler Toledo DSC 822e). For this measurement, the temperature was changed from 243 K to 573 K with the temperature increment of 10 K/min.

Pure paraffin was supplied by Schweizerhall Chemie, Basel, Switzerland. Average carbon length, n, is 29. The PEG 3000 ($HO\text{-}(CH_2CH_2O)_m\text{-}H$, average molecular weight: 2700-3000, density: 1.1-1.2 g/cm^3) is obtained from Clariant GmbH, Division Tenside, Musterlager Werk Gendorf as Polyglykol 3000 Schuppen.

Table 1. Chemical structure, symbolic expression, molecular weight and melting point of paraffin base PEG polymers, pure paraffin and PEG 3000.

PEG number	Chemical structure	Symbolic expression	Molecular weight	Melting point
0	C_nH_{2n+2}	(paraffin)	413	220 K
1	$H(CH_2)_{22}$–(OCH_2CH_2) OH	$C_{22}E_1$	371	336 K
2	$H(CH_2)_{22}$–$(OCH_2CH_2)_2OH$	$C_{22}E_2$	359	333 K
3	$H(CH_2)_{18}$–$(OCH_2CH_2)_3OH$	$C_{18}E_3$	415	315 K
8	$H(CH_2)_{22}$–$(OCH_2CH_2)_8OH$	$C_{22}E_8$	679	323 K
10	$H(CH_2)_{18}$–$(OCH_2CH_2)_{10}OH$	$C_{18}E_{10}$	711	313 K
40	$H(CH_2)_{18}$–$(OCH_2CH_2)_{40}OH$	$C_{18}E_{40}$	2033	325 K
80	$H(CH_2)_{18}$–$(OCH_2CH_2)_{80}OH$	$C_{18}E_{80}$	3795	334 K
∞	$H(OCH_2CH_2)_mOH$	(PEG3000)	2700-3300	321 – 327 K

Dielectric Measurements

The complex permittivity was measured using Vector Network analyzer (Agilent Technologies Inc. USA-Palo Alto CA 94304-1185, HP 8720D 50 MHz – 20 GHz) with the connecting cable of High Temperature 20 GHz, Type-N female 1250-1743, 2.4 mm male 11901D, and the "High temperature probe kit 8570E Agilent technologies Inc." The real and imaginary parts of complex permittivity were obtained by the software program HP 85070 of Agilent Technologies Inc., also used for the measurments of the dielectric permittivity.

The measurement vessel was a double-layer Pyrex-Glass with internal diameter 25 mm and height of 25 mm, and the external diameter of 50 mm and height of 50 mm. Between these layers, temperature controlled water flowed. The water entered from the

upper aperture of the vessel and exited from the lower one. In this way, we obtained the best circulation around the sample. This vessel was designed in the Institute of Pharmaceutical Technology, University of Basel, Switzerland and was manufactured by Glastechnik-Rahm (Muttenz/BL, CH-4132, Switzerland).

The samples were brought to the required temperature using a Thermostat / circulating water bath (B. Braun Biotech International GmbH D-34209 Melsungen, Thermomiux UB; 852 042/9; 90120498, Frigomix U-1; 852 042/0; 8836 004) with the temperature control accuracy of $\pm$0.1 K. The temperature of the sample and the probe were measured using Infrared thermometer (Fluke 66 Ir Thermometer) with the accuracy of $\pm$0.1 K.

Sufficient amounts of material were placed into the measuring vessel and were brought to the required temperature using circulating water bath. The temperature were increased and/or decreased with thermostat of the circulating water bath. The measurement was carried out by first melting the sample, inserting the calibrated probe, increasing the temperature up to 343 K and then gradually decreasing it. The dielectric permittivities were measured at the required temperatures during this process.

RESULTS

Dielectric permittivity

Figure 1 shows the experimental results of (a) real part, ε', and (b) imaginary part, ε'', of complex permittivity of the paraffin base PEG polymers, PEG 3000 and pure paraffin. Pure paraffin exhibits constant value for real part of complex permittivity, $\varepsilon'_{\text{paraffin}} = 2.4$, at all measured frequencies, and the imaginary part of complex permittivity is as expected nearly zero. From these results, it is evident that pure paraffin has no polar structure. Instead, PEG 3000 has an electric dipole moment and the real part of complex permittivity, $\varepsilon'_{\text{PEG}}$, becomes maximum value about 9 at the lowest measured frequency. The peak of the imaginary part of complex permittivity, $\varepsilon''_{\text{PEG}}$, appears at 7 GHz and its value is 2.6. Paraffin base-PEG polymers have intermediate permittivity values between pure paraffin and PEG 3000. The higher the PEG numbers in the polymer, the larger both real and imaginary parts of the complex permittivity. All paraffin base-PEG polymers have one peak in the dielectric loss, and all of their peaks are located at nearly the same frequency as PEG 3000.

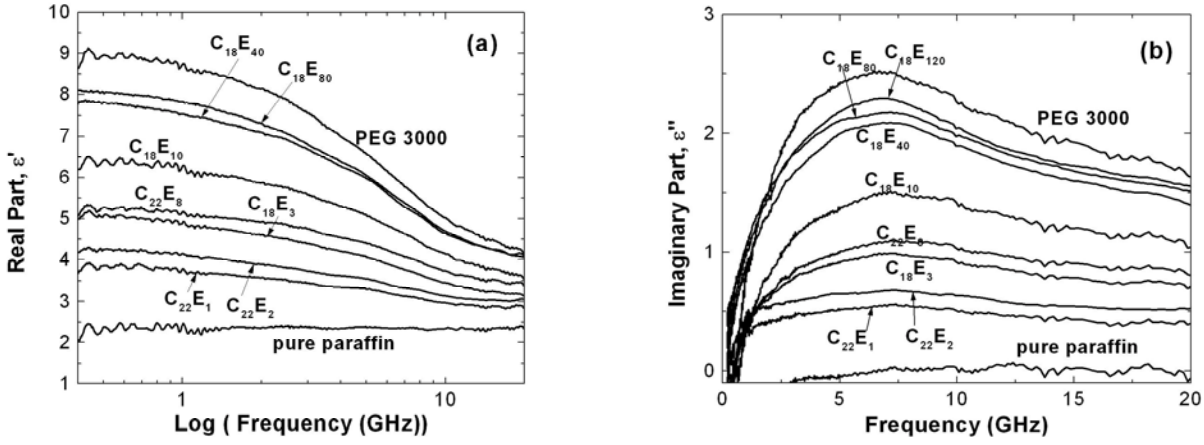

Figure 1. (a) Real and (b) imaginary part of dielectric permittivity of paraffin base PEG polymers, pure paraffin and PEG 3000.

Effect of PEG chain length

To observe the effect of the PEG chain length on the dielectric properties of the whole paraffin base-PEG polymers, we plotted these values as a function of logarithm of the PEG chain length. The real part is shown in Figure 2 (a) and the imaginary part is in Figure 2 (b). The frequency of 2.4 GHz was chosen as it is the most commonly available frequency for industrial and daily use, and the frequency of 20 GHz was chosen for comparison. Both, real and imaginary parts increase with increasing PEG chain length as also indicated in Figure 1. However, a different behavior is observed depending on the carbon chain length of 18 and 22. Compared to the group of carbon chain length 18, the group of carbon chain length 22 which has PEG chain length of 1, 2, and 8 has slightly lower values of the dielectric permittivity for both real and imaginary part. From these results we understand that the dielectric permittivity of paraffin based PEG polymers is influenced not only by the PEG chain length but also by the carbon chain length at the paraffin side.

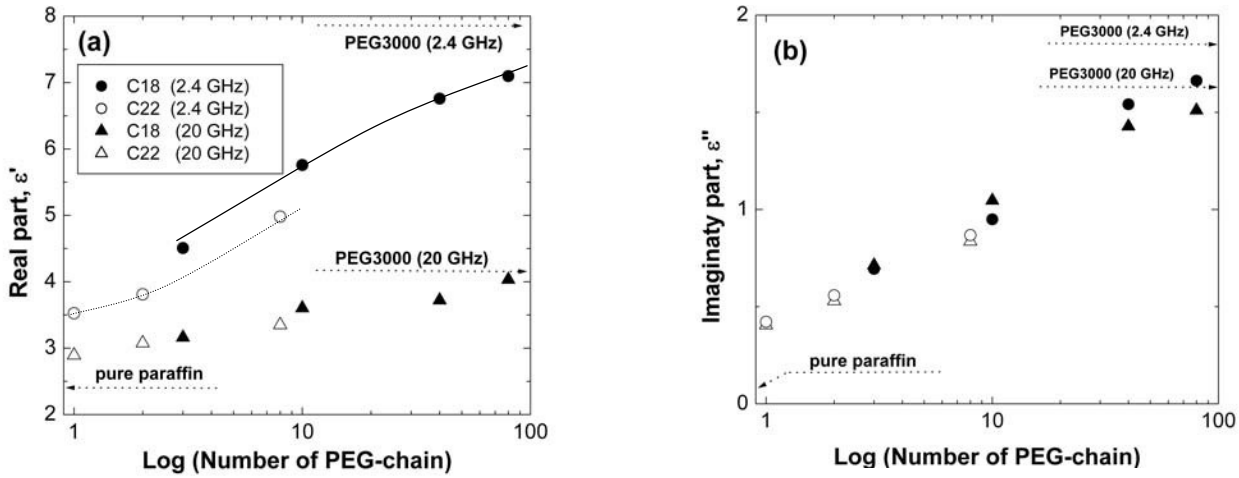

Figure 2. Real (a) and imaginary (b) part of dielectric permittivity plotted against number of PEG chain. Closed circles denote the carbon chain length 18 at 2.4 GHz, open circles denote the carbon chain length 22 at 2.4 GHz, closed triangles denote the carbon chain length 18 at 20 GHz and open triangles denote the carbon chain length 22 at 20 GHz. ε' and ε'' of pure paraffin (same value at both frequencies at 2.4 GHz and 20 GHz) and PEG 3000 at 2.4 GHz and 20 GHz are also shown in the figure.

DISCUSSION

Molecular weight fraction of PEG

To discuss how the dielectric permittivity of whole paraffin based PEG polymer is affected by the carbon chain length and/or PEG chain length, we introduced the fraction of molecular weight of PEG part divided by the molecular weight of the whole polymer (Mw fraction of PEG) in this paper as follows:

$$\text{Mw fraction of PEG} = \frac{Mw_{\text{PEG}}}{Mw_{\text{PEG}} + Mw_{\text{Paraffin}}} \quad (1)$$

where Mw_{PEG} is a molecular weight of PEG part and Mw_{Paraffin} is the paraffin part of the

whole paraffin-base PEG polymer. Mw fraction of PEG = 0 indicates pure paraffin and 1 indicates pure PEG. Though molecular weight of paraffin part with carbon chain length 18 and 22 become 254 ($C_{18}H_{37}$-) and 310 ($C_{22}H_{45}$-), respectively, the molecular weight fraction of the polymers used here can be calculated as shown in Table 2.

Table 2. Molecular weight fraction of paraffin-base PEG polymers

Material	PEG part		Mw fraction of PEG
	Molecular weight	Chemical structure	
Paraffin	413		0
$C_{22}E_1$	61	$-(OCH_2CH_2)_1-OH$	0.165
$C_{22}E_2$	105	$-(OCH_2CH_2)_2-OH$	0.253
$C_{18}E_3$	149	$-(OCH_2CH_2)_3-OH$	0.370
$C_{22}E_8$	369	$-(OCH_2CH_2)_8-OH$	0.544
$C_{18}E_{10}$	458	$-(OCH_2CH_2)_{10}-OH$	0.643
$C_{18}E_{40}$	1779	$-(OCH_2CH_2)_{40}-OH$	0.875
$C_{18}E_{80}$	3542	$-(OCH_2CH_2)_{80}-OH$	0.933
PEG 3000	2700-3000		1

The Mw fraction of PEG represents the molecular weight contribution of PEG in the whole polymer. This value is nearly independent on the carbon chain length of the paraffin (here 18 or 22).

The relationship between the Mw fraction of PEG and the dielectric permittivities is plotted in Figure 3. The frequencies are chosen at 2.4 GHz and 20 GHz. The carbon chain length of 18 is shown by solid symbles and that of 22 by open symboles. The data of pure paraffin and PEG 3000 are also shown on these figures by solid symboles. As is seen from these figures, the plots of the permittivity for different carbon chain lengths (18 and 22) at the same frequency (in particular Fig. 3.(a) at 2.4 GHz) are closer to a single line than the plots in Figure 2. This phenomenon indicates that the dielectric permittivity of paraffin-base PEG ploymers depends more on the molecular weight fraction of PEG than on the carbon chain length. The molecular weight fraction of the dipole moment affects the total dielectric permittivity of the polymer.

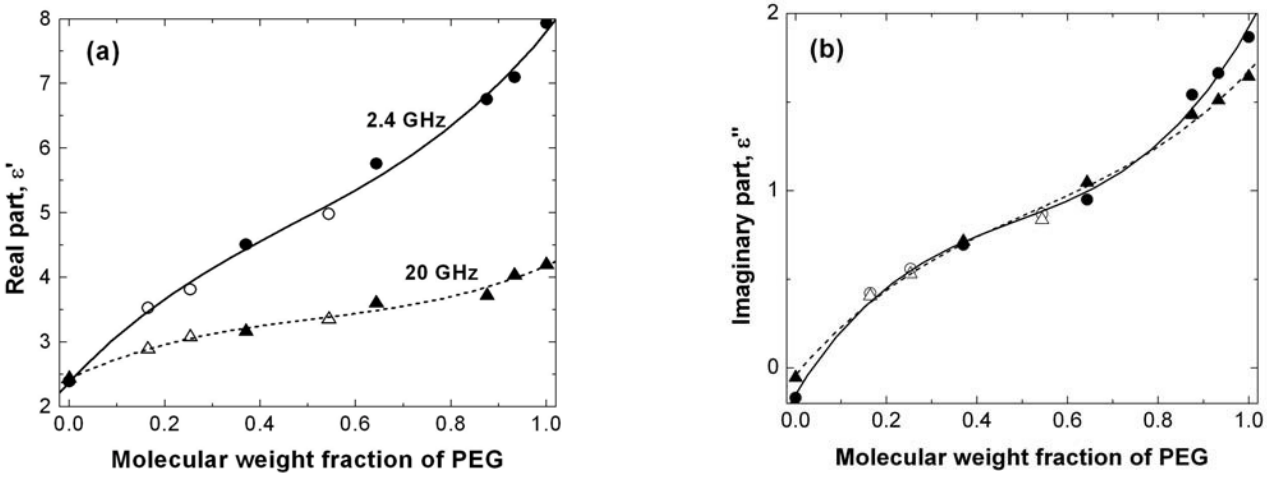

Figure 3. Real (a) and imaginary (b) part of the dielectric permittivity plotted against the molecular weight fraction of PEG. Closed circles denote the carbon chain length 18 at 2.4 GHz, open circles denote the carbon chain length 22 at 2.4

GHz, closed triangles denote the carbon chain length 18 at 20 GHz and open triangles denote the carbon chain length 22 at 20 GHz. Solid lines indicate the cubic polynomial curve fit result for frequency of 2.4 GHz, and the dashed line indicates the fit at 20 GHz.

For a more detailed investigation of these plots, we performed polynomial curve-fitting for both, real and imaginary part at frequencies of 2.4 GHz and 20 GHz. The data of pure paraffin and PEG 3000 are also included for the curve-fit. All these four curves exhibit cubic dependence agatinst Mw fraction. The curve-fitted results of 2.4 GHz and 20GHz are respectively shown by solid and dashed lines in Figure 3. The r-square became more than 0.99 for all curve-fitting results. This indicates a good fit with a cubic polynomial.

Loss tangent and PEG chain length

Loss tangent can express by using real and imaginary part of dielectric permittivity as $\tan\delta = \varepsilon''/\varepsilon'$. This means dielectric energy absorption. Polymers with larger loss tangent absorb more electro-magnetic energy and can efficiently heat up and/or induce pyrolysis. Using the experimental data of real and imaginary part of dielectric permittivity shown in Figure 3, the loss tangent of paraffin base-PEG polymers are calculated at frequencies of 2.4 GHz and 20 GHz. The calculated results are shown in Table 3. Though the experimental data of pure Paraffin's imaginary part contains errors, the loss tangent of pure paraffin was not calculated.

Table 3. Loss tangent at frequencies 2.4 GHz and 20 GHz calculated from the experimental data of real and imaginary part of dielectric permittivity shown in Figure 3.

Mw fraction of PEG	Loss Tangent	
	2.4 GHz	20 GHz
0	--	--
0.165	0.120	0.140
0.253	0.146	0.172
0.370	0.154	0.226
0.544	0.165	0.250
0.643	0.174	0.290
0.875	0.228	0.384
0.933	0.234	0.374
1.000	0.235	0.391

Though both real and imaginary parts of dielectric permittivity of Paraffin base-PEG polymers have cubic polynomial relations to the Mw fraction of PEG, for the loss tangent, we found a linear relation with Mw fraction of PEG. The linear-fit of loss tangents for 2.4 GHz and 20 GHz was performed using Table 3, and the fitting results are expressed by the following equations;

$$(\text{Loss tangent}) = 0.101 + 0.136 \cdot (\text{Mw fraction of PEG}) \quad \text{for 2.4 GHz} \tag{2}$$

$$(\text{Loss tangent}) = 0.096 + 0.305 \cdot (\text{Mw fraction of PEG}) \quad \text{for 20 GHz} \tag{3}$$

R-square of these linear-fit equations are 0.971 and 0.992 for 2.44 GHz and 20 GHz, respectively. This indicates a good linear relation of loss tangent and Mw fraction of PEG

at both frequencies, though the increment of loss tangent following the increment of Mw fraction of PEG is much larger for 20 GHz. The extrapolated line towards the axis of Mw fraction =1 means the loss tangent of PEG 3000. These values are 0.237 and 0.401 for 2.44 GHz and 20 GHz, and are in a good agreement with the experimental data of PEG 3000. Instead in a pure paraffin side where Mw fraction of PEG becomes 0, the extrapolated loss tangetnt at both 2.44 GHz and 20 GHz, are in the almost same value of 0.101 and 0.096. Though pure paraffin has no dipole moment in its molecular structure, it is adequate to have the same value of the loss tangent independent of the measuring frequencies. However the pure paraffin's loss tangent of 0.1 instead of 0 can be explained that the extrapolated loss tangent of pure paraffin from paraffin base-PEG polymers remains the effect of dielectric permittivity of PEG at very high frequencies. They are an effect of high enery absorption of PEG, which can occor only at very high frequenciy region. For this reason the extrapolated loss tangent of pure paraffin is different from the experimentally obtained loss tangent of pure paraffin. High-enegy absorption of PEG has to be considered in the limited high frequency dielectric constant, ε_∞, of PEG compared to the ε_∞ of pure paraffin.

Calculation of loss tangent by PEG chain length

Using the linear relationship between loss tangent and Mw fraction of PEG obtained in equations (2) and (3), the effect of PEG chain number on paraffin base-PEG polymer is calculated. This calculation is useful to predict the dielectric properties of paraffin base-PEG polymers, when the dielectric loss of paraffin base PEG polymers has to be engineered for an application (among other properties as mechanical and thermal properties). The calculation was performed for the carbon chain length 18 of paraffin.

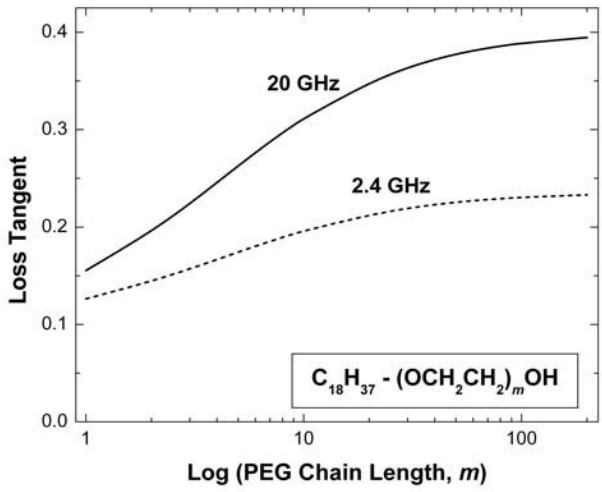

Figure 4. Calculated loss tangent of paraffin base-PEG polymers as a function of number of PEG chain length. The carbon chain length of 18 was used for the calculation

From this figure we can understand that the efficiency of increasing loss tangent i.e. the efficiency of heating and doing pyrolysis of the polymers, by increasing PEG chain length decreases when the PEG chain length becomes longer. Considering the increment of loss tangent from pure paraffin (Loss tangent = 0) to PEG 3000, in the PEG chain length of 2, the loss tangent of paraffin base-PEG polymers already reaches 50 % to the loss tangent of PEG 3000 at 20 GHz. When the PEG chain length arrives at 10 at this

frequency, the polymer's loss tangent reaches 75% of that of PEG 3000. Considering the frequency dependence of loss tangent, the effect of PEG chain is more efficient for the frequency of 20 GHz than 2.4 GHz. This efficiency is significant when the number of PEG chain length becomes longer. Moreover, by using the equation (1) together with equation (2) for 2.4 GHz and equation (3) for 20 GHz, we can predict the relationship between PEG chain length and loss tangent of whole polymer for any carbon chain length of the paraffin base-PEG polymers. These predicted curves help us to design the suitable paraffin base-PEG polymers depending on our particular requirement of the material's properties of the polymer.

CONCLUSIONS

The effect of the PEG chain length on the dielectric permittivity of paraffin base-PEG polymers was studied experimentally and analyzed in detail at frequencies of 2.4 GHz and 20 GHz. The molecular weight fraction of PEG explains well the effect of PEG chain length on the dielectric permittivity of whole polymer, and the effect of carbon chain length of the paraffinn is negligible. With increasing Mw fraction of PEG, both real and imaginary parts of dielectric permittivity exhibit a cubic dependence. The loss tangent increases linearly. Using the linear fit-line of the loss tangent we could simulate the loss tangent of the polymer and its dependency on the PEG number, also with taking into account the carbon chain length. At both frequencies, 2.4 GHz and 20GHz, the PEG chain contributes to the increment of loss tangent of the whole polymer and this increment is most efficient when the carbon chain length is short. At the PEG number of 10, the loss tangent reaches 75% of its maximum, i.e. loss tangent of PEG 3000.

REFERENCES

[1] Budarin, V.L., Clark, J.H., Tavener, S.J., Wilson, K (2004).Chemical reactions of double bonds in activated carbon: microwave and bromination methods. *Chem.Commun*., 2736-2737.

[2] Liu, H., Hu, C., Zhu, X., Hao, H., Luo, J., Zhou, J., Ouyang, S. (2004). Solid chemical reaction in microwave and millimeter-wave fields for the sysntheses of $LiMn_2O_4$ compound. *Mater. Chem. Phys.*, 88, 290-294.

[3] Babaritskiĭ, A.I., Gerasimov, E.N., Demkin, S.A., Zhivotov, V.K., Knizhnik, A.A., Potapkin, B.V., Rusanov, V.D., Ryazantsev, E.I., Smirnov, R.V., Sholin, G.V. (2003), The repetitive microwave discharge as a catalyst for a chemical reaction. *Tech. Phys.*, 45, 1411-1416.

[4] Adachi, K., Iwamura, T., Chujo, Y. (2005). Microwave assisted synthesis of organic-inorganic polymer hybrids. *Polym. Bull.*, 55, 309-315.

[5] Chevalier, S., Meyer, O., Weil, R., Fourrier-Lamer, A., Petit, A., Loupy, A., Maurel, F. (2001). New instrumentation for the comprehension of chemical reactions under microwave and classical heating with the aid of a wide frequency band dielectric spectroscopy. *Eur. Phys. J. AP*, 15, 223-229.

[6] Törmälä, P., Lättilä, H., Lindberg, J.J. (1973). Solid and liquid state relaxations in spin-labelled poly (ethylene glycol) at high temperatures ($T>T_g$). *Polymer*, 14, 481-487.

[7] Purohit, H.D., Sengwa, R.J. (1991). Dielectric relaxation studies of oligether of ethylene glycol at microwave frequencies, *Bull. Chem. Soc. Jpn.*, 64, 2030-2031.

[8] Sengwa, R.J., Purohit, H.D. (1992), Dielectric relaxation in poly (ethylene glycols) at 9.83 GHz, P*olymer International*, 29, 25-28.

[9] Yoshioka, S., Aso, Y., Otsuka, T., Kojima, S. (1995), Water mobility in poly (ethylene glycol)-, poly (vinylpyrrolidone)-, and gelatin-water systems, as indicated by dielectric relaxation time, spin-latice relaxation time, and water activity. *J. Pharm. Sci.*, 84,

1072-1077.
[10] Sengwa, R.J., Kaur, K., Chaudhary, R. (2000) Dielectric properties of low molecular weight poly (ethylene glycol)s, *Polym. Int.*, 49, 599-608.
[11] Rodnikova, M.N., Syrnikov, Y.P., Penkina, N.V., Kayumova, D.B., Chumaevskii, N.A. (2005). Estimation of the structural relaxation time for ethylene glycol at 298 K. *Russ. J. Phys. Chem.*, 12, 2060-2061.

Cole-Cole plot analysis of dielectric behavior of paraffin labeled with different PEG-chains

Yoko Yamada [a,*], Dana Daneshvari [b], Raniero Pittini [c], Sébastian Vaucher [a], Lukas Rohr [a], Susanne Leparoux [a], Hans Leuenberger [d]

[a] *Swiss Federal Institute for Materials Research and Testing, EMPA, Feuerwerkerstrasse 39, CH-3602 Thun, Switzerland*
[b] *Institute of Pharmaceutical Technology, Pharmacenter, Klingelbergstrasse 50, University of Basel, CH-4056 Basel, Switzerland*
[c] *Maxon motor ag, Brünigstrasse 220, CH-6072 Sachseln, Switzerland*
[d] *Institute of Pharmaceutical Technology, Pharmacenter, Klingelbergstrasse 50, University of Basel, CH-4056 Basel, Switzerland,*
present address: *Institute for Innovation in Industrial Pharmacy, CH-4148 Pfeffingen, Switzerland*

* Responsible author:
Feuerwerkerstrasse 39, CH-3602 Thun, Switzerland
Tel.: +41-33 228 42 41, Fax: +41-33 228 44 90
E-mail address: yoko.pittini@empa.ch (Y. Pittini Yamada)

Abstract

Complex permittivity of paraffin labeled with different PEG-chains was measured above melting point at frequencies from 0.2 to 20 GHz. The number of PEG-chain length is varied from 0 to 120 for observing the effect of PEG-chain length on dielectric permittivity of whole polymer. The measured real and imaginary parts of complex permittivity of these polymers were analyzed by Cole-Cole plot using the graphical analysis proposed by Havriliak-Negami. This analysis makes us understand that, at low frequency region, the shape of Cole-Cole plot behaves as an isotropic shrinkage of PEG. The proportion of this shrinkage is larger with decreasing the number of PEG-chains bonded with paraffin. At high frequency region, Cole-Cole plot of all polymers put on one single line and the extrapolation of this line towards real-axis of Cole-Cole plot arrives at complex permittivity of pure paraffin. This phenomenon explains the contribution of PEG's dipole movement to the complex permittivity of the whole polymer depending on different PEG chain length and microwave frequencies.

Keywords: Dielectric constants, Complex permittivity, Polymers, Havriliak-Negami's

graphical analysis

1. Introduction

Dipolar losses in the microwave range are used in modern technology for accelerating thermal processing of polymers (tempering, curing etc...) [1-3]. Optimal heating conditions can be achieved by combining conventional and dielectric heating. A fast volumetric heating can affect the thermal decomposition kinetic of the polymers, and, for example, prevent undesired oxidation reactions and decompositions. Furthermore, the presence of the electro-magnetic field has been shown to lower the onset temperature of chemical reactions and also can lead to different reaction products.

In molecular systems submitted to microwave, the conversion of electro-magnetic energy into heat is essentially due to the interaction of the electric field with dipoles. Apolar molecules such as *n*-alkanes or paraffin are not suitable for microwave heating. On the other hand, polar structures such as poly(ethylene glycols) (PEG) are dissipative [4,5]. In this study we investigate the dielectric properties of molecules of general formula: $H(CH_2)_n$-$(OCH_2CH_2)_mOH$. These molecules are composed of one straight part containing electric dipoles chemically linked to an inert *n*-alkane part. We investigate how the PEG-chain length, *m*, effects the dielectric properties of the whole compounds. The number of chemically bonded PEG-chain varies between 1 and 120. Pure paraffin and PEG3000 were also studied for comparison.

For analyzing the experimentally obtained dielectric constants, we plotted the real part of complex permittivity in *x*-axis and imaginary part of that in *y*-axis. This is known as Cole-Cole plot. Havriliak and Negami's analytical method [6, 7], which is succeeded to explain the skewed circle of polymer's Cole-Cole plot, is introduced in this paper. The definitions and theoretical background of this analytical method are briefly summarized in chapter 2. This analytical technique helps us to understand the effect of chemically bonded PEG to the paraffin on the transition of the shape and size of the skewed Cole-Cole plot.

2. Definitions and theoretical background of Cole-Cole plot

The data analysis of experimentally obtained complex permittivity is usually performed

by a curve-fitting technique using several models such as Debye model, Cole-Cole model, Davidson-Cole model, Havriliak-Negami model and KWW model. The curve-fitting technique using these models is used to find relaxation time. However, a Cole-Cole plot, which is led from dielectric constants, has been also used for analyzing dielectric parameters including relaxation time. A graphical analysis using Cole-Cole plot proposed by S. Havriliak and S. Negami [6, 7] is efficiently applied, especially in case of polymers. In their work they studied the shape of many polymers' Cole-Cole plots and found that they all have approximately the same shape. The curve becomes linear at high frequency region and becomes semi-circular at low frequency region.

In order to represent this behavior quantitatively, they proposed the following relaxation function:

$$\frac{\varepsilon^*(\omega)-\varepsilon_\infty}{\varepsilon_0-\varepsilon_\infty}=\left\{1+(i\omega\tau_0)^\alpha\right\}^{-\beta} \tag{1}$$

where ε^* is the complex permittivity, ε_∞ is the limited high frequency dielectric constant, ε_0 is the limited low frequency (static) dielectric constant , ω is the angular frequency and τ_0 is the average relaxation time. α is the distribution parameter indicating the broadness of the symmetric relaxation curve and β is the distribution parameter indicating the skew of the circular curve. Equation (1) can separate the real and imaginary parts of complex permittivity (ε', ε'') as follows [6]:

$$\varepsilon'(\omega)-\varepsilon_\infty=r^{-\beta/2}(\varepsilon_0-\varepsilon_\infty)\cos\beta\theta \tag{2}$$

$$\varepsilon''(\omega)=r^{-\beta/2}(\varepsilon_0-\varepsilon_\infty)\sin\beta\theta \tag{3}$$

where

$$r^2=\left[1+(\omega\tau_0)^{1-\alpha}\sin\alpha(\pi/2)\right]^2+\left[(\omega\tau_0)^{1-\alpha}\cos\alpha(\pi/2)\right]^2 \tag{4}$$

$$\theta=\arctan\left[\frac{(\omega\tau_0)^{1-\alpha}\cos\alpha(\pi/2)}{1+(\omega\tau_0)^{1-\alpha}\sin\alpha(\pi/2)}\right] \tag{5}$$

Equations (2) to (5) indicate that, with $\omega\tau_0$ going toward infinitive value, $\varepsilon'(\omega)$ reaches ε_∞ and $\varepsilon''(\omega)$ reaches zero. In addition, with $\omega\tau_0$ going toward zero, $\varepsilon'(\omega)$ reaches ε_0 and $\varepsilon''(\omega)$ reaches 0. For these reasons two of the dispersion parameters, ε_0 and ε_∞, can be evaluated as the high and low frequency intercepts of the experimental quantities with the real axis of Cole-Cole plot.

3. Experimental Method

3.1 Materials

Pure paraffin was supplied by Schweizerhall Chemie, Basel, Switzerland. The PEG3000 ($H(OCH_2CH_2)_mOH$, average molecular weight: 2700-3000, density: 1.1-1.2 g/cm^3, melting temperature range: 321-327 K) is obtained from Clariant GmbH, Division Tenside, Musterlager werk Gendorf as Polyglykol 3000 schuppen.

Paraffin labeled with different PEG-chains (C_nE_m) were obtained from Zschimmer & Schwarz GmbH & Co. KG in Germany (n=18 or n=22, $1 \leq m \leq 120$). The number of PEG chain length is varied between 1 and 120. Their chemical structures and symbolic expressions are shown in Table 1.

PEG number	Chemical structure	Symbolic expression	Molecular weight	Melting point	Specific enthalpy ΔH/g (J/g)
0	C_nH_{2n+2}	—	—	220 K	55
1	$H(CH_2)_{22}-(OCH_2CH_2)$ OH	$C_{22}E_1$	371	336 K	188
2	$H(CH_2)_{22}-(OCH_2CH_2)_2OH$	$C_{22}E_2$	359	333 K	117
3	$H(CH_2)_{18}-(OCH_2CH_2)_3OH$	$C_{18}E_3$	415	315 K	111
8	$H(CH_2)_{22}-(OCH_2CH_2)_8OH$	$C_{22}E_8$	679	323 K	106
10	$H(CH_2)_{18}-(OCH_2CH_2)_{10}OH$	$C_{18}E_{10}$	711	313 K	144
40	$H(CH_2)_{18}-(OCH_2CH_2)_{40}OH$	$C_{18}E_{40}$	2033	325 K	160
80	$H(CH_2)_{18}-(OCH_2CH_2)_{80}OH$	$C_{18}E_{80}$	3795	334 K	169
120	$H(CH_2)_{18}-(OCH_2CH_2)_{120}OH$	$C_{18}E_{120}$	5558	333 K	163
∞	$H(OCH_2CH_2)_mOH$: PEG3000	—	2700-3300	321 – 327 K	—

Table 1: Materials used for the dielectric measurement of this study. Peak temperature of melting point and specific enthalpy are measured by DSC for paraffin labeled with different PEG-chains and pure paraffin.

3.2 Equipments for Dielectric Measurement

The complex permittivity (real part, ε', and imaginary part, ε'') were measured using Vector Network analyzer (Agilent Technologies Inc. USA-Palo Alto CA 94304-1185, HP

8720D 50 MHz – 20 GHz) with the connecting cable of High Temperature 20 GHz, Type-N female 1250-1743, 2.4 mm male 11901D, and the "High temperature probe kit 8570E Agilent technologies Inc.". The ε' and ε" were obtained by Software Program of HP 85070 by Agilent Technologies Inc. which is also used for the measurments of dielectric permittivity.

The measuring vessel is a double layer Pyrex-Glass with internal diameter of 25 mm and height of 25 mm, and the external diameter of 50 mm and height of 50 mm. Between these layers temperature controlled water flows. The water enters from the upper entering of the vessel and goes out from the lower one. In this way we obtain the best circulation around the sample. This vessel was designed in the Institute of Pharmaceutical Technology, university of Basel, Switzerland and was manufactured by Glastechnik-Rahm (Muttenz/BL, CH-4132, Switzerland). The photos of this vessel are shown in Fig.1.

Fig. 1 Photos of a vessel used for controlling sample temperatures and measuring dielectric constants by immersing the dielectric probe in to the melted samples in this vessel.

The samples were brought to required temperature using Thermostat / circulating water bath (B. Braun Biotech International GmbH D-34209 Melsungen, Thermomiux UB; 852 042/9; 90120498, Frigomix U-1; 852 042/0; 8836 004) with the temperature control of +0.1K. The temperature of the sample and the probe were measured using Infrared thermometer (Fluke 66 Ir Thermometer) with the control of $\pm$0.1K.

3.3 Method

Sufficient amounts of material were placed into the measuring vessel and were brought to required temperature using circulating water bath. The probe was calibrated before the measurement of each sample using three standards, *i.e.* air, short block and water. After complete melting of the samples, the calibrated measuring probe was inserted into the sample.

The temperature were increased / decreased with thermostat of the circulating water bath. The temperature of the probe and the sample were checked using infrared thermometer before each measurement to insure that they have the same temperature. The measurement was carried out by first melting the sample, inserting the calibrated probe, increasing the temperature up to 343 K and then gradually decreasing it. The dielectric constants were measured in required temperatures during this process.

3.4 Melting point measurement

Melting point is measured by DSC (Mettler Toledo DSC 822e). The temperature is changed from 243 K to 573 K with the temperature increment of 10 K/min. In this study the melting temperature is determined by the peak of the DSC curve. The experimentally obtained melting point and specific enthalpy are shown in Table 1.

4. Results

Figure 2 shows the experimental results of dielectric properties, (a) real part of complex permittivity and (b) imaginary part of complex permittivity of the paraffin labeled with different PEG-chains, PEG3000 and pure paraffin. Pure paraffin exhibits constant value for real part of complex permittivity, $\varepsilon'_{\text{paraffin}} = 2.36$, at all measured frequencies, and the imaginary part of complex permittivity, $\varepsilon''_{\text{paraffin}}$, is as expected zero. From this result, it is evident that pure paraffin has no polar structure. Instead, PEG3000 has an electric dipole moment and the real part of complex permittivity, $\varepsilon'_{\text{PEG}}$, becomes maximum at the lowest frequency among the measurements performed in this study, and the value is about 9. The peak of imaginary part of complex permittivity, $\varepsilon''_{\text{PEG}}$, appears at 6.7 GHz and its value is 2.52. Paraffins labeled with different PEG-chains have intermediate values

between pure paraffin and PEG3000. The longer PEG chain length in the polymer, the larger both real and imaginary parts of the complex permittivity. All paraffins labeled with different PEG-chains have one peak in imaginary part, and all of their peaks are located at the same frequency as PEG3000.

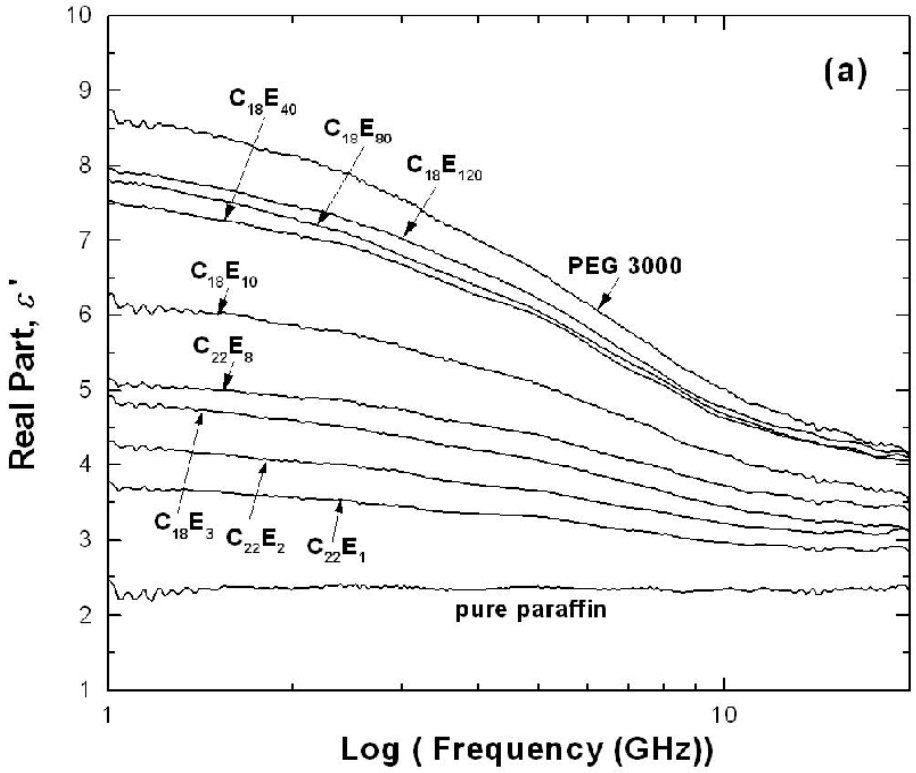

Fig.2 Experimental results of dielectric properties, (a) real part and (b) imaginary part of paraffins labeled with different PEG-chain, PEG 3000 and pure paraffin.

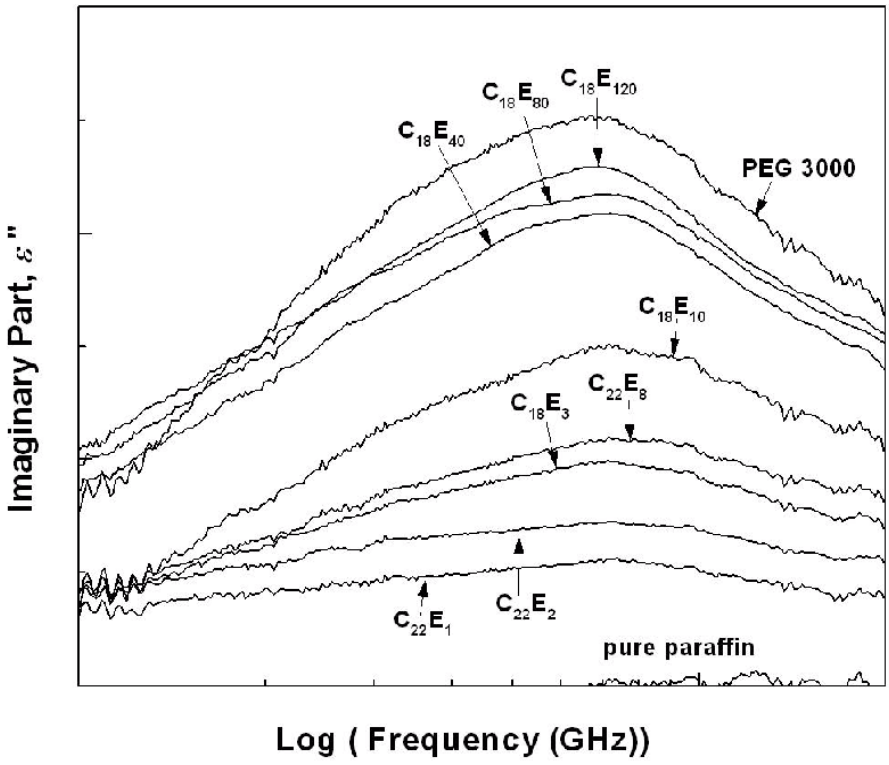

Fig.2 (b)

Figure 3 shows the Cole-Cole plot of paraffin labeled with different PEG-chains, pure paraffin and PEG3000. They are plotted following the definition in chapter 2 by using the experimental results of real and imaginary part of complex permittivity shown in Fig.2. The values of pure paraffin appear as a single point on a Cole-Cole plot. It is evident from the experimental data of ε' and ε'' that these values remains constant over the frequency range of interest. The values of ε' and ε'' of paraffin on a Cole-Cole plot are 2.36 and 0, respectively. PEG3000 appears as a semi-circular shape within the measured frequencies. The paraffins labeled with different PEG-chains are located between the PEG3000 curve and the point of pure paraffin. At frequency below 9.7 GHz, circular shape tendency is found similar to PEG3000, while the magnitude depends on the number of PEG units involved in the labeling. In contrast, at higher frequencies above 9.7 GHz, the shape of Cole-Cole plot becomes significantly flattens. This is not likely to PEG3000. This behavior of Cole-Cole plot is consistent with the discussion by S. Havriliak and S. Negami [6] that nearly all polymeric dispersions have a circular dependence at low frequencies while being linear at high frequencies.

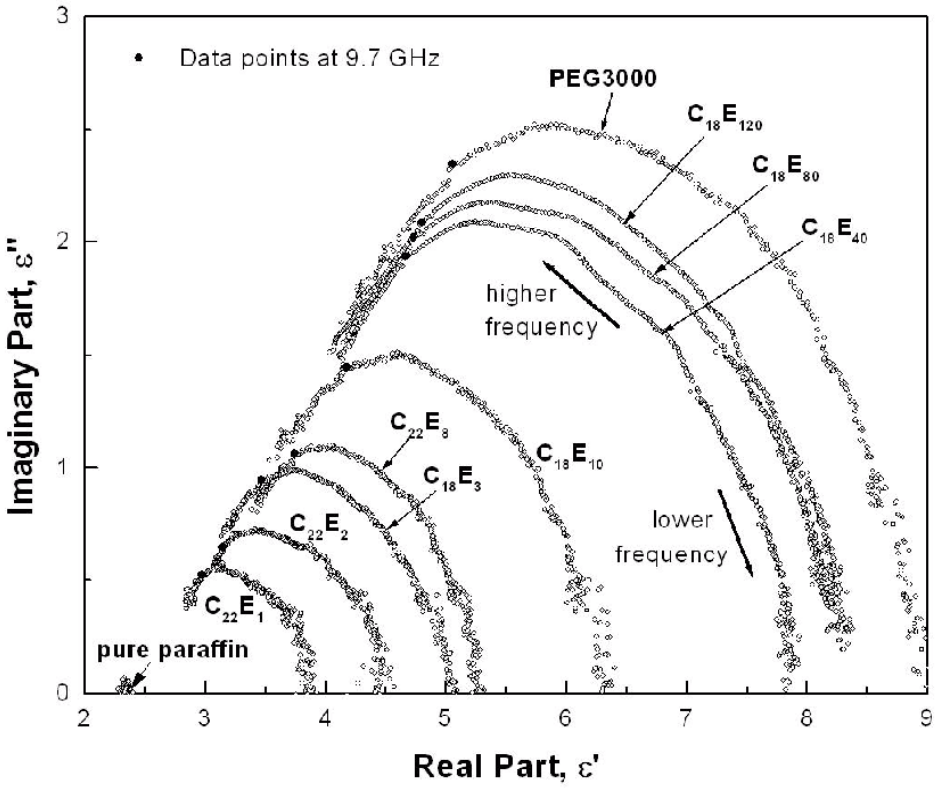

Fig. 3 Cole-Cole plots of paraffins labeled with different PEG-chain, PEG3000 and pure paraffin. Solid circles indicate the data point at 9.7 GHz.

5. Discussion

5.1 Linear region of Cole-Cole plot

For a more detailed investigation of the linear behavior of the Cole-Cole plot in high frequency region, the experimental data of paraffin labeled with different PEG-chains from 9.7 GHz to 20 GHz are sorted out and fitted by a linear line. The fitted results, *i.e.* slopes and intersections with ε'-axis, are shown in Table 2. According to Havriliak and Negami [6], this slope corresponds to the graphical parameter of $\alpha\beta \cdot \pi/2$ (see eq.(1) for the meaning of α and β), and the intersection with ε'-axis corresponds to high frequency limiting value of permittivity, ε_∞. The Cole-Cole plot of this region is linear for all the paraffins labeled with different PEG-chains with good statistical error (r-square) values of the linear fits. Although the slopes vary from 0.61 to 1.07, the intersections with the ε'-axis (ε_∞) correspond well to an average value of 2.17 with the error range of ±16%.

Sample	High frequency region			Low frequency region	
	slope	intersection with	r^2	intersection with	r^2

	real axis (ε_∞)			real axis (ε_0)	
Pure paraffin	—	2.36	—	2.36	
C_{22} E_1	0.87	2.39	0.828	3.83	1.000
C_{22} E_2	1.07	2.53	0.988	4.30	1.000
C_{18} E_3	0.74	2.19	0.984	4.89	1.000
C_{22} E_8	0.65	2.13	0.972	5.28	1.000
C_{18} E_{10}	0.61	1.82	0.986	6.16	1.000
C_{18} E_{40}	0.82	2.30	0.998	7.86	1.000
C_{18} E_{80}	0.71	1.87	0.999	8.18	1.000
C_{18} E_{120}	0.77	2.12	0.997	8.31	1.000
All C_nE_m	0.87	2.40	0.996	—	—
PEG 3000	—	—	—	8.87	1.000

Table 2 Curve-fitting results from Cole-Cole plot of pure paraffin, paraffins labeled with different PEG-chains and PEG3000. At high frequency region (from 9.7 GHz to 20 GHz) the fitting is performed by linear-fit. The intersection with real axis obtained by a linear extrapolation corresponds to high frequency limiting value of permittivity, ε_∞. At low frequency region (below 9.7 GHz) the low frequency limiting value of permittivity, ε_0, is obtained by a circular arc extrapolation of the experimental points to the real axis. In 'All C_nE_m', all data with different number of labeled PEG are fitted linearly together.

Fig.4 shows the experimental data of all paraffins labeled with different PEG-chains at frequencies between 9.7 GHz and 20 GHz. To take into account the effect of different value ranges of ε' and ε'' depending on the number of the labeled PEG, all the experimental data shown in Fig.4 were put together and fitted linearly all data together. A line on this figure is a linear-fitted result. The slope of this line is 0.87 and the intersection with ε'-axis is ε_∞ = 2.40 as is shown in Table 2. This intersection value of (ε', ε'') = (2.40, 0), is closed to the complex permittivity of pure paraffin, *i.e.* ($\varepsilon'_{\text{paraffin}}$, $\varepsilon''_{\text{paraffin}}$) = (2.36, 0) (see chapter 4) . Therefore, we presume that the extrapolation of the linear region of the paraffin labeled with different PEG-chain to the ε'-axis goes toward the value of dielectric permittivity of pure paraffin. These results indicate that, above 9.7 GHz, the dipole associated to the ether group of PEG label can no longer contribute to dipolar relaxation, and only the effect of paraffin part remains for the dielectric permittivity.

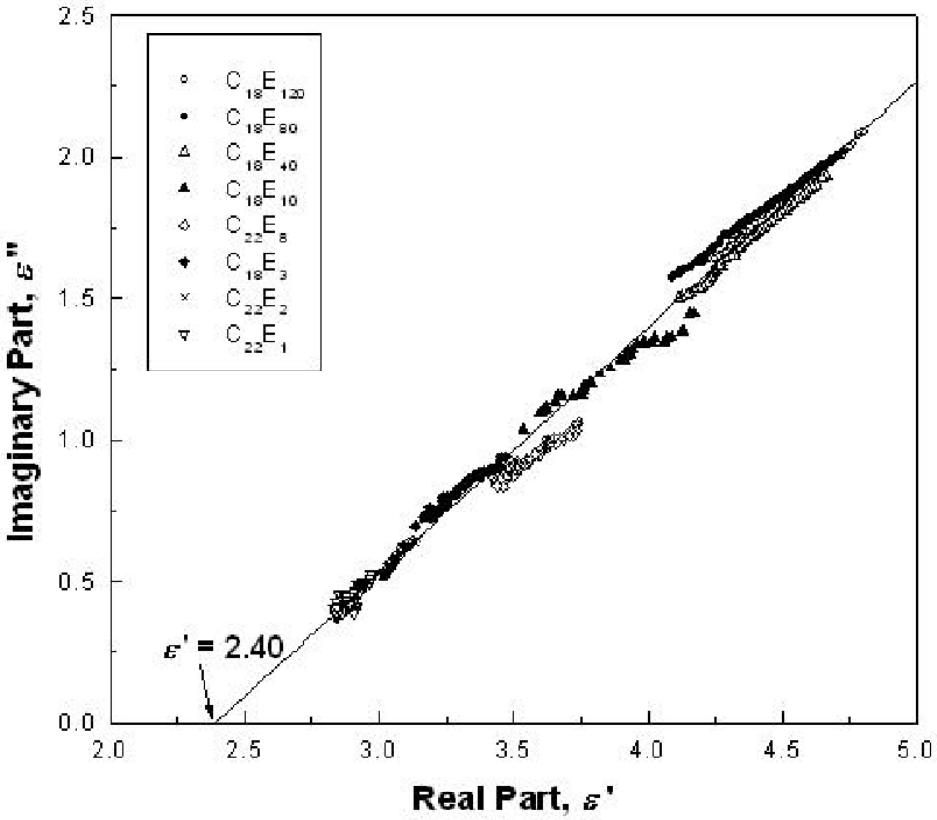

Fig.4 Experimental data of paraffins labeled with different PEG-chain at frequency range from 9.7 to 20 GHz. The line is obtained by linear fitting by using all data together.

5.2 Circular region of Cole-Cole plot

Looking at the circular region of Cole-Cole plot of the paraffin labeled with different PEG-chains in Fig.3, the shape of this circular region is similar to the Cole-Cole plot of PEG but is shrunken in size and shifted towards a point (ε', ε'')=(2.36, 0), which is the complex permittivity of pure paraffin. With an assumption that the circular region of the Cole-Cole plot of paraffin labeled with different PEG-chain are shrunken compared to PEG's Cole-Cole plot, this contribution can be expressed as the following formula.

$$\varepsilon'_{\text{paraffin}-\text{PEG}} = \varepsilon'_{\infty} + k\left(\varepsilon'_{\text{PEG}} - \varepsilon'_{\infty}\right) \tag{6}$$

$$\varepsilon''_{\text{paraffin}-\text{PEG}} = k\varepsilon''_{\text{PEG}} \tag{7}$$

where ε'$_{\text{paraffin-PEG}}$ and ε''$_{\text{paraffin-PEG}}$ are the real and imaginary part of complex permittivity of paraffin labeled with different PEG-chains, and ε'$_{\text{PEG}}$ and ε''$_{\text{PEG}}$ are those of PEG. ε'_{∞}

is the limiting high-frequency permittivity of the paraffin labeled with different PEG-chain, and this has the same value as the real part of the complex permittivity of pure paraffin, $\varepsilon'_{\text{paraffin}}$. k is the proportionality constant from Cole-Cole plot of PEG to paraffin labeled with different PEG-chains. The value of k varies in the range $0 \leq k \leq 1$. $k = 1$ indicates the value of PEG, and when $k = 0$, every value of the Cole-Cole plot converges to the complex permittivity of pure paraffin, $(\varepsilon', \varepsilon'') = (\varepsilon'_{\infty}, 0)$. Lines in Fig.5 show the calculated results of shrunken PEG's Cole-Cole plot. The shrunken proportionality constant of k varies from 0.1 to 0.9 with intervals of 0.1 in Fig. 5. The experimentally obtained Cole-Cole plots of paraffin labeled with different PEG-chain are also displayed by points on this figure. Comparing the simulated results with the experimental ones, the simulated curve follows well the measured data within the low frequency region, where the Cole-Cole plot becomes circular. This indicates that the PEG labels of paraffin labeled with different PEG-chain behaves like PEG itself. Only the intensity of the values for the complex permittivity decreases depending on the chain length of PEG.

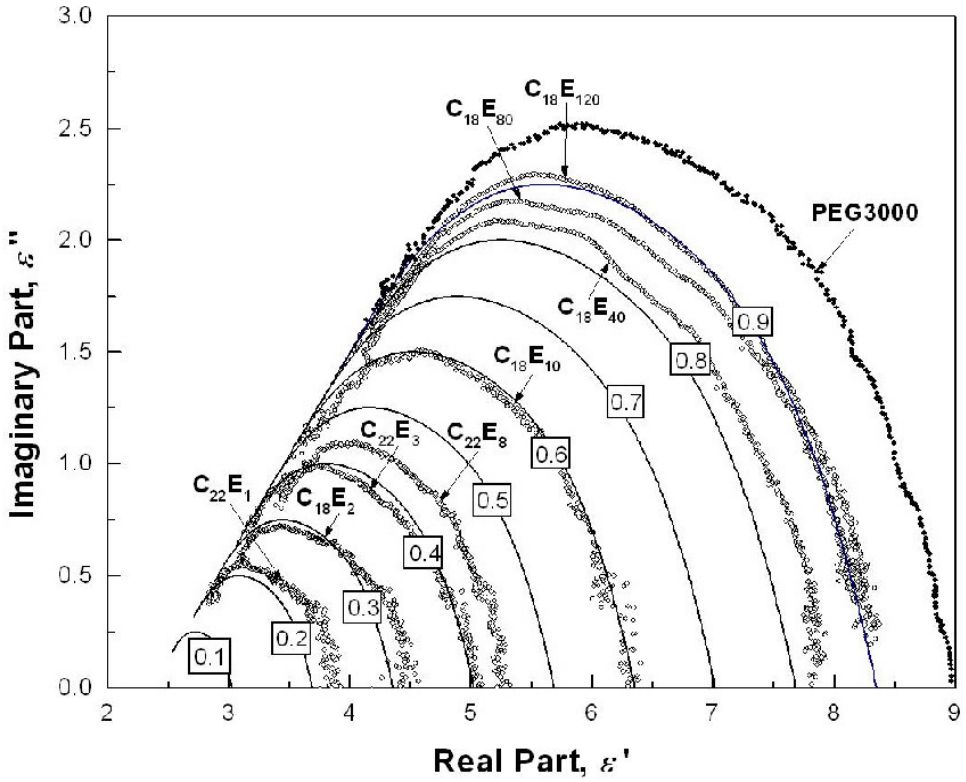

Fig.5 Lines show the simulated Cole-Cole plots of paraffin labeled with different PEG-chain with corresponding k values. Experimental data are shown by dots.

5.3 Transition from circular to linear curve

From the discussions of 5.1 and 5.2, we clarified the behavior of linear region and circular region of the Cole-Cole plot of paraffin labeled with different PEG-chain. The next discussion is about the transition from circular to linear regions by increasing the frequency. Observing the frequency corresponding to the cross-over between the circular and the linear region, this transition is found to take place at the same frequency of 9.7 GHz for all the paraffins labeled with different PEG-chain. Because in eq.(1) the frequency is tied to the scattering time τ_0 in form of the product $\omega\tau_0$, it follows that at 9.7 GHz the scattering time τ_0 is the same for all the studied paraffin labeled with different PEG-chain, and τ_0 is approximately frequency-independent in the region around 9.7 GHz. Furthermore, the extrapolation of the linear fit (shown in Fig.4) towards the Cole-Cole plot of PEG also crosses the PEG curve at the same frequency. This phenomenon indicates that at frequencies below 9.7 GHz the dielectric behavior of PEG governs the dielectric function of the paraffin labeled with different PEG-chain. The intensity of the contribution of PEG depends on the number of the PEG bonded to the paraffin. This phenomenon is also reported by R.J. Sengwa et al. [4] at low molecular weight of poly(ethylene glycol)s. When the frequency is increased to 9.7 GHz, the motion of PEG molecules by the applied electro-magnetic field is hindered by the chemical bonding with paraffin. This phenomenon eliminates the contribution of the PEG to the paraffin labeled with different PEG-chain and the dielectric function becomes linear in the Cole-Cole plot with slope $\alpha\beta\,\pi/2$ and ε' crossing at $\varepsilon_{\text{paraffin}}$. From the slope of 0.87 of the linear part in the Cole-Cole plot, we find, for all the measured paraffin labeled with different PEG-chains, an $\alpha\beta$ product of 0.55, close to the Schoenhals et al. [8] value of 0.5, describing "local chain motion", which could occur in the transition from PEG to paraffin. This bonding is the same in all the measured paraffin labeled with different PEG-chain. Therefore, the same local mode can be excited in all these polymers, and the same $\alpha\beta$ product is observed for all measured paraffin labeled with different PEG-chain.

6. Conclusion

The dielectric behavior of paraffin labeled with different PEG-chain with different number of PEG structural units, pure paraffin and PEG3000 were measured, and the dielectric constants were analyzed by Cole-Cole plot. It is found that all of the Cole-Cole plots of paraffin labeled with different PEG-chain showed a skewed arc shape. Pure PEG3000 showed as well a skewed arc shape but there is no linear region, and pure

paraffin is just one point in the Cole-Cole plot as to be expected. The linear region of all of the paraffin labeled with different PEG-chain were observed at the frequency between 9.7 to 20 GHz, and the linearly extrapolated line towards $\varepsilon''=0$ axis tend invariably to the value of pure paraffin. The circular region of paraffin labeled with different PEG-chain has the shrunken shape as PEG. From these behaviors of Cole-Cole plot, we can conclude that at higher frequencies when the PEG's dipole movement cannot follow the electro-magnetic field, no effect of the derivatives can be measured. The number of chemically bonded PEG structural units on paraffin contributes only to intensity of the values of the complex permittivity in the region of lower frequencies.

Acknowledgement

The authors gratefully acknowledge the funding provided by CTI.

References

[1] C. Leonelli, G.C. Pellacani, C. Siligarde, P. Veronesi, Key Eng. Mater. 264-268 (2004) 739-742.

[2] Zhipeng Xie, Yong Huang, Jianguang Wu, Longlei Zheng, J. Mater. Sci. Lett. 14 (1995) 794-795.

[3] E.H. Moore, D.E. Clark, R. Hutcheon, Mat. Res. Soc. Symp. Proc. 269 (1992) 341-346.

[4] R.J. Sengwa, K. Kaur, R. Chaudhary, Polym. Int. 49 (2000) 599-608.

[5] R. J. Sengwa, H. D. Purohit, Polym. Int. 29 (19920) 25-28.

[6] S. Havriliak, S. Negami, J. Polym. Sci., Part C 14 (1966) 99-117.

[7] S. Havriliak, S. Negami, Polymer 8 (1967) 161-210.

[8] A. Schönhals, E. Schlosser, Colloid Polym. Sci. 267 (1989) 125-132.

Appendix

							One Debye	
V_{wa}/V %	V_{wa}/V	Dielectric constant	E_i/E - values	g - values	Density [g/cm^3]	Refractive index	τ [ns]	R^2
0	**0.0**	47.5082	-13.2559	1.1856	1.09502	1.4765	0.020	0.995
7	**0.07**	55.0777	-15.7465	1.2033	1.09744	1.4754	0.027	0.991
14	**0.14**	60.8573	-17.6852	1.2165	1.09863	1.4741	0.036	0.991
20	**0.20**	64.60548	-18.9586	1.2163	1.09824	1.4710	0.042	0.991
30	**0.30**	69.6115	-20.6348	1.2377	1.09398	1.4648	0.048	0.993
40	**0.40**	73.0568	-21.7469	1.2778	1.08487	1.4525	0.045	0.988
45	**0.45**	74.3568	-22.1452	1.3050	1.07877	1.4460	0.041	0.995
50	**0.50**	75.1955	-22.3711	1.3415	1.07210	1.4385	0.037	0.995
55	**0.55**	76.0865	-22.5899	1.3876	1.06469	1.4308	0.032	0.995
58	**0.58**	76.4486	-22.6544	1.4214	1.06031	1.4232	0.030	0.994
64	**0.64**	77.0945	-22.7333	1.4970	1.05090	1.4075	0.025	0.993
70	**0.70**	77.6537	-22.7339	1.5956	1.04108	1.3911	0.020	0.993
80	**0.80**	78.1455	-22.4500	1.8216	1.02555	1.3757	0.015	0.994
90	**0.90**	78.8803	-21.9266	2.1924	1.01057	1.3607	0.011	0.997
100	**1.00**	79.4399	-20.7270	2.8465	0.99704	1.3461	0.009	0.999

E_i/E-parameter from the modified Clausius-Mossotti Eq., g-values obtained from the Kirkwood-Fröhlich Eq., density, refractive index, relaxation time τ in the investigated DMSO-water binary mixtures at room temperature (25°C).

							One Debye	
V_{wa}/V %	V_{wa}/V	Dielectric constant	E_i/E - values	g - values	Density [g/cm^3]	Refractive index	τ [ns]	R^2
0	**0.0**	33.3170	-8.20061	1.359002573	0.95896	1.4695	0.022	0.997
7	**0.07**	38.4528	-9.76681	1.416619297	0.97396	1.4685	0.037	0.998
14	**0.14**	42.7977	-11.14425	1.454636024	0.98569	1.4630	0.050	0.998
20	**0.20**	46.1843	-12.22819	1.484768276	0.99302	1.4566	0.058	0.998
30	**0.30**	51.7862	-13.99228	1.550723199	1.00088	1.4440	0.061	0.997
40	**0.40**	57.0432	-15.62104	1.630680218	1.00450	1.4293	0.054	0.995
45	**0.45**	59.5301	-16.37684	1.678128919	1.00515	1.4210	0.050	0.994
50	**0.50**	59.96660	-16.30281	1.767950591	1.00520	1.4198	0.046	0.993
55	**0.55**	64.09849	-17.73681	1.779369799	1.00477	1.4052	0.041	0.990
58	**0.58**	65.31928	-18.09000	1.81228982	1.00434	1.4004	0.037	0.990
64	**0.64**	67.51454	-18.67440	1.89401651	1.00333	1.3913	0.032	0.988
70	**0.70**	69.86557	-19.33080	1.977189115	1.00186	1.3789	0.027	0.987
80	**0.80**	73.1352	-20.08596	2.150698713	0.99945	1.3648	0.020	0.987
90	**0.90**	76.1068	-20.55207	2.411834582	0.99744	1.3488	0.014	0.991
100	**1.00**	78.6726	-20.53681	2.819767023	0.99672	1.3325	0.009	0.999

E_i/E-parameter from the modified Clausius-Mossotti Eq., g-values obtained from the Kirkwood-Fröhlich Eq., density, refractive index, relaxation time τ in the investigated DMAC-water binary mixtures at room temperature (25°C).

							One Debye	
V_{wa}/V %	V_{wa}/V	Dielectric constant	E_i/E - values	g - values	Density [g/cm^3]	Refractive index	τ [ns]	R^2
0	**0.0**	37.5739	-10.22488	1.161179758	0.94382	1.4283	0.012	0.990
7	**0.07**	42.48708	-11.77074	1.202233928	0.95711	1.4255	0.017	0.994
14	**0.14**	46.68602	-13.11328	1.230346487	0.96865	1.4223	0.024	0.991
20	**0.20**	50.35467	-14.27023	1.263187746	0.97705	1.4185	0.030	0.988
30	**0.30**	55.85577	-15.99013	1.321254645	0.98711	1.4115	0.036	0.986
40	**0.40**	61.61922	-17.72827	1.413575959	0.99315	1.4018	0.037	0.987
45	**0.45**	63.51140	-18.29795	1.450593598	0.99483	1.3957	0.036	0.993
50	**0.50**	65.49290	-18.87439	1.496286312	0.99593	1.3902	0.033	0.995
55	**0.55**	67.42156	-19.41170	1.551891064	0.99649	1.3845	0.031	0.993
58	**0.58**	68.22580	-19.62715	1.581734246	0.99664	1.3808	0.029	0.994
64	**0.64**	70.11479	-20.10696	1.65969112	0.99666	1.3739	0.026	0.992
70	**0.70**	71.64773	-20.44151	1.750053214	0.99646	1.3670	0.023	0.997
80	**0.80**	74.1934	-20.86332	1.961124733	0.99600	1.3553	0.018	0.999
90	**0.90**	76.3573	-20.92802	2.274855417	0.99588	1.3443	0.013	0.999
100	**1.00**	78.0951	-20.34993	2.800228243	0.99679	1.3321	0.009	0.999

E_i/E-parameter from the modified Clausius-Mossotti Eq., g-values obtained from the Kirkwood-Fröhlich Eq., density, refractive index, relaxation time τ in the investigated DMF-water binary mixtures at room temperature (25°C).

							One Debye	
V_{wa}/V %	V_{wa}/V	Dielectric constant	E_i/E - values	g - values	Density [g/cm^3]	Refractive index	τ [ns]	R^2
0	**0.0**	33.2690	-8.95438	1.046557746	1.02749	1.4669	0.018	0.993
7	**0.07**	38.9597	-10.63452	1.13429785	1.03543	1.4632	0.037	0.995
14	**0.14**	44.0418	-12.17227	1.203312189	1.04175	1.4574	0.057	0.997
20	**0.20**	47.9769	-13.37925	1.254111306	1.04526	1.4512	0.071	0.997
30	**0.30**	53.9050	-15.20238	1.334981117	1.04683	1.4392	0.079	0.997
40	**0.40**	59.3029	-16.83955	1.424681146	1.04366	1.4256	0.073	0.996
45	**0.45**	61.6544	-17.53383	1.475727578	1.04082	1.4179	0.065	0.995
50	**0.50**	62.87100	-17.78698	1.545168249	1.03883	1.4137	0.057	0.995
55	**0.55**	65.91002	-18.78161	1.578098717	1.03297	1.4019	0.049	0.993
58	**0.58**	67.00504	-19.08759	1.613304344	1.03035	1.3968	0.044	0.992
64	**0.64**	69.21089	-19.67947	1.692368131	1.02492	1.3878	0.037	0.991
70	**0.70**	71.07958	-20.13798	1.783029782	1.01944	1.3782	0.030	0.989
80	**0.80**	73.937	-20.70549	1.982601946	1.01074	1.3630	0.018	0.995
90	**0.90**	76.3553	-20.90803	2.282066382	1.00287	1.3475	0.013	0.999
100	**1.00**	78.5519	-20.50642	2.814993006	0.99672	1.3326	0.009	0.999

E_i/E-parameter from the modified Clausius-Mossotti Eq., g-values obtained from the Kirkwood-Fröhlich Eq., density, refractive index, relaxation time τ in the investigated NMP-water binary mixtures at room temperature (25°C).

							One Debye	
V_{wa}/V %	V_{wa}/V	Dielectric constant	E_i/E - values	g - values	Density [g/cm^3]	Refractive index	τ [ns]	R^2
0	**0.0**	7.48942	-0.72066	1.235426179	0.88196	1.4049	0.015	0.940
7	**0.07**	11.66523	-1.14125	1.743769066	0.89658	1.4001	0.017	0.981
14	**0.14**	15.78429	-1.84058	2.061624755	0.91018	1.3987	0.020	0.989
20	**0.20**	19.56503	-2.61773	2.279904709	0.92056	1.3958	0.022	0.992
30	**0.30**	26.76454	-4.27607	2.600690861	0.93669	1.3900	0.024	0.993
40	**0.40**	34.53259	-6.28648	2.833127274	0.95058	1.3833	0.025	0.977
45	**0.45**	38.39797	-7.38310	2.903259689	0.95746	1.3791	0.024	0.978
50	**0.50**	42.44093	-8.52946	2.980473472	0.96312	1.3741	0.025	0.980
55	**0.55**	46.94808	-9.84056	3.039095103	0.96914	1.3721	0.024	0.982
58	**0.58**	49.12822	-10.53389	3.045453762	0.97228	1.3687	0.023	0.992
64	**0.64**	54.00767	-12.04467	3.077268628	0.97760	1.3628	0.021	0.992
70	**0.70**	58.85642	-13.58765	3.08118907	0.98248	1.3588	0.020	0.994
80	**0.80**	66.1354	-16.03211	3.033062293	0.98829	1.3503	0.017	0.997
90	**0.90**	72.8191	-18.37204	2.949339779	0.99225	1.3409	0.013	0.999
100	**1.00**	79.1879	-20.66623	2.838940845	0.99669	1.3324	0.009	0.999

E_i/E-parameter from the modified Clausius-Mossotti Eq., g-values obtained from the Kirkwood-Fröhlich Eq., density, refractive index, relaxation time τ in the investigated THF-water binary mixtures at room temperature (25°C).

							One Debye	
V_{wa}/V %	V_{wa}/V	Dielectric constant	E_i/E - values	g - values	Density [g/cm^3]	Refractive index	τ [ns]	R^2
0	**0.0**	44.3524	-12.69629	0.988295196	1.26557	1.4827	0.035	0.998
7	**0.07**	47.78493	-13.74655	1.038843303	1.24770	1.4716	0.031	0.996
14	**0.14**	50.77732	-14.67187	1.081006322	1.22925	1.4615	0.030	0.992
20	**0.20**	53.07704	-15.38659	1.11419989	1.21421	1.4528	0.029	0.988
30	**0.30**	57.07275	-16.60310	1.181483692	1.18910	1.4386	0.027	0.984
40	**0.40**	59.64404	-17.39432	1.229787618	1.16324	1.4254	0.023	0.996
45	**0.45**	61.74981	-18.00370	1.280123665	1.14938	1.4176	0.021	0.997
50	**0.50**	63.72479	-18.56807	1.333106326	1.13700	1.4092	0.020	0.998
55	**0.55**	65.54325	-19.07636	1.386919185	1.12353	1.4017	0.019	0.998
58	**0.58**	66.54024	-19.33901	1.425340894	1.11581	1.3966	0.018	0.998
64	**0.64**	68.07008	-19.73650	1.487589487	1.09949	1.3887	0.015	0.999
70	**0.70**	70.01955	-20.20580	1.581864763	1.08270	1.3796	0.014	0.999
80	**0.80**	73.4851	-20.93047	1.795928915	1.05503	1.3656	0.012	0.999
90	**0.90**	75.7932	-21.04450	2.118732026	1.02636	1.3501	0.010	0.999
100	**1.00**	78.7079	-20.54602	2.820899953	0.99677	1.3325	0.009	0.999

E_i/E-parameter from the modified Clausius-Mossotti Eq., g-values obtained from the Kirkwood-Fröhlich Eq., density, refractive index, relaxation time τ in the investigated Sulfolane-water binary mixtures at room temperature (25°C).

							One Debye	
V_{wa}/V %	V_{wa}/V	Dielectric constant	E_i/E - values	g - values	Density [g/cm^3]	Refractive index	τ [ns]	R^2
0	**0.0**	108.285	-30.84987	2.181582435	1.12857	1.4404	0.034	0.980
7	**0.07**	109.5908	-31.41959	2.145198736	1.12051	1.4372	0.030	0.979
14	**0.14**	109.9565	-31.67086	2.121389302	1.11251	1.4303	0.027	0.978
20	**0.20**	109.5196	-31.63313	2.10356675	1.10562	1.4237	0.025	0.976
30	**0.30**	107.7520	-31.19920	2.082680961	1.09391	1.4125	0.022	0.974
40	**0.40**	104.7820	-30.33440	2.070601133	1.08183	1.4019	0.020	0.968
45	**0.45**	102.9734	-29.77814	2.072376993	1.07557	1.3960	0.018	0.967
50	**0.50**	101.3787	-29.26157	2.084982186	1.06926	1.3907	0.017	0.966
55	**0.55**	99.31734	-28.58569	2.100396206	1.06290	1.3850	0.016	0.968
58	**0.58**	98.02997	-28.16359	2.10966621	1.05880	1.3816	0.015	0.967
64	**0.64**	95.36444	-27.25299	2.142522314	1.05093	1.3750	0.014	0.961
70	**0.70**	92.67952	-26.31088	2.187263895	1.04242	1.3682	0.013	0.963
80	**0.80**	88.0791	-24.60061	2.306284681	1.02799	1.3567	0.012	0.971
90	**0.90**	83.4002	-22.70343	2.501087323	1.01287	1.3449	0.010	0.988
100	**1.00**	78.7341	-20.55236	2.821549908	0.99674	1.3326	0.009	0.999

E_i/E-parameter from the modified Clausius-Mossotti Eq., g-values obtained from the Kirkwood-Fröhlich Eq., density, refractive index, relaxation time τ in the investigated Formamide-water binary mixtures at room temperature (25°C).

							One Debye	
V_{wa}/V %	V_{wa}/V	Dielectric constant	E_i/E - values	g - values	Density [g/cm^3]	Refractive index	τ [ns]	R^2
0	**0.0**	174.8919	-47.92274	4.267133371	0.99876	1.4286	0.115	0.928
7	**0.07**	151.4659	-42.23320	3.465299583	1.00325	1.4251	0.089	0.880
14	**0.14**	134.6828	-38.06177	2.935508004	1.00754	1.4196	0.073	0.919
20	**0.20**	124.5443	-35.51103	2.627897108	1.01066	1.4151	0.063	0.927
30	**0.30**	112.4383	-32.39149	2.294789051	1.01437	1.4066	0.049	0.942
40	**0.40**	104.0521	-30.14534	2.103276039	1.01597	1.3974	0.039	0.963
45	**0.45**	100.8685	-29.25845	2.048340865	1.01599	1.3921	0.035	0.968
50	**0.50**	98.09128	-28.45373	2.01259917	1.01556	1.3874	0.031	0.973
55	**0.55**	95.46079	-27.66788	1.990964005	1.01469	1.3819	0.028	0.979
58	**0.58**	94.01103	-27.21745	1.976036797	1.01397	1.3824	0.026	0.981
64	**0.64**	91.28309	-26.33619	1.992847773	1.01220	1.3724	0.023	0.988
70	**0.70**	88.85742	-25.49289	2.025991368	1.01005	1.3660	0.020	0.991
80	**0.80**	85.261	-24.08451	2.147814834	1.00580	1.3552	0.015	0.996
90	**0.90**	81.8531	-22.49485	2.381299585	1.00118	1.3439	0.012	0.998
100	**1.00**	78.6657	-20.53507	2.818710046	0.99672	1.3327	0.009	0.999

E_i/E-parameter from the modified Clausius-Mossotti Eq., g-values obtained from the Kirkwood-Fröhlich Eq., density, refractive index, relaxation time τ in the investigated N,methylformamide-water binary mixtures at room temperature (25°C).

						One Debye	
$V_{dioxane}/V$ %	$V_{dioxane}/V$	Dielectric constant	E_i/E - values	Density [g/cm^3]	Refractive index	τ [ns]	R^2
0	**0.0**	47.086	-13.05057	1.09492	1.4282	0.024	0.979
7	**0.07**	43.50269	-11.82270	1.09054	1.4263	0.023	0.979
14	**0.14**	40.25978	-10.70054	1.08636	1.4269	0.024	0.978
20	**0.20**	37.19126	-9.67331	1.08234	1.4265	0.024	0.977
30	**0.30**	32.34948	-8.05804	1.07586	1.4255	0.025	0.974
40	**0.40**	27.46662	-6.46853	1.06940	1.4245	0.026	0.970
45	**0.45**	24.95958	-5.67725	1.06611	1.4240	0.025	0.969
50	**0.50**	22.86679	-4.97949	1.06319	1.4234	0.026	0.959
55	**0.55**	20.35476	-4.21330	1.05956	1.4231	0.025	0.970
58	**0.58**	18.90076	-3.77425	1.05756	1.4230	0.024	0.965
64	**0.64**	16.12710	-2.94122	1.05351	1.4225	0.021	0.993
70	**0.70**	13.45923	-2.15983	1.04936	1.4220	0.020	0.993
80	**0.80**	9.28793	-0.99837	1.04244	1.4214	0.019	0.991
90	**0.90**	5.50896	-0.08506	1.03527	1.4208	0.016	0.984
100	**1.00**	2.28474	0.26344	1.02768	1.4198	-	-

E_i/E-parameter from the modified Clausius-Mossotti Eq., density, refractive index, relaxation time τ in the investigated DMSO-1,4-dioxane binary mixtures at room temperature (25°C).

						One Debye	
$V_{dioxane}/V$ %	$V_{dioxane}/V$	Dielectric constant	E_i/E - values	Density [g/cm^3]	Refractive index	τ [ns]	R^2
0	**0.0**	34.4177	-8.44609	0.95902	1.4721	0.022	0.997
7	**0.07**	29.73286	-7.26192	0.96377	1.4687	0.022	0.994
14	**0.14**	26.91104	-6.48854	0.96847	1.4657	0.021	0.994
20	**0.20**	24.57337	-5.84401	0.97251	1.4626	0.023	0.992
30	**0.30**	21.00270	-4.84467	0.97925	1.4568	0.022	0.992
40	**0.40**	17.55389	-3.88827	0.98610	1.4529	0.021	0.993
45	**0.45**	15.92012	-3.43619	0.98953	1.4488	0.020	0.993
50	**0.50**	13.94563	-2.94146	0.99277	1.4468	0.021	0.991
55	**0.55**	12.79247	-2.58254	0.99637	1.4453	0.019	0.993
58	**0.58**	12.05926	-2.36006	0.99819	1.4418	0.019	0.993
64	**0.64**	7.75049	-1.64841	1.00227	1.4398	0.019	0.992
70	**0.70**	6.34203	-1.32246	1.00635	1.4356	0.021	0.987
80	**0.80**	4.17458	-0.89196	1.01334	1.4304	0.017	0.991
90	**0.90**	2.51385	-0.64408	1.02383	1.4255	0.013	0.990
100	**1.00**	2.33774	0.31576	1.02755	1.4199	-	-

E_i/E-parameter from the modified Clausius-Mossotti Eq., density, refractive index, relaxation time τ in the investigated DMAC-1,4-dioxane binary mixtures at room temperature (25°C).

						One Debye	
$V_{dioxane}/V$ %	$V_{dioxane}/V$	Dielectric constant	E_i/E - values	Density [g/cm^3]	Refractive index	τ [ns]	R^2
0	**0.0**	37.2953	-10.15389	0.94359	1.4282	0.012	0.990
7	**0.07**	34.77212	-9.24069	0.94949	1.4263	0.013	0.984
14	**0.14**	31.80499	-8.24768	0.95534	1.4269	0.013	0.987
20	**0.20**	29.23127	-7.41128	0.96041	1.4265	0.013	0.990
30	**0.30**	25.39028	-6.15598	0.96887	1.4255	0.013	0.982
40	**0.40**	21.62629	-4.95594	0.97726	1.4245	0.011	0.980
45	**0.45**	19.71571	-4.36613	0.98171	1.4240	0.012	0.978
50	**0.50**	17.90895	-3.80639	0.98595	1.4234	0.012	0.987
55	**0.55**	16.19276	-3.27232	0.99027	1.4231	0.011	0.994
58	**0.58**	15.15993	-2.95675	0.99286	1.4230	0.011	0.986
64	**0.64**	13.12444	-2.34293	0.99780	1.4225	0.011	0.901
70	**0.70**	11.08130	-1.75416	1.00321	1.4220	0.016	0.993
80	**0.80**	7.94746	-0.86187	1.01195	1.4214	0.016	0.993
90	**0.90**	5.02937	-0.10043	1.02068	1.4208	0.013	0.973
100	**1.00**	2.33376	0.30814	1.02973	1.4198	-	-

E_i/E-parameter from the modified Clausius-Mossotti Eq., density, refractive index, relaxation time τ in the investigated DMF-1,4-dioxane binary mixtures at room temperature (25°C).

						One Debye	
$V_{dioxane}/V$ %	$V_{dioxane}/V$	Dielectric constant	E_i/E - values	Density [g/cm^3]	Refractive index	τ [ns]	R^2
0	**0.0**	33.0795	-8.90758	1.02746	1.4674	0.018	0.993
7	**0.07**	31.49468	-8.38122	1.02775	1.4652	0.018	0.980
14	**0.14**	27.47972	-7.26549	1.02775	1.4622	0.018	0.976
20	**0.20**	25.26025	-6.60497	1.02785	1.4593	0.017	0.974
30	**0.30**	21.82118	-5.56844	1.02795	1.4546	0.017	0.967
40	**0.40**	18.58501	-4.58530	1.02804	1.4496	0.020	0.991
45	**0.45**	16.93028	-4.09193	1.02806	1.4474	0.019	0.991
50	**0.50**	15.37972	-3.62406	1.02808	1.4447	0.019	0.990
55	**0.55**	13.89875	-3.17386	1.02808	1.4423	0.019	0.989
58	**0.58**	13.13750	-2.92673	1.02808	1.4408	0.019	0.988
64	**0.64**	11.27511	-2.38626	1.02808	1.4377	0.019	0.987
70	**0.70**	9.62689	-1.88916	1.02806	1.4344	0.018	0.985
80	**0.80**	6.99575	-1.10432	1.02800	1.4302	0.017	0.980
90	**0.90**	4.56204	-0.37885	1.02790	1.4258	0.015	0.959
100	**1.00**	2.25891	0.23785	1.02778	1.4238	**-**	**-**

E_i/E-parameter from the modified Clausius-Mossotti Eq., density, refractive index, relaxation time τ in the investigated NMP-1,4-dioxane binary mixtures at room temperature (25°C).

Appendix

(A1)

KDP/H2O	e'							
V H20	**10°C**	**20°C**	**25°C**	**30°C**	**40°C**	**50°C**	**60°C**	**70°C**
1	83.7055	80.4504	78.5514	77.8285	74.9422	70.5707	69.4406	67.4669
0.995	84.5749	81.4944	74.7706	78.9351	76.0751	73.4102	70.9721	68.8592
0.983	87.9171	85.2289	83.5728	82.8178	80.0942	78.2234	76.0084	74.1057
0.966	90.2412	87.9453	86.9642	85.7718	83.817	82.0304	80.8939	81.958
0.948	92.9378	90.963	90.1674	89.2226	87.3897	85.9826	84.7079	84.9929
0.931	95.5739	93.9589	92.3368	92.3523	90.9567	89.4945	88.5922	87.9832
0.914	96.751	95.5251	94.8583	94.3904	93.0962	92.0798	91.5375	93.6235
0.897	98.0473	96.8073	95.6228	95.6131	94.4756	93.3576	92.8607	95.4731
0.871	97.5446	96.5973	96.1851	95.5984	94.7617	93.8111	93.1806	94.1699

(B1)

KDP/H2O	e''							
V H20	**10°C**	**20°C**	**25°C**	**30°C**	**40°C**	**50°C**	**60°C**	**70°C**
1	2.5283	2.0188	1.7931	1.7098	1.4171	1.293	1.1859	1.1716
0.995	20.5181	23.752	23.0122	27.2047	31.9961	37.3204	44.1971	51.3286
0.983	64.5767	76.215	79.9055	88.5994	107.4323	120.7057	140.5933	159.9556
0.966	111.5135	131.9864	137.8972	154.0253	183.4907	214.2751	256.9724	325.749
0.948	151.4263	179.745	190.5084	209.3901	246.9945	285.9306	334.9772	404.1606
0.931	188.7851	223.6514	233.0085	259.9559	307.1445	358.5628	418.4013	473.0233
0.914	217.9802	257.6232	272.2834	299.6361	352.9886	411.7993	482.4296	583.4705
0.897	230.447	271.0402	285.0786	315.2959	375.1138	436.3751	514.0636	644.8626
0.871	228.3972	270.4252	288.8012	312.8055	369.0437	430.801	497.2678	578.9286

A1) real and B1) imaginary part of complex permittivity measured at 500 MHz.

(A2)

KDP/H2O	e'							
V H20	**10°C**	**20°C**	**25°C**	**30°C**	**40°C**	**50°C**	**60°C**	**70°C**
1	83.3222	80.2549	76.6586	77.5232	74.5834	70.1693	68.8939	66.8793
0.995	83.5098	80.5609	72.9777	77.9481	74.9352	72.1167	69.4412	67.1448
0.983	84.9524	82.2135	80.1881	79.6955	76.4452	74.2049	71.536	69.1491
0.966	85.2689	83.0267	81.7997	80.8374	78.3762	75.9251	73.8763	73.2128
0.948	85.7514	83.806	83.1241	81.9202	79.55	77.202	74.9523	73.5377
0.931	86.4264	84.9862	83.5809	83.3538	81.1675	78.9751	76.8464	74.922
0.914	85.7451	84.8742	84.4286	83.6097	81.7881	79.7385	77.8312	77.1336
0.897	86.1336	85.2738	84.2721	83.9472	82.0158	80.0204	77.7108	76.8546
0.871	85.3431	84.5695	84.5299	83.3664	81.5891	79.6061	77.5693	76.2416

(B2)

KDP/H2O	e''							
V H20	**10°C**	**20°C**	**25°C**	**30°C**	**40°C**	**50°C**	**60°C**	**70°C**
1	4.3077	3.0611	4.0956	2.279	1.6586	1.1885	0.8777	0.6404
0.995	14.8713	15.451	14.4068	16.474	18.2973	20.5146	23.6733	27.0188
0.983	38.4762	43.0859	43.6618	48.3962	57.1315	63.1878	72.7452	82.1486
0.966	62.2169	71.0837	73.5176	80.9807	94.7832	109.5072	130.4013	164.6111
0.948	83.7051	96.2816	100.8031	109.849	127.4476	146.1948	170.5132	204.7631
0.931	103.3711	119.2687	123.0726	136.1045	158.401	183.2482	212.4463	239.7153
0.914	118.8711	137.2461	143.8344	156.8532	182.2539	210.4436	245.0225	296.5153
0.897	126.5248	145.1101	150.7247	165.975	194.6232	224.0122	262.3888	328.3785
0.871	125.2495	144.8897	152.7734	164.7003	191.581	221.6372	254.1809	294.8715

A2) real and B2) imaginary part of complex permittivity measured at 1 GHz.

(A3)

KDP/H2O	e'							
V H20	**10°C**	**20°C**	**25°C**	**30°C**	**40°C**	**50°C**	**60°C**	**70°C**
1	79.9164	78.0896	76.5922	75.9639	73.341	69.096	69.0978	66.8525
0.995	79.5341	77.8672	71.6517	75.9964	73.5594	71.0903	68.747	66.4603
0.983	78.6295	77.49	76.271	75.9938	73.5009	71.7488	69.4438	67.2244
0.966	75.6642	75.1635	75.0772	74.208	72.6828	70.8636	68.8839	67.3768
0.948	74.0517	74.0657	73.9631	73.6136	72.5969	71.1754	69.3946	67.6964
0.931	72.1275	72.6048	71.9287	72.5283	71.8903	70.7022	69.0892	67.4626
0.914	69.3837	70.1723	70.5395	70.3853	70.1109	69.2707	67.8233	65.9605
0.897	69.4554	70.4152	69.4914	70.7351	70.4518	69.6625	68.1976	65.7612
0.871	68.7313	69.6467	69.557	70.0717	69.9423	69.203	68.0484	66.5751

(B3)

KDP/H2O	e''							
V H20	**10°C**	**20°C**	**25°C**	**30°C**	**40°C**	**50°C**	**60°C**	**70°C**
1	16.2222	12.4928	11.7858	9.9263	7.8973	6.2235	5.2875	4.4318
0.995	19.6894	16.7961	15.0522	14.9776	13.6869	13.139	13.006	13.3132
0.983	29.1771	27.9193	27.3677	27.6239	28.4986	29.3564	31.4505	33.9415
0.966	39.0886	39.7113	39.6164	41.1471	44.0527	47.5475	53.7055	65.2394
0.948	46.9684	49.2373	50.4447	52.1025	56.4031	61.2813	68.4255	79.5824
0.931	54.7843	58.4802	59.2576	62.7008	68.652	75.7384	84.4989	92.6784
0.914	60.5073	65.4239	67.3507	70.8623	78.0984	86.3838	97.0884	114.9308
0.897	63.1934	68.2297	70.0069	74.1168	82.5412	91.3696	103.2746	126.3792
0.871	62.5676	68.0868	70.755	73.7272	81.573	90.7533	100.4875	113.9764

A3) real and B3) imaginary part of complex permittivity measured at 3 GHz.

(A4)

KDP/H2O	e'							
V H20	10°C	20°C	25°C	30°C	40°C	50°C	60°C	70°C
1	56.8472	61.7271	62.2023	64.5883	65.901	64.5385	65.1555	64.3405
0.995	56.2844	61.0355	58.5641	63.8171	65.2759	65.2234	64.5461	63.3121
0.983	54.2449	58.7925	60.5521	61.4331	62.9546	63.0182	62.5096	61.5937
0.966	51.5574	55.7523	57.6464	58.2435	59.7416	60.0669	59.6063	58.431
0.948	50.7589	54.7305	55.5055	57.2446	58.7602	59.3665	59.0806	58.0731
0.931	48.6228	52.2856	52.79	54.7369	56.3487	57.0339	56.8821	56.5746
0.914	45.9294	49.5043	50.8299	51.8904	70.1109	54.388	54.24	52.5416
0.897	45.3274	48.8546	49.7015	51.2733	52.8007	53.5073	53.4759	51.1936
0.871	45.0953	48.6798	49.7071	50.9695	52.6747	53.5017	53.6759	52.8403

(B4)

KDP/H2O	e''							
V H20	10°C	20°C	25°C	30°C	40°C	50°C	60°C	70°C
1	36.8367	32.1143	30.0935	27.752	23.3034	19.2964	16.6459	14.4327
0.995	37.3076	32.805	29.458	28.8135	24.3964	21.0723	18.3426	16.4662
0.983	39.0353	35.465	33.3572	32.3069	28.6033	26.6996	24.9191	23.886
0.966	40.0247	37.5426	36.2018	35.4091	33.4758	32.2101	32.1381	34.6621
0.948	40.3986	38.6208	38.4105	37.2625	36.195	35.5606	36.0465	38.3299
0.931	41.5961	40.6205	40.0176	39.9677	39.64	40.0303	41.0795	42.4232
0.914	41.9351	41.6949	41.5705	41.6278	42.0723	42.9628	44.9023	49.3347
0.897	42.3463	42.2101	41.8857	42.4398	43.1639	44.3433	46.5765	52.2078
0.871	41.973	42.0202	42.1132	42.1987	42.8437	44.1258	45.8434	48.8365

A4) real and B4) imaginary part of complex permittivity measured at 10 GHz.

(A5)

KDP/H2O	e'							
V H20	10°C	20°C	25°C	30°C	40°C	50°C	60°C	70°C
1	32.2892	38.4418	40.0873	43.6901	48.3343	50.7856	54.1875	56.1086
0.995	32.2116	38.33	38.0718	43.3751	48.4332	51.8335	54.5739	56.0506
0.983	31.3219	37.0097	39.8715	41.657	46.9062	49.2894	51.6443	52.9184
0.966	30.4225	35.5177	37.9936	39.7804	43.6791	46.436	48.0892	47.8602
0.948	30.7869	35.6534	36.9118	39.6253	43.2532	45.9239	47.4093	47.5693
0.931	29.6837	34.207	35.3287	37.8502	41.2394	43.5533	44.9961	45.6198
0.914	28.4616	32.5335	34.2623	35.963	38.99	41.1866	42.2599	41.2524
0.897	28.2304	32.3002	33.588	35.5865	38.569	40.5895	41.7401	40.0519
0.871	28.0285	32.0546	33.5899	35.2293	38.2912	40.4538	41.6715	41.4208

(B5)

KDP/H2O	e''							
V H20	10°C	20°C	25°C	30°C	40°C	50°C	60°C	70°C
1	36.6204	36.6779	36.3905	36.4067	34.963	32.8366	30.9007	29.3145
0.995	36.6926	36.828	35.9871	36.6674	35.35	33.6891	31.7251	29.7626
0.983	36.5619	37.0683	37.0008	37.0257	36.0779	35.1098	33.6981	32.7156
0.966	35.9793	36.6729	37.0177	36.8555	36.6117	35.9394	35.3125	35.99
0.948	36.0228	36.6753	36.9292	37.1661	37.1547	36.8282	36.5197	37.2145
0.931	35.581	36.5557	36.4819	37.1074	37.441	37.6204	37.725	38.1542
0.914	34.7453	35.9628	36.2731	36.787	37.4045	37.8388	38.3885	39.8079
0.897	34.4676	35.6169	35.9427	36.5868	37.353	37.8553	38.546	39.9022
0.871	34.4871	35.7394	36.0674	36.644	37.3238	37.9708	38.4392	39.4588

A5) real and B5) imaginary part of complex permittivity measured at 20 GHz.

(A6)

ADP/H2O	e'							
V H20	10°C	20°C	25°C	30°C	40°C	50°C	60°C	70°C
1	83.7055	80.4504	78.5514	77.8285	74.9422	70.5707	69.4406	67.4669
0.993	86.58617	83.59593	82.15867	80.65927	77.76133	75.0164	72.36953	70.43257
0.973	88.8722	86.25317	84.8748	83.6861	81.36233	78.99573	76.92167	75.32497
0.946	91.3206	88.64423	87.4683	86.27403	84.0933	82.26717	80.52827	79.3928
0.920	93.7821	91.78107	90.6602	89.67313	88.05343	86.57207	85.41133	84.55207
0.894	95.74027	94.1826	93.4316	92.70677	91.27063	89.8672	88.7702	87.99273
0.868	97.22893	95.99893	95.41207	94.88147	93.61493	92.50737	91.66333	91.05957
0.817	98.82577	98.7622	98.57473	98.46873	97.98477	97.41073	96.6688	96.18293
0.790	98.56103	100.3049	100.4909	100.5345	100.443	100.0261	99.6504	99.40983

(B6)

ADP/H2O	e''							
V H20	10°C	20°C	25°C	30°C	40°C	50°C	60°C	70°C
1	2.5283	2.0188	1.7931	1.7098	1.4171	1.293	1.1859	1.1716
0.993	23.441	27.0581	29.346	31.99	37.6344	44.8184	51.2844	59.5181
0.973	67.763	81.0949	89.4513	97.7367	115.8123	139.0066	162.8849	190.5856
0.946	112.4627	136.9124	150.0242	165.7041	199.0807	229.8052	272.9231	320.788
0.920	150.1374	179.4764	200.5183	222.4692	264.2702	314.6861	364.0651	425.8167
0.894	184.4368	222.1403	242.7801	267.1751	317.6527	372.8694	437.0411	498.8367
0.868	209.0647	254.4674	278.2511	305.7863	364.6721	435.9697	501.9874	576.8038
0.817	250.1481	303.4431	335.2866	366.1862	432.6055	521.5407	604.0598	698.4928
0.790	266.5258	322.7566	357.5593	389.2668	463.361	547.2405	650.5774	744.7734

A6) real and B6) imaginary part of complex permittivity measured at 500 MHz.

(A7)

ADP/H2O	e'							
V H20	10°C	20°C	25°C	30°C	40°C	50°C	60°C	70°C
1	83.3222	80.2549	76.6586	77.5232	74.5834	70.1693	68.8939	66.8793
0.993	85.306	82.3387	80.8558	79.32187	76.265	73.3785	70.53237	68.36693
0.973	85.13333	82.67727	81.31613	80.03183	77.32023	74.4057	71.72983	69.4276
0.946	85.49833	83.20143	81.95463	80.6737	77.96537	75.438	72.85257	70.54443
0.920	85.91223	84.32833	83.21213	81.9964	79.74667	77.31603	74.99003	72.97697
0.894	85.9451	84.86903	84.12267	83.22663	81.22383	78.78633	76.4401	74.41503
0.868	84.38507	84.9753	84.77747	83.74303	81.94507	79.70883	77.65937	75.65533
0.817	82.929	83.53977	83.50233	83.35303	82.3214	80.60563	78.53397	76.48837
0.790	81.0449	83.10783	83.43637	83.47087	82.8846	81.519	79.30337	77.23473

(B7)

ADP/H2O	e''							
V H20	10°C	20°C	25°C	30°C	40°C	50°C	60°C	70°C
1	4.3077	3.0611	4.0956	2.279	1.6586	1.1885	0.8777	0.6404
0.993	14.783	17.2241	18.0527	18.9925	21.313	24.5144	27.4847	31.612
0.973	39.7307	45.1257	48.6236	52.4485	60.5795	71.4858	83.0624	96.8269
0.946	63.7014	74.1516	80.0349	87.2116	102.8105	117.5706	138.562	162.1678
0.920	83.5523	96.4794	106.0816	116.1781	136.0296	159.9232	184.7137	214.5219
0.894	101.7655	118.8722	128.3405	139.5943	163.6116	190.1057	221.8724	251.6037
0.868	115.1283	136.0869	147.1355	160.0863	188.0051	222.6069	255.007	291.8691
0.817	138.3905	163.5693	178.7044	193.4158	225.2013	267.8319	308.8393	354.3064
0.790	147.1089	174.2622	190.8697	206.0581	241.633	282.2935	333.182	376.7648

A7) real and B7) imaginary part of complex permittivity measured at 1 GHz.

(A8)

ADP/H2O	e'							
V H20	10°C	20°C	25°C	30°C	40°C	50°C	60°C	70°C
1	79.9164	78.0896	76.5922	75.9639	73.341	69.096	69.0978	66.8525
0.993	81.88127	80.06367	78.9506	77.64463	74.90593	72.1387	69.2331	66.93787
0.973	78.53827	77.72347	76.94107	76.1511	74.1061	71.5534	69.05187	66.65077
0.946	75.4705	75.23177	74.8782	74.33863	72.801	70.98717	68.74047	66.42533
0.920	72.90703	73.32007	73.2641	73.006	72.03007	70.44327	68.5496	66.56913
0.894	70.47813	71.38347	71.56227	71.61213	71.1517	69.9918	68.2216	66.39127
0.868	68.56593	69.27193	69.6732	69.91927	69.81653	68.86807	67.516	65.75097
0.817	62.5698	64.50183	65.32987	65.9419	66.59683	66.649	65.76607	64.165
0.790	59.6629	62.13827	63.04413	63.73327	64.76313	64.98123	63.84583	62.2356

(B8)

ADP/H2O	e''							
V H20	10°C	20°C	25°C	30°C	40°C	50°C	60°C	70°C
1	16.2222	12.4928	11.7858	9.9263	7.8973	6.2235	5.2875	4.4318
0.993	21.7542	18.7185	17.6147	16.7879	15.6599	15.3797	15.2639	16.0409
0.973	31.1511	30.0089	29.775	29.9402	30.8416	33.0311	35.8635	39.8626
0.946	40.53	41.2469	42.0509	43.2782	46.5994	50.0599	55.84	63.1332
0.920	48.2746	50.5589	52.5469	54.8431	59.7829	66.3025	73.4335	82.9748
0.894	55.1097	59.0903	61.4586	64.386	70.8052	78.134	87.4854	97.0254
0.868	60.0791	65.6618	68.7352	72.3073	80.2708	90.5399	100.351	111.8018
0.817	68.0761	75.9124	80.6221	85.2516	95.095	108.3946	121.137	136.3685
0.790	70.6818	79.6854	85.1025	90.0009	101.4928	114.3098	130.4124	145.2396

A8) real and B8) imaginary part of complex permittivity measured at 3GHz.

(A9)

ADP/H2O	e'							
V H20	10°C	20°C	25°C	30°C	40°C	50°C	60°C	70°C
1	56.8472	61.7271	62.2023	64.5883	65.901	64.5385	65.1555	64.3405
0.993	54.8714	60.84963	62.62603	63.69107	64.2537	63.37963	61.71057	60.1968
0.973	52.113	57.75027	59.7477	61.07673	62.264	61.60257	60.91113	59.5336
0.946	49.9767	55.17037	57.00307	58.51623	60.1912	60.63153	60.29863	59.40983
0.920	47.5951	52.39617	54.45353	56.08133	57.752	58.36927	58.30463	57.77953
0.894	45.51883	50.0678	51.84593	53.39243	55.32883	56.35757	56.4736	56.1797
0.868	46.52577	47.82497	49.56353	51.10613	53.19873	54.29067	54.60647	54.35457
0.817	38.22433	42.498	44.3899	45.8616	48.10023	49.77357	50.32	50.01503
0.790	36.18387	40.4275	42.2865	43.71707	46.13607	47.7054	48.04463	47.7502

(B9)

ADP/H2O	e''							
V H20	10°C	20°C	25°C	30°C	40°C	50°C	60°C	70°C
1	36.8367	32.1143	30.0935	27.752	23.3034	19.2964	16.6459	14.4327
0.993	42.2202	35.8411	32.6759	29.6107	24.1914	20.2145	17.2526	15.6367
0.973	41.8963	37.4079	34.8553	32.7936	29.0297	26.2088	24.5083	23.8559
0.946	40.7313	38.0284	36.7316	35.5242	33.5546	32.3311	31.7852	32.4293
0.920	41.2442	39.8325	38.8378	38.1627	37.2907	37.1381	37.4657	38.9705
0.894	41.6113	40.9622	40.6568	40.4433	40.3102	40.6541	41.8506	43.3884
0.868	41.7148	41.8352	41.8596	42.0421	42.6665	44.0076	45.6256	47.8751
0.817	41.4184	42.9245	43.694	44.5026	46.2905	48.8862	51.584	55.1649
0.790	40.6364	42.873	44.0496	45.1012	47.5206	50.2618	53.9609	57.3373

A9) real and B9) imaginary part of complex permittivity measured at 10 GHz.

(A10)

ADP/H2O	e'							
V H20	10°C	20°C	25°C	30°C	40°C	50°C	60°C	70°C
1	32.2892	38.4418	40.0873	43.6901	48.3343	50.7856	54.1875	56.1086
0.993	27.62017	35.631	39.70163	43.78823	51.24977	56.90007	60.6335	62.32897
0.973	27.0837	34.51973	38.4787	42.02207	48.2165	52.86137	55.53253	56.79823
0.946	28.9352	34.93777	37.63233	40.27417	44.59217	47.4631	49.40687	50.28527
0.920	28.15497	33.37517	36.19037	38.77873	42.42657	45.1189	46.73377	47.49973
0.894	27.51017	32.3145	34.58287	36.8004	40.3164	43.05117	44.66077	45.34063
0.868	30.58397	31.1776	33.27057	35.32883	38.75833	41.2836	42.6842	43.25803
0.817	24.0846	27.98153	29.99867	31.67677	34.59823	37.2027	38.47767	38.65867
0.790	23.39653	26.99863	28.8366	30.36527	33.2706	35.44337	36.51133	36.64937

(B10)

ADP/H2O	e''							
V H20	10°C	20°C	25°C	30°C	40°C	50°C	60°C	70°C
1	36.6204	36.6779	36.3905	36.4067	34.963	32.8366	30.9007	29.3145
0.993	35.4617	37.1704	37.4025	37.0622	35.0685	31.5981	27.3835	24.4429
0.973	35.7498	36.9338	37.0402	36.9305	35.3783	32.7545	30.0853	27.8951
0.946	36.0006	36.6827	36.8386	36.9605	36.5796	35.8825	35.0032	34.7911
0.920	35.1655	36.3608	36.6474	37.036	37.1036	36.9896	36.6593	36.7615
0.894	34.4781	35.8053	36.3458	36.8199	37.3832	37.5479	37.8206	38.1213
0.868	33.5774	35.2358	35.8718	36.5856	37.525	38.1518	38.7192	39.5373
0.817	31.4782	33.5873	34.5938	35.4879	37.0893	38.4869	39.7313	41.1933
0.790	30.145	32.473	33.6827	34.7271	36.6656	38.2732	39.883	41.2354

A10) real and B10) imaginary part of complex permittivity measured at 20 GHz.

(A11)

Seignette Salt/H2O	e'							
V H20	10°C	20°C	25°C	30°C	40°C	50°C	60°C	70°C
1	83.7055	80.4504	78.5514	77.8285	74.9422	70.5707	69.4406	67.4669
0.94	84.448	82.080	81.214	80.278	78.801	77.461	76.424	75.935
0.88	81.309	79.865	79.387	78.874	77.945	77.481	76.982	76.546
0.77	74.455	74.187	74.138	74.286	74.334	74.559	74.851	74.797
0.66	65.032	65.890	66.471	67.116	67.953	68.788	69.108	66.903
0.61	61.547	62.823	63.403	64.165	65.345	66.622	67.556	65.330

(B11)

Seignette Salt/H2O	e''							
V H20	10°C	20°C	25°C	30°C	40°C	50°C	60°C	70°C
1	2.5283	2.0188	1.7931	1.7098	1.4171	1.293	1.1859	1.1716
0.94	116.826	144.5157	158.4398	174.119	207.0508	248.3078	291.1246	347.841
0.88	188.8832	233.5285	256.8255	282.9737	360.9468	405.8491	477.4581	590.1924
0.77	253.0576	317.2777	359.4989	384.5982	463.9456	550.6255	648.8916	746.0609
0.66	235.8718	305.2657	341.4058	381.0198	463.0504	552.4592	641.9475	667.4833
0.61	215.6949	284.5357	316.4548	351.2237	430.693	522.8593	610.0378	622.5601

A11) real and B11) imaginary part of complex permittivity measured at 500 MHz.

(A12)

Seignette Salt/H2O	e'							
V H20	10°C	20°C	25°C	30°C	40°C	50°C	60°C	70°C
1	83.3222	80.2549	76.6586	77.5232	74.5834	70.1693	68.8939	66.8793
0.94	79.228	76.566	75.434	74.138	71.723	69.287	67.060	64.929
0.88	74.180	72.002	70.980	69.925	66.873	65.280	62.921	59.977
0.77	64.974	63.498	62.653	62.171	60.558	58.797	56.734	54.458
0.66	55.780	55.437	55.351	55.249	54.572	53.772	52.441	49.240
0.61	52.408	52.316	52.291	52.183	51.894	51.382	50.449	47.573

(B12)

Seignette Salt/H2O	e''							
V H20	10°C	20°C	25°C	30°C	40°C	50°C	60°C	70°C
1	4.3077	3.0611	4.0956	2.279	1.6586	1.1885	0.8777	0.6404
0.94	63.62673	76.45477	83.01893	90.45173	106.2822	126.4971	147.5367	175.5004
0.88	99.98007	121.3539	132.582	145.4374	183.6602	205.9762	241.7893	298.2991
0.77	132.0523	163.3422	184.0601	196.4458	235.7597	279.1346	328.0483	377.3643
0.66	122.4574	156.5217	174.3212	193.8194	234.4582	278.9452	324.0258	336.5463
0.61	112.4222	146.2275	162.0817	179.1973	218.6613	264.33	307.8605	314.3988

A12) real and B12) imaginary part of complex permittivity measured at 1 GHz.

(A13)

Seignette Salt/H2O	e'							
V H20	**10°C**	**20°C**	**25°C**	**30°C**	**40°C**	**50°C**	**60°C**	**70°C**
1	79.9164	78.0896	76.5922	75.9639	73.341	69.096	69.0978	66.8525
0.94	73.783	72.205	71.293	70.233	68.133	65.830	63.601	61.291
0.88	67.386	66.227	65.515	64.652	62.056	60.510	58.161	54.636
0.77	57.200	56.624	56.027	55.656	54.263	52.497	50.164	47.382
0.66	47.565	47.861	47.855	47.707	46.946	45.800	44.143	40.243
0.61	43.758	44.402	44.403	44.269	43.824	42.950	41.515	38.039

(B13)

Seignette Salt/H2O	e''							
V H20	**10°C**	**20°C**	**25°C**	**30°C**	**40°C**	**50°C**	**60°C**	**70°C**
1	16.2222	12.4928	11.7858	9.9263	7.8973	6.2235	5.2875	4.4318
0.94	35.7791	37.3449	38.58947	40.26743	44.22863	49.9873	56.33993	65.37197
0.88	47.68407	52.6347	55.5705	59.1374	70.35537	77.21773	88.4982	107.3529
0.77	57.4071	66.1616	72.3179	76.08097	88.331	102.0975	118.0923	134.4744
0.66	53.12937	63.14353	68.60517	74.72567	87.6735	102.1923	116.9175	120.6879
0.61	49.38703	59.41747	64.26747	69.6276	82.18727	97.08887	111.5796	113.5707

A13) real and B13) imaginary part of complex permittivity measured at 3 GHz.

(A14)

Seignette Salt/H2O	e'							
V H20	**10°C**	**20°C**	**25°C**	**30°C**	**40°C**	**50°C**	**60°C**	**70°C**
1	56.8472	61.7271	62.2023	64.5883	65.901	64.5385	65.1555	64.3405
0.94	52.763	57.163	58.354	59.144	59.735	59.222	58.218	56.642
0.88	47.202	50.929	51.985	52.756	53.128	52.732	51.671	49.317
0.77	39.125	42.417	43.710	44.264	45.145	45.110	44.205	42.577
0.66	32.308	35.668	36.948	37.984	39.235	39.752	39.335	35.898
0.61	29.059	32.357	33.444	34.372	35.846	36.628	36.449	33.502

(B14)

Seignette Salt/H2O	e''							
V H20	**10°C**	**20°C**	**25°C**	**30°C**	**40°C**	**50°C**	**60°C**	**70°C**
1	36.8367	32.1143	30.0935	27.752	23.3034	19.2964	16.6459	14.4327
0.94	39.2472	35.57577	34.08693	32.70953	30.5261	29.4402	29.05997	30.12987
0.88	40.15283	38.2542	37.5449	36.9633	36.66403	37.0359	38.4384	42.35697
0.77	38.11207	38.5253	38.9084	39.23367	40.6501	43.15143	45.71547	49.2074
0.66	32.04153	33.96073	34.95533	36.03423	38.37053	41.1818	44.2482	44.3646
0.61	29.0527	31.52027	32.5231	33.56767	36.13193	39.24127	42.272	42.08217

A14) real and B14) imaginary part of complex permittivity measured at 10 GHz.

(A15)

Seignette Salt/H2O	e'							
V H20	**10°C**	**20°C**	**25°C**	**30°C**	**40°C**	**50°C**	**60°C**	**70°C**
1	32.2892	38.4418	40.0873	43.6901	48.3343	50.7856	54.1875	56.1086
0.94	30.680	37.153	39.680	42.058	46.087	48.845	50.535	50.872
0.88	27.679	33.146	35.342	37.543	41.501	42.871	43.813	42.900
0.77	24.425	28.505	30.692	31.834	34.546	36.318	36.929	36.359
0.66	21.713	25.046	26.558	28.015	30.345	31.969	32.577	30.078
0.61	20.162	23.080	24.304	25.478	27.690	29.419	30.119	28.073

(B15)

Seignette Salt/H2O	e''							
V H20	**10°C**	**20°C**	**25°C**	**30°C**	**40°C**	**50°C**	**60°C**	**70°C**
1	36.6204	36.6779	36.3905	36.4067	34.963	32.8366	30.9007	29.3145
0.94	36.4985	36.65523	36.57213	36.29387	35.3116	34.00673	32.72393	31.9367
0.88	34.34577	34.97717	34.99387	35.0091	34.48663	34.08273	33.70757	34.21403
0.77	29.92023	31.37417	32.03553	32.37777	33.117	33.70227	34.3422	35.02787
0.66	24.503	26.61327	27.53043	28.44773	29.87997	31.1354	32.1701	30.9204
0.61	21.6926	24.04933	24.93687	25.78153	27.4906	29.0563	30.22707	28.98063

A15) real and B15) imaginary part of complex permittivity measured at 20 GHz.

Resume

Dana Daneshvari
Pharmacist

Personal Details

Name:	Dana Daneshvari
Date and place of birth:	5 September 1975
Nationality:	Iran
Current address:	Mülhauserstrasse 114, 4056 Basel, Switzerland
Office phone:	+41 61 267 15 05
Cell phone:	+41 76 330 05 56
E-Mail:	dana.daneshvari@unibas.ch

PhD Study

October 2004 – present	PhD study at Institute of Pharmaceutical Technology (University of Basel) under the supervision of Prof. Dr. Hans Leuenberger. Work title: ”Investigation of binary polar solvent mixtures, solubilized ferroelectric salts and Paraffin-based derivatives using dielectric spectroscopy.” Lectureship in practical courses of semi-solid dosage forms

Presentations

20 – 21 April 2007	3rd World Congress of the Board of Pharmaceutical Sciences of FIP (PSWC 2007), Pre-Satellite Sessions, Amsterdam, Holland Poster presentation
22 – 25 April 2007	3rd World Congress of the Board of Pharmaceutical Sciences of FIP (PSWC 2007), Amsterdam, Holland Poster presentation

Education

September 1998 – June 2004	Pharmacy studies at Semmelweis University, Budapest, Hungary Master in Pharmaceutical Sciences Final result state examination: Good Final result practical diploma thesis: 5 (maximum 5.00)
September 1997 – June 1998	Pre-medical course, Collage International Budapest, Hungary

1995 – 1997	Obligatory military services
August 1990 – July 1994	High school diploma at 7th of Tir High school, Tehran, Iran

Work Experience

July 2000 – September 2000	Damatco Chemical Co, Tehran, Iran
July 2002 – September 2002	Namy Pharmacy, Tehran Iran
June 2003 – August 2003	City Apotheke, Lucerne, Switzerland
January 2004 – June 2004	Dorotya Apotek, Budapest, Hungary

Additional Skills

Trainings

March 2007	Freeze-Drying of Protein-Based Pharmaceuticals, Bio Up Foundation, held at Novartis Foundation, London, U.K.
March 2007	Innovative Dosage Forms & process Technology, Basel, Switzerland
March 2007	Quality and GMP 2007, ETH Zürich – Unibasel, Basel, Switzerland
February 2007	Robust dosage form design: Innovative and effective tools for a science based road map in pharmaceutical R&D. Technology Training Center (TTC) Binzen, Germany
November 2006	Pan Coating. Technology Training Center (TTC) Binzen, Germany
May 2006	Granulation & Tabletting. Technology Training Center (TTC) Binzen, Germany
November 2005	Key Issues In Drug Discovery & Development, ETH Zürich – Unibasel, Basel, Switzerland

Languages	Persian (native speaker) English (fluent) German (good, oral and written) Hungarian (Basic)
PC Literacy **Applications**	Proficient user Good command of Microsoft Office and Excel applications